1998

A study of the overoxidation of the conducting polymer polypyrrole

Trevor W. Lewis
University of Wollongong

A STUDY OF THE OVEROXIDATION OF THE CONDUCTING POLYMER POLYPYRROLE

A thesis submitted in fulfilment of the requirements for the award of the degree of

DOCTOR OF PHILOSOPHY

from the

University of Wollongong

by

TREVOR W. LEWIS BSc

Supervisors: Professor G. G. Wallace and Dr G. M. Spinks

The work presented in this thesis was carried out by the candidate and any assistance has been duly acknowledged.

Department of Chemistry,

August, 1998.

"There's no use trying" she said: "one *can't* believe impossible things."

"I daresay you haven't had much practice," said the Queen.

"..... Why, sometimes I've believed as many as six impossible things before breakfast."

Through the Looking Glass.

Lewis Carroll, 1872.

ACKNOWLEDGMENTS

Firstly, I would like to formally thank Professor Gordon Wallace and Dr Geoff Spinks for the opportunity to do this project and for their encouragement, support and friendship throughout it. In particular I appreciate the freedom Gordon allowed me to do pretty well whatever I thought was appropriate, almost essential for someone of my age and disposition, but extremely difficult for him.

My appreciation also goes to the members of the IPRI laboratories for their assistance and time, and for giving me access to, and advice on, instruments whenever I needed either. Special thanks go to Drs Dezhi Zhou and Peter Innis and Mr Ian Norris for their help in the laboratory and in proof reading and assembling this thesis, and to Professor Leon Kane-Maguire, for his almost unbelievable enthusiasm on nearly everything, including proof reading, and insights into kinetics.

I would also like to thank many (ex?) friends in the Chemistry Department at this University for their help in areas ranging from computer hardware and software through organic chemistry and mass spectrometry, to showing an interest in my progress on Friday nights in the bar. This thesis would not be possible without their assistance and the allowances they, and the broader Chemistry Department and its Chair, Professor John Bremner, made for me as I worked on the project. I would like to make specific mention of Associate Professor John Ellis, who suggested to me many years ago that I should do a PhD and Mrs Susan Butler and Jenny Vasquez, for their help and time in running samples on the UV-vis and Mass Spectrometer. I am also indebted to Associate Professor Margaret Sheil and Dr Will Price, for their help in interpreting the MS data and Leon's kinetics. Thanks also to Professor Stephen Pyne for his patience in dealing with my lack

of understanding of organic chemistry and Dr Stephen Wilson for his with my inability to comprehend the workings of a computer.

My thanks also go to Drs Chung Yup Kim and Dong Young Kim at the Division of Polymer Science and Engineering, Korean Institute of Science and Technology, Seoul, Korea, and Professor Danillo De Rossi, Centro E Piaggo, University of Pisa, Italy, for their time and assistance in the work carried out in their laboratories on the UV / vis and Raman studies and the two electrode system, respectively.

To Kaius, Benno, Prin, Morgy, Timmy and Truds, you always knew I could do it, so can you.

Finally, to my wife and best friend Janey, for being there almost all of the time, mille, mille grazie!!!

ABSTRACT

Linear sweep voltammetry - resistometry, UV-vis and Raman spectroscopy, Matrix Assisted Laser Desorption Ionisation mass spectrometry (MALDI-MS) and cyclic voltammetry were employed to study the overoxidation of polypyrrole and substituted polypyrroles. Consideration was given to a range of parameters that affect the degradation of this polymer in an aqueous environment: incorporated counterion, supporting electrolyte solutes and pH, substrate, film thickness, scan rate and applied potential.

From these studies it was observed that the major contributions to ease the overoxidation potential of polypyrrole are the applied potential and supporting electrolyte pH. It was also found that variations in the overoxidation potential corresponded to the ordering of cations and anions in the lyotropic series. The most stable non-substituted polypyrrole films were those containing mono-cationic sulphonates as dopants. However, the substituted polymer poly(3-octylpyrrole) was shown to have by far the highest stability.

Based on Raman spectroscopic studies, a mechanism for the facile overoxidation of poly(3-methylpyrrole-carboxylic acid) was proposed. Further, a chain breaking mechanism for the overoxidation of polypyrrole was supported by MALDI-MS studies. This commenced with the formation of adjacent imine-nitrogens (-N=) at one end of a six pyrrole unit to initiate chain breaking by oxygen attack. At various levels of overoxidation, oxygen-containing and oxygen-free pyrrole dimers, trimers, tetramers, hexamers and heptamers were observed.

From this study it is suggested that realistic anodic limits for practical applications of polypyrrole in an acidic aqueous environment are as low as 0.5 V (vs Ag/AgCl). However, polypyrrole is so susceptible to degradation in basic conditions that it is not possible to suggest any anodic limit. In free-standing two-electrode polypyrrole devices

operating in air long term operation can be ensured by limiting the potential difference to ±1.5 V.

PUBLICATIONS ARISING FROM THIS AND RELATED WORK

T. W. Lewis, G. G. Wallace

Communicative polymers: the basis for development of intelligent materials.

Journal of Chemical Education, 74 (6), 1997, 703 -8.

T. W. Lewis, G. M. Spinks, S. E. Moulton, G. G. Wallace

Optimisation of a polypyrrole based actuator.

Synthetic Metals, 85 (1 - 3), 1997, 1419 - 20.

T. W. Lewis, G. G. Wallace, C. Y. Kim, D. Y. Kim

Studies of the overoxidation of polypyrrole.

Synthetic Metals, 84 (1 - 3), 1997, 403-4.

T. W. Lewis, G. M. Spinks, G. G. Wallace, D. De Rossi and M. Pachetti

Development of an all polymer electromechanical actuator.

Polymer Pre-prints, 38 (2), 1997, 520-1.

H. Zhao, F. Chen, T. W. Lewis, W. E. Price, G. G. Wallace

Studies of electropolymerisation of sodium 2-(3-thienyl)ethyl sulphonate.

Reactive and Functional Polymers, 34, 1997, 27-36.

P. R. Teasdale, A. I. Minett, K. Dixon, T. W. Lewis, G. E. Batley

Methodoligical notes on redox potential (E_H) measurements and the application of a multiple-electrode redox probe (MERP) for characterising sediments in-situ.

Analytica Chimica Acta, 367, 1998, 210 - 213.

T. W. Lewis, L. A. P. Kane-Maguire, A. S. Hutchison, G. M. Spinks, G. G. Wallace

Development of an all-polymer, axial force electrochemical actuator.

Synthetic Metals, In Press (1998).

J. N. Barisci, T. W. Lewis, G. M. Spinks, C. O. Too, G. G. Wallace

Responsive systems based on conducting polymers.

Journal of Intelligent Polymer Material Systems and Structures, Submitted (1998).

G. G. Wallace, T. W. Lewis, M. R. Smyth

Electrofunctional polymers: their role in the development of new analytical sensors.

Analytica Chimica Acta, Submitted (1998).

J. N. Barisci, T. W. Lewis, G. M. Spinks, C. O. Too, G. G. Wallace

Responsive systems based on conducting polymers.

Journal of Intelligent Polymer Material Systems and Structures, Submitted (1998).

T. W. Lewis, M. M. Sheil, J. A. Vasquez, G. G. Wallace

The application of MALDI-MS to studies of the overoxidation of polypyrrole.

In Preparation.

T. W. Lewis, G. G. Wallace, C. Y. Kim, D. Y. Kim

Raman spectroscopic studies of the overoxidation of polypyrrole and substituted polypyrroles.

In Preparation.

T. W. Lewis, G. G. Wallace

Chaotropes, kosmotropes and polypyrrole.

In Preparation.

T. W. Lewis, G. M. Spinks, G. G. Wallace

Applied potential limits in a conducting polymer two-electrode solid-state device.

In Preparation.

ABBREVIATIONS

A	ampere
A^-	anion
Å	angstrom
[A]	concentration of species A
AcN	acetonitrile
Ani	aniline monomer
aq	aqueous
atm	atmosphere
BS	benzenesulphonate anion
C	coulomb
C^+	cation
CEP	conducting electroactive polymer
CR	cyclic resistommetry
c	centi
CSA	camphor sulphonic acid anion
CV	cyclic voltammetry
°C	degrees Centigrade
d	density
D	diffusion coefficient
D_{app}	apparent diffusion coefficient
Da	Dalton
DBS	dodecylbenzenesulphonate anion
DC	direct current
DDS	dodecylsulphate anion
DS	decylsulphate anion
dyn	dyne
ΔH°_f	standard enthalpy of formation change

ΔG^{o}_{f}	standard Gibbs free energy of formation change
E	potential
E_a	activation energy
E_{app}	applied potential
E_{meas}	measured potential
$E_{O\text{-}Ox}$	overoxidation potential
E_{pa}	oxidation peak potential
eV	electron volts
F	Faraday's Constant, 9.649×10^4 C mol^{-1}
FT	Fourier Transform
g	gram
GC	glassy carbon
h	hour
i	current
IR	infrared spectroscopy
i_D	current at disk electrode in an RRDE experiment
ITO	indium - tin oxide
i_R	current at ring electrode in an RRDE experiment
J	joules
k	kilo
K	degrees Kelvin
L	film thickness (μm)
LSR	linear sweep resistometry
LSV	linear sweep voltammetry
m	meter (length)
m	milli
m	molal concentration
M	molar concentration
M	mega

Me	methyl group
min	minute
mol	mole
m/z	mass to charge ratio (Dalton per charge)
μ	micro
n	nano
o-ox	overoxidation
OS	octanesulphate anion
Pa	Pascal
PAni	polyaniline
PC	propylene carbonate
P(MPyC)	poly(3-methylpyrrole-carboxylic acid)
P(3-OPy)	poly(3-octylpyrrole)
ppm	parts per million
PPy	polypyrrole
PSS	polystyrenesulphonate anion
PS	pentanesulphonate anion
PTh	polythiophene
pTS	paratoluenesulphonate anion
PVS	polyvinylsulphate anion
Py	pyrrole monomer
R	resistance
Q	charge
rpm	revolutions per minute
s	second
SCE	saturated calomel electrode
SS	stainless steel
t	time
T	temperature

τ	time constant
TBA	tetrabutylammonium cation
TEA	tetraethylammonium cation
Th	thiophene monomer
Tir	tiron anion
UV-vis	ultra-violet - visible spectroscopy
V	volt
W	watts
XPS	X-ray photoelectron spectroscopy

CONTENTS

1 GENERAL INTRODUCTION

1.1 BACKGROUND

"Pyrrole black" was first obtained by Angeli in 1916 from solutions containing pyrrole and hydrogen peroxide [1]. Its conducting nature was recognised in 1963 when McNeil et al [2] synthesised polypyrrole (PPy) by pyrolysis of tetraiodopyrrole. Conductivities of between 0.005 and 1.0 Scm^{-1} were observed for this material. McNeil also noted that this conductivity decreased with exposure to water vapour and oxygen. The first electrochemical preparation of PPy was reported by Dall'Olio et al [3] in 1968, followed by the preparation of a free-standing film by Diaz and Kanazawa in 1979 [4]. From this point strong interest in this novel material lead to extensive research into the chemical, physical and engineering properties of polypyrrole.

As a result of this research activity a wide range of applications for polypyrrole have been considered, for example: biosensors [5, 6], chemical sensors [7, 8], electrochemical catalysts [9], solar cells [10], electronics components [11, 12], corrosion protection [13], separation membranes, batteries [14], electrochromics [15], actuators [16] and anti-static coatings [17].

Many of these applications rely on the polymer retaining its electroactivity and / or conductivity under an applied potential in environments containing oxygen and water. Under such conditions the polymer is often degraded irreversibly or "overoxidised". Overoxidised PPy exhibits losses of conductivity, charge storage ability, electrochromism [18, 19], electroactivity [20], conjugation [21], mechanical properties [22] and adhesion to the substrate [23]. Though a number of applications are proposed for deactivated PPy (eg anion exclusion membranes [24, 25], *in-vivo* sensors [26, 27], enzyme immobilisation matrices [28] and size exclusion membranes [29]), Neoh et al have

observed that the "stability of a conducting polymer is one of the most important factors determining its potential practical applications." [22].

The focus of this work is to further investigate a number of combinations of operating environments and the film chemistries that may have a role in the degradation of polypyrrole in an aqueous environment.

1.2 POLYMERISATION OF PYRROLE

1.2.1 Growth mechanism

Polypyrrole can be readily produced from the pyrrole monomer by chemical oxidation from aqueous solution [30] or electrochemical oxidation from aqueous [31] or non-aqueous [4] solutions. Dependent on the polymerisation conditions employed, polypyrrole may be produced as either a powder, film or colloidal suspension [32]. The mechanism proposed by John and Wallace [33] (Scheme 1.1) involves firstly the oxidation of the monomer to form a radical cation with three resonance forms. Due to its higher spin density, the most stable of these forms is the α-radical [34], leading to radical - radical coupling largely through the α-positions. Deprotonation of the coupled radical cations leads to the formation of a pyrrole dimer which may be oxidised to form a radical cation. Chain propagation then occurs by reaction between this species and other radical cations (monomers, dimers, trimers etc) [35]. Coupling reactions continue until the solubility of the oligomers is exceeded (up to nine monomer units [36]) and they precipitate to initiate film growth at the electrode surface [37].

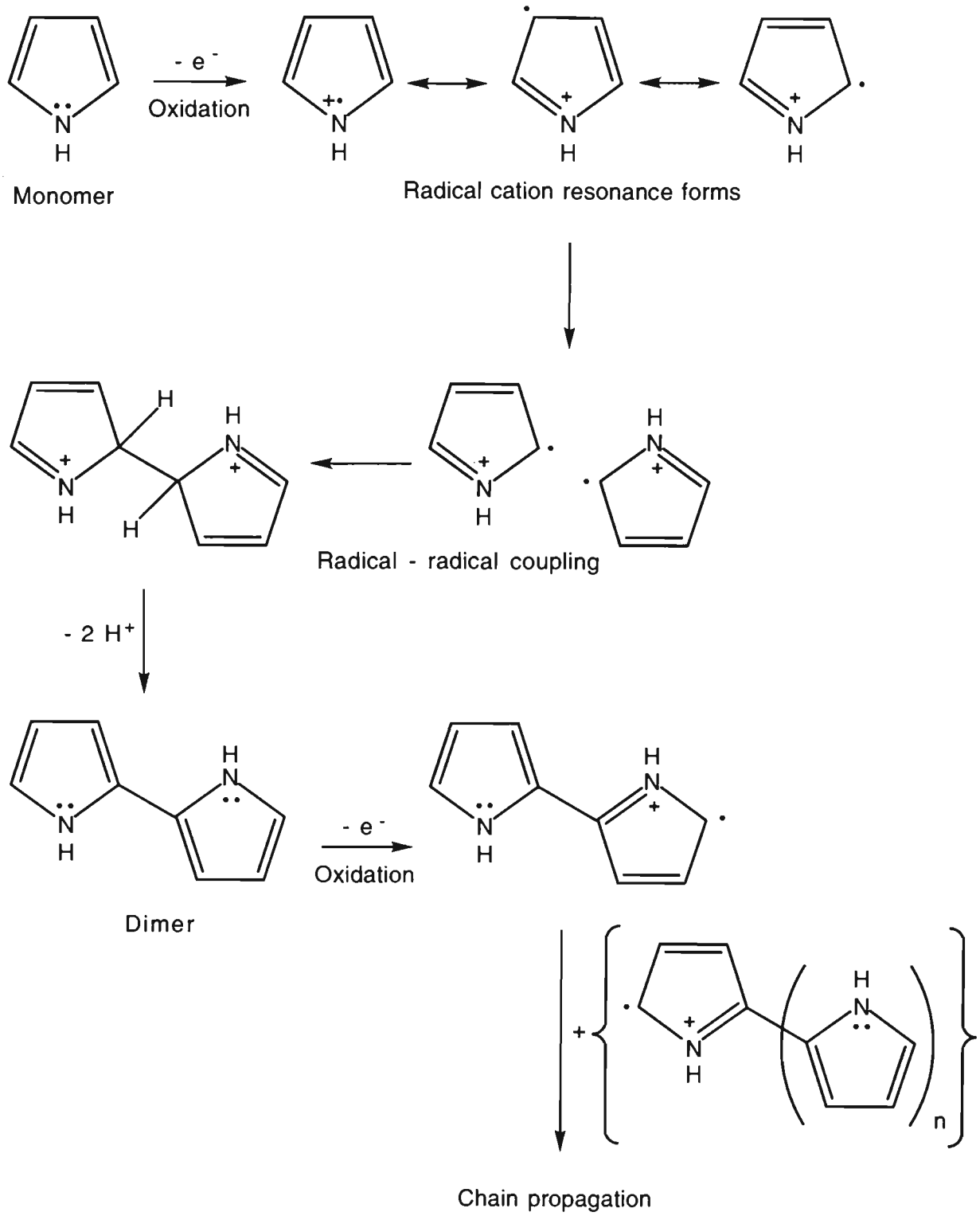

Scheme 1.1: Oxidative polymerisation of polypyrrole (after John and Wallace [33]).

According to John and Wallace [33] film growth occurs as a result of continual precipitation of these oligomers from solution and not heterogenous reactions at the film surface. On the other hand, Schlarifker and Fermin [37] and Bilger and Heinze [38] report that while soluble intermediate species participate in the initial stages of formation, film growth occurs by direct reaction of the pyrrole monomer at the PPy surface. In

contrast, Kim et al [39] claim that the initial stages of film growth is initiated by adsorption of monomer at the electrode surface followed by two dimensional nucleation, coalescence and densification.

Regardless of which mechanism is correct, growth continues until the polymer is terminated by either nucleophilic attack at an α-carbon [35] or prevention of further reaction by steric hindrance [40]. This limits the polymer chain length to an average of 34 monomer units in the case of galvanostatic growth of PPy/ClO_4 from 0.1 M Py / 1 M $NaClO_4$ [41].

Under potentiodynamic conditions the initial step in Scheme 1, monomer oxidation, occurs at an applied potential of 0.6 V (vs Ag/AgCl) and polymer growth typically occurs at around 0.8 V [42]. Otero and Santamaria [43] claim that PPy/ClO_4 can be grown from aqueous solutions at applied potentials of up to 2.4 V (vs SCE). They further report that over 10 to 120 s these potentials give good yields of polymers with high charge storage capacity and good electrochemical responses. During galvanostatic polymerisation polymer growth is effected at about 0.65 V (vs SCE) [44]. In both circumstances it is necessary to maintain the application of potential as the polymerisation is not autocatalytic and will cease in the absence of suitable oxidative conditions [45].

1.2.2 Structural defects

The mechanism presented in Scheme 1.1 is obviously idealised and would result in purely α–α coupling throughout the chain. However, a number of structural defects have been observed in PPy ([1] and references therein). These include α–β couplings and adjacent rings with hydrogens in the cis-position, both of which will eventually limit chain growth by steric hindrance. A second group of defects, which lead to poor conjugation in the polymer, include hydrogenation and attachment of hydroxyl and carbonyl groups. Scheme 1.2 illustrates the common defects found in polypyrrole.

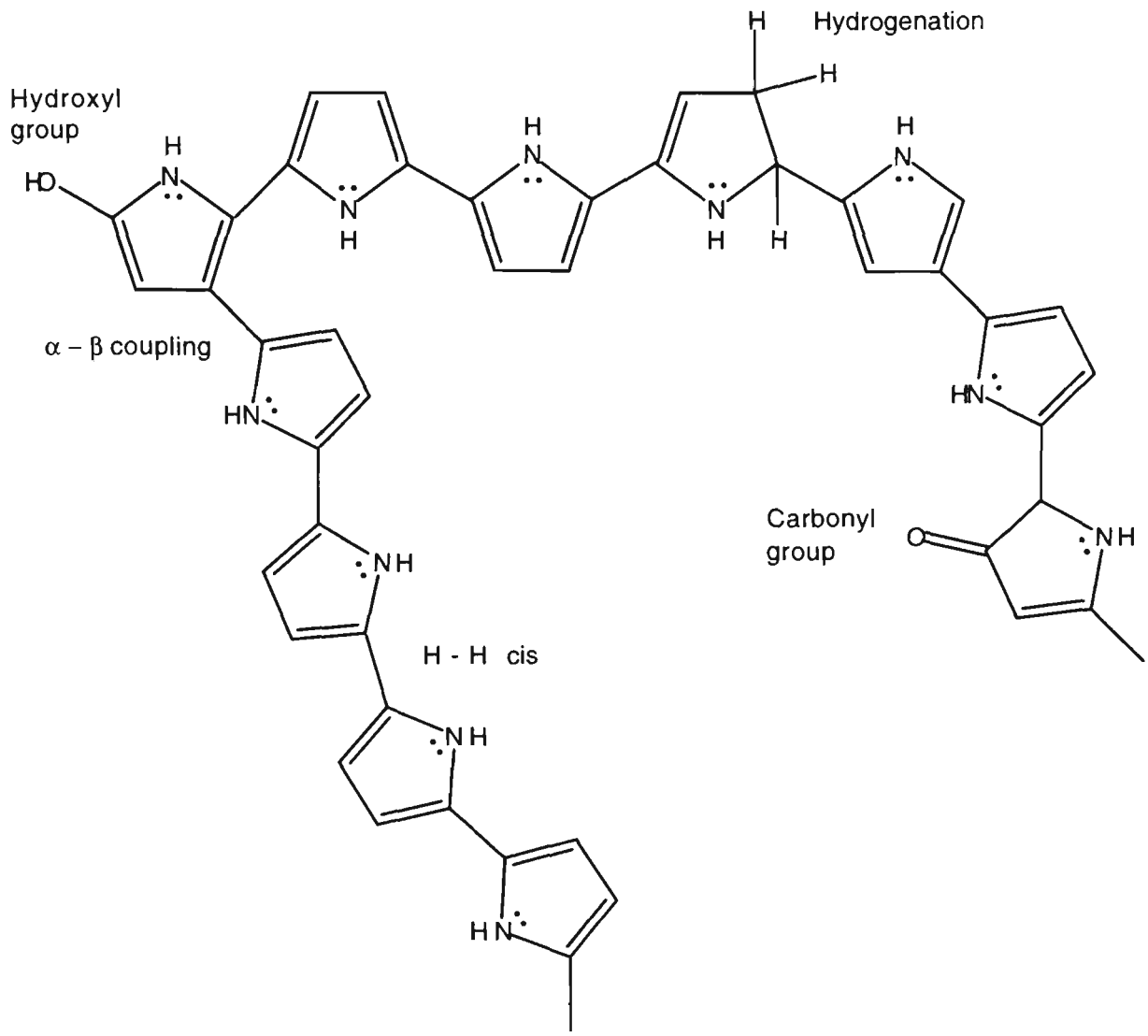

Scheme 1.2: Possible defects in the structure of polypyrrole (after Saunders [1]).

As early as 1982 Street et al [46] recognised that hydrogenation occurred during electrochemical growth of PPy from dry, oxygen-free AcN. The hydrogen content was found to be in 10 % excess over its stoichiometric requirement. These workers also recognised that α–β coupling occurs, causing a deviation from chain linearity. These deviations will increase steric hindrance and lead to early cessation of chain propagation.

In the following year the same group observed [47] the presence of oxygen in electrochemically cycled PPy, even though "considerable care" had been taken to exclude it from all processes. Only by rigorous drying of all reagents (including distillation, recrystallisation and drying under vacuum) and total exclusion of both water and air from the AcN growing solution, did Lei and Martin [48-50] succeed in producing oxygen - free

PPy films. However, these extreme measures would appear impractical for routine production of PPy especially for many of the large scale applications mentioned earlier. In more practical growing conditions (1 % water in AcN with N_2 degassing), oxygen has been observed either singly or doubly bonded to a pyrrole ring carbon [51, 52]. The addition of water is more practical because of higher quality film obtained when PPy is polymerised from a growing solution containing a minimum of 1 % water [53].

Due to cost, safety and environmental considerations, the most suitable solvent for large scale production of polypyrrole must surely be water. When water is employed during galvanostatic growth, the level of excess oxygen incorporated has been reported to be as high as 0.74 mol of O per mol of Py in $PPy/NO_{3\,[54]}$. This is not all necessarily present as structural defects on the pyrrole backbone as Ge et al [55] note that only 7 % of the carbons in PPy/ClO_4 grown under similar conditions are in the form of -COH, -C-O-C- or C=O. Lei and Martin [49] claim that this is largely in the form of C-OH as tautomerisation to the carbonyl group only occurs during very slow polymerisation in water. It is relevant to the current work that, according to Satoh et al [56], there is no difference in the conductivity of a PPy film prepared in the presence or absence of aerial oxygen. Beck et al [57] and Warren et al [58] also note that aerial oxygen has little effect on the electrochemistry and stability of polypyrrole.

1.2.3 Oxidation states of polypyrrole

Polypyrrole exists in three oxidation states, namely neutral PPy, the singly charged polaron (radical cation) and the doubly charged bipolaron (dication) (see Scheme 1.3). These can be reversibly interconverted from one to another by the application of suitable cathodic or anodic potentials. Though polarons and bipolarons are often present in PPy films in the as-grown state [59], their relative levels during potential cycling are controlled by the applied potential. Even though the neutral species predominates in reduced PPy, polarons have been observed by Christensen and Hamnett [41] in UV-vis absorption

studies in aqueous $NaClO_4$ at -0.6 V (vs SCE). As applied potential is scanned in the anodic direction the relative level of polarons increases until it plateaus at -0.2 V, the oxidation peak potential for this polymer. This has since been confirmed by Mostany and Scharifker [60] in a direct microcalorimetric study of the oxidation processes in PPy/Cl. Christensen and Hamnett also note some bipolaron features at potentials as low as -0.5 V, but their presence only becomes significant at -0.2 V and their relative levels increase until 0.7 V. In similar studies of PPy/Cl in aqueous NaCl, Osaka et al [61] determine that the level of the bipolaron species continues to increase up to about 0.45 V (vs SCE) and at potentials more positive than this nucleophilic attack by OH^- occurs. This phenomena will be explored more thoroughly in Section 1.6.

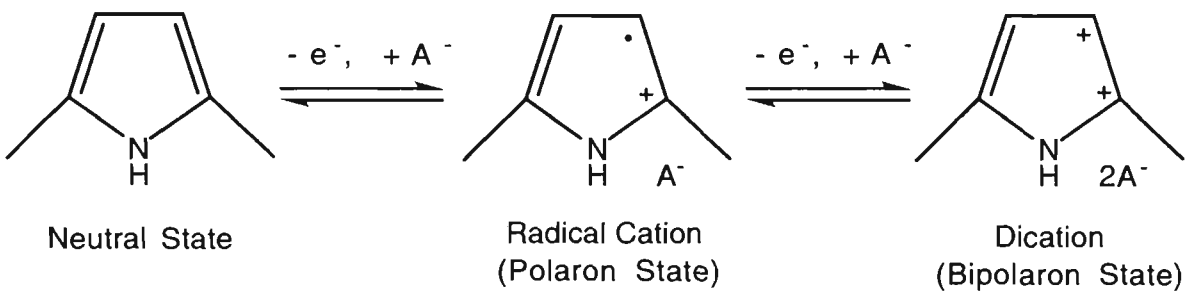

Scheme 1.3: Simplified representation of the oxidation states of polypyrrole as depicted by Beck et al [21].

As the formation of polarons from the neutral polymer disrupts the π-bonding of the conjugated polymer backbone, the reaction is endothermic in the early stages of oxidation [60]. Mostany and Scharifker postulate that the generation of polarons and bipolarons may be represented by:

PPy^0 ----> $PPy^+ + e^-$ (i, oxidation of neutral PPy, endothermic)

PPy^+ ----> $PPy^{2+} + e^-$ (ii, oxidation of PPy^+, exothermic)

$2\ PPy^+$ ----> $PPy^0 + PPy^{2+}$ (iii, combination of two polarons, exothermic),

where PPy represents "neutral polypyrrole segments". Further oxidation will tend to form bipolarons by (ii) or (iii) instead of additional polarons in the same segment, since the

energy of the bipolaronic state is about 38 $kJmol^{-1}$ lower than that of two adjacent polarons.

This appears to contradict the earlier work of Christensen and Hamnett mentioned above. They determined that the average chain length of PPy was 34 monomer units (under certain growing conditions) and that this chain could be considered as a number of "unit cells" which could be either neutral, polaronic or bipolaronic [41]. If a unit cell is already in a polaronic state, further oxidation will favour the formation of another polaron in any remaining neutral cells in the chain. Bipolarons will only be formed when all of the unit cells in a chain are polarons. According to Christensen and Hamnett, polarons exist over about 12 monomer units within a chain and bipolarons over about 3 units.

If the "neutral polypyrrole segments" of Mostany and Scharifker correspond to the "unit cells" of Christensen and Hamnett, it appears possible to reconcile these two works into a single working hypothesis: the first stage of oxidation will create a polaron approximately every 12 monomer units along the length of a PPy chain; further oxidation will then create bipolarons in preference to increasing the number of polarons in each unit; full oxidation will lead to a bipolaron over each 3 monomer units.

Theoretically, the amount of charge that could be cycled during these redox processes is given [62] by:

$Q_{rev} = Q_s / (2\,y)$,

where Q_{rev}: reversible charge available,

Q_s: charge consumed during growth,

y: number of pyrrole monomer units per dopant anion (Section 1.2.4).

Maia et al point out that during idealised PPy growth a charge of 2 electrons are consumed for the addition of each molecule of Py and 0.33 electrons per monomer unit for the addition of doping anion to the polymer chain [44]. Based on this, $Q_{rev} = (2 + 0.33) / (2 \times 3) = 0.39$ electrons per Py monomer unit, or 17 % of growing charge. Practically, it

is found that around 8 to 12 % of the charge passed during growth can be cycled during the redox processes indicated in Scheme 1.3 [31].

1.2.4 Charge compensation

As the growing potential of PPy is higher that its oxidation potential, the polymer will be oxidised during growth [1]. To maintain charge neutrality counter-anions (or "dopants") present as the supporting electrolyte anion, are incorporated into the polymer during growth. One of the major benefits of water as a growing solvent is that it allows the incorporation of an extensive range of dopant anions with extremely broad chemical and biochemical properties. These include: small inorganic mono-anions (ClO_4^-, NO_3^-, BF_4^-) [53], halogens (F^-, Cl^-, Br^-) [63], hydroxide [61], larger inorganic mono-anions (eg HSO_4^-, $H_2BO_3^-$, $H_2PO_4^{2-}$) [53], inorganic dianions (eg SO_4^{2-}, CO_3^{2-}) [64], salts of organic acids (eg salts of trifluoracetic acid, oxalic acid, maleic acid) [65], sulphonated organic salts (eg pTS, DBS, PSS) [58], redox probes (eg $Re_2Cl_8^{2-}$) [66], luminescence probes (eg pyrene sulphonate, naphthalene sulphonate) [67], chelating agents (eg dithiocarbamate) [68], enzymes (eg urease) [69], antibodies (eg anti-HSA) [70] and proteins [71].

Though the anions incorporated during growth do not effect the electrochemical switching pattern they do have a major impact on the morphology, conductivity, doping level [66] and mechanical properties [59] of the film. In general, larger anions produce a more regular chain structure with more extensive conjugation and lower oxidation potential [66].

Among the more common anions employed (eg small inorganic mono- and di-anions and sulphonated anions), sulphonates and sulphates would appear to impart special properties. Compared with inorganic dopant anions, PPy films incorporating sulphonates or sulphates exhibit higher electrical conductivity, good physical and mechanical properties and anistropic molecular behaviour [72]. For example, Zotti et al in a

comparison of PPy/ClO_4 and PPy/pTS, the most studied polypyrroles, note that PPy/ClO_4 is a hard, brittle material, while PPy/pTS is a flexible, plastic, highly ordered material [73]. Table 1.1 gives a range of parameters for PPy/ClO_4 and PPy/pTS.

Table 1.1: Representative physical, mechanical and electrochemical properties of PPy/ClO_4 and PPy/pTS.

Parameter	PPy/ClO_4	Py/pTS
Density (gcm^3) [74]	1.53	1.37
Tensile strength (MPa) [54]	2.6	74
Doping ratio (A / Py) [74]	0.25	0.43
Conductivity (Scm^{-1}) * [75]	36	30
Diffusion coefficient of incorporated anion (cm^2s^{-1}) [59] **	3×10^{-9}	10^{-10}
Appearance [59]	Rough	Smooth
Adhesion to GC [59]	Fair	Good
Anisotopicity [76]	Isotropic	Anistropic
E_{pa} (V vs SCE) *** [59]	-0.13	-0.45
E_{pc} (V vs SCE) *** [59]	-0.14	-0.88

* Films grown from aqueous solution.

** Films grown potentiostatically from aqueous solution, diffusion coefficients determined in 0.1 M Na salt of the counterion.

*** E_{pa}: oxidation peak potential at 10 mVs^{-1} in 0.1 M Na salt of the counterion.

*** E_{pc}: reduction peak potential at 10 mVs^{-1} in 0.1 M Na salt of the counterion.

During cycling, many anions will exchange with the supporting electrolyte anion and alter a number of the properties of the film [77, 78]. For example, Iseki et al report that pTS fully exchanges with NO_3^- in less than 10 cycles at 200 mVs^{-1} between -1.0 and 0.5 V (vs Ag/AgCl) [72]. This is despite the observation of Walton et al [79] that pTS is an

"immobile anion" in comparison to ClO_4^-, BF_4^- and PF_6^-. Zotti et al [73] have studied the effects of this counterion exchange on film conductivity. They exchanged pTS with a range of counterions by firstly dipping PPy/pTS in aqueous base to dedope the film, followed by treatment with 1 M solutions of acids of the anions. The base treatment time was kept below 10 min to avoid degradation of the film (see Section 1.4). During acid treatment of the dedoped film, the anion of the acid was incorporated as the counterion. Table 1.1 gives the conductivity of the resulting PPy/A films.

Table 1.2: Conductivities of PPy/pTS films after exchange of pTS with a range of anions by base / acid treatment (Zotti et al [73]).

Anion	Conductivity (Scm^{-1})	Anion	Conductivity (Scm^{-1})
pTS *	100	BF_4^-	80
F^-	90	CF_3COO^-	80
Cl^-	100	CH_3COO^-	70
Br^-	100	$CH_3CH_2COO^-$	70
NO_3^-	90	$PhCOO^-$ **	70
HSO_4^-	90	PhO^- **	25
ClO_4^-	85	OH^-	3×10^{-2}

* Grown from 1 % H_2O / AcN

** Ph: phenyl group

Zotti et al point out that the size, shape and length of aliphatic / aromatic groups of the replacement ions have little impact on the resultant conductivities of the exchanged PPy. The most significant influence is the basicity of the inserted anion. Anions of strong acids have little impact on the conductivity while the more basic anions (carboxylates, PhO^- and OH^-) decrease the conductivity appreciably. They assign this to "pinning" of the positive charges in the polymer, thus preventing easy charge movement along the backbone.

A similar experiment was performed by Yamaura et al [74], who exchanged PF_6^- with a range of anions by immersing PPy/PF_6 films in 0.1 M salt solutions at rest potential for 48 h at 20 °C. The range of anions studied in this case was small inorganic ions, halides and sulphonates. Yamaura et al observed that all anions with radii less than 10 Å fully exchanged with PF_6. The conductivity remained unchanged for all of these smaller anions, with the exception of the halides, which decreased both the conductivity and the ductility of the film. For the sulphonates with radii greater than 10 Å, only poor exchange was observed while conductivity remained constant. This study indicates that even under static conditions ion movement occurs readily, though it is limited by the pore size created by the incorporated anion.

The mobility of ions in PPy is crucial in the kinetics of the electrochemical processes occurring during oxidation and reduction [80-83]. For small, mobile anions effectively all of the charge balancing is by anion movement. However, if large, less mobile anions are incorporated during growth, the supporting electrolyte cations will diffuse through the PPy to maintain electroneutrality [84]. Values of diffusion coefficients of anions in PPy range from 10^{-8} to 10^{-13} cm^2s^{-1} (cf ~10^{-5} cm^2s^{-1} in water [67]) and of cations from 1 x 10^{-10} to 5 x 10^{-11} cm^2s^{-1} [85]. The values determined depend on the type of ion, solvent and concentration of the electrolyte, direction of the potential scan, film thickness and polymer growing conditions [77]. Tamm et al [86] classify anions into three size groups (Table 1.3) according to their hydrated radii and redox behaviour (similarities between wave shape and kinetic behaviour).

Considering firstly the "small" anions, Schlenoff and Chen [87] report that the diffusion coefficients of ClO_4^- in PPy/ClO_4 (grown galvanostatically from PC) in water, AcN and PC are 4.2 x 10^{-8}, 3.6 x 10^{-10} and 3 x 10^{-13} cm^2s^{-1}, respectively. This is in excellent agreement with the value of 3 x 10^{-8} cm^2s^{-1} determined for Cl^- through PPy/Cl (grown potentiostatically from H_2O) by Grzeszczuk and Zabinska-Olszak [77]. However, Matencio et al [88] report far faster diffusion of ClO_4^- and Cl^- through PPy grown with

the relatively large dodecylbenzenesulphonate anion (DBS) incorporated. The diffusion coefficients of ~3 x 10^{-5} cm^2s^{-1} for both anions imply that the ease of movement of small anions through the large pores created by DBS approach that in bulk water.

Table 1.3: Classification of anions according to hydrated radii and electrochemical behaviour induced in PPy [86].

"Size"	Anion
Small	ClO_4^-, Cl^-, Br^-, NO_3^-, BF_4^-, PF_6^-
Medium	pTS, BS^-, pentanesulphonate
Large	DDS, PSS, polyvinylsulphate

To explain fast and slow Faradaic processes observed in thin (<1 μm) PPy/Cl films, Amemiya et al [89, 90] break small ion movement into two types of ionic trapping. Slow Faradaic processes are associated with "deeply trapped" Cl^- ions that are held in the double layer formed at the polymer electrode interface. On the other hand, the fast Faradaic processes involve ions which are "shallowly trapped" and exist in the bulk of the film. This is particularly significant in partially oxidised films (~ -0.3 V vs SCE) as the electric double layer in this oxidation state is quite broad and extends over the maximum number of ions. In either fully oxidised or fully reduced films, this effect is not observed.

Li and Qian [91] also report a pH effect on the movement of small anions in PPy/Cl. They claim that in acid solution (pH 3) oxidation and reduction occur by anion movement only, whereas in neutral conditions both cations and anions are involved in maintaining charge neutrality.

In the work mentioned above, Tamm et al [86] point out that the sulphate anion, though of a similar hydrated radii and molecular shape to other small anions, induces very different electrochemistry in PPy. This is assigned to the very compact PPy structure

created by SO_4^{2-} and the difficulties associated with charge balancing intermediates as the di-anion diffuses. The unusual behaviour of sulphate is confirmed by Reynolds et al who consider the EQCM responses for sulphate during electrochemical cycling to be "reminiscent" of (3,6-(carbaz-9-yl)propanesulphonate) or PSS [78].

With regard to anions of "medium" size (eg pTS), Iseki et al [72] observe that both anions and cations participate in the redox process of PPy incorporating these counterions. In aqueous solutions of alkali metal cations (M^+) electroneutrality is maintained by cation movement during the first few cycles, while pTS exchanges with any mobile supporting electrolyte anion with repeated cycling. The moderate mobility of pTS is exemplified by the observation that PPy/pTS is electrochemically deactivated when cycled in aqueous solutions of alkaline earth metals (M^{2+}) or large tetraalkylammonium ions (R_4N^+). This occurs as, over the first few cycles, neither the pTS nor the dicationic M^{2+} or large R_4N^+ are sufficiently mobile to maintain electroneutrality during electrochemical switching. However, as discussed above, over repeated scanning or extended contact with solutions of other anions, pTS is sufficiently mobile to exchange fully with other ions.

Contrary to this, "large" anions (eg dodecylbenzenesulphonate (DBS), dodecylsulphate (DDS) and polystyrenesulphonate (PSS)) do not participate in the redox cycle and instead charge balance is achieved by supporting electrolyte cation and anion movement [92]. This is shown in an idealised form in Scheme 1.4. De Paoli et al [81] assign the immobility of DBS to both its size and interactions between the alkyl chain and non-polar sections of PPy, particularly in the neutral state. Poly-anions are likely to be effectively immobile due to both their size and attachment at multiple binding sites. Wainwright and Zorman [93] observed that "only under extreme conditions was the very large PSS anion mobile". As the supporting electrolyte cation plays such a critical role in charge compensation in PPy employing immobile anions, the switching potentials of these polymers will be dependent on the relative mobilities and charge distribution of these ions. For example, Tamm et al [94] report that E_{pa} of PPy/DDS cycled in aqueous

chloride solutions of TEA^+ and Li^+ shifts from -0.15 to -0.42 V (vs Ag/AgCl), respectively.

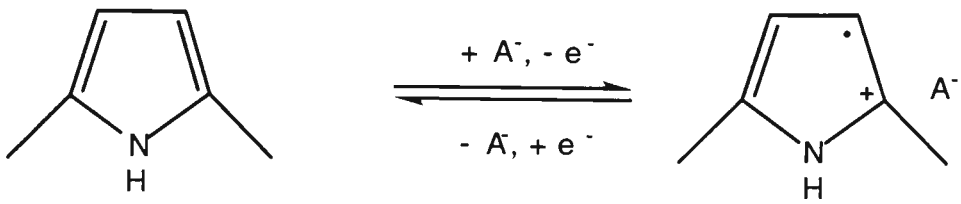

A^-: Mobile anion, eg Cl^-, ClO_4^-, NO_3^-

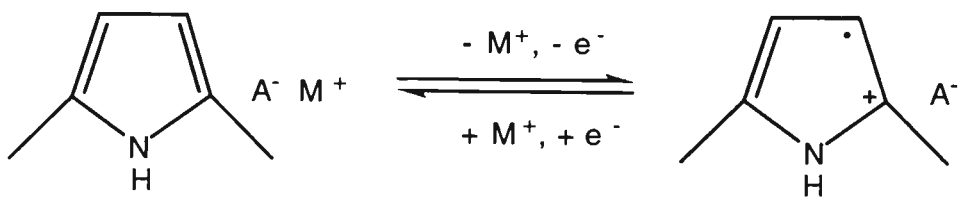

A^-: Immobile anion, eg DBS, DDS,PSS

M^+: Mobile cation, eg Na^+, K^+, Li^+

Scheme 1.4: Idealised representation of the extremes of charge compensation for PPy with mobile and immobile counterions incorporated.

In many cases, the real situation lies somewhere between these two extremes and charge compensation occurs by movement of both anions and cations into and / or out of the polymer.

1.2.5 Calculation of film thickness

The thickness of the PPy film prepared by electrochemical means is proportional to the charge passed during polymerisation. Throughout this work, film thickness will be estimated based on charge passed during growth per μm film thickness (see Table 1.4). It should be noted that the film thicknesses calculated by this means are only approximate due to variations in film porosity and growing efficiency of the films in the presence of varying concentrations of monomer and counterion.

Table 1.4: Charge passed per μm film thickness for the growth of PPy containing various anions.

Anion	Charge per μm ($mC\ cm^{-2}\ \mu m^{-1}$)	Reference
NO_3^-	410	[95]
ClO_4^-	380	[53, 80, 96, 97]
pTS^-	300	[53]
BF_4^-	390	[53, 80]
DS^-	400	[97]
BS^-	240	[9]
PSS^-	400	[67]
Cl^-	295	[89]

1.3 CONDUCTION IN POLYPYRROLE

1.3.1 Conduction band model

Two possible modes for charge transport in oxidised polypyrrole are reported, the band model and the charge hopping model [98]. The band model has its origins in conductivity in metals and semi-conductors. As metal atoms approach each other to form a crystal lattice, the atomic orbitals overlap forming bonding and anti-bonding molecular orbitals [98-100]. The shared electrons will reside in the (lower energy) bonding orbitals and the (higher energy) anti-bonding orbitals will remain empty. Due to the extremely high number of molecular orbitals formed, the energies of these orbitals lie at closely spaced intervals between the highest and lowest energy orbitals (Figure 1.1). This effectively forms a band of allowed energy states spread across the entire metal lattice. As not all of the allowed orbitals within this conduction band are filled, a small energy input (eg heat, applied potential difference) will readily raise electrons to a slightly higher (vacant) energy

level. Once in this higher energy level, the electrons are free to move throughout the lattice leading to the good thermal and electrical conduction characteristic of metals.

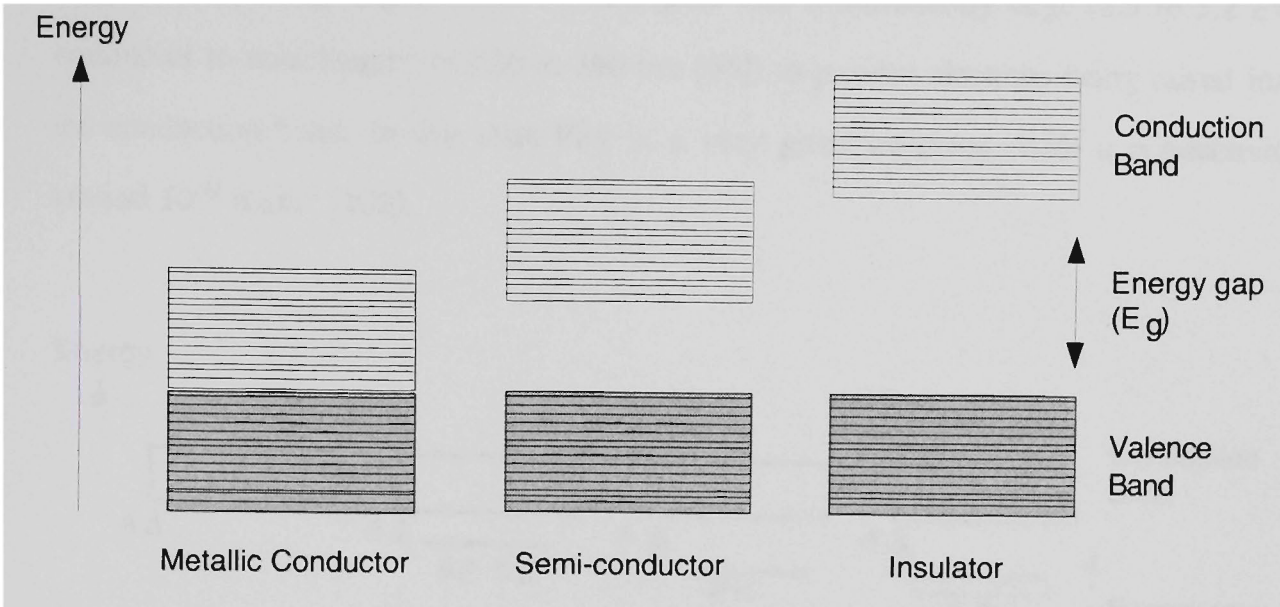

Figure 1.1: Energy bands of a metallic conductor, a semi-conductor and an insulator.

Due to the overlap of atomic orbitals, valence and conduction bands also form in many other solid materials, for example diamond, germanium and silicon. In these materials the valence band is completely filled with an appreciable energy gap (E_g) between it and the conduction band. If E_g is sufficiently large (eg diamond, E_g = 6 eV [100]), it will not be possible to impart sufficient energy to raise electrons from the valence band to the conduction band. In this case, with no possibility of electrons residing in the conduction band, the material will be a excellent insulator. If E_g is sufficiently small, as it is in germanium and silicon (E_g = 0.72 and 1.1 eV, respectively [100]), it will be possible to thermally excite some electrons into the conduction band. Once in the conduction band, these electrons will behave as they would in a metal and are capable of conducting electricity. However, as only a small number of electrons will be promoted to the conduction band, the conductivity will be lower than in metals. The material will be a semiconductor, with a conductivity somewhere between a metal and an insulator.

In the polymerisation of polypyrrole, filled valence and empty conduction bands [101] are created by the overlap of carbon π-bonds in the conjugated backbone. In the neutral polymer, the energy gap (π–π*, "*A*" in Figure 1.2) is sufficiently large (2.9 to 3.2 eV, equivalent to wavelengths of 430 to 390 nm [66]) to prevent electrons being raised into the conduction band. In this state PPy is a very good insulator, with a conductivity around 10^{-12} S cm^{-1} [102].

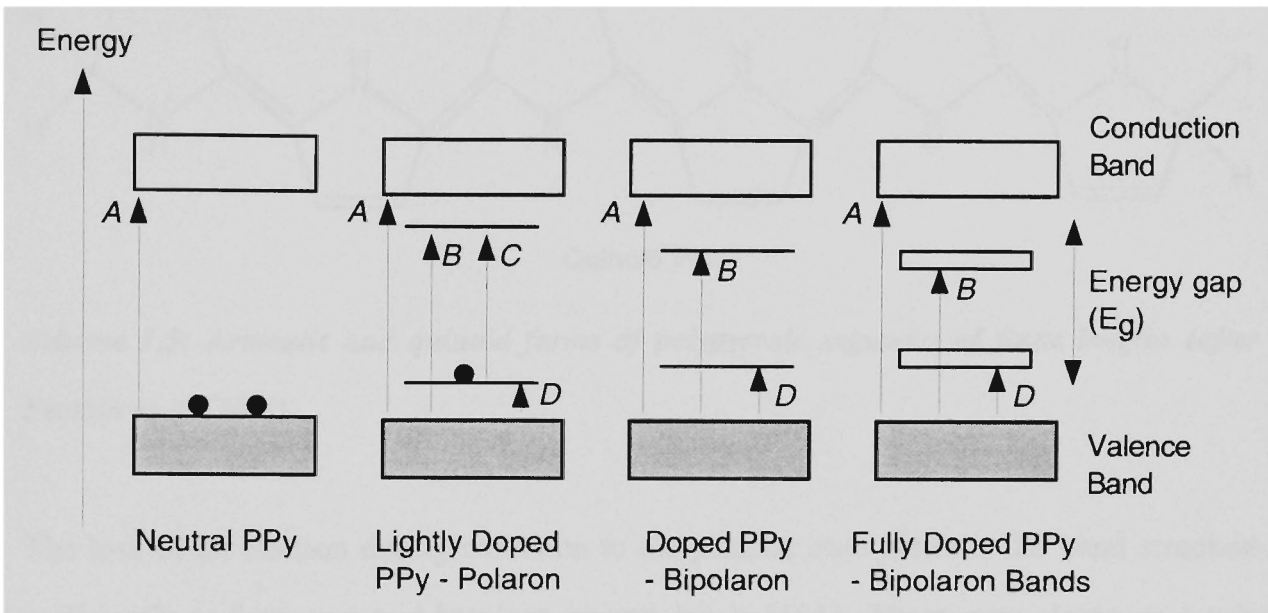

Figure 1.2: Energy bands of neutral, lightly doped, doped and fully doped polypyrrole (after Cheung et al [66]).

Fermin et al [103] and Kim et al [39] report far larger bandgaps for neutral PPy, ie 3.9 eV (320 nm) and 4.0 eV (310 nm), respectively. According to Fermin, two distinct π–π* transition energies are seen as a result of the two non-degenerate ground states of PPy shown in Scheme 1.5. Fermin notes that the aromatic form is more stable in neutral PPy, while Forsyth et al [104] report that the quinoid form is stabilised by oxidation of the neutral polymer. On the other hand, Kertesz [105], Jenden et al [106] and Blanking et al [107] postulate that both aromatic and quinoid forms may be present in a single PPy chain. Fermin further claims that within a polaron or bipolaron "defect", both forms are structurally and energetically equivalent, leading to a single set of energy transitions for each form.

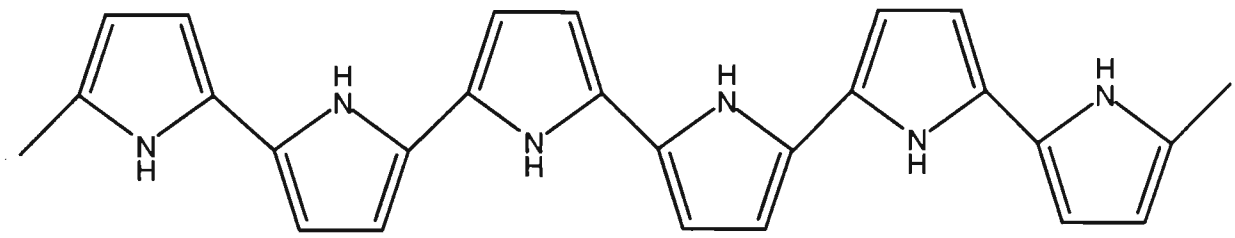

Aromatic Form

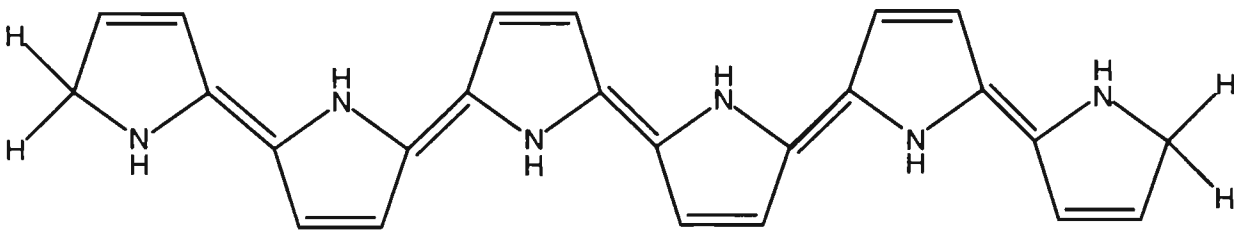

Quinoid Form

Scheme 1.5: Aromatic and quinoid forms of polypyrrole segments of finite lengths (after Fermin et al [103]).

The loss of an electron during oxidation to the polaron state perturbs the band structure sufficiently to form two mid-bandgap energy levels [101]. These new electronic levels allow thermal excitation of electrons, indicated as transitions "*B*", "*C*" and "*D*" in Figure 1.2, which gives the PPy some conductivity. Table 1.5 gives the energies associated with the transitions indicated in Figure 1.2.

Table 1.5: Allowed transitions for the polaronic state of PPy (from Bredas et al [108]). The symbols given refer to Figure 1.2.

Symbol	Transition	Energy (eV)	Wavelength (nm)
A	Valence Band ---> Conduction Band	3.2	390
B	Valence Band ---> Antibonding Polaron State	2.1	590
C	Bonding Polaron State ---> Antibonding Polaron State	1.4	880
D	Valence Band ---> Bonding Polaron State	0.7	1770

Further oxidation to the bipolaron (dication) causes greater lengthening of double bonds and shortening of single bonds than observed for the oxidation to the polaron [108]. This shifts the energy levels associated with the bipolaron (bonding bipolaron and antibonding bipolaron states) further from the valence and conduction band edges. On full doping (1: 3 dopant : monomer) the bipolaron and anti-bipolaron states broaden to form bands of about 0.2 eV [39] to 0.45 eV [108] wide. The creation of these bipolaron bands between the valence and conduction bands allows easier thermal excitation of electrons, increasing the conductivity of the material. The energies determined for the allowed transitions are given in Table 1.6.

Table 1.6: Allowed transitions for the fully doped bipolaronic state of PPy (from Bredas et al [108]). The symbols given refer to Figure 1.2.

Symbol	Transition	Energy (eV)	Wavelength (nm)
A	Valence Band ---> Conduction Band	3.6	340
B	Valence Band ---> Antibonding Bipolaron Band	2.7	460
D	Valence Band ---> Bonding Bipolaron Band	1.0	1240

1.3.2 Hopping model

The band structure in PPy has been shown theoretically and confirmed experimentally by the authors mentioned above and many others (for example [109-112]). However, it is unlikely to be the sole contribution to charge movement. Firstly, it applies only to a crystalline lattice containing no disorders which could act as traps or defects to delay or scatter the charge carrier [98]. As was discussed in Section 1.2.2, polypyrrole contains a wide range of structural defects which would limit conduction by this mechanism alone. Secondly, as mentioned in Section 1.2.1, Christensen and Hamnett [41] report that the

average length is only 34 monomer units. This chain length would be far too short for the conduction band model to explain the high conductivities of PPy on its own.

Thirdly, as pointed out by Singh et al [113] and Satoh et al [56] the conductivity of PPy shows a linear dependence on the inverse of the fourth root of temperature ($T^{-1/4}$). Such linear dependence of conductivity on $T^{-1/4}$ fits the Mott variable-range hopping model of charge transport in disordered systems [114] used to explain conduction in amorphous germanium and silicon. In this model, electrical conduction arises due to movement ("hopping") of charge carriers through the material over variable distances. Singh et al claim that the observed temperature dependence "cannot be explained either by the band conduction model or by assuming the existence of a temperature-dependent energy gap". They then postulate that the dominant conduction mechanism is variable-range polaron hopping over a distance of about 5.8 Å (1.5 monomer units [41]). On the other hand, Goedel et al [115] observe that PPy attains its maximum conductivity when equal numbers of polarons and bipolarons are present. This is offered as evidence for a hopping model of conduction in which charge transfer between these two states is the predominant mechanism of conduction.

According to Singh et al [113] and Yakushi et al [116] the total conductivity of polypyrrole may best be described by a combination of intrachain conductivity (described by the band model) and the interchain conductivity (described by charge hopping). Montemayor et al claim that, due to the anistropic nature of an electrodeposited PPy film, conduction parallel to the substrate is largely intrachain, while interchain conduction prevails perpendicular to the substrate. Cheung [66] proposes a three stage conduction mechanism: (i) intrachain transport; (ii) interchain transport; (iii) interparticle transport (see Figure 1.3). This is supported by Sixou et al [117] who propose charge hopping between "conducting grains" separated by insulating barriers. This is justified on the basis of a decrease in grain size and increase in barrier size, and hence conductivity, with ageing in air.

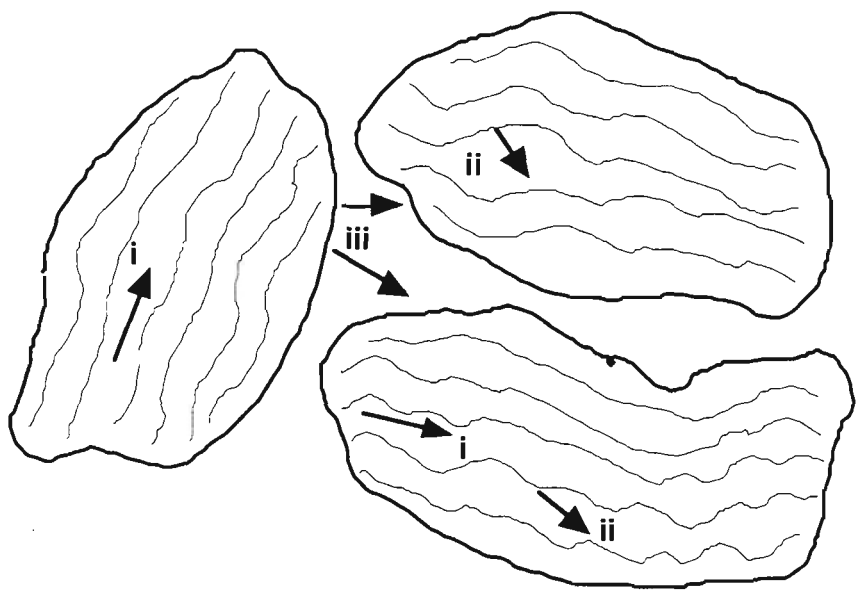

Figure 1.3: Conductivity network of oxidised polypyrrole showing (i) intrachain charge transport, (ii) interchain charge transport and (iii) interparticle charge transport (after Cheung et al [66]).

1.4 THE FORMS OF NITROGEN AND BASE TREATMENT

In early X-ray Photoelectron Spectroscopy (XPS) studies Pfluger et al [47] noted that nitrogen existed in only one form in PPy that had not been previously been oxidised. Oxidation of PPy led to chemical changes to as many as 30 % of the nitrogen sites, including bonding to oxygen during cycling. These changes however, did not affect the conductivity of the film and were completely reversible by electrochemical reduction. These forms of nitrogen have been confirmed by a number of authors [22, 51, 52, 55, 118-120] as "amine", "pyrrolylium" or "neutral" nitrogen (-NH-), "positively charged" or "positively charged pyrrolylium" nitrogen ($-NH^+-$) and "imine" or "imine-like" nitrogen (=N-).

Studies of PPy/ClO_4 by Tan et al [120] reveal that as-grown PPy has largely pyrrolylium (-NH-) and positively charged ($-NH^+-$) nitrogens present. Ge at al [55] have determined the relative abundance of these species in as-grown PPy/ClO_4 to be: 67.5 % -NH-; 29.9 % $-NH^+-$; 3.6 % -N=. Tan et al have also observed that in this oxidation state

the fraction of the positively charged species approximates the fraction of the ClO_4^- dopant. Base treatment (0.5 M NaOH) of this film leads to complete removal of the dopant, conversion of the positively charged nitrogens into imine nitrogens (=N-) and loss of conjugation. A similar study by the same group [22] reveals identical results for PPy/pTS treated for 1 h with 0.5 M NaOH with a slower dedoping and conversion of positively charged to imine nitrogens over 20 h in water.

Both papers point out that redoping and reconversion of imine to positively charged nitrogen is brought about by acid treatment of the base dedoped PPy (Scheme 1.6). In these studies the base dedoping led to a decrease of ca. 3 orders of magnitude in the conductivity of the as-grown PPy while redoping by acid treatment recovered ca. 50 % of this [119]. The lowering of conductivity in the redoped material is assigned to subsequent oxygen attack on the PPy in the dedoped state, leading to the formation of -COOH, -C=O or -COH and, hence, permanent loss of conjugation. They claim that these base induced degradation processes only occur in the presence of air and that PPy is stable in 1 M NaOH over their base treatment period (1 h). This is confirmed by Li et al [121] who report that PPy/NO_3 is stable in 1 M NaOH for up to 8 h in the absence of oxygen and retains its electroactivity at applied potentials less than -0.2 V (vs SCE).

Wernet and Wegner [62] and Forsyth and Truong [75] also report the possibility of the formation of C-OH at a β-carbon when base treatment is performed in air. However, Forsyth and Truong do not completely rule out deprotonation of nitrogen as an alternative mechanism consistent with their results. While Inganas et al [122] note that PPy conductivity changes during base treatment are only seen for $[OH^-] > 0.5$ M, Wernet and Wegner [62] report rapid loss of electroactivity during electrochemical cycling at any pH > 9. Gustafsson et al [123] report that ammonia is a sufficiently strong base to deprotonate and, ultimately, degrade PPy. Exposure of PPy/pTS to 27 ppm dry NH_3 in Ar for 30 min decreases the film conductivity by about 15 %. When exposed to 1 atm dry ammonia for 10 min the conductivity reversibly decreases by a factor of 30, while

exposure to the same concentration of NH_3 gas saturated with water vapour for 7 days irreversibly alters the conductivity.

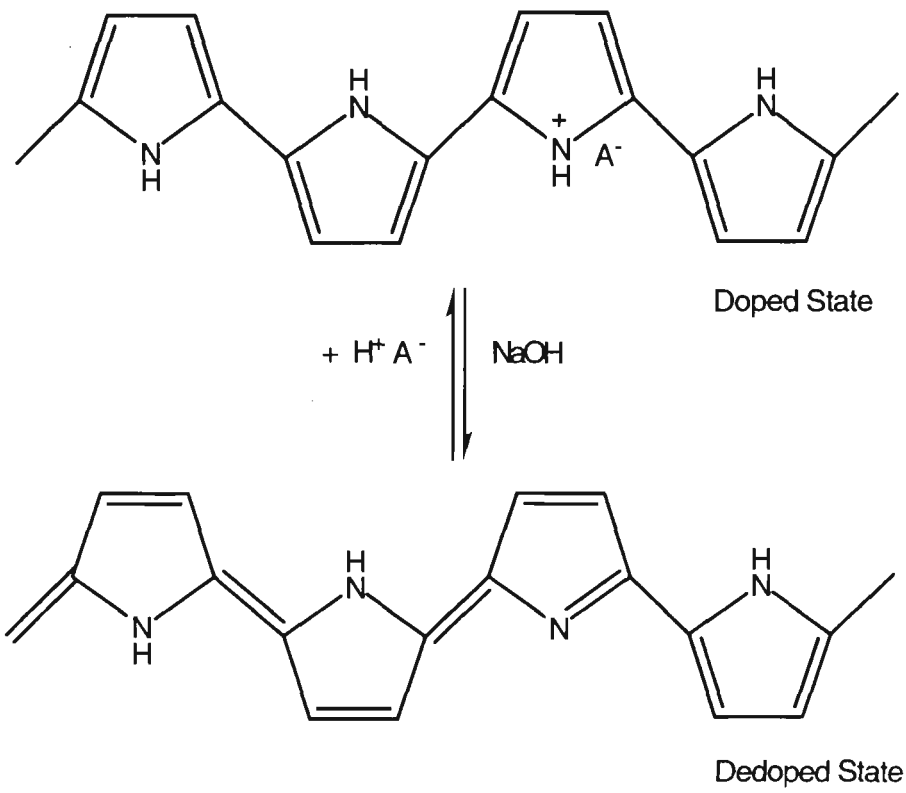

Scheme 1.6: Idealised dedoping / redoping of PPy by base / acid treatment showing changes from positively charged nitrogen to imine nitrogen with pyrrolylium nitrogen present in both structures [119].

Pei and Qian [95] and Li et al [124-127] propose a rather different mechanism for the base dedoping of PPy based on a delocalisation a double bond around an α-carbon and protonation centred on an β-carbon (Scheme 1.7). They observed two types of doping sites in PPy: the traditional positively charged conjugated chain (Site 1) and a protonated β-carbon in a Py unit (Site 2). According to these authors, base treatment at any pH > 7 will lead to deprotonation of Site 2 and a drop in conductivity of about 70 %. Full dedoping with strong base leads to identical results to those discussed above for deprotonation of nitrogen.

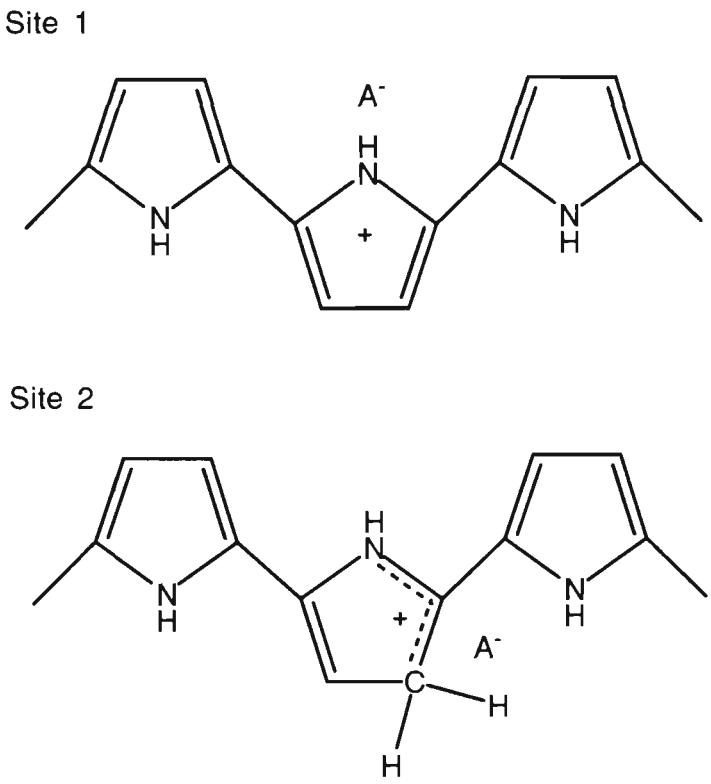

Scheme 1.7: Doping sites proposed by Pei and Qian [95] and Li and Qian [124]. Site 1: Positively charged conjugated PPy chain; Site 2: Protonation of β-carbon of a Py unit.

1.5 THERMAL STABILITY AND DEGRADATION IN AIR

This section considers degradation of PPy under two different "dry state" conditions: short term ageing at elevated temperature and long term degradation in air at around ambient temperature. These conditions not only represent possible operating environments for a number of the applications mentioned in Section 1.1, but are useful indicators of the storage life and degradation mechanism of polypyrrole.

1.5.1 Thermal stability

Much of the stability, or lack thereof, of PPy at elevated temperature is associated with the low stability or high volatility of the dopant counterion. For example, Mathys and Truong [128] investigated the thermal ageing of PPy/$FeCl_4$ at 90 °C in both N_2 and air. They report that dopant degradation, in this instance to yield Cl_2 and / or HCl, led to degradation of the polymer, with CO, CO_2, H_2O and NH_4Cl given off. They suggest that the source of oxygen when the experiment is performed under N_2 is likely to be O_2^- present initially in the polymer as a dopant.

Similarly, Ansari and Wallace [129] report weight loss, associated with counterion loss, commencing for PPy/DS at about 170 °C, for PPy/pTS at 240 °C and for PPy/Cl at 90 °C. This is despite the observation that the conductivities of PPy/DS and PPy/pTS increase by 30 % and 20 % respectively at 100 °C under N_2. The same group report [130] the loss of Cl^- from PPy/Cl (by formation of HCl), decomposition of DDS from PPy/DDS and vaporisation of pTS from PPy/pTS at elevated temperatures. Forsyth et al [104] also observe the decomposition of DDS at elevated temperature, with 90 % of DDS dopant lost from PPy/DDS at 150 °C in air over 24 h. However, some anionic species remained in the polymer after treatment and it was believed that these could either be OH^-, O_2^- (from reactions with aerial oxygen) or SO_4^{2-} or HSO_4^- (from decomposition of DDS). This report also considered that oxygen played a critical role in the decomposition of DDS as, when the thermal treatment was performed under Ar, the loss or degradation of the DDS was not as pronounced. Possible cross-linking of PPy chains was postulated to explain the change in physical parameters observed under these conditions. On the other hand, PPy/pTS aged in air at 150 °C over 48 h exhibited no loss of pTS, though this does occur over 3 months under these conditions.

In another study of the thermal stability of PPy/pTS, Moss and Burford [131] report that the conductivity of PPy/pTS aged in air at temperatures between 65 and 170 °C shows first-order decay rates, with an activation energy of 56 kJ mol^{-1}. As this is close to the activation energy for triplet oxygen insertion into a conjugated chain, they propose the following mechanism for insertion of triplet oxygen at a pyrrole free radical site:

$Py^{\bullet} + O_2$ ---> $PyOO^{\bullet}$,

$PyOO^{\bullet} + PyH$ ---> $PyOOH + Py^{\bullet}$,

PyOOH ---> C=O + C-OH.

They also note that PPy/pTS was stable at these temperatures under N_2. However, again over this temperature range, ClO_4^- decays to Cl^- and $2O_2$, while BF_4^- decays to $BF_3 + F^-$.

A number of studies of the kinetics of aerial degradation have also been performed which give an insight into the micro-structure of PPy. Among these Tansley and Maddison [132] reported that PPy/pTS heated to 80 - 200 °C showed two degradation processes: one over the first 120 min (diffusion of O_2 onto surface of PPy fibrils) and the other over longer time (diffusion through the bulk of the fibrils). Sixou et al [117] extended this work by observing that conductivity decrease for short term ageing of PPy at 120 °C in air is proportional to √time, whereas in long term ageing it is proportional to the exponential of √time. From this they proposed the concept of PPy composed of a series of "conducting grains" separated by "insulating barriers" (not dissimilar to PPy "fibrils" above). Short term oxygen attack occurs on the exterior of the grains, decreasing their size and extending the insulating barriers. Long term oxygen attack then requires further oxygen to diffuse through the (thicker) insulating barriers. This is supported by the studies of Khedkar and Radhakrishnan [133] involving PPy/Cl blended in polystyrene to give conducting domains imbedded in an insulating matrix. With ageing in air (at ambient temperature), the distance separating the conducting domains is increased as the surface of the domains is degraded by oxygen attack. This leads to an initial (over 100 days) rapid decrease in conductivity followed by a very gradual decrease over the next 500 days.

Truong et al [134] and Cheah et al [118] report that it is possible to enhance the thermal stability of PPy by acid treatment (0.5 or 1 M H_2SO_4 at 100 °C for 1 h). Both reports note an increase in protonation of PPy during acid treatment leading to an increase in conductivity. Though it may be due to decreased permeability of the treated films, no mechanism for the stabilisation has been confirmed.

1.5.2 Ambient temperature stability

As is the case at elevated temperatures, the stability of PPy at ambient temperature is also dopant dependent. Masuda and Kaeriyama [135] note that the stability in air and darkness is in the order BF_4^- < ClO_4^- < PF_6^- < pTS, with PPy/PF_6 retaining 60 % of its initial

conductivity over 200 days under these conditions. Again the oxidation process proceeds in two discreet stages, with 50 % of the total loss occurring over the first 10 days.

As a final point on the stability of PPy under normal environmental conditions, the effects of UV irradiation on PPy/BS in the dry state were reported by Adachi and Yamauchi [136]. Though the film conductivity increases under UV light, once the source is removed (after 40 to 60 min) conductivity returns to somewhat below its original level due to chain scission. They claim that conductivity increases by 0.5 to 14 % (dependent on the UV power employed) due to UV induced coalescence of polarons to bipolarons and chain scission to produce "dangling bonds". As not all of these dangling bonds reform when the UV source is removed, it is reasonable to assume that the polymer will degrade with repeated exposure.

1.6 OVEROXIDATION

Overoxidation is the irreversible, electrochemical oxidative degradation of a conducting polymer under an anodic applied potential [23]. As mentioned in Section 1.1, during overoxidation a polymer loses conductivity, charge storage ability, electrochromism, electroactivity, conjugation, mechanical properties and adhesion to the substrate. In fact, almost all of the beneficial features of a conducting polymer are destroyed by this process.

Though it is known that extending the anodic potential limits beyond about 1 V (vs Ag/AgCl) in an aqueous environment leads to overoxidation [41, 137], repeated cycling to much lower anodic limits also degrades the polymer with time. For example, Rangamani et al [138] observe significant loss of electroactivity of PPy/NO_3 over 120 cycles between -0.7 and 0.7 V (vs Ag/AgCl) at 50 mVs^{-1} in aqueous KNO_3 and almost total deactivation over 90 cycles between -0.7 and 0.8 V. They also note that the anodic current associated with irreversible overoxidation increases sharply at only 0.75 V (vs Ag/AgCl).

Somewhat slower overoxidation has been reported at similar potentials in "dry" organic solvents. Pyo et al [139] observe that PPy/pTS loses 10 % of its electroactivity over 1100 cycles between -0.6 and 0.4 V (vs Ag/AgCl) at 100 mVs^{-1} in a dry solution of 0.1 M $LiClO_4$ in PC under Ar. Under similar conditions PPy/Cl retained 90 % of its electroactivity for 500 cycles and then deteriorated quickly. Novak and Vielstich [140] report similar results for PPy/ClO_4 cycled between 3.0 and 4.0 V (vs Li/Li^+, or -0.18 to 0.74 V vs Ag/AgCl) in dry PC, with 20 % of the original capacity lost after 20,000 cycles. However, if the anodic potential limit was extended only marginally to 4.2 V (vs Li/Li^+, or 0.94 V vs Ag/AgCl), degradation was found to be "rather rapid".

Surprisingly, Otero et al [19] contradict many of these findings when they claim that PPy/ClO_4 (electrogenerated from AcN) could be repeatedly stepped from -0.5 to 1.0 V (vs SCE) in either AcN, H_2O or PC solutions of $LiClO_4$ for 42 h before losing half of their charge storage capacity.

A number of factors other than the applied potential and nature of the supporting electrolyte have also been recognised to effect the rate of overoxidation. These include: pH [141], the incorporated counterion [60, 139] and the method of polymerisation [142]. Based on diverse experimental studies of the electrochemical degradation of PPy, three quite different mechanisms for overoxidation have been proposed: nucleophilic attack at a β-carbon [21], nucleophilic attack at a α-carbon leading to ring opening [143] and nucleophilic attack at an α-carbon leading to chain breaking [144].

1.6.1 Nucleophilic attack leading to the formation of pyrrolinones

The first of these mechanisms, by Beck, Braun and Oberst [21], reported that the conjugation of the PPy backbone was disrupted by nucleophilic attack at a β-carbon, with no chain breaking (see Scheme 1.8).

In this mechanism, nucleophilic attack (indicated by OH^- in Scheme 1.8) occurs at a β-carbon of the polypyrrole bipolaron yielding 3-hydroxypyrrole. Oxidation of the carbonyl tautomer of 3-hydroxypyrrole generates a pyrrolinone, which may be further oxidised to give 4-hydroxypyrrolin-3-one. Six electrons are consumed from the neutral state to the final product (4-hydroxypyrrolin-3-one). Beck et al point out that overoxidation by nucleophilic attack will occur at water concentrations (in AcN) as low as 0.1 % and that at pH > 10, PPy is more prone to nucleophilic attack by OH^-. Other strong nucleophiles (CN^-, Br^-, CH_3COO^-) are also reported to lead to rapid overoxidation.

It is interesting to note that in the year of Beck's publication (1987) a very similar mechanism was proposed by Wegner, Wernet et al [145] to explain OH^- attack on PPy in aqueous base (0.1 M NaOH). In this mechanism, as in Beck's, oxidation of 3-hydroxypyrrole, in this case formed by base treatment at rest potential, led to a pyrrolinone and disruption of the conjugation. This paper seems to be largely ignored in comparison to Beck's work.

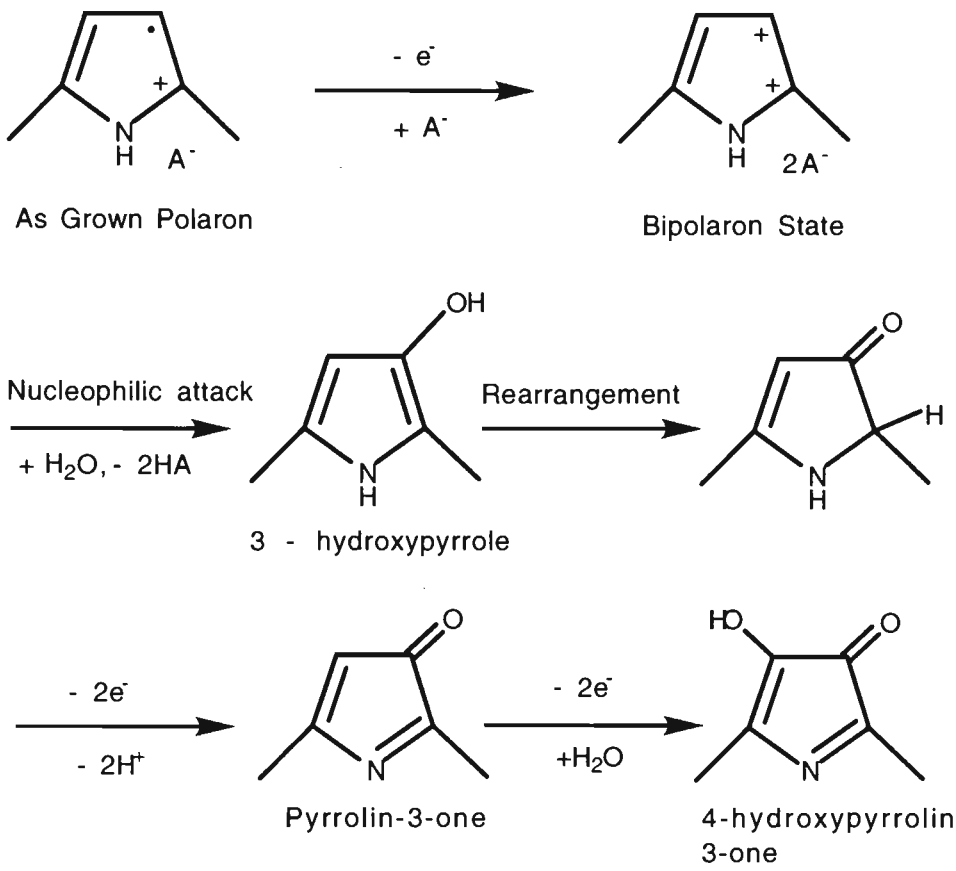

Scheme 1.8: Nucleophilic attack at a β-carbon of a polypyrrole ring (after Beck et al [21].

In later papers Beck et al [57, 146] provide indirect support of their mechanism by a series of electrochemical and corrosion experiments of PPy under open circuit and controlled potential conditions. Direct confirmation of the mechanism by FT-IR studies of the overoxidation of PPy has been offered not only by Beck et al in the original paper, but also by Novak et al [140, 147] and Schlenoff and Xu [20]. All of these studies confirm the presence of C-O and C=O groups in overoxidised PPy. They also note that C-O, a precursor for the formation of C=O, is observed in all films grown in aqueous solution and Novak et al [148] note both C-O and C=O are present in all PPy polymerised in water.

The levels of C-O and C=O have been quantified by Ge at al [55] in XPS studies of PPy/ClO_4 during electrochemical growth and overoxidation (1.2 V vs Ag/AgCl, for 2 min), as shown in Table 1.7. This study clearly shows the increase in the level of

oxidised carbon (and changes nitrogen forms) during overoxidation, as would be expected from Scheme 1.8.

Table 1.7: Abundance of carbon and nitrogen species in as-prepared and overoxidised PPy/ClO_4. The film was overoxidised at 1.3 V (vs Ag/AgCl) [55].

Species	Relative Abundance - as-prepared (%)	Relative Abundance - overoxidised (%)
C	77.2	69.3
C-OH	9.8	12.7
C=O	9.0	12.3
COOH	4.0	5.8
-N=	3.6	14.3
-NH-	67.5	73.4
$-NH^+-$	29.9	12.3

As support for Beck's mechanism, it is significant to note that no N-O species were observed, indicating that oxygen attack is at a carbon site and that ring breaking is not a significant contribution to overoxidation. Similarly Anglada et al [149] note that though the deprotonation of the nitrogen plays a significant role in the overoxidation of disubstituted PPys, it is not the reactive centre for this process. In the studies mentioned above, Novak and Vielstich [150] and Novak et al [147] also conclude that N is not involved in the overoxidation of N-substituted PPy. On the other hand, Beck et al [21] themselves note that ring cleavage and polymer bond disruption may occur under extreme potentials and / or nucleophilic attack.

1.6.3 Nucleophilic attack leading to ring opening

The second mechanism for overoxidation of PPy at high anodic potentials was proposed by Otero, Tejada and Elola [143] to explain the loss of deactivation of PPy/ClO_4 when cycled between -0.5 and 0.7 V (vs SCE) in 0.1 M $NaClO_4$. Though no analytical

evidence was offered for this mechanism, it was considered that nucleophilic attack by water at an α-carbon would lead to ring opening by rearrangement. This mechanism is given in Scheme 1.9.

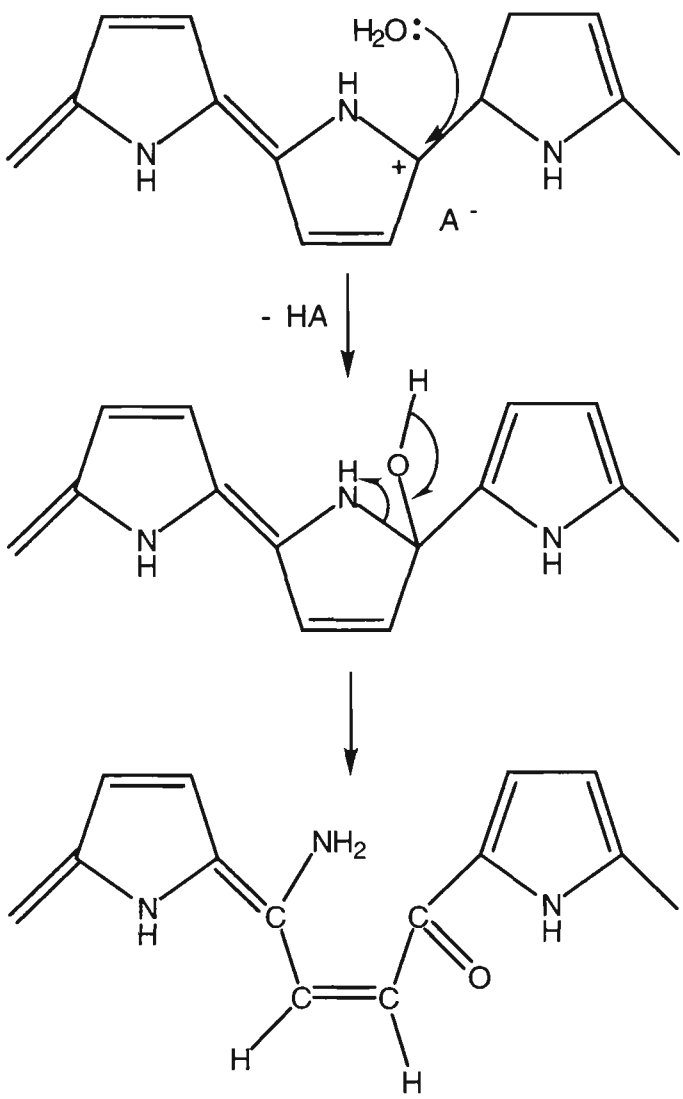

Scheme 1.9: Nucleophilic attack at an α-carbon on a pyrrole ring leading to chain opening (after Otero et al [143]).

Based on elemental analysis results, ring opening was also invoked by Mengoli et al [151] to explain the overoxidation of PPy during electrochemical growth from H_2SO_4 at potentials above 0.8 V (vs SCE). Direct analytical support for this mechanism has been offered by Gustafsson et al [123]. They note that UV-vis, FTIR and XPS data obtained for PPy/pTS and PPy/ClO_4 treated with $NH_{3(g)}$ in air are consistent with both mechanisms

given in Schemes 1.8 and 1.9. However, elemental analysis of the degradation product did not fit either mechanism particularly well.

1.6.2 Nucleophilic attack leading to chain breaking

Based on a UV-vis study of the solution products of the overoxidation of PPy/BF_4 by the application of 1.2 V (vs SCE) in 1 M H_2SO_4, a chain breaking mechanism has been proposed by Park and Shim [144] (Scheme 1.10). The Py units shown in this Scheme represent the units at one end of a polymer chain that undergo a series of nucleophilic attacks followed by oxidative chain breaking to form maleimide and succinimide. These products were confirmed by comparison to UV-vis, IR, NMR and mass spectra of the pure materials.

Maleimide (though not succinimide) has also been observed by Thieblemont et al [152] during chemical growth of PPy employing $FeCl_3$ as an oxidant. UV-vis and HPLC studies of the growing solution failed to find the expected Py oligomers. However, maleimide was "unambiguously identified" and was postulated to be formed by overoxidation during synthesis.

Strong support for this mechanism also comes from Palmisano, Malitesta et al [153] and Malitesta et al [154]. This group employed far milder conditions of 0.7 V (vs SCE) in an aqueous solution of 0.2 M phosphate buffer (pH = 7) for periods up to 7 h. By employing XPS and Chemical Derivatisation-XPS, they confirmed that C-O and C=O are present in as-grown PPy in the β-position. They further note that overoxidation increases the levels of C-O and C=O and forms new oxygen containing species, COOH. However, they also determine that C-O and C=O are found at α-carbons in overoxidised PPy, indicating that chain breaking must occur and identify an amide-type carbonyl as the major final product (see Scheme 1.11).

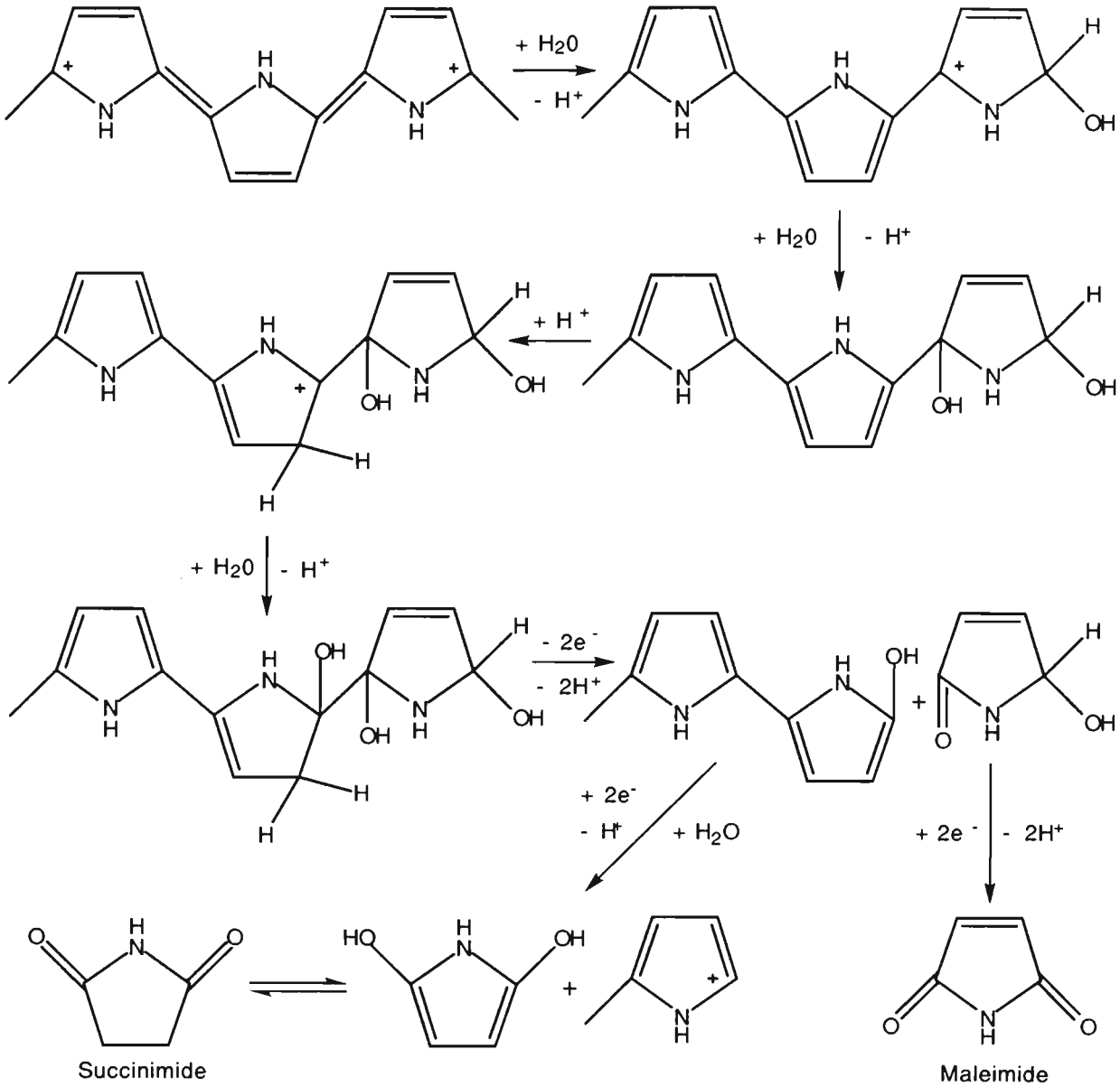

Scheme 1.10: Nucleophilic attack at an α-carbon on a terminal pyrrole ring leading to the formation of maleimide and succinimide by chain breaking (after Park and Shim [144]).

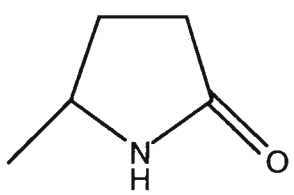

Scheme 1.11: Amide-type carbonyl resulting from chain breaking during overoxidation (after Maltitesta [154]).

1.7 AIM

In a recent publication, Chen et al [142] noted "Despite the enormous volume of scientific literature published on PPy and its composites, relatively few papers concentrate systematically on the stability of the electrical conductivity of PPy and its composites under different conditions. In fact, the stability of the electrical conductivity is very important for the industrial application of PPy and its composites.". This thesis addresses specifically the problem of overoxidation of PPy and substituted PPy in their most common environment, ie either immersed in, or in contact with, water. The aim is to further the understanding of the overoxidation of these materials and define their limits of operation for practical devices operating in air.

CHAPTER 2: IN-SITU RESISTOMETRY STUDIES

2.1: INTRODUCTION

As discussed in the General Introduction, resistance or conductance measurements are one of the most common techniques used to monitor the viability, stability and degradation of conducting polymers.

Long term stability studies in air, employing dry-film conductivity as the measure of stability, include those by Cheah [118], Masuda [135], Tansley [132], Truong [134, 155], Forsyth [75], Thieblemont [156], Khedkar [133], Moss [131] and Chen [142, 157]. Four point probe conductivity, again in the dry state, has been used to monitor the effects on PPy of a diverse range of parameters, including: substituents at the 3-position [158]; substrate [159]; degree of protonation [126]; base treatment [122]; counterion incorporated during growth [54, 66, 160]; solvent employed during growth [161] and chemical changes during aerial oxidation [47]. Of specific interest in this project is a study of overoxidation by Beck et al [146] which also employs ex-situ four point probe conductivity.

However, it is not possible to directly relate dry state conductivity to an applied potential in the study of electrochemical processes in conducting polymers. Most practical applications of CEPs will be either in solution or at least in contact with moisture and it would seem advantageous to study the electrochemistry, particularly stability, of these materials in-situ. Consequently, Feldman et al [162] in 1985 employed PPy sandwiched between two Pt electrodes held in a supporting electrolyte solution to determine in-situ conductivities. He stated that although the absolute values of conductivities determined under different circumstances (dry state, pressed pellet, wet state) are different "we see no reason to suspect that the relative conductivities....are not meaningful" and the results

may be used for comparison of the stability / instability of polymers tested under these different conditions.

Since then, in-situ conductivity has been used to monitor the effects on the conductivity of PPy of: basicity of organic acid counterions incorporated during growth [65]; electrodeposition conditions [163]; ion exchange after growth [73]; application of high (up to 5V) potential in vacuum [164] and base treatment [165].

The usefulness of in-situ conductivity for the investigation of the properties of conductive electroactive polymers is greatly enhanced when combined directly with cyclic voltammetry. Results of such studies have been reported by a number of authors: Kittleson [166] studied PPy and poly(N-methylpyrrole) for possible microelectronic applications (diodes, transistors) with an interdigitated Au array; Paul [167] similarly investigated PAni; Zhang [168] employed carbon fibres fixed around a GC macro-electrode with PPy film grown across the entire electrode to study counterion and solvent effects on the electrochemical properties of PPy in the -0.8 to +0.6V (vs SCE) range.

Cyclic resistometry, invented by Deutsher, Fletcher and Hamilton [169], is ideally suited to simultaneous, in-situ cyclic voltammetry / conductivity studies of any conducting material at an electrode surface in a standard three electrode cell. The technique is based on the application of square galvanostatic pulses, sufficiently short (< 200 μs) to avoid Faradaic reactions and double layer charging effects, to measure resistance. The pulses are applied every 30 ms during a voltammetric scan while the potentiometer is switched to a dummy cell, enabling resistance measurements with applied potential to be determined (Scheme 2.1). This technique has been used to study deposition / dissolution of metals and redox cycling of electrochromic films of iridium oxide [169] and the characterisation of conducting polymers [64, 170-172].

One possible criticism of the application of this technique to CEPs is that it measures resistance across the film, as opposed to other in-situ techniques where resistance or conductivity are measured along the film parallel to the substrate. It has been reported that the conductivity of PPy is highly anisotropic, with resistivity perpendicular to the substrate being as much as ten times higher than parallel to it [173] and even that the conductivity of PPy aged in air decreases more quickly at right angles to the substrate than parallel to it [133].

However, Sun and Burford [174] report that the variation of conductivity of PPy parallel to and at right angles to the substrate depends on both growing temperature and substrate shape. They state that on a square substrate the conductivity along a film is only 1.2 times higher than across it, whereas on a long, thin substrate this may increase to 3.3 times. As the substrates discussed in this chapter are all circular, it is reasonable to assume that anisotropy will be towards the lower end of the range. Saunders et al [1], take this one step further and claim that even though the structure of an electrochemically deposited PPy film is anisotropic, with the chains laying parallel to the substrate, its conductivity is isotropic. This is ascribed to a short effective chain length of PPy brought about by defects and structural disorder within the plane of the film, which leads to interchain transport of charge carriers being the dominant mechanism of conduction. If interchain transport is the major or even a significant mechanism of charge transport, the conductivity of the film becomes isotropic and measurement of the resistance across or along the film should provide equivalent information on the degree of overoxidation.

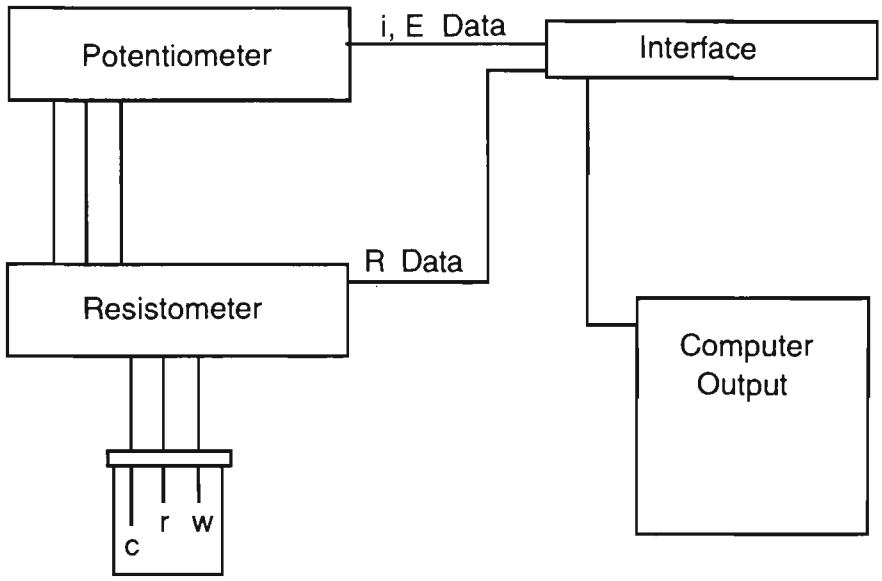

Scheme 2.1: Schematic of linear sweep voltammetry / linear sweep resistometry (LSV / LSR) instrumental set-up.

2.2 EXPERIMENTAL

2.2.1 Reagents and materials

All chemicals used were analytical reagent grade unless otherwise stated. Pyrrole (Sigma) was distilled before use and stored at -16 °C in the dark under N_2 where necessary. Reagent grade water was obtained from a Millipore Milli-RO/Milli-Q™ water purification system.

Electrodeposition and characterisation of polymer films were carried out on either gold (Beckman), platinum (Beckman) or glassy carbon (in-house) disk electrodes with diameters of 6 mm (0.283 cm^2), 6 mm (0.283 cm^2) and 5.5 mm (0.238 cm^2) respectively. Platinum gauze (Engelhard) was used as an auxiliary electrode throughout. All potentials were measured against a Ag/AgCl reference electrode (Hart Analytical) via a salt bridge containing 0.1 or 1 M $NaNO_3$ or KCl.

2.2.2 Instrumentation

Electropolymerisation of polymer films was carried out using an in-house galvanostat. Characterisation was performed using a CV-27 (BAS) Potentiostat and a CSIRO

(Australia) Resistometer. Data was collected by a Macintosh (Apple) computer interfaced through a MacLab (ADI, Australia) four channel interface. Rotating ring disk electrode studies were performed on a PAR 366 Bipotentiostat and 636 Ring Disk Electrode (EG&G).

2.2.3 Procedures

The electrodes were firstly polished to a mirror finish, initially on 1 μm and then 0.3 μm Al_2O_3 slurry, followed by ultrasonication for 30 s in Milli-Q water and rinsing with water. PPy was electrodeposited galvanostatically using a standard three electrode cell with a current density of 0.5 or 1 $mAcm^{-2}$ for periods of between 5 and 20 min (unless stated otherwise) from a solution of 0.2 M pyrrole and 0.05 M counterion in H_2O (unless stated otherwise). After growth the polymer films were rinsed thoroughly with Milli-Q water, inserted into a second standard three electrode cell containing a 1 M solution of the supporting electrolyte and cycled three times from -0.1 to 0.5 V (vs Ag/AgCl), to condition the polymer, before characterisation. All growing and characterisation solutions were purged with N_2 gas (5 min) before use and kept under a N_2 atmosphere during characterisation.

As interpretation of the resistometry experiments relied only on changes in resistance during an experiment, absolute resistances were not important in this work. As such it was not necessary to ensure that the internal resistance of the cell was absolutely minimised, only that it was constant throughout any particular experiment. Even so, by employing 1 M supporting electrolyte, the resistances obtained for any given polymer / supporting electrolyte system were reasonably reproducible throughout this work. It was also assumed that, due to the relatively low porosity of PPy, the major resistive losses in the system would occur across the polymer film. This assumption was considered valid as the diffusion of ions through PPy is of the order of 10^3 to 10^8 slower than in water (see Section 1.2.4).

2.3 RESULTS AND DISCUSSION

2.3.1 Linear voltammetry / resistometry

As stated above (Section 2.1) there are significant advantages in studying the electrochemistry of CEPs employing simultaneous CV / CR techniques compared to many other techniques. Figure 2.1 gives the current versus time and resistance versus time outputs for a CV / CR experiment on a Py/NO_3 film scanned in 1 M H_2SO_4 supporting electrolyte at 20 mVs^{-1}.

As can be seen from Figure 2.1, scan 1 for both the CV and CR showed the normal electroactive response expected for PPy/NO_3 in 1 M H_2SO_4. This response includes the increase in resistance apparent in the CR as the polymer was reduced at about 0.1 V with an associated reduction peak in the CV commencing at about the same potential. The CV also displayed the large current associated with overoxidation commencing at around 0.7 V in scan 1 in the anodic direction. However, both the CV and CR lost many of their electroactive features after only seven cycles up to 0.9 V, even at 20 mVs^{-1}.

However, it is very difficult to determine the precise potential at which overoxidation commences from this technique, short of performing a very large number of experiments while increasing the positive switching potential in very small increments. For a relatively slow phenomena like overoxidation, cycling (typically at greater than 25 mVs^{-1}) may not be the most suitable technique as it "allows less time for equilibration with the external solution than holding the potential at a suitable constant value" [175]. Another possibility is a potential step technique, but again it is often very difficult to determine the precise potential at which overoxidation of a polymer film either commences or is complete with this technique, as both the effects of time and potential need to be taken into account.

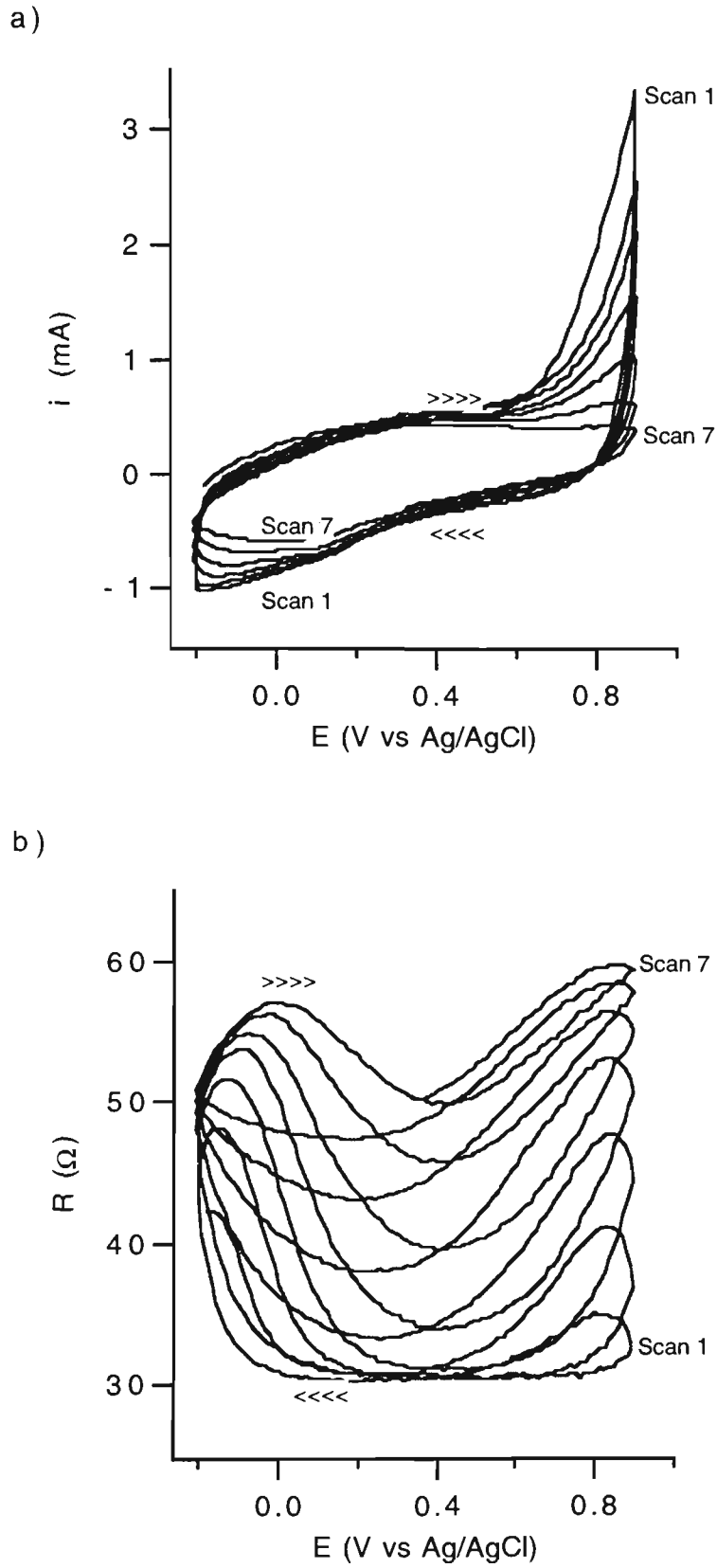

Figure 2.1: (a) Cyclic voltammetry and (b) cyclic resistometry output for a 0.6 μm PPy/NO_3 film grown on GC from 0.2 M Py and 0.05 M $NaNO_3$ solution. Film was scanned in 1 M H_2SO_4 at 20 mVs^{-1} between -0.2 and 0.9 V vs Ag/AgCl.

To overcome these problems a new approach of simultaneous linear sweep voltammetry (LSV) and linear sweep resistommetry (LSR) was adopted. This involved slow (0.5 to 5 mVs^{-1}) linear scans, in which current, resistance and potential were simultaneously measured and plotted against time. The advantage of this approach was that it allowed sufficient time for even reasonably thick films (up to 1.5 μm) to be fully overoxidised while still producing current and resistance versus time plots that were analytically useful. That is, inflection points, peaks and plateaus could be readily distinguished to allow the determination of the onset and completion of overoxidation.

Figure 2.2 below is a typical output from a simultaneous LSV / LSR experiment, in this case for a PPy/NO_3 film scanned from 0.1 V in 1M $NaNO_3$ at 5 mVs^{-1}. The initial potential was chosen to ensure that the polymer was in the oxidised state, thus avoiding current flow associated with normal, reversible oxidation.

In Figure 2.2 (a) the current began to rise at about 0.41 V as the film was fully oxidised to the bipolaron state with an associated incorporation of anions continuously between 0.20 V and 0.70 V (vs SCE) [41] to form the maximum number of bipolarons. Beck and Michaelis report that significant chemical changes can occur at these potentials with no associated conductivity changes [47]. Current then began an almost linear increase at around 0.70 V at the onset of overoxidation, indicated by the initial increase in resistance. This commencement of overoxidation at potentials greater than 0.70 V is in agreement with Christensen [41] and Beck [21]. However, it is assumed in the current work that as the resistance was not yet increasing significantly, this stage of overoxidation may be reversible. This will be further discussed in Section 2.3.3 below.

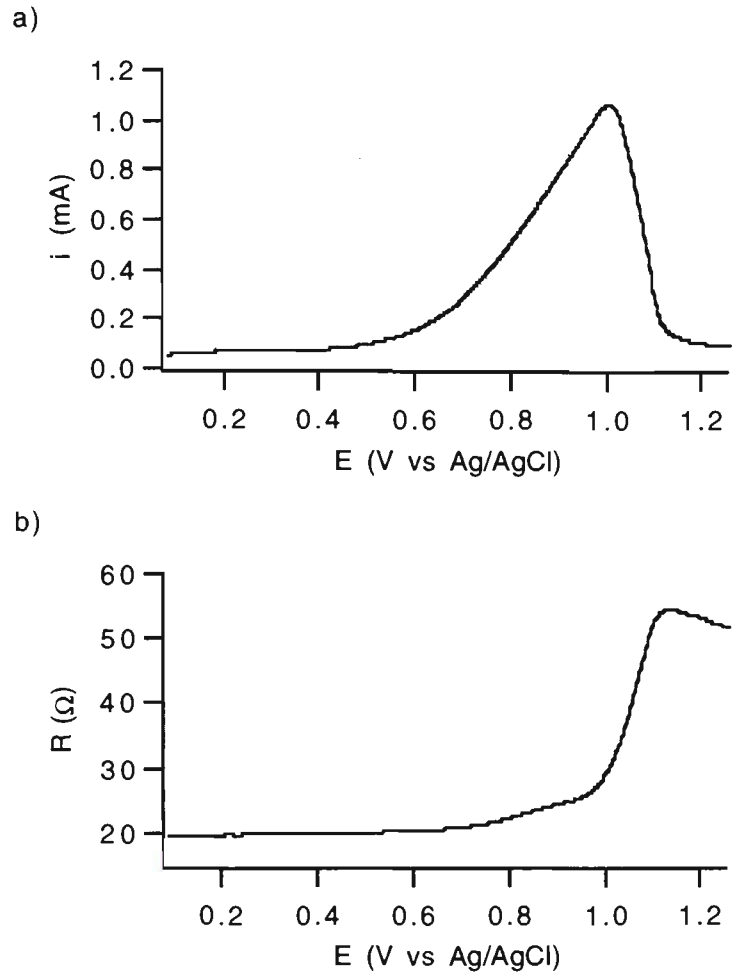

Figure 2.2: LSV / LSR output for a 1.2 μm PPy/NO_3 film grown on GC and scanned in 1 M $NaNO_3$ at 5 mVs^{-1} showing (a) current / potential and (b) resistance / potential outputs.

The increase in resistance remained quite gradual up to a potential of 0.98 V, after which it increased almost linearly. From this point overoxidation presumably became irreversible as the properties of the bulk polymer were now being altered, as indicated by the rapid change in resistance. The current maxima occurred part way through this increase in resistance at 1.07 V, indicating that a large proportion of the film was now overoxidised. The lag time between maximum current flow and maximum resistance was not unexpected, as Talaie reported a similar lag when scanning from an oxidised to reduced form and he postulated that "changes in resistance are not purely an electrochemical phenomena and that some slower process (ion diffusion or reconformation of polymer) is involved" [171]. The resistance maxima and local current minima occurred at 1.15 V and at this potential the film is completely overoxidised and all conducting pathways are "shut

off" [172]. Integration of the area under the current peak between 0.4 V, the commencement of its rise, and 1.07 V indicated that 66 mC was passed during the overoxidation of this film, 60% of the 114 mC passed during growth. This is rather lower than the 70% reported by Kras'ko et al [137]. After overoxidation was complete the resistance dropped to plateau at a level somewhat below its maximum, presumably due to relaxation and further chemical reactions within the film.

The gradual initial increase in resistance is not surprising as PPy films are heterogeneous materials [63, 117, 140] and heterogeneity increases with oxidation level [63]. Otero and Angulo reported that oxidation does not occur uniformly throughout a film, but commences at points that expand initially on the surface and then through the film [176]. Thus, regions in various states of oxidation / overoxidation, and hence with various conductivities, coexist in the polymer at any given potential. This is compounded by the findings of Ge et al that the onset of overoxidation is initially at the electrode / polymer interface [55] and not evenly through the body of the film.

It is interesting that after complete overoxidation the resistance drops below its maximum but does not return to its original level or even lower, despite the fact that at this point the porosity of the film has increased greatly [19, 41] as has the content of electrolyte phase within it. However, the original oxidised film also contained a large excess of electrolyte, with up to 40% of the polymer being electrolyte phase, some balancing the bipolaron (PPy^+/A^-) and some in excess (C^+A^-) [177]. The total conductivity of the original film is made up of contributions from both of these charge carriers and the film is both an electronic and ionic conductor. Even though one ion pair (C^+A^-) has increased its level in the film with overoxidation, the other (PPy^+/A^-) has decreased its level. The overoxidised film is now only an ionic conductor [178], but with an effective surface area less than the bare electrode substrate [24], meaning that the conductivity will still be less than at a bare electrode. This leads to an overall increase in the resistance of a PPy film up to complete

overoxidation and a final resistance below the maximum at this point, but still well above the level of the original film.

2.3.3 Reversibility of resistance changes

To investigate the above assumption that changes in the resistance between 0.70 and 0.98 V in Figure 2.2 are at least partly reversible, a number of potential step experiments were performed followed by CV / CR scans to check the remaining electroactivity of the films. Figure 2.3 shows the changes in resistance of a PPy film held at 0.80V for 7 min followed by 3 min at rest potential.

The current / time output is not shown in Figure 2.3. However, three points should be made: (i) there was no current flow associated with the return of resistance to its original level after the potential was switched off; (ii) integration of the current / time plot indicated that 30.8 mC was passed during the application of this potential, compared with 85 mC consumed during growth of this film (36%); and (iii) the potential was switched off before the current peak and, hence, the resistance plateau was reached, that is before overoxidation was complete.

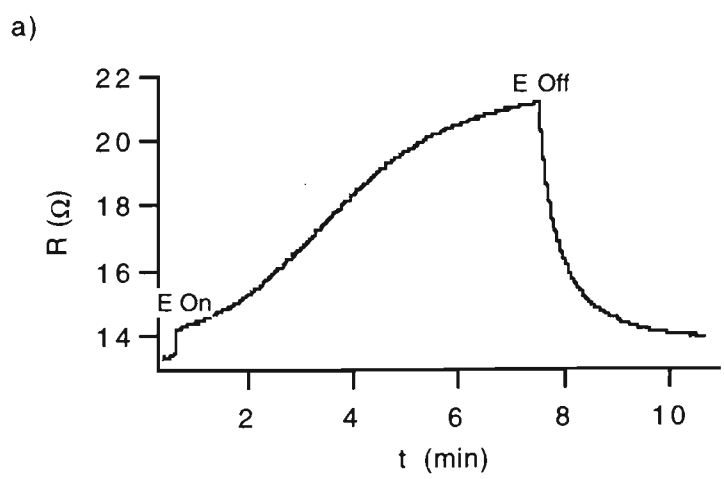

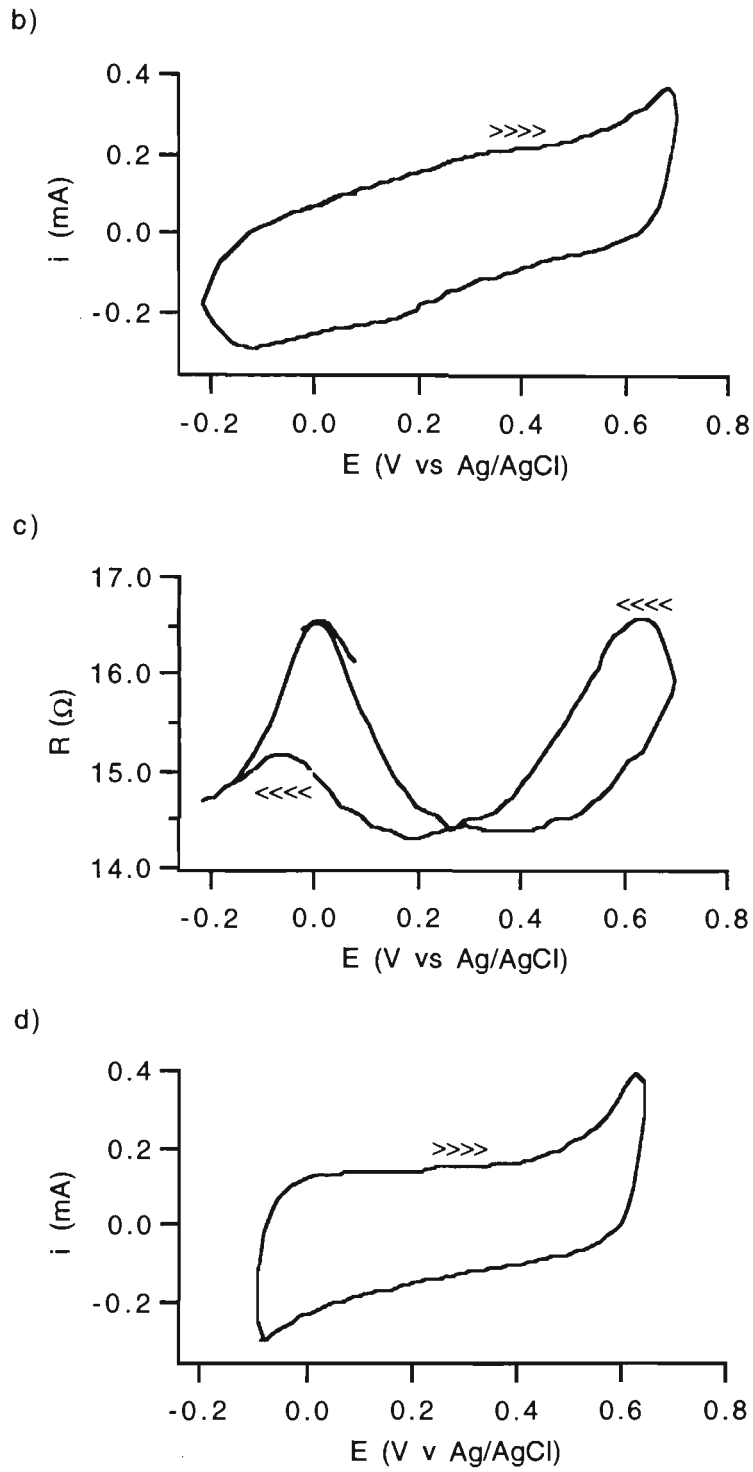

Figure 2.3: (a) Resistance versus time plot of a 0.75 μm PPy/BF_4 film on Pt in 1M H_2SO_4 during the application of 0.8V for 7 min followed by 3 min at rest potential, (b) CV and (c) CR (both 20 mVs^{-1}) of the polymer after this period, (d) CV of a pristine PPy/BF_4 film on Pt in 1 M H_2SO_4 at 20 mVs^{-1}.

Figure 2.3, reveals an almost immediate (currentless) decrease in resistance, to slightly above its initial level, when the potentiometer was switched to a dummy cell. This

indicates that overoxidation at this potential for this period may be reversible. This is supported by the CV and CR run after 3 min at rest potential. The CV still showed oxidation and reduction peaks at 0.3 and 0.1 V, respectively, as well as a peak associated with further overoxidation at above 0.7 V. The CR showed the normal increase in resistance during reduction, although it exhibited a much larger increase than would be expected (Scan 1, Figure 2.1) for a pristine film at potentials above 0.4 V. This indicates that the overoxidation may be partly reversible at this potential, or that it is incomplete (even after 7 min at 0.8 V) and sufficient conducting pathways remain to allow the resistance to return to its initial level and the film to retain significant electroactivity.

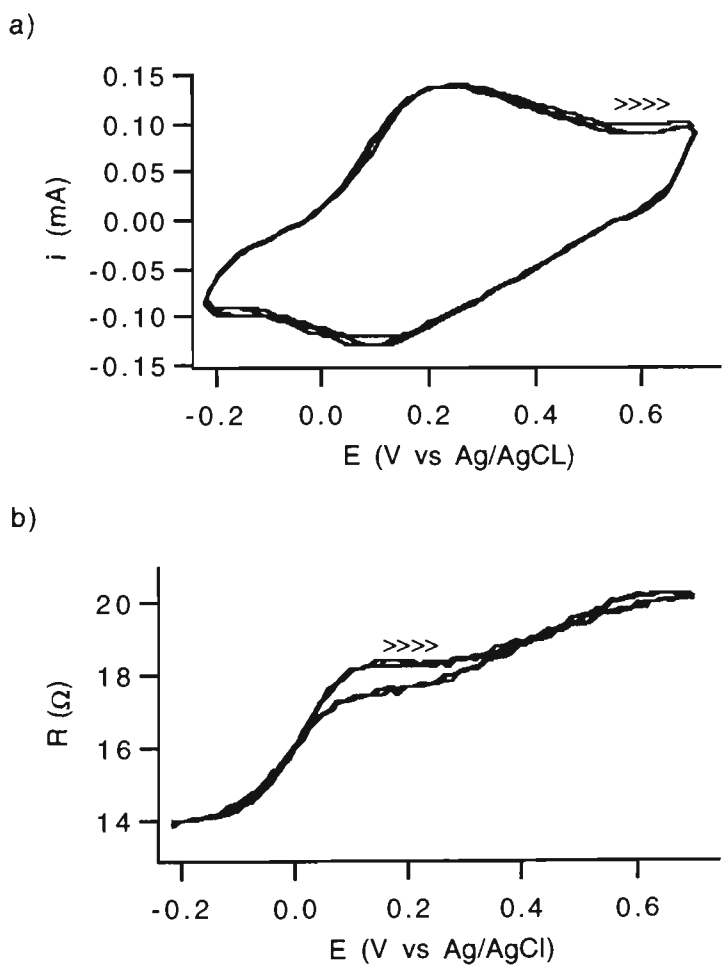

Figure 2.4: (a) CV and (b) CR of a 0.75 μm PPy/BF_4 film on Pt in 1M H_2SO_4 after the application of 0.75V for 40 min followed by 15 min at rest potential. Scan rate 20 mVs^{-1}.

The results in Figure 2.4, where the potential (now only 0.75 V) was applied for a considerably longer period of 40 minutes provide an interesting comparison to Figure 2.3. Even here, the film is not completely overoxidised, as shown by both its CV and CR. Although the CV was quite different to that of a pristine PPy/BF_4 film in 1 M H_2SO_4, the film was still clearly electroactive, with strong oxidation and reduction peaks at 0.2 and 0.1 V, respectively. Of greater interest is the CR for this film. As opposed to the expected increase in resistance at potentials below the reduction potential of the film (0.1 V), in this instance the resistance significantly decreased. Similarly the resistance increase above the oxidation potential (0.2 V) was larger than expected. These phenomena, both in the CV and CR, may be explained by the fact that the film is only partially overoxidised and at least part of the overoxidation at this potential is reversible.

Partial overoxidation, where some of the conducting channels are closed, leads to an increase in the "baseline" resistance of the film. However, if parts of this are reversible, reduction of the polymer will open these channels and resistance will decrease. Scanning to above the oxidation potential will again cause the (reversible) overoxidation of these parts of the film, increasing the resistance, as is seen in the CR in Figure 2.3 (b). If this hypothesis is true, the oxidation and reduction peaks seen in Figure 2.3 (a) are not associated with the normal oxidation / reduction of the PPy backbone, but are oxidation and reduction of a reversible overoxidation intermediate or product. This would also explain the differences in the shape of this CV compared to that of the pristine film shown in Figure 2.3 (d).

The nature of this "reversible" overoxidation product may be explained in terms of the possible chemistries of nitrogen in PPy, which were discussed more fully in Chapter 1. Briefly, in oxidised PPy nitrogen exists in one of three forms: amine-like or neutral pyrrolylium nitrogen (-NH-), positively charged pyrrolylium nitrogen ($-N^+H$) and imine-like or quinoid nitrogen (=N-) [22, 47, 51, 75, 120]. During chemical [51] and electrochemical [21, 146, 153] overoxidation, the positively charged pyrrolylium N atoms

are transformed to imine-like N atoms (with an increase in hydrophobicity [153]) which decreases conductivity due to disruption of the PPy conjugation [122]. Similarly, strong base treatment also leads to deprotonation of the pyrrolylium N to give imine-like N and this is at least partly reversible by treatment with strong acid [22, 119, 120, 122].

During overoxidation some of the imine-like N is oxidised to give a positively charged species which may then bind the supporting electrolyte or dopant anion to the polymer as indicated in Scheme 2.2 [21]. Fixing of the SO_4^{2-} anion, the supporting electrolyte anion in the current experiment, in a manner similar to this has specifically been reported by Mengoli et al [151].

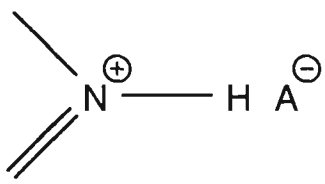

Scheme 2.2: A possible anion fixing mechanism for overoxidised PPy, where A^- is fixed in the solid as HA, linked to the N in a highly oxidised form (after Beck et al [21]).

Beck et al [21] also pointed out that when high concentrations of H_2SO_4 (10 M) are employed as the supporting electrolyte during overoxidation of PPy, extensive sulphonation of the pyrrole ring occurs. In the same paper they also noted that if HBr is used at the supporting electrolyte, reversible bromination occurs.

Whether nitrogen fixing of the anion or sulphonation of the PPy backbone occur, the conjugation of the polymer is disrupted and its resistance will increase in each case. In both cases there is evidence that the process may be reversible, and it is believed that this occurs here. As the potential is scanned below 0.1 V either the nitrogen is reduced or the backbone is de-sulphonated, giving rise to the reduction peak and a decrease in resistance as conjugation is restored. Similarly, at potentials above 0.2 V, either the nitrogen is

oxidised (with charge balancing by HSO_4^-) or the backbone is resulphonated, either of which would lead to an increase in film resistance.

From similar potential step experiments it was also found that if a polymer was held at a potential between the point where the steep rise in resistance commenced and one where the current maximum occurred, its resistance plateaued at a level similar to films subjected to an ongoing potential ramp, but more slowly than if an ongoing potential ramp were applied. It was also found that in these cases if the potential was switched off, even after the plateau had been reached, the resistance would drop almost to its original level. For example, for a PPy/BF_4 film held at 0.75 V for 25 min in 1M H_2SO_4 the resistance increased from around 14 Ω to plateau at 21 Ω and then fell back to 16 Ω over 20 min at open circuit.

Another surprising result from these experiments was the consistency of the time taken to reach the resistance plateau irrespective of the film thickness and the charge passed during overoxidation. Table 2.1 gives the average of at least two overoxidation experiments for each thickness where 0.8 V was applied to a PPy/BF_4 film on Pt in 1M H_2SO_4.

Table 2.1: Time and charge passed to reach the resistance plateau (R_{max}) for a PPy/BF_4 film on Pt in 1M H_2SO_4 with an applied potential of 0.8 V vs Ag/AgCl.

Charge during growth (mC)	Film thickness (μm)	Time to R_{max} (min)	Charge passed to R_{max} (mC)	mC to R_{max} / mC during growth (%)
150	0.38	21	57	38
300	0.75	25	161	53
450	1.13	25	271	60
600	1.5	27	374	62

For the first of the three thicker films, Table 2.1 shows that the time to R_{max} and charge (as a percentage of total charge passed during growth) were very similar for these films, namely about 25 min and 55 - 60 %, respectively, for an applied potential of 0.8 V. Again the latter result is lower than reported by Kras'ko et al [137]. On the other hand, the thinnest film (0.38 μm) though still taking 21 min to reach R_{max}, only consumed 38% of its growth charge in reaching this plateau. The unexpected consistency of the time to reach the resistance maximum (24.5 +/- 14% min) indicated that at a constant 0.8 V, the period of the overoxidation reaction(s) is relatively independent of film thickness. This is also indicated by the constant final resistance of each of these films, namely 21 to 22 Ω (from initial levels close to 14 Ω). This could imply that the overoxidation reactions occur only at one surface of the film, as suggested by Ge et al [55] and not through the bulk of the film. If this were the case, the charge passed during overoxidation would also be independent of film thickness. This is not the case and for the thicker films it remains at a reasonably constant percentage of the charge passed during growth (50 - 60%). This would suggest that at a constant potential well below the overoxidation-current peak potential and in strong acid conditions, the chemical reactions that close the conductive pathways occur throughout the entire film over the same period of time regardless of film thickness.

This can be explained by considering that in a fully oxidised polymer nearly half of the polymer volume is occupied by the electrolyte [177]. The pore space can be considered as being filled with PPy chains, which act as molecular wires. In this model the critical interface is now between the wires and the internal electrolyte solution. Here charge is removed from the wire, counterions are bound to the surface of the wire and overoxidation, certainly in the initial stages, takes place. Overoxidation, as measured by changes in resistance and current flow, should then occur over a reasonably constant period as the process occurs uniformly at the surfaces of these wires, since all parts of the film are in direct contact with the electrolyte phase. This is particularly significant if the polymer is anisotropic, at least in terms of its structure, as overoxidation at the surface of

the wires would limit intrachain charge movement and hence increase resistance. This does not contradict the heterogeneous nature of PPy films mentioned above, as now the heterogeneity is at the molecular wire level, with chemistries occurring first on the outside of the wires and then through their entire volume.

As the relationship between overoxidation and film thickness / scan rate will be discussed in Sections 2.3.5.5 and 2.3.5.6, should be emphasised that the potential applied to the films here is constant and well below the overoxidation potential of the polymer. If the potential ramp is employed to ensure complete overoxidation the LSR technique will allow the investigation of the effects of variables such as: incorporated counterion, growth solvent, supporting electrolyte, substrate, scan rate and film thickness on the overoxidation potential of a CEP.

2.3.5 Verification of the linear resistometry method

2.3.5.1 Precision of the method

To ensure that the determination of the overoxidation potential employing the LSV / LSR technique was reproducible, replicate samples of PPy/BF_4 grown from water and acetonitrile were run over a period of weeks. For thirteen separate 0.77 μm PPy/BF_4 films grown galvanostatically on Pt from an aqueous solution and scanned at 2 mVs^{-1} in 1 M H_2SO_4, the average overoxidation potential, as determined from the resistance maxima, was 0.97 ± 0.02 V vs Ag/AgCl. The overoxidation current peaks were measured at 0.93 ± 0.03 V for the same set of films. Similarly, for nine 0.77 μm PPy/BF_4 films grown galvanostatically on Pt from an acetonitrile solution and scanned at 2 mVs^{-1} in aqueous 1 M H_2SO_4, the resistance maxima were found at 0.98 ± 0.02 V and the overoxidation current peak at 0.94 ± 0.02 V. In general, due to uncertainties in estimating the potential at which the resistance plateaued, results will be quoted to two decimal places. However for any mathematical or graphical manipulation, the full three decimal points available from the instrumental set up will be used.

These results show that the precision of the method is extremely good, especially considering the difficulty of growing reproducible polypyrrole films. They also reveal the advantages of using a slow linear potential ramp in an LSV / LSR technique (over CV or potential step methods) for the determination of the precise potential of either the onset or completion of overoxidation.

2.3.5.2 Rotated ring disk electrode (RRDE) verification

Rotated ring disk electrodes have been employed in overoxidation studies by Stilwell and Park in the case of PAni [179] and by Park, Shim and Park [180] and Hsueh [25] for PPy. Scharifker and Fermin have also employed the technique to study the growth of PPy [37]. It was hoped that in the present study it could be employed simultaneously with in-situ resistometry to further study the overoxidation of PPy. However, due to excessive noise levels in the resistometer output when connected between the cell and the bipotentiostat, it was not possible to gather any useful data from this instrument. This was possibly due to the fact that the bipotentiostat employs a common reference electrode for monitoring potential at the disk and the ring electrodes simultaneously. As the resistometer switched the disk electrode to a dummy cell, part of the cell was still in use as a component of the ring electrode cell, leading to noise feedback to the resistometer. However, the RRDE technique was still of use as an independent verification technique, but without the benefit of simultaneous resistometry data.

In the RRDE studies a number of variables required optimisation: disk electrode size and material; ring electrode size and material; applied potential at the disk and the ring electrodes; and the rate of rotation. Other variable studied were the nature of the: supporting electrolyte and the counterion as well as the PPy film thickness.

The PPy film was grown on a disk electrode in the normal manner and then, while the RRDE was rotated in a suitable supporting electrolyte, a slow linear ramp was applied to

the disk electrode via the bipotentiostat. As the film is overoxidised electroactive overoxidation products will be released [180], as will any soluble oligomers formed [36, 37] and trapped in the film during polymerisation and, by applying an appropriate cathodic potential to the ring electrode, these species may be detected at the ring.

Various rates of rotation (1000 to 2000 rpm), ring / disk configurations (Pt / Pt, GC / GC, GC / Pt) and ring potentials (-0.15 to -0.4 V) were trialed. Of these, rotation rate and ring / disk configurations did not appear to affect the results significantly. However, the potential applied to the ring electrode improved the peak response at this electrode during overoxidation of a PPy/BF_4 film in 1 M $NaNO_3$ from around -5 μA when it was held at -0.15 V to about 130 μA at -0.4 V. Therefore, all further work with the RRDE was performed at 2000 rpm, on a Pt / Pt electrode, with the ring held at -0.4 V. Figures 2.5 and 2.6 show the RRDE outputs for PPy/NO_3 and PPy/Tir films, respectively, using these conditions.

In Figure 2.5, the current at the ring electrode (i_R) began to decrease at 0.44 V, at the same potential that the current at the disk electrode (i_E) increased slightly from a baseline of 0.05 mA to 0.06 mA. Even though this potential is very low for the commencement of overoxidation, Anglada [149] reports that overoxidation commences at any potential above the oxidation potential of the film. The fact that currents were generated at both electrodes indicates that this is the case here. These currents could also be associated with the polymer opening up as it is fully oxidised to the bipolaron state, which would release trapped oligomers that are then detected at the ring electrode. Both peaks then increased gradually to peak at about 1.00 V, with i_D peaking 0.01 V above i_R before dropping to their respective local maxima (i_R) and minima (i_D) at about 1.15 V. When related to an LSV / LSR experiment where the resistance peak corresponds to the current returning to its baseline (see Figure 2.2 above), the return of i_D and i_R to near their baselines indicates that the conducting pathways are fully shut off only after all electroactive products of overoxidation are produced, ie both i_D and i_R effectively cease. In the case of the ring

electrode, the current does not entirely return to its original level as electroactive material continues to bleed out of the film, even though the overoxidation is complete and i_D has returned to its baseline level.

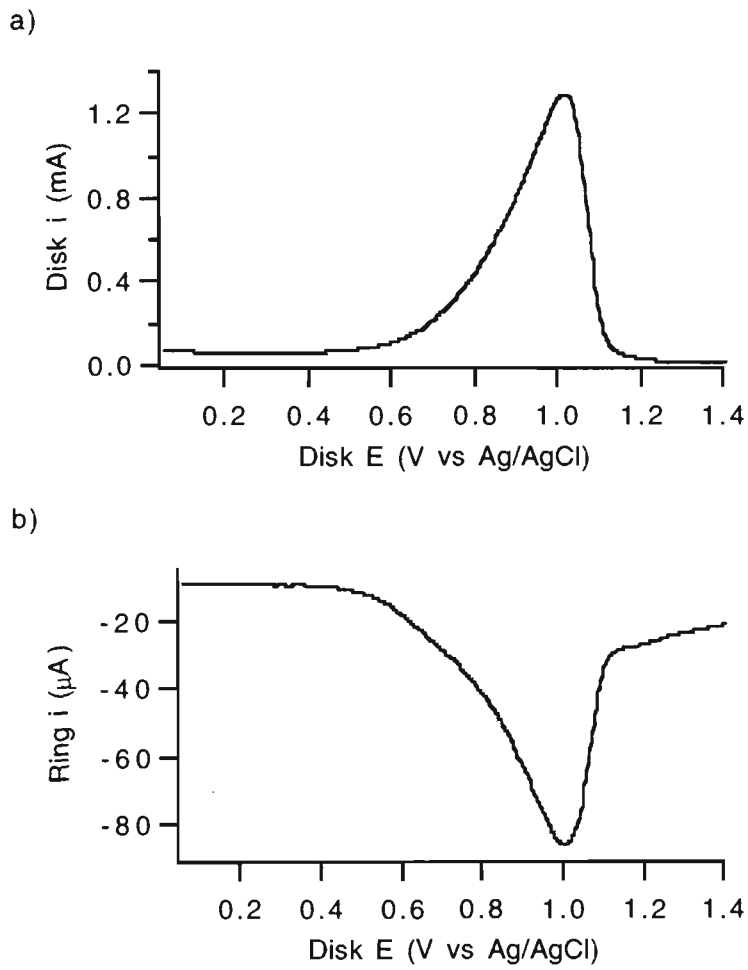

Figure 2.5 : RRDE outputs for a 0.37 μm PPy/NO_3 film rotated at 2,000 rpm in 1M $NaNO_3$, disk electrode potential ramped at 5 mVs^{-1} : (a) disk current vs disk potential; (b) ring current vs disk potential, ring held at -0.4 V vs Ag/AgCl.

On the other hand Figure 2.6 shows a somewhat different current potential relationship due to the presence of the electroactive counterion Tiron (Tir), shown in Schematic 2.3. In this case i_R begins to decrease at a significantly lower potential of 0.30 V, at which point i_D increases slightly from a baseline of 0.02 mA to 0.03 mA. This is expected as the electrocatalytic nature of Tiron shifts the polymerisation potential of Py in a cathodic

direction from 0.34 to 0.20 V [181], and the electrocatalytic effect may also shift the onset of overoxidation to lower potentials.

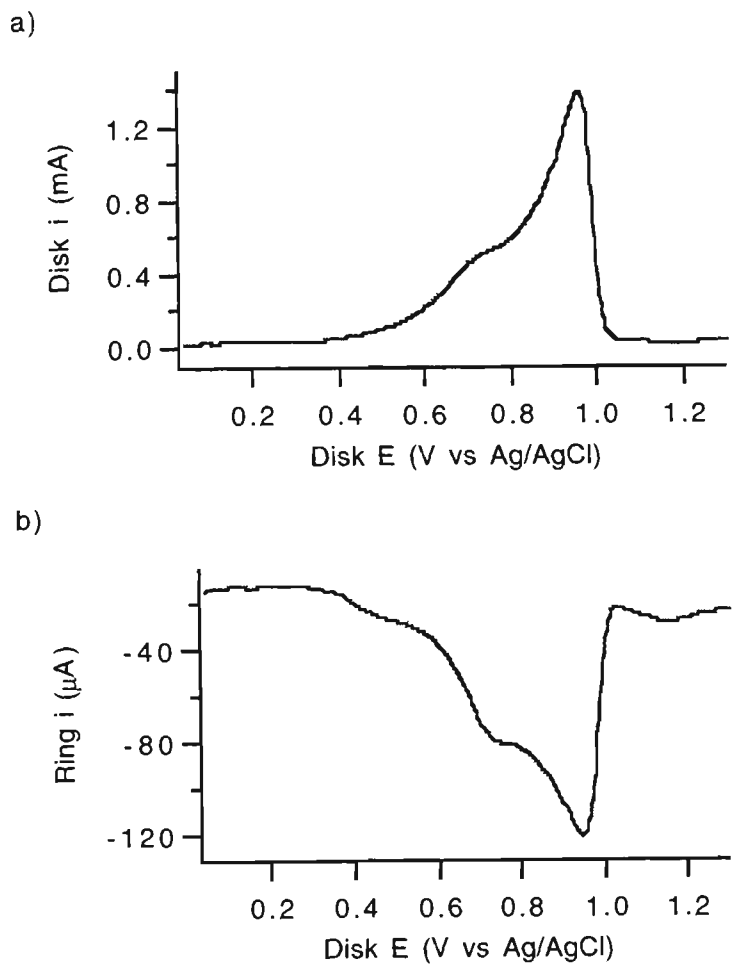

Figure 2.6 : RRDE outputs for a 1.5 μm PPy/Tir film rotated at 2,000 rpm in 1M $NaNO_3$, disk electrode potential ramped at 5 mVs^{-1} : (a) disk current vs disk potential; (b) ring current vs disk potential, ring held at -0.4 V vs Ag/AgCl.

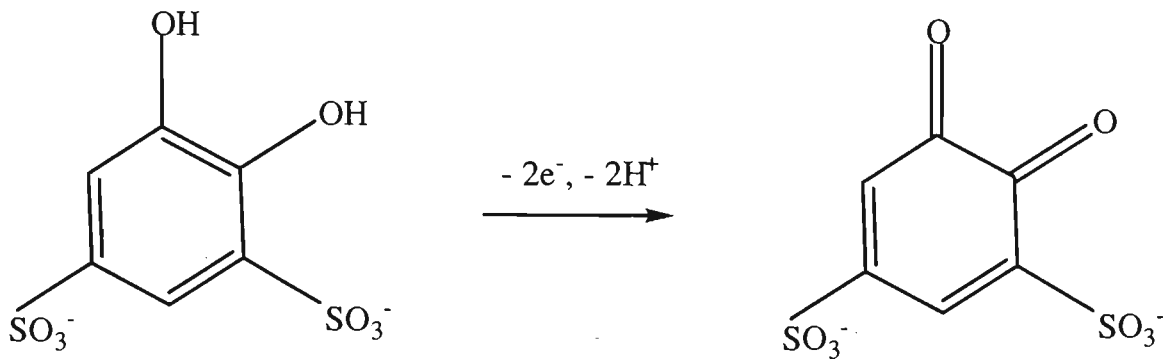

Tiron Ortho-quinone

Scheme 2.3: Oxidation of the 4,5-dihydroxy-1,3-benzenedisulphonate (Tiron) anion.

The current at the ring electrode then displayed a shoulder at 0.47 V, with no similar feature obvious in i_D, presumably as excess Tir leaches from the film as it expands during full oxidation or initial overoxidation, or catalytic overoxidation occurs. Both of these are possible as counterion in excess of strict charge balancing requirements has been reported in PPy films [177]. Also as the film is fully oxidised to maximise the number of bipolarons or overoxidation commences, it would be difficult for a dianion like Tir to bind to positive sites within the polymer. In either case, oxidised Tiron would leach from the film. Both i_D and i_R exhibited shoulders at about 0.75 V, indicating that an oxidation in the film was leading directly to a reducible product at the ring electrode. This presumably could be be trapped oligomers released from the PPy and reduced at the ring. Both peaks then increased to peak at about 0.95 V, with i_D peaking 0.01 V above i_R before dropping to their respective local maxima (in the case of i_R) and minima (for i_D) at about 1.04 V. This is appreciably lower than for PPy/NO_3 above, indicating that Tiron did in fact play an electrocatalytic role in the overoxidation of the film. It is in good agreement with an LV / LR experiment run separately under identical conditions (with the exception of the film thickness of 1.2 μm instead of 1.5 μm for the RRDE experiment) which had a current peak at 0.91 V and resistance plateau (indicating complete overoxidation) at 0.95 V. Again, the current at the ring electrode does not entirely return to its original level as electroactive material continues to bleed out of the film.

2.3.5.3 Chronopotentiometry

Kras'ko reported [137] the "irreversible oxidation" of PPy films under the application of a constant current and calculated the ratio of the charge associated with overoxidation against that for reversible oxidation and growth. He found that the overoxidation charge was around 70% of that consumed during growth. To confirm the LSV / LSR results discussed in the current work, a series of experiments employing chronopotentiometry was run using a variety of film thicknesses with various charge densities. The chronopotentiograms, presented in Figure 2.7, show four distinct regions: an initial increase in potential from 0.2 to 0.7 V (where the film is largely being fully oxidised and initial overoxidation commences) as indicated by the gentle curve into the next region; an almost horizontal section during overoxidation at above 0.8 V; an almost vertical increase in potential after overoxidation is complete and no further electrochemical reactions occur; and a final almost horizontal region where the oxidation of water occurs. To estimate the overoxidation potential, which lies at the intersection of the horizontal overoxidation region and the vertical increase immediately after it, these sections of the plot were extrapolated and the potential at the point of intersection was estimated graphically.

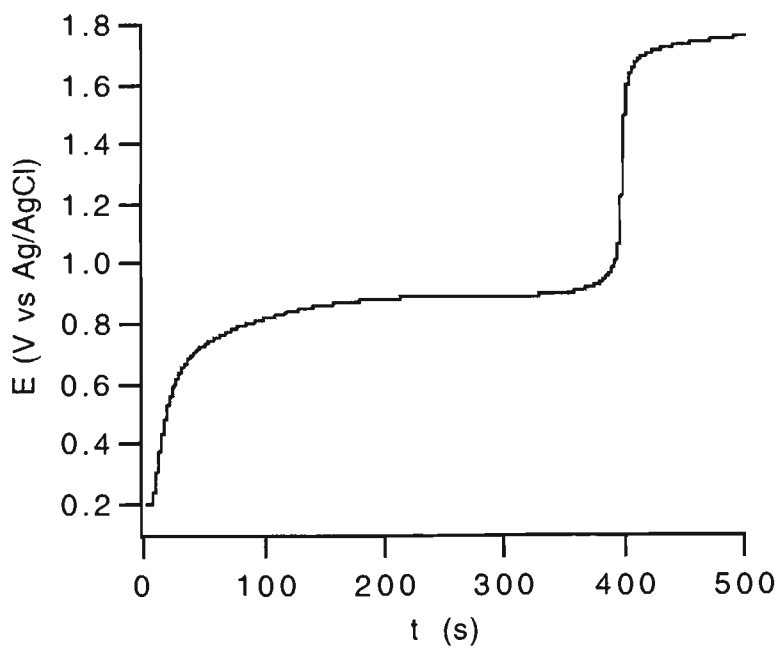

Figure 2.7: Chronopotentiogram of 1.46 μm PPy/NO_3 on Pt in 1M $NaNO_3$ at 1 $mAcm^{-2}$. Ag/AgCl reference.

The results of these experiments are given in Tables 2.2, 2.3 and 2.4. Excellent agreement was observed between the results in Table 2.3 and previous LSV / LSR determinations of the overoxidation potential of PPy/NO_3 films on Pt in 1 M $NaNO_3$. For a 0.35 μm film the overoxidation potential determined from the resistance plateau was 0.94V, from Table 2.2 it was 0.94 V for a 0.29 μm film. Similarly, LSR gave an overoxidation potential of 0.92 V for a 0.73 μm film, while chronopotentiometry indicated 0.90 V for a 0.88 μm film. Again, this is surprising agreement considering the variability in film growth of conducting polymers. Table 2.2 also shows that an average of 61% of the charge used to grow these films was consumed during overoxidation, compared with 70% noted by Kras'ko. The difference between the two sets of data can be accounted for by the fact that Kras'ko appears to have applied charge to the polymer in the fully reduced state, whereas in the experiments reported here the polymer was in the "as grown" state. This is confirmed by Diaz, who reported [80] that the charge consumed during an oxidation scan of a PPy film from fully reduced to fully oxidised state was about 9% of total amount of charge used to grow that film. This accounts precisely for the remaining 9% of growth charge not included in the present experiments.

From Table 2.2 the overoxidation potential obtained by chronopotentiometry for the 1.17 μm film (0.92 V) is in excellent agreement with the result of 0.92 V obtained for a 0.75 μm PPy/NO_3 film scanned at 1 mVs^{-1} in 1 M $NaNO_3$.

It is also worth of noting that the overoxidation potential and the percentage growth charge consumed during overoxidation summarised in Table 2.2 are independent of film thickness when 1 mA cm^{-2} is applied to the films. However, when charge density was varied and film thickness kept constant, the charge density had a significant role in the effectiveness of overoxidation as shown in Table 2.3.

Table 2.2: Results of chronopotentiometric determination of the overoxidation potential of various film thicknesses of PPy/NO_3 on Pt in 1M $NaNO_3$ by application of 1 $mAcm^{-2}$. Average of at least two determinations for each result.

Growth		Overoxidation			
Charge (mC)	Film Thickness (μm)	Charge Density ($mAcm^{-2}$)	Potential (V vs Ag/AgCl)	Charge (mC)	Growth mC / O-ox mC (%)
204	1.75	1	0.92	129	63
170	1.46	1	0.93	112	66
135	1.17	1	0.92	76	57
102	0.88	1	0.90	57	55
68	0.59	1	0.92	43	64
34	0.29	1	0.94	21	61

Table 2.3: Results of chronopotentiometric determination of the overoxidation potential of PPy/NO_3 on Pt in 1M $NaNO_3$ overoxidised at various charge densities. Average of two determinations for each result.

Growth		Overoxidation			
Charge (mC)	Film Thickness (μm)	Charge Density ($mAcm^{-2}$)	Potential (V vs Ag/AgCl)	Charge (mC)	Growth mC / O-ox mC (%)
135	1.17	2	0.92	70	52
135	1.17	1	0.92	76	57
135	1.17	0.5	0.89	89	66
135	1.17	0.25	0.90	110	82

The results in Table 2.3 indicate that not only applied potential, supporting electrolyte and incorporated counterion (to be discussed in the following sections) play a role in how

thoroughly a PPy film is overoxidised, but the current density also has a major contribution to overoxidation. Although the overoxidation potentials for the four film thicknesses studied here were very similar (average 0.91 V) the percentage of growth charge consumed during overoxidation varied from 52 to 82%, with the lowest value being for the highest charge density. From this it would appear that at higher charge densities (eg 2 $mAcm^{-2}$) the polymer is only partially overoxidised, possibly on the exterior of the "conducting wires" mentioned above, before further reaction is prevented. Overoxidation at these high current densities may prevent effective overoxidation throughout the entire polymer since, based on the conducting islands or conducting wires concept, an overoxidised casing is built up protecting any underlying material from the applied potential and nucleophiles. Alternatively, based on the conducting wires concept, the conducting pathways under these extreme conditions are completely severed at some point (rather like blowing a fuse wire by overloading it), preventing overoxidation along the entire length of the polymer. If the overoxidation is performed more gently, ie at a lower current density of 0.25 $mAcm^{-2}$, the polymer is more completely overoxidised. The protective shield is not established nor the pathways disrupted abruptly, allowing the passing of a higher percentage of the growth charge before overoxidation ceases.

The results of a chronopotentiogram run on a PPy/NO_3 film in 1 M H_2SO_4 are given in Table 2.4. Again, the overoxidation potential was estimated from this technique at 0.91 V, in perfect agreement with the LSR result of 0.91 V obtained for the same film thickness scanned at 1 mVs^{-1} in 1 M H_2SO_4. However, the percentage of the growth charge consumed during overoxidation was well above an identical film in 1 M $NaNO_3$, presumably due to extensive sulphonation which occurs when high concentrations of H_2SO_4 are used as the supporting electrolyte [21]. This sulphonation would also be expected to consume charge, and would account for some of the increase in charge determined in this electrolyte.

Table 2.4: Results of chronopotentiometric determination of the overoxidation potential of PPy/NO_3 on Pt in 1 M H_2SO_4. Average of two determinations.

Growth		Overoxidation			
Charge (mC)	Film Thickness (μm)	Charge Density ($mAcm^{-2}$)	Potential (V vs Ag/AgCl)	Charge (mC)	Growth mC / O-ox mC (%)
135	1.17	1	0.91	101	75

2.3.6 Studies employing LSV / LSR

A number of reports have been published on the chemical and physical factors that effect the oxidation potential of PPy [9, 21, 29, 60, 62, 63, 72, 73, 78, 122, 135, 138, 139, 144, 160, 182-185] and this section will investigate the contributions of these parameters to the overoxidation of PPy and their effects on overoxidation potential.

2.3.6.1 Effects of incorporated counterion on overoxidation potential

Tamm [86] found sufficient similarities in the normal redox behaviour (ie similar wave shapes and close kinetic parameters) of PPys to group the anions based on their Pauling's or hydrated radii, namely small (ClO_4^-, Cl^-, Br^-, NO_3^-, BF_4^-), medium (pTS^-) or large (PVS^-, DS^-). However, these similarities are not apparent under the extreme conditions encountered during overoxidation. On the contrary, Tang reported [186] that the rate of overoxidation of PAni is strongly dependent on the counterion incorporated in the film during growth and that anions promote growth and overoxidation of PAni with similar effect. Table 2.5 presents the results of LSR studies of PPy films containing different counterions incorporated during growth.

From Table 2.5 it is apparent that the counterion incorporated into PPy has an appreciable effect on the overoxidation of PPy in aqueous media, with variations of up to 0.19 V between counterions. This variation occurred even though the films were cycled thrice from 0.5 and -0.1 V in the relevant supporting electrolyte to condition the polymer.

During this cycling it is possible that some of the more mobile monovalent anions (eg NO_3^-, BF_4^-, Cl^-) may have exchanged with the supporting electrolyte anion, though less mobile multianions and polyelectrolytes (eg PVS, Tir, SO_4^{2-}) would not be expected to exchange at all [44, 78]. However, even for those that exchange readily, the degree of exchange will be small in only three cycles. Iseki reported that up to 100 cycles may be necessary for full exchange between mobile anions [72] and Yamuara indicated that 100 h at open circuit was required to complete the exchange [74].

Table 2.5: Overoxidation potential of PPy with various counterions incorporated during galvanostatic growth from 0.2 M Py and 0.05 M counterion in water. The films were grown on Pt or GC by passing 480 $mCcm^{-2}$ (to give approximately 1.2 μm films), with the exception of PPy/F which was grown potentiostatically, and scanned in 1 M $NaNO_3$ at 1 mVs^{-1}.

Counterion - on Pt	Overoxidation potential (V vs Ag/AgCl)		Counterion - on GC	Overoxidation potential (V vs Ag/AgCl)	
	Supp. Elect. $NaNO_3$	Supp. Elect. H_2SO_4		Supp. Elect. $NaNO_3$	Supp. Elect. H_2SO_4
Br^-	0.92	ND*	DS	1.00	1.02
Cl^-	0.96	1.06	NO_3^-	1.03	0.96
F^- **	0.97	ND	pTS	1.06	1.03
I^-	1.01	ND	PVS	0.92	0.97
NO_3^-	0.92	0.89	SO_4^{2-}	0.97	0.96
pTS	0.99	1.01	Cl^-	ND	1.07
Tir	0.90	0.94	F^- **	0.94	ND
BF_4^-	ND	0.89			

* ND: Not Determined

** PPy/F grown potentiostatically at 0.85V.

For the halide anions, all electroactive and reasonable nucleophiles, the highest overoxidation potential was determined for PPy/I. This is expected as Rangamani reports [138] that I^- will scavenge oxidising intermediates responsible for overoxidation, possibly by reduction of $OH^\bullet$, O^-, $O^\bullet$, O_2^- (generated from oxidation of water). Mostany, when studying the effects on overoxidation of halide ions (by exchanging them with PPy/NO_3 by cycling) reported that F^- and Br^- increase the ease of overoxidation in comparison to Cl^- and NO_3^- [60]. Bromide, being the most nucleophilic halide, attacks PPy directly, while F^- destabilises PPy due to its extremely tight hydration shell. This shields fluoride's high charge density, and so it does not compensate charge well (Cl^- and NO_3^- have higher charge densities in aqueous solution), and so it is easily substituted by OH^-. Accumulation of dopant OH^- increases the local pH within the polymer, favouring overoxidation by incorporation of oxygen. Mostany also reported that when PPy / NO_3 is cycled in an aqueous solution of F^-, the NO_3^- exchanges with F^- and overoxidation commences at potentials as low as 0 V (vs SCE) [63].

This should lead to PPy/F and PPy/Br having the lowest overoxidation potential in this group. However, in $NaNO_3$ the overoxidation potential of PPy/F is seen from Table 2.5 to be somewhat above PPy/Cl and significantly above PPy/Br. This may be due to the fact that the PPy/F was grown potentiostatically at 0.85 V, as it could not be grown galvanostatically at any current density, this method of growth at a relatively high potential, in some way affected the final polymer or its morphology and hence increased its stability.

Considering other anions in Table 2.5, PPy/BF_4 and PPy/NO_3 have reasonably low overoxidation potentials, especially in comparison to PPy/DS and PPy/pTS. This may be due to a very high degree of order and packing in the PPy/DS and PPy/pTS films, to the extent that they are known to have a very high degree of anisotropic molecular organisation [58, 72]. In general, larger anions produce a more regular chain structure in PPy [66] and the influence of this ordering on stability is indicated by the fact that

PPy/BF_4 is far less stable in air than PPy/pTS [135]. The relatively high overoxidation potential of PPy/DS and PPy/pTS may in part be attributed to the increased hydrophobicity of the polymer with these incorporated anions (due to their relatively non-polar carbon groups) which is also a significant factor in their high degree of order. Increased hydrophobicity would slow overoxidation by excluding H_2O, or at least limiting wetting of the polymer, decreasing the level of contact with the most likely nucleophile.

Turning to the multi- or polyanions, even though they are larger ions than the group discussed above, their PPy salt films are still relatively easily overoxidised. It is known that SO_4^{2-} stabilises PPy under normal electrochemical conditions due to its double charge [86] and it may be anticipated that PPy/SO_4 would more stable to overoxidation than other polypyrroles. This, however, is not the case. The latter polymer in fact has one of the lower overoxidation potentials of the examples presented in Table 2.5. This may be in part due to the strongly hydrophilic nature of the sulphate anion [1] which is present as SO_4^{2-} in PPy/SO_4, not as HSO_4^-, even at low pH [86]. This hydrophilicity would effectively wet the polymer at a molecular level, making water readily available for participation in overoxidation.

A further contribution to the relative ease of overoxidation of PPy/SO_4 may be that it, along with Tir and PVS, is a multiply charged anion, which will localise charge carriers on the polymer chain to match their multi-charged nature [79]. Hence, as each anion normally compensates more than a single charge in the polymer, once one of the bonds is disrupted by overoxidation of the backbone, these counterions have excess negative charge. However, they are still attached at least one point and actually destabilise the polymer, hastening overoxidation. Alternatively, the fact that the charge carriers are concentrated around the dianion may facilitate overoxidation, as Beck [21] reports that overoxidation occurs more readily at the site of a polaron or bipolaron. These multianions localise such sites, possibly making nucleophilic attack easier. This hypothesis is

supported by the observation (Table 2.5) that these three anions each have relatively low overoxidation potentials.

The role of pH, as seen by the variation between overoxidation potentials of the same counterion in $NaNO_3$ and H_2SO_4, will be discussed in Section 2.3.5.3 and Chapter 3, while the differences recorded for the same anion will be discussed in Section 2.3.5.4.

2.3.6.2 Effects of supporting electrolyte ions on overoxidation potential

As reported by Diaz [80], the electrolyte salt clearly influences the normal redox reactions of PPy. Not only are the kinetics of the redox processes influenced by the mobility of the ions, but the differences observed depend on both the anion and cation of the salt. As mentioned in Section 2.3.5.2 above, even though it is expected that little exchange between the growth counterion and the supporting electrolyte counterion will occur in the three "forming" cycles from -0.1 to 0.5 V, the supporting electrolyte will still play a significant role in overoxidation. In particular, in fully oxidised PPy a large portion of the polymer volume is occupied by the electrolyte phase [177], which will obviously include the cation. Cation incorporation during overoxidation occurs to such a high degree that Rangamani reports [138] small crystals appearing on the surface of an overoxidised film after washing and drying.

In this section the effects of the supporting electrolyte cation and anion on overoxidation potential will be investigated separately.

2.3.6.2.1 Cations - the lyotropic series: kosmotropes and chaotropes.

Table 2.6 presents the LSR results (each the average of at least two determinations for each result) for the overoxidation of PPy/NO_3 on Au scanned at 1 mVs^{-1} in various NO_3^-

salts in water. There are significant differences between the overoxidation potentials, even though only the cations of the supporting electrolyte were varied. This is a little unexpected, as the roles of the cation in overoxidation appear only to be: as part of the supporting electrolyte to fill the increasing pore space created during overoxidation; and to compensate some of the charge of the polymer counterion as it is released during overoxidation.

Table 2.6: Overoxidation potential of PPy/NO_3 scanned in various supporting electrolytes (1M) at 2 mVs^{-1}. The films were grown galvanostatically on Au from 0.05M Py and 0.02 M NO_3 in water by passing 150 $mCcm^{-2}$ to give a film thickness of approximately 0.36 μm.

Supporting Electrolyte	Incorporated Counterion	Overoxidation potential on Au (V vs Ag/AgCl)
HNO_3	NO_3	0.98
NH_4NO_3	NO_3	0.93
$NaNO_3$	NO_3	0.99
KNO_3	NO_3	0.94
$Ca(NO_3)_2$	NO_3	0.99
$Mg(NO3)_2$	NO_3	0.95
$Sr(NO_3)_2$	NO_3	0.93

A number of physical parameters for these cations that may effect their interactions with PPy during overoxidation are given in Tables 2.7 and 2.9. Their hydrated radii may be significant, as it will effect the rate of diffusion of the cations into the polymer where the pore size of an overoxidised film is dictated by the pore size of the dopant anion [29]. The radii listed in Table 2.7 suggest that diffusion alone would not explain the differences in Table 2.6. On this basis all of the singly charged cations would have similar diffusion rates as they all have ionic radii either less than or of the same order as NO_3^- (3.35 Å, [187]). Hence, ion movement will not only be anions diffusing out as a charge

compensation mechanism, but will also involve cations diffusing in to compensate charge (as well as to fill the voids before, during and after overoxidation). On the other hand, all of the dications also have similar ionic radii and all are appreciably larger than NO_3^-. Thus, if diffusion does have a significant contribution to differences in overoxidation potential, the mono-cations as a group should have lower overoxidation potentials than the dications. Clearly from Tables 2.6, this is not the case. There is no obvious relationship between the hydrated radii of these cations and the overoxidation potential of PPy in a supporting electrolyte containing them.

Table 2.7: Ionic [188] and Hydrated Radii [187] of various cations and their Standard Enthalpy (ΔH^o_f) and Standard Gibbs Free Energy (ΔG^o_f) Changes of Hydration [99, 188, 189].

Cation	Ionic radii (Å)	Hydrated radii of cation (Å)	Ratio of Hydrated to Ionic Radii	ΔH^o_f (kcal mol^{-1})	ΔG^o_f (kcal mol^{-1})
H^+	1.54	2.82 *	1.83	0	0
NH_4^+	1.43	3.31	2.31	-31.7	-19.0
Na^+	0.97	3.58	3.69	-57.3	-62.6
K^+	1.33	3.31	2.49	-60.4	-67.5
Ca^{2+}	0.99	4.12	4.16	-130.0	-132.2
Mg^{2+}	0.66	4.28	6.48	-110.4	-109.0
Sr^{2+}	1.12	4.12	3.68	-130.4	-133.2

* Uncertain.

Considering the thermodynamic parameters, ΔH^o_f and ΔG^o_f, for the hydration of the cations presented in Table 2.7, it is apparent that all of these cations (with the exception of H^+) have energy advantages in binding a solvation layer to them. The cation hydration most thermodynamically favoured is that of Sr^{2+} (most negative Gibbs free energy and

enthalpy changes) and the least favoured is H^+ (least negative ΔG°_f and ΔH°_f). The order of increasing thermodynamic stability of the hydrated cations:

$Sr^{2+} > Ca^{2+} > Mg^{2+} > K^+ \approx Na^+ > NH_4^+ > H^+$.

If this order is reversed, the cations are then ranked according to the lyotropic series [190-197], originally proposed by Hofmeister in 1888 and "rediscovered" a number of times over the intervening years [190, 197], to explain the water-solute interactions of proteins. At the simplest level proteins are high molecular weight biopolymers formed by the condensation of amino acids, with a repeat unit based on the peptide bond, as shown in Scheme 2.4.

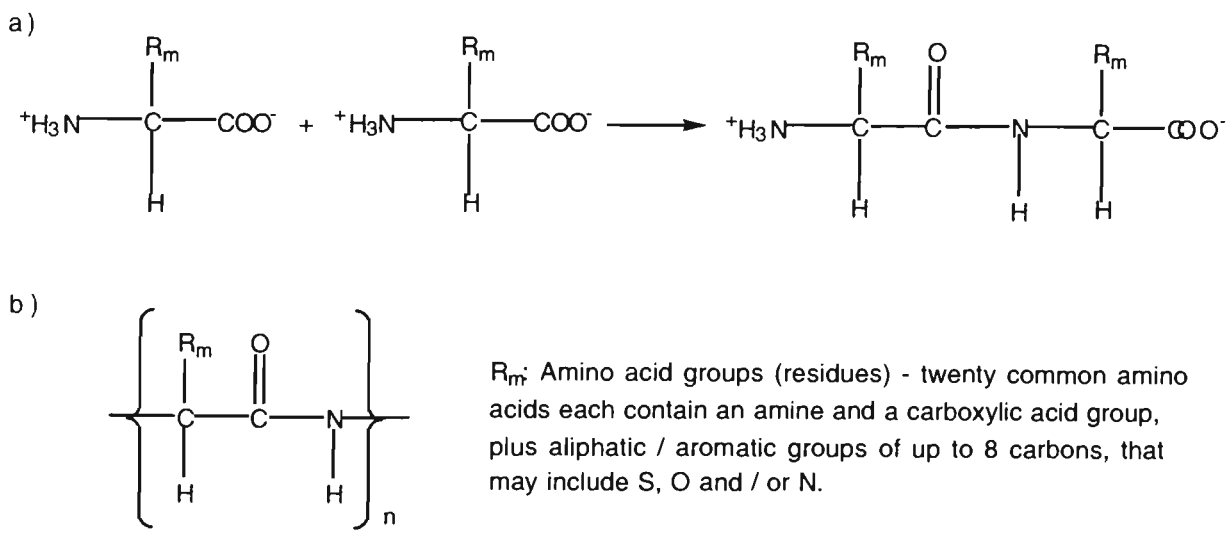

Scheme 2.4: (a) Condensation of the α-carboxyl group of one amino acid and the α-amino group of another to form a peptide bond; (b) the protein repeat unit, where R_m is one of twenty amino acid groups (after Darby [192]).

The repeating nature of the peptide bond in the polymer structure means that proteins resemble synthetic homopolymers with repeating backbone structures and variable side chains, for example vinyl, acrylic and polyether derivatives [198]. Importantly for the current work, proteins also contain hydrophobic (aliphatic or aromatic groups) and hydrophilic (hydrophilic peptide bonds, carboxylic acid and amine groups) regions that are repeated at regular intervals. Repeating hydrophobic / hydrophilic groups also occur to

a greater or lesser extent in conducting polymer / counterion systems: neutral parts of the polymer backbone (including substituents) and any long chain or aromatic counterions being hydrophobic; and the hydrophilic regions being the charged regions in both the backbone (polarons and bipolarons) and counterion, and any carbonyl group formed due to OH attack.

Some 110 years now Hofmeister postulated that all the observed ion specific interactions with proteins were due to the "power of ions to bind water" [197]. The lyotropic series proposed by him ranks both cations and anions according to their ability to solubilise proteins in aqueous solutions. Table 2.8 ranks anions and cations in the lyotropic series according to their interactions with proteins. The ranking of a cation or anion within this series has also been found to influence micelle formation of surfactants, flocculation of colloids [193] and the solubility of non-polar compounds in water [197].

These effects on protein structure and solubility may be explained by considering the interactions of both proteins and ions with water. Due to the unfavourable thermodynamics of the water / carbon interface [199], hydrophobic sections of a protein cause a strong organisation of water molecules immediately adjacent to them. Addition of any ionic species to a solution of a protein increases the surface tension of the solvent and decreases the amount of water available at the surface for hydration. However, in the presence of strong kosmotropes (eg Na_2SO_4), molecular water organisation is strongly encouraged around the hydrophobic sections and excludes the ionic species from binding to the charged regions or dipoles of the protein. This allows the molecule to fold since the intra- and inter-molecular electrostatic forces that keep proteins unfolded and solubilised are screened out [192] by the closely packed hydration layer. As the protein folds it expels water, reducing its exposed surface area. It becomes more compact, then aggregates and precipitates.

Table 2.8 : The Hofmeister lyotropic series for cations and anions [194] with the implications for protein structure and solubility, and other hydrophobic interactions displayed at the relevant end of the ranking [190, 194, 196, 197, 199].

$(CH_3)_2 NH_2^+ > NH_4^+ > K^+ \approx Na^+ > Cs^+ > Li^+ > Mg^{2+} > Ca^{2+} > Ba^{2+}$ $F^- > PO_4^{3-} > SO_4^{2-} > CH_3COO^- > Cl^- > Br^- > I^- > SCN^-$	
Kosmotropes	Chaotropes
Water-structure makers	Water-structure breakers
Enhance water clusters around protein	Ions bind to protein at charged groups or dipoles, reducing number of water clusters
Reduce solubility of hydrophobic units, and non-polar compounds generally, in water by increasing surface tension of water relative to chaotropes	Increase solubility of hydrophobic units, and non-polar compounds generally, in water by decreasing surface tension of water relative to kosmotropes
Fold (stabilise) protein	Unfold (destabilise) protein
- expels water and decreases surface area exposed to water	- increases surface area exposed to water
- leads to aggregation (salting out)	- leads to solubilization (salting in)
Increase micellar formation of surfactants	Reduce micellar formation of surfactants

In the presence of reasonable (0.15 to 2 M [194]) concentrations of chaotropic salts (eg LiSCN) the water organisation is broken and water is displaced by these chaotropic ions binding at the dipolar and charged regions. The protein unfolds due to repulsion between the now exposed hydrophobic sections and the polar components of the protein, as well as the stronger interactions between these polar sections and the polar solvent. Due to these ionic interactions, the unfolded or denatured protein is able to be completely solubilised.

The folding and unfolding of proteins in the presence of different kosmotropes and chaotropes, and concomitant inclusion or expulsion of water, would obviously have less effect on a more rigid conducting polymer film than on a protein in solution. However, it can clearly have a measurable effect since changes in the conformation of substituted polythiophenes in different supporting electrolytes have been reported by Levesque [200]. Changes in the conformation of PAni in different solvents and solvent vapours have also been reported by a number of authors [201-204], indicating that solvent effects (though rather different ones to those under discussion here) are recognised as having a major impact on polymer conformation. Of more import to this work is the fact that the changes in conformation of proteins are associated with changes in the degree of interaction between the hydrophobic regions of a polymer, the sites of nucleophilic attack, and water, the most common nucleophile.

As mentioned above, strongly chaotropic solute ions such as SCN^- and Mg^{2+} bind to polymers with alternating hydrophobic / hydrophilic regions very effectively, maximising the polymer surface area and generating the maximum number of solute binding sites. Strongly kosmotropic solutes such as SO_4^{2-} and K^+ create a hydration shell around the polymer, but are themselves excluded from binding with the protein, which minimises the polymer surface area. Considering the important role of water in the overoxidation of PPy, the ranking of a supporting electrolyte cation in the lyotropic series may contribute to the overoxidation potential in the following ways:

i) kosmotropic (water structuring) cations may order water so well that it is less available to participate in overoxidation, while chaotropic ions may increase its availability. This is not inconceivable, as ions in solution may have up to 15 water molecules in their solvation shell [190]. In the current study the concentration of salt solutions used was 1 M in all cases. With 15 water molecules per ion implies 30 moles water per litre is "fixed" about the solute (of the possible 55.6 moles). In the presence of a strong kosmotrope, up to 54% of the water will be tightly bound and less available for reaction with PPy. This is a little misleading, as kosmotropes also enhance water

structure around the hydrophobic components of a molecule, thus forming water clusters at the surface of the pyrrole ring. However, the structuring of over 50% of the water may have a minor effect on the freedom of waters to participate in any reaction.

ii) as polymers containing hydrophobic and hydrophilic regions are contracted in the presence of kosmotropic cations, water is excluded and the polymer surface area is minimised. This would also tend to reduce contact of the polymer surface with free water, with the converse applying to chaotropic cations.

iii) the mono- or di-layer of water bound to the hydrophobic regions of the polymer may be so highly organised as to prevent the diffusion of any ionic species to or away from the polymer surface [190, 205]. This would prevent OH^- (from the self dissociation of water) from contributing to overoxidation at the polymer surface. This may well be a significant contribution since OH^- is a much better nucleophile than H_2O itself [206]. The latter exhibits such low nucleophilicity towards an aromatic carbon that Mostany [60] reports overoxidation of PPy by OH^- (not H_2O) attack in neutral solutions of NaF. Thus, limiting OH^- diffusion to the pyrrole ring by the use of a strong kosmotrope would tend to increase the overoxidation potential. Again, the converse would apply for chaotropic cations, with the polymer surface having no protective hydration sheath over it and ions in solution having more ready access to the polymer surface. It is also conceivable that, due to the high water-stabilising nature of kosmotropes in the bulk solution, the degree of water dissociation, and hence the concentration of OH^- (and H^+), may be decreased. Furthermore, chaotropes bind their first hydration shell so loosely that the water adjacent to them is more mobile than that in the bulk solution [190].

iv) The layer of water bound to the hydrophobic regions of the polymer may be oriented or stabilised by a strong kosmotrope in such a way that it will be less effective as a nucleophile. Collins [190], in his excellent paper on the Hofmeister effect and solvent / protein interactions, reports that the ordered solvation layer at hydrophobic regions of a

polymer is expected to be at most two molecules thick and that this layer is very highly stabilised by the waters in the adjacent layers and the solutes in the bulk solution. He also postulates that the water molecules in this hydration layer are oriented in such a way that, due to a decrease in hydrogen bonding interactions in the surface waters, their oxygen carries a slight absolute negative charge. In the presence of a suitably high concentration of kosmotropic ions in the bulk water layers, the negative charge, and hence the electron density, on the surface oxygen is increased. In the case of chaotropes it is decreased. This may enhance the likelihood of nucleophilic attack by water and decrease the overoxidation potential of PPy in the presence of a kosmotrope. There are, however, two possible contributions to negate this effect, ranked in order of increasing importance:

a. as the oxygen of the water adjacent to the PPy ring carries an increased negative charge it will be repelled more strongly by the electron rich aromatic ring than would a water molecule in the absence of kosmotrope or the presence of a chaotrope. This effect will, of course, be overcome when the polymer is oxidised sufficiently to form a radical cation that more strongly attracts the higher negative charge density on the oxygen.

b. as the surface water is strongly stabilised by waters in the adjacent layer and the kosmotrope in the bulk solution, it will require more energy to extract it from its environment across the solution / polymer interface and into the carbon environment. This extra energy will result in higher overoxidation potential in the presence of kosmotropic cations and, conversely, lower the potential with chaotropic cations.

In summary, all of these above contributions will act in concert to increase the overoxidation potential of PPy in the presence of a kosmotrope and decrease it the case of a chaotrope. It would therefore appear worthwhile to look further at the order of cations in the lyotropic series.

The ranking of both anions and cations within this series can be estimated by many different measures (Collins [190] and references therein) including: protein solubility and aggregation; entropy change upon hydration; heats of hydration; surface tension at the air-water interface; solute hydrodynamic radius; solubility of low molecular weight organic solutes; self diffusion coefficient of water and many others. It is important to note though that all measures give a similar, characteristic ordering of ions, with only slight variations.

Surface tension is clearly relevant to the lyotropic series as it is a direct measure of how well a salt organises water at its surface [207]. At a constant concentration, a higher surface tension for one salt compared to another indicates that the former salt is able to organise water molecules at the surface more effectively than the latter. It thus excludes itself from the surface layer and fixes water molecules in this layer instead. Two factors contribute to surface tension at a constant temperature, the degree of organisation of waters by the salt and the concentration of salt in solution. Molal surface tension increment, σ, is a means of measuring the degree a salt increases or decreases the surface tension of the solvent ($\Delta\gamma = \gamma - \gamma^{o}$), while taking into account concentration effects and is given by:

$$\gamma = \gamma^{o} + \sigma\, m,$$

where: γ: surface tension of aqueous salt solution at a given concentration (dyn cm^{-1});

γ^{o}: surface tension of pure water (dyn cm^{-1});

σ: molal surface tension increment (dyn kg cm^{-1} mol^{-1});

m: molal concentration of salt solution (mol kg^{-1}) {molality concentration units are employed as molality is independent of temperature [207]};

σ is determined from the slope the linear region of a plot of γ vs molal concentration for a range of concentrations.

Table 2.9 presents the surface tension increments and molal surface tension increments of the nitrate salts employed in the current study.

Before further examining the ranking of the cations under consideration here they will be broken into three groups based on a combination of their charge, thermodynamic properties, hydrated to ionic radii ratio, molal surface tension increments and contribution to pH namely: (i) small, singly charged neutral, cations Na^+, K^+, NH_4^+; (ii) larger neutral dications Ca^{2+}, Mg^{2+}, Sr^{2+}; and (iii) finally H^+.

Table 2.9: Surface Tension Increments ($\Delta\gamma$) and Molal Surface Tension Increments (σ) of various nitrate salts in aqueous solution [207-212].

Cation	$\Delta\gamma$ *	σ
	(dyn cm^{-1})	(dyn kg cm^{-1} mol^{-1})
H^+	- 0.8	- 0.6
NH_4^+	1.0	0.85
Na^+	1.20	1.06
K^+	1.03	1.00
Ca^{2+}	2.4 **	2.9 **
Mg^{2+}	2.3 **	2.6 **
Sr^{2+}	2.3	2.6

* $\Delta\gamma$ is the difference between the surface tension of a solution and that of the pure solvent at the same temperature. Values are quoted in molal concentration terms and given for concentration = 1 m. Positive values of $\Delta\gamma$ indicate that the surface tension of the solution is greater than that of the solvent, negative values the reverse [213].

** Estimated from the relationship between surface tensions of chlorides and nitrates of other cations (Na^+, K^+, Sr^{2+}, Ba^{2+}) [207, 212] and the ionic contributions to surface tension of chloride and sulphate [213], and assumes that surface tension increments are linear over a reasonable concentration range [214, 215].

The separation of H^+ from the other cations is warranted on a number of points: it defines pH, the significance of which will be discussed briefly in the next section and in detail in Chapter 3; it has very different thermodynamic, hydrated to ionic radii and surface tension properties; and the theory of the lyotropic series only applies to neutral salts.

From the molal surface tension data in Table 2.9 the cations may be ordered within the groups discussed above as follows:

(highest water ordering) $Na^+ > K^+ \approx NH_4^+$ (lowest water ordering);

and $Ca^{2+} >> Mg^{2+} \approx Sr^{2+}$.

This is in extremely good and pleasing agreement with the experimental results for the overoxidation potentials in the presence of these cations given in Table 2.6:

(highest overoxidation potential) $Na^+ >> K^+ \approx NH_4^+$ (lowest overoxidation potential);

and $Ca^{2+} > Mg^{2+} \approx Sr^{2+}$.

From this it is clear that the cation of the supporting electrolyte has a significant role in the overoxidation potential of PPy films. It would also appear that the molal surface tension increment is a suitable means of determining the ranking of cations within the lyotropic series for this application.

To conclude this section some comments should be made on overoxidation in the presence of high concentrations of hydrogen ion. The data in Table 2.8 indicates that H^+ should increase the overoxidation potential of PPy if it follows the trends observed for other cations in the lyotropic series. However, H^+ does not fit into this series for reasons mentioned earlier. The most significant of these is its role in decreasing the concentration of OH^-, which is pivotal in the overoxidation of PPy. At lower pHs (in this case pH $\approx$ 0), the concentration of OH^- will approach 10^{-14} M and, with no other species added to the solution, water (at a concentration of 55 M) effectively becomes the only nucleophile involved in overoxidation. As water is a far less effective nucleophile than OH^-, this will slow down the process of overoxidation, ie increase the overoxidation potential.

However, there are a number of contradictory reports on this matter. For example, Gao et al [27] observed stabilisation of PPy against nucleophilic attack in 1 M HCl, and Pei et al [95] reported that PPy/NO_3 is stable in 1 M HNO_3 under open circuit conditions. Beck et al [21] quoted an increase of ≈ 0.05 V in the overoxidation potential of PPy/BF_4 in 0.1 M H_2SO_4 using chronoamperometry. On the other hand, Park et al [144] reported destabilisation of PPy in 1 M H_2SO_4 during CV studies and potential step experiments [180], possibly due to the effects of SO_4^{2-} mentioned above. Kang et al [184] also reported that the stability of PPy during cycling is decreased in high concentrations of strong acids (1 M), as these encourage higher levels of swelling and contraction during oxidation and reduction cycles. From work to be presented in Chapter 3, lowering the pH will hinder overoxidation under linear sweep conditions where repeated swelling and contraction do not occur, that is the polymer will be stabilised in reasonable (up to 1 M) acidic conditions.

On the other hand, in the work currently under discussion 1 M HNO_3 was employed as the supporting electrolyte. Nitric acid is a strong oxidising acid commonly used for the digestion of metals and organic matter. This could negate the expected increase in the overoxidation potential expected from the presence of a relatively high concentration of H^+ in the supporting electrolyte. From Table 2.6 the overoxidation potential of PPy/NO_3 in 1 M HNO_3 is 0.98 V, towards the top of the 0.93 to 0.99 V range given in the table, but not as high as anticipated in 1 M H^+.

To confirm that strong acids generally do stabilise PPy against overoxidation, at least when the films are not repetitively cycled, the overoxidation potential of PPy/Tir and PPy/pTS in 1 M acid solutions and their corresponding sodium salts were determined by LSR. The results are given in Table 2.10.

In each case the overoxidation potential in acid was higher, by between 5 and 8 %, than in the sodium salt of that anion. This would be expected if the argument that increased

acidity, which decreases the concentration of OH^- (the strongest nucleophile likely to be present in these systems), increases the stability of PPy to overoxidation. In these experiments the concentration of OH^- was decreased by about six orders of magnitude with the pH of the sodium salt solutions approximately 6, ie $[OH^-] \approx 10^{-8}$ M, compared with a $[OH^-]$ in 1 M acid $\approx 10^{-14}$ M. The effects of pH on the rate of overoxidation will be investigated thoroughly in Chapter 3.

Table 2.10: Overoxidation potential of PPy/Tir and PPy/pTS scanned in various supporting electrolytes (1M) at 1 mVs^{-1}. The films were grown on Pt galvanostatically from 0.05M Py and 0.02 M Tiron in water by passing 480 $mCcm^{-2}$ to give an approximate film thickness 1.2 μm.

Supporting Electrolyte Anion	Incorporated Counterion	Overoxidation potential (V vs Ag/AgCl)	
		Na^+	H^+
Cl^-	Tiron	0.92	0.98
NO_3^-	Tiron	0.88	0.95
SO_4^{2-}	Tiron	0.89	0.94
SO_4^{2-}	pTS	0.96	1.01

Finally, an identical set of experiments to those whose results were presented in Table 2.8 were performed on a Pt substrate (rather than Au). The results are summarised in Table 2.10, each overoxidation potential being the average at least two determinations.

From Table 2.11 it can be seen that again the overoxidation potential of PPy in the presence of H^+ is among the highest observed, but is no higher than with Na^+ and Sr^{2+} cations. The order of overoxidation potentials for the other cations, after breaking them into the groups discussed previously, is:

(highest overoxidation potential) $Na^+ > K^+ \approx NH_4^+$ (lowest overoxidation potential)

{σ order: $Na^+ > K^+ \approx NH_4^+$, overoxidation order on Au: $Na^+ >> K^+ \approx NH_4^+$};

and $Sr^{2+} > Ca^{2+} \approx Mg^{2+}$

{σ order: $Ca^{2+} >> Mg^{2+} \approx Sr^{2+}$, overoxidation on Au: $Ca^{2+} > Mg^{2+} \approx Sr^{2+}$}.

Table 2.11: Overoxidation potential of PPy/NO_3 scanned in various supporting electrolytes (1M) at 2 mVs^{-1}. The films were grown galvanostatically on Pt from 0.05M Py and 0.02 M NO_3 in water by passing 150 $mCcm^{-2}$ to give a film thickness of approximately 0.36 μm.

Supporting Electrolyte	Incorporated Counterion	Overoxidation potential on Pt (V vs Ag/AgCl)
HNO_3	NO_3^-	0.94
NH_4NO_3	NO_3^-	0.91
$NaNO_3$	NO_3^-	0.94
KNO_3	NO_3^-	0.90
$Ca(NO_3)_2$	NO_3^-	0.91
$Mg(NO3)_2$	NO_3^-	0.90
$Sr(NO_3)_2$	NO_3^-	0.94

Again, excellent agreement between the order of the molal surface tension increment and the overoxidation potentials is observed for the mono-cations. However, the order for overoxidation in the presence of dications is effectively the reverse of that expected. No reasonable explanation for this can be offered, as the only variation in the experimental conditions was the use of a Pt substrate (to be discussed in Section 2.3.5.3).

2.3.6.2.2 Anions

It is far more difficult to select an extensive range of anions as supporting electrolyte anions for a study of their effects on the overoxidation potential of PPy than is the case for cations. Ideally these would need to be small, singly charged, non-electroactive, non-nucleophilic ions with high water solubility. The effects of incorporating a number of anions during growth that fit into one or more of these groups were discussed in Section

2.3.6.1. Therefore, only two significant issues will be discussed here: confirmation of the relevance of the lyotropic series to anions and the effect of OH^- concentration on overoxidation.

Table 2.12 presents the molal surface tension increments of aqueous $NaNO_3$, NaCl and $NaSO_4$ solutions and the overoxidation potentials for PPy/pTS films overoxidised in these supporting electrolytes. From this table, even though the results could overlap within experimental error (see Section 2.3.5.1), a general trend may be observed that both NO_3^- and Cl^- have overoxidation potentials in the order predicted by their respective molal surface tension increments (Cl^- > NO_3^-). This again indicates the applicability of the lyotropic series to conducting polymer chemistry. However, the overoxidation potential for SO_4^{2-} is much lower, relative to Cl^- and NO_3^-, than predicted by its ranking in the lyotropic series. This is not unexpected in the light of the earlier discussion on the effects of SO_4^{2-} in Section 2.3.6.1 above. The factors discussed there obviously outweigh any contribution by its kosmotropic nature.

Table 2.12: Molal surface tension increments of various aqueous supporting electrolyte solutions (from Ref (Melander, 186)) and overoxidation potential of PPy/pTS scanned in 1 M solutions of these at 1 mVs^{-1}. The films were grown galvanostatically on Pt from 0.05M Py and 0.02 M pTS in water by passing 480 $mCcm^{-2}$ to give a film thickness of approximately 1.2 μm.

Supporting Electrolyte	σ (dyn kg cm^{-1} mol^{-1})	Overoxidation potential (V vs Ag/AgCl)
$NaNO_3$	1.06	0.90
NaCl	1.64	0.92
Na_2SO_4	2.73	0.89

As was the case above, the pH of the supporting electrolyte plays a pivotal role in the overoxidation of conducting polymers. The increasing rate and ease of overoxidation of PPy in basic conditions has been reported widely [9, 21, 31, 58, 62, 73, 78, 86, 121, 122, 165, 178, 184, 185]. Unlike the contradictory reports on the effects of strong acids, there is universal consensus on the effects of increasing pH and the importance of the hydroxide ion on the overoxidation of PPy. For example, PPy/ClO_4 and PPy/BF_4 exhibit decreases of up to four orders of magnitude in their conductivities when soaked in 2M NaOH for 2 to 4 minutes at 50°C in air [122]. Even though base treatment may stabilise PPy for long term aging in air [118] and base-treated films are stable between -0.2 and -1.0V (vs SCE) [121], Reynolds et al reported [78] that PPy/Cl degrades rapidly at any pH > 9 when scanned between -1.2 and + 0.4V (vs Ag/AgCl). Haimerl et al pointed out [9] that "owing to the increasing nucleophilicity with increasing pH, nucleophilic attack (overoxidation) on PPy should be pH dependent".

Table 2.13 summarises the overoxidation potentials observed for PPy/pTS when 0.1 M NaOH is employed as the supporting electrolyte in an LSR determination, results for 1 M $NaNO_3$ and Na_2SO_4 employed under similar conditions are given for comparison.

Table 2.13: Overoxidation potential of PPy/pTS scanned in various supporting electrolytes at 1mVs^{-1}. The films were grown galvanostatically on Pt from 0.05M Py and 0.02 M pTS in water by passing 480 mCcm^{-2} to give a film thickness of approximately 1.2 μm.

Supporting Electrolyte	Incorporated Counterion	Overoxidation potential (V vs Ag/AgCl)
$NaNO_3$ (1 M)	pTS	0.99
Na_2SO_4 (1 M)	pTS	0.96
NaOH (0.1M)	pTS	0.45

As stated in the Experimental section of this Chapter, 1 M solutions would generally be employed throughout the LSR work to avoid contributions to the film resistance by the supporting electrolyte. However, 1 M NaOH was employed as the supporting electrolyte the point of inflection around the resistance plateau could not be determined, due to an ill-defined rise in resistance from the commencement of the potential ramp. It is possible of course that the resistance changes had largely occurred before the potential ramp was begun. This was not unexpected, as Wernet et al [62] has noted that PPy/DS loses 60% of its electroactivity (charge passed in each scan) after only 9 complete scans (-0.75 to +0.25 V vs SCE at 50 mVs^{-1}) when the supporting electrolyte pH was adjusted to 9.

Even in the case of 0.1 M NaOH reported Table 2.13, the determination of the resistance plateau was only possible with the aid the LSV data to assist in locating the plateau. This is not of great import, as the intention here was only to verify that reasonable levels of OH^- would have a major impact on the overoxidation potential. This is clearly the case, as the overoxidation potential was reduced by more than 50% when 0.1 M NaOH was employed as the supporting electrolyte. As mentioned above, the effects of pH will be studied in greater depth in Chapter 3.

2.3.6.3 Effects of substrate on overoxidation potential - gold, platinum and glassy carbon

The growth substrate is known to have a significant effect on the porosity of the overoxidised films, with Witkowski and Brajter-Toth reporting [141, 175] that PPy overoxidised on rough pyrolytic carbon has an apparent diffusion coefficient from 5 to 10 times higher than one grown on glassy carbon. Farrington et al [29] also observed that overoxidised PPy grown on GC gives larger pores, with different morphology, than one grown on Au, and that this difference is sufficient to allow higher rates of transport of dopamine through the latter [29]. According to Mengoli et al [151], PPy/SO_4 grown from H_2SO_4 has much better adhesion on GC than on Pt or Au. However, Teasdale [216] reports that PPy/NO_3 grown on oxidised Pt is far more difficult to remove chemically (by

chromic acid) in comparison to PPy/NO_3 on GC, due to bonding of the polymers to the platinum substrate through a covalent oxygen linkage. Pigois-Landureau also notes the likelihood of these metal-oxygen-polymer linkages leading to good adhesion between PPy and Pt [217].

Of the three electrodes under consideration here, Pt has the greatest propensity to form an oxide layer on its surface [218, 219]. Pt exhibits a strong oxidation wave at about 0.6 V (vs Ag/AgCl) in 1 M H_2SO_4, while Au has a similar peak at about 1.0 V [219]. GC exhibits no oxidation peak under these conditions up to 1.0 V [218]. These surface oxide layers not only increase the adhesion of PPy to the substrate, but also promote electron transfer through a redox mediation mechanism where oxygen-containing surface redox groups [218] transfer electrons between the electrode surface and the attached polymer film. This oxygen attachment would allow better (possibly more even) transfer of electrons from the electrode to the polymer film for Pt than for the other electrode materials, reducing the measured overoxidation potential of PPy on this substrate. The uneven, less efficient contact in the cases of Au and GC is also indicated by the more gradual initial increase in resistance and less clearly defined resistance plateau of polymers on these electrodes, as can be seen in Figure 2.8.

The overoxidation potentials determined from these, and similar experiments employing different supporting electrolyte salts during the overoxidation of PPy/NO_3, are given in Table 2.14. In all cases, the overoxidation potential on gold was greater than on Pt (by an average of 0.04 V over the 7 tests) and almost identical to the only determination under identical conditions for GC. This strongly supports the hypothesis above that Pt forms strong oxygen linkages to the polymer film, which then allows more efficient electron transfer, as indicated by the lower overoxidation potentials for this substrate.

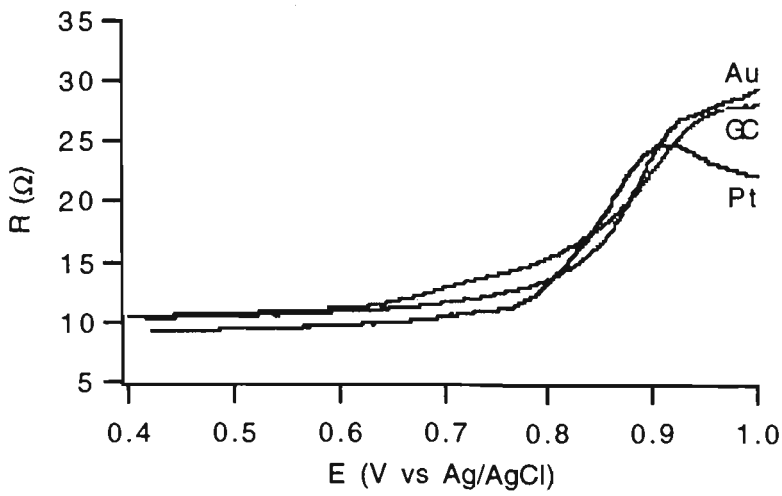

Figure 2.8: LSR output for 0.37 μm PPy/NO_3 films grown galvanostatically from H_2O on Pt, GC and Au electrodes scanned in 1M $NaNO_3$ at 2 mVs^{-1}.

Table 2.14: Overoxidation potential of PPy/NO_3 scanned in various supporting electrolytes (1M) at 2 mVs^{-1}. The films were grown galvanostatically on Pt, Au or GC from 0.05M Py and 0.02 M NO_3 in water by passing 150 $mCcm^{-2}$ to give a film thickness of approximately 0.36 μm.

Supporting Electrolyte	Overoxidation potential on Pt (V vs Ag/AgCl)	Overoxidation potential on Au (V vs Ag/AgCl)	Overoxidation potential on GC (V vs Ag/AgCl)
HNO_3	0.94	0.98	ND*
$NaNO_3$	0.94	0.99	1.00
KNO_3	0.90	0.94	ND
NH_4NO_3	0.91	0.93	ND
$Sr(NO_3)_2$	0.94	0.93	ND
$Ca(NO_3)_2$	0.91	0.99	ND
$Mg(NO_3)_2$	0.90	0.95	ND

* ND: Not Determined

A final note on substrates - gold is the most cantankerous material to use as a substrate for characterisation by this method, at least in the case of the small, singly charged counterions employed here. Warren and Anderson [220] report that PPy/NO_3 when

grown on Au gives uneven, irreproducible films, while Schirmeisen and Beck [53]274) report that it gives "irregular" voltammetric curves and that successful deposition of this polymer on Au is very much dependent on the growing conditions. On the other hand, Kim [39] observed that PPy/NO_3 deposited from water onto sputter-coated Au gave smooth, even films. As can be seen from Figure 2.8, the LSR output for PPy/NO_3 on Au is far from ideal, in that it does not plateau, but after an inflection point continues to rise. This was often the case for this substrate material, which frequently exhibited two resistance features that could be best described as "peaks", as opposed to plateaus. In the case of unsubstituted PPy films grown on Au, this occurred in 8 out of the 20 tests performed, compared with 1 out of over 230 LSR determinations on either GC or Pt.

It is recognised that gold is readily complexed in the presence of Cl^- and other complexing agents [219]. Any gold complexes formed may contribute to these unusual resistance curves by the formation of a resistive layer between the overoxidised PPy and the gold. Even though these experiments were performed in the presence of either NO_3^- or BF_4^- / NO_3^-, impurities in the solution, leakage from salt bridges, sloppy technique or PPy overoxidation products may have provided a suitable complexing material to create a gold complex at the electrode. The latter possibility is considered to be the most likely for the following reasons: (i) the resistance continued to increase slowly after a clear inflection point as the overoxidation is complete, as indicated by the LSV data; and(ii) as Farrington et al noted [29], even though the pore size of overoxidised PPy is normally dictated by the size of the dopant anion, the pore size of a PPy film overoxidised on gold is larger than for one on GC. These features suggest that the gold substrate imparts some unique chemistry to the overoxidation process involving an interaction between the gold and the film or its overoxidation products.

2.3.6.4 Effects of growing solvent on overoxidation potential - water and acetonitrile

Although water, due to safety and environmental aspects, is the most practical growing solvent for any large scale preparation of PPy films, a number of organic solvents are often employed in this role including propylene carbonate [79, 127], methanol [161] and acetonitrile [31, 53, 79, 84, 96]. The impact of utilising an organic solvent during growth would have on the overoxidation potential of PPy has therefore also been studied here. Acetonitrile (AcN) was selected for this purpose as it is the most common non-aqueous solvent used, generally with the addition of a small amount of water [31, 96]. In the current work, AcN was "dried" over molecular sieves. However it is extremely unlikely that this would remove all water and, as the AcN was handled in air and no special precautions were taken to dry the N_2 used for deoxygenation, it is assumed that a significant amount of water remained. After preparation in the respective solvents, both films were rinsed with water and then overoxidised in aqueous 1 M H_2SO_4. The LSR output for both films is presented in Figure 2.9.

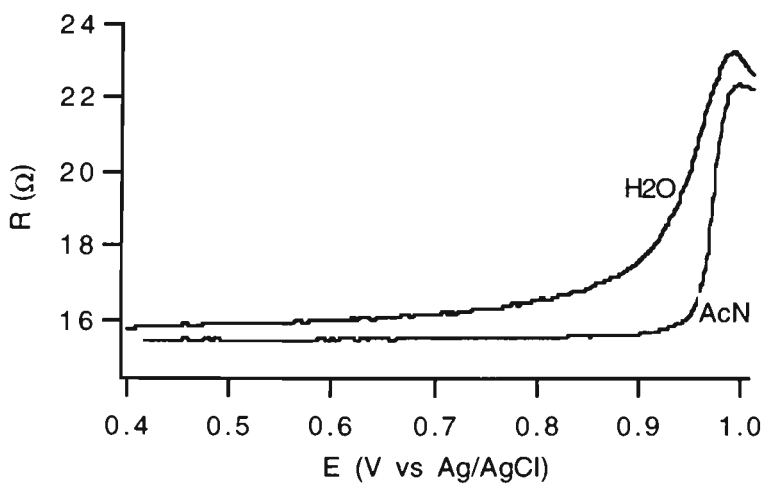

Fig 2.9: LSR output for 0.77 μm PPy/BF_4 films grown galvanostatically at 0.5 $mAcm^{-2}$ on Pt from solutions of 0.05 M Py / 0.02 M $TBABF_4$ in "dry" AcN or water. Film thickness 0.73 mm, potential scanned at 2 mVs^{-1} in 1 M H_2SO_4.

The overoxidation potential determined for a PPy/BF_4 film grown from water (PPy/BF_4/H_2O) was 0.98 ± 0.02 V (vs Ag/AgCl, average of 9 results). This is in excellent agreement with the value of 0.97 ± 0.02 V (average of 13 results) determined for PPy/BF_4 grown from AcN (PPy/BF_4/AcN) run under identical conditions. From this it is obvious that the growing solvent has no impact on the overoxidation potential of the polymer. However, from comparison of the two curves in Figure 2.9, it clearly has a large impact on the shape of the resistance / potential curve and the onset of overoxidation. For PPy/BF_4/H_2O there was a clearly discernible increase in resistance starting around 0.6 V. This was followed by a gradual increase until around 0.92 V, and then a more rapid rise until the maximum is reached near 0.97 V. On the other hand, PPy/BF_4/AcN showed effectively no increase in resistance before about 0.90 V, rises steadily until around 0.95 V and then almost vertically to its maximum around 0.97 V.

These variations are best explained by recognising that when PPy is grown in AcN and transferred to water for characterisation, it contracts markedly [84] during the initial potential cycles. As the film contracts, it will expel considerable amounts of supporting electrolyte and pack the polymer chains more closely. This leads to much lower diffusion rates of ions into and out of the polymer, which retards overoxidation. It also provides better contact between the molecular wires, opening up more conducting pathways to compensate for any destroyed in the early stages of overoxidation. However, once the potential is sufficiently high to fully overoxidise PPy, at around 0.9 V, the polymer begins to open up and the rate of the reaction increases rapidly, leading to the almost vertical rise in resistance from 0.95 to 0.97 V. It is important though to realise that the growing solvent does not alter the actual (irreversible) overoxidation potential of the polymer as determined by this method, but alters the potential at which the onset of overoxidation is observed.

2.3.6.5 The role of scan rate

The LSR technique is a dynamic one with the potential continually increasing from the onset of overoxidation, through its completion and onwards. Even though the scan rates selected here were slow compared to normal CV rates, complete overoxidation is also a relatively slow process. If the scan rate is too high, a clear lag time exists between potential, current and resistance changes. However, it is not possible to perform potential scans or steps at infinitely slow rates or small amplitudes. Hence, an overoxidation potential determined by any dynamic electrochemical means will clearly be dependent on the scan rate or step amplitude chosen. On the other hand, this Section aims to determine the "inherent" overoxidation potential of the polymer, ie the potential at which irreversible overoxidation of the entire polymer would occur if it were stepped to that precise potential and held there for some finite time. Stated in another way, the "inherent" overoxidation potential represents the overoxidation potential at an "infinitely slow scan rate", as opposed to the "actual" overoxidation determine by some real, dynamic technique.

Table 2.15: Overoxidation potential of PPy films scanned in various supporting electrolytes (1M) at various scan rates. The films were grown galvanostatically on Pt from 0.05M Py and 0.02 M anion in water by passing 480 mCcm^{-2} to give a film thickness of approximately 1.2 μm.

Incorporated Anion / Supporting Electrolyte	NO_3^- / H_2SO_4	pTS / $NaNO_3$	pTS / H_2SO_4	pTS / Na_2SO_4	SO_4^{2-} / Na_2SO_4	Tir / $NaNO_3$
Scan Rate (mVs^{-1})	Overoxidation Potential (V vs Ag/AgCl)					
0.5	0.89	0.94	0.97	0.90	0.89	0.88
1	0.91	0.99	1.01	0.96	0.93	0.90
2	0.93	1.04	1.04	1.01	0.98	0.95
3	0.95	1.06	1.06	1.06	1.04	ND*
5	0.98	1.11	ND	ND	1.13	1.01

* ND: Not determined

Table 2.15 presents the overoxidation potentials determined by LSR of a number of 1.2 μm PPy films that were overoxidised in the supporting electrolytes indicated at various scan rates. It is clear that scan rate has a major impact on the overoxidation potential, as variations of around 10 % are evident for the same polymer system between the slowest and fastest scan rates employed.

Figure 2.10, shown here only to emphasise the variation in the slopes for the different polymer / supporting electrolyte combinations, is a plot of the square root of the scan rate versus the overoxidation potential of the data presented in Table 2.15. These plots allow easy determination of the "inherent" overoxidation potential at zero scan rate (Y-intercept) for any particular counterion / supporting electrolyte combination. These results, along with the r-values and slopes for the lines of best fit, are given in Table 2.16.

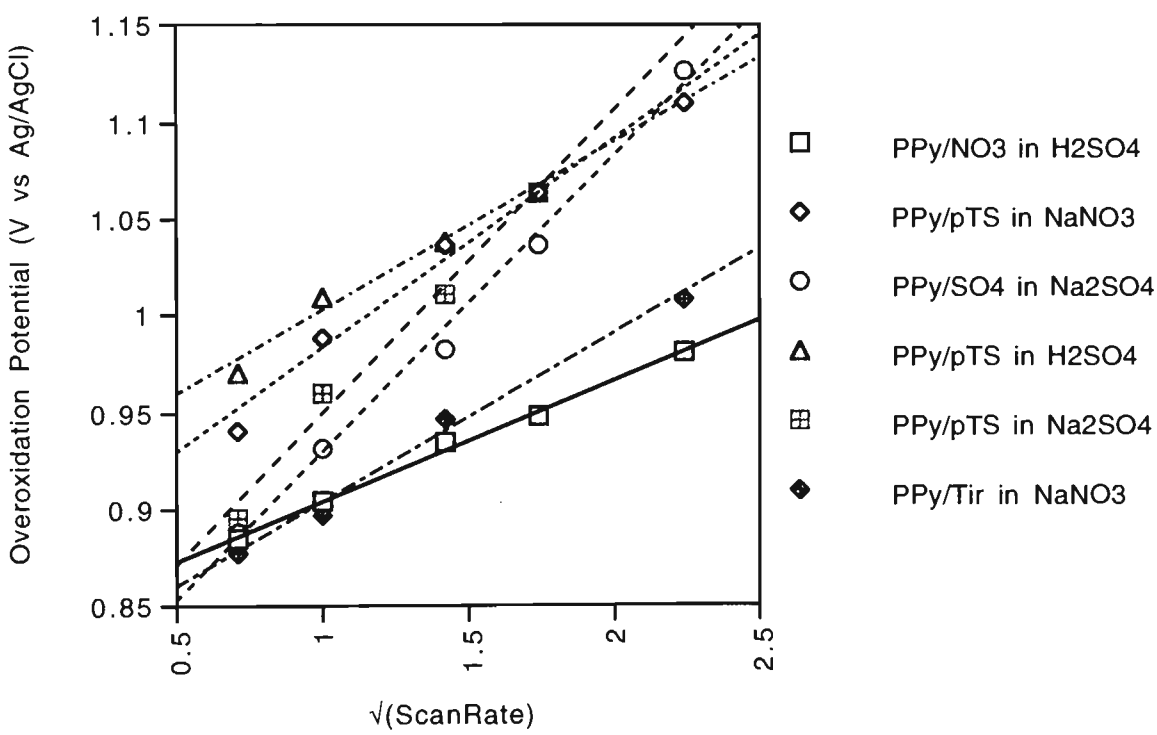

Figure 2.10: Graph of √Scan Rate against the measured overoxidation potential for a range of 1.2 mm PPy films on Pt in various supporting electrolytes.

Table 2.16: Slope, Y-intercept and r value of the plots of (√Scan Rate) against (Overoxidation Potential) as determined by LSR for various polypyrroles in various supporting electrolytes.

Incorporated Anion / Supporting Electrolyte	NO_3 / H_2SO_4	pTS / $NaNO_3$	pTS / H_2SO_4	pTS / Na_2SO_4	SO_4 / Na_2SO_4	Tir / $NaNO_3$
Slope of {√(Scan Rate) v (O-ox Pot)} Plot	0.062	0.108	0.087	0.157	0.154	0.087
Y-intercept: Inherent Overoxidation Potential	0.84	0.87	0.92	0.79	0.77	0.82
r value	0.998	0.992	0.991	0.994	0.997	0.995

The "inherent" overoxidation potentials (Y-intercepts) determined from Figure 2.10 and presented in Table 2.16 show many of the trends for these polymer / electrolyte systems expected from the discussions above:

i. PPy/pTS is one the most stable polymers, having the highest inherent overoxidation potential for each of the supporting electrolytes in this group;

ii. H_2SO_4 inhibits overoxidation and extends the overoxidation potential;

iii. and SO_4^{2-}, except as sulphuric acid, destabilises polymers during overoxidation and reduces the overoxidation potential of these polymers, resulting in PPy/SO_4 in Na_2S0_4 having the lowest inherent overoxidation potential in this group.

As these linear relationships involve √Scan Rate, the rate determining step in the redox mechanism may be ion transport by diffusion and migration within the film. According to Levi et al [221], the rate controlling step for thick PPy films scanned in the normal redox region is ionic movement by diffusion through the polymer / solution. In this case i is proportional to $\upsilon^{1/2}$. The validity of this is supported by the results given in Table 2.16 where the slopes at least superficially reflect the ease of diffusion of the ions through the respective polymers.

PPy/pTS is a very closely packed polymer with a high degree of order [58, 66] due to the planar nature of the anion [72]. PPy/pTS films exhibited the highest slopes of any of the films investigated here. Within this group the magnitudes of these slopes reflected the relative mobilities of the anions and/or cations of the supporting electrolyte in a PPy/pTS film: $Na_2SO_4 < NaNO_3 < H_2SO_4$. In the first instance, Na^+ alone would be the mobile species; in the second both Na^+ and NO_3^- would have high mobility; and in the third the mobile species would be H^+, which has an extremely high mobility. By the same reasoning Na_2SO_4, would be less mobile in the highly compact [86] PPy/SO_4 than $NaNO_3$ is in PPy/Tir and H_2SO_4 in PPy/NO_3.

As the measured overoxidation potential at faster scan rates increased more rapidly for more stable films, higher slopes for plots of √Scan Rate versus Overoxidation Potential were associated with increasing electrochemical stability of the films. This is not necessarily related to the inherent overoxidation potential of the film (which is defined at "zero scan rate"), but will indicate the stability of the film under dynamic conditions, including normal conditions at potentials below the overoxidation potential. From perusal Table 2.16 it can be seen that the slopes for all pTS films are larger than those for the other polymers, irrespective of the supporting electrolyte used, the anions incorporated in the other films and the inherent overoxidation potentials determined for the films. The relative stability of PPy/pTS films in an aqueous solution parallels reports of the high stability of PPy/pTS films compared to other polypyrroles in air [66, 130, 131]. In the former case, degradation relies on diffusion of hydrated ions through the polymer at an anodic potential, while in the latter case it is the diffusion O_2 in the dry state at open circuit.

2.3.6.6 The role of film thickness

The work discussed in Section 2.3.5.5 above involved a constant film thickness of 1.2 μm and a relationship between scan rate and overoxidation potential was determined. It would also be expected that a relationship should exist between the measured

overoxidation potential and the film thickness, and this will also be investigated here. Table 2.17 presents the LSR results for the overoxidation of two PPy films with a range of film thicknesses.

It was expected that the relationship between film thickness and the overoxidation potential would involve proportionality between the overoxidation potential and the square of film thickness, as Beck reported [21] that the time constant for diffusion of ions in a PPy film during a normal voltammetric experiment is given by:

$\tau = L^2 / 4 D$,

where L: film thickness,

D: diffusion coefficient, in this case through the polymer.

Table 2.17: Overoxidation potential of PPy/BF_4 and PPy/NO_3 scanned in 1M H_2SO_4 and $NaNO_3$ at 2 and 1 mVs^{-1}, respectively. The films were grown on Pt or GC at 1.0 or 0.5 $mAcm^{-2}$, respectively, from 0.05M Py and 0.02 M anion in water.

PPy/BF_4 on Pt		PPy/NO_3 on GC	
Film Thickness (μm)	Overoxidation Potential (V vs Ag/AgCl)	Film Thickness (μm)	Overoxidation Potential (V vs Ag/AgCl)
0.38	0.95	0.29	0.96
0.77	0.97	0.58	0.97
1.15	1.00	1.17	1.03
1.53	1.03	-	-

As overoxidation in the experiments carried out in the current work involves diffusion of ions through the polymer under the influence of a linear potential, it was expected that a similar relationship would exist. This belief was vindicated as shown in Figure 2.11.

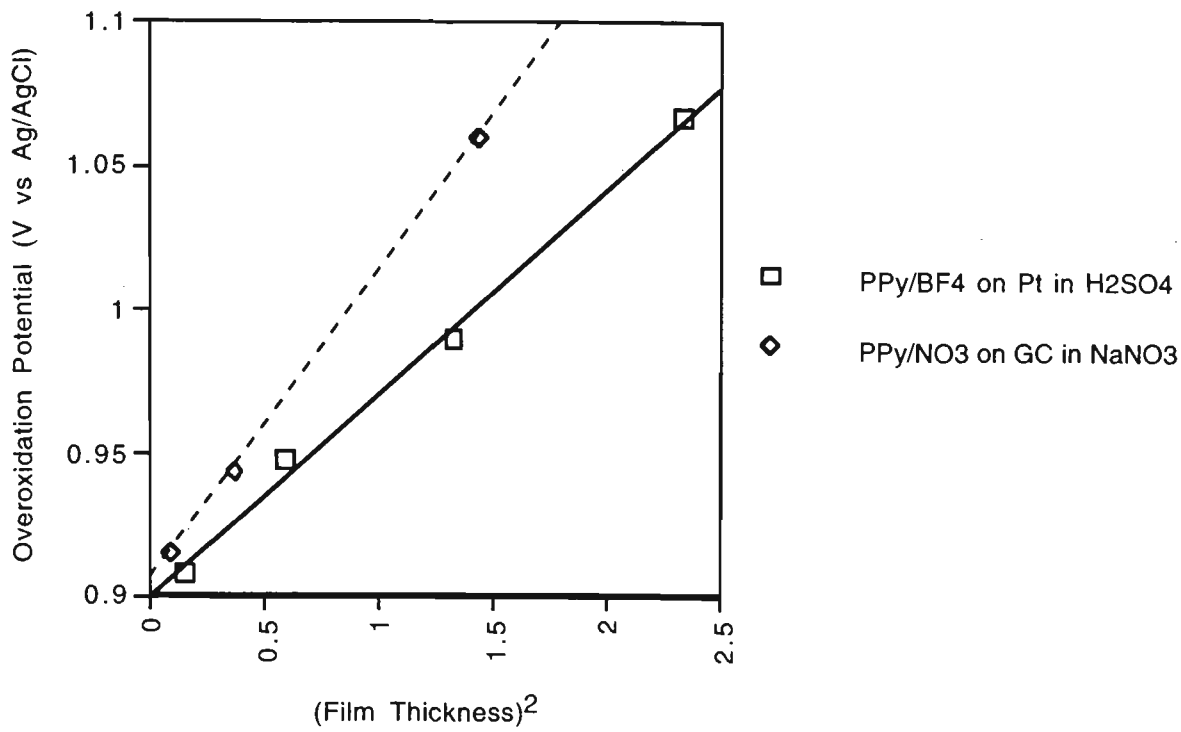

Figure 2.11: Plot of (Film Thickness)^2 against Overoxidation Potential for various thicknesses of PPy/BF_4 in H_2SO_4 and PPy/NO_3 in $NaNO_3$.

The slope, Y-intercept and r-values derived for these plots are given in Table 2.18.

Table 2.18: Slope, Y-intercept and r value of the plots of (Film Thickness)^2 against Overoxidation Potential as determined by LSR experiments for various thicknesses of PPy/BF_4 in H_2SO_4 and PPy/NO_3 in $NaNO_3$.

Counterion / Supporting Electrolyte	BF_4^- / H_2SO_4	NO_3^- / $NaNO_3$
Slope of {(Film Thickness)^2 v (O-ox Pot)} Plot	0.07	0.11
Y-intercept	0.90	0.91
r value	0.997	1.000

A surprising observation from Table 2.18 is that at zero thickness the calculated overoxidation potentials of the films are 0.90 V for the PPy/BF_4 and 0.91 V for

PPy/NO_3, which is the same result within experimental error. This was not expected as, even though both polymers fit into the "small spherical anion" class with no special structure ordering, they were overoxidised on substrates and in supporting electrolytes that should produce very different results, as discussed in Sections 2.3.5.3.2 and 2.3.5.3 above. In the case of PPy/BF_4 the supporting electrolyte was 1 M H_2SO_4, which would be expected lead to a higher overoxidation potential for this film compared to PPy/NO_3 in 1 M $NaNO_3$. However, the former film is grown on Pt, compared to GC in the latter case, which would be expected to result in a lower overoxidation for the latter. It would appear that these two influences may coincidentally cancel each other out in this work or that for an infinitely thin film, the effects of the counterion and substrate are negligible.

It is apparent that these limiting overoxidation potentials at "zero film thickness" are much higher than the inherent overoxidation potentials calculated in Section 2.3.5.5 for 1.2 μm films in similar polymer / supporting electrolyte combinations. The inherent overoxidation potentials determined for PPy/NO_3 in H_2SO_4 and PPy/Tir in $NaNO_3$ were 0.84 and 0.82 V, respectively. Even taking into account the variations brought about by different counterion / supporting electrolyte / substrate combinations, the results obtained in the current section are very high in comparison. It was assumed that the results determined for overoxidation at "zero scan rate" (where a polymer can be held precisely at its overoxidation potential for an infinite time if necessary and thus film thickness should not be critical) and "zero film thickness" (where an infinitely thin film should be overoxidised instantaneously at its overoxidation potential) would be reasonably independent of film thickness and scan rate. This is clearly not the case.

This may be explained in part by appreciating that, in both cases above, the dependence of the overoxidation potential on scan rate or film thickness is based on diffusion of ions into or out of a film of some finite thickness (in practical terms greater than about 0.3 μm in the films studied here). As the film thickness approaches zero, the role of diffusion becomes less significant and the rate of the reaction becomes dependent only on the

kinetics of nucleophilic attack, which will be discussed in detail in Chapter 3. Obviously, extrapolation of film thickness to zero gives an erroneously high overoxidation potential, as it does not take into account the range of film thicknesses where diffusion is no longer a significant contribution. In this region, overoxidation will not be hindered by diffusion rates and the overoxidation potential will drop below the line of best fit obtained in Figure 2.11, possibly approaching the inherent overoxidation potentials given in Table 2.18.

While remembering that the comparison here is between PPy on Pt in acid and PPy on GC in neutral supporting electrolyte, making it difficult to compare the absolute overoxidation potentials, there is still a significant difference between the slopes of PPy/NO_3 in $NaNO_3$ (slope 0.071) and PPy/BF_4 in H_2SO_4 (slope 0.107). This highlights the importance of ion diffusion in the overoxidation process in films of finite thickness. In the presence of extremely mobile H^+, compared with Na^+ and NO_3^-, overoxidation proceeds more rapidly though the film leading to a smaller lag time between applied potential and measured overoxidation potential and a lower value of the slope.

On the other hand, in the special case of an infinitely thin film, none of the above considerations may have any impact. As the film is theoretically a monolayer, diffusion has no role and all molecules have good contact with the substrate. The Y-intercept of Figure 2.11 may represent the fundamental overoxidation potential of a PPy film in water without the other real-world contributions of counterions, supporting electrolyte salts, substrates, etc.

2.3.6.7 Effects of ring substituents on overoxidation potential

If it assumed, as was discussed in the Introduction, that the predominant mechanism of overoxidation of PPy is nucleophilic attack at the β-carbons, it would seem logical that polypyrroles with substituent groups at either or both the 3- or 4- positions may be stabilised against overoxidation. It is this possible stabilisation that will be investigated in this section.

A wide range of substituted polypyrroles have been grown electrochemically [149, 222, 223] including those from the two monomers chosen for this study: 3-methylpyrrole-4-carboxylic acid (MPyC) [224] and 3-octylpyrrole (3-OPy) [135, 225], see Scheme 2.5. These were selected due to their ease of polymerisation, availability of the monomers, reasonable conductivities of their polymers and their differing chemistries. They provide a disubstituted PPy and one with a large, hydrophobic substituent.

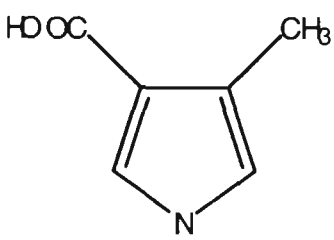

a) 3-methylpyrrole-carboxylic acid (MPyC)

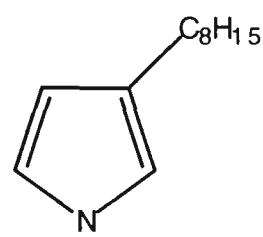

b) 3-octylpyrrole (3-OPy)

Scheme 2.5: Structures of 3-methylpyrrole-carboxylic acid and 3-octylpyrrole.

Owing to the poor water solubilities of these monomers, the solvents and supporting electrolyte salts given in Table 2.19 were employed for polymer growth. It is worth noting that no suitable combination of monomers / supporting electrolyte / solvent could be found to grow even, reproducible films of these substituted PPys on Pt. This is possibly associated with the increased hydrophilicity of this material over Au and GC due to the oxygen attachment described above (Section 2.3.5.3) and the relative hydrophobicity of these monomers. Hence, gold and glassy carbon were employed as substrates for the majority of this work.

From an LSV / LSR study of a 0.75 μm P(MPyC)/DS film scanned at 1 mVs^{-1} in 1 M H_2SO_4 the overoxidation potential of this material was determined to be 1.03 V, not significantly higher than un-substituted PPy under similar conditions. This is despite the fact that both β-positions are occupied by a substituent group, conceivably making

nucleophilic attack more difficult. However, Anglada reports that disubstituted PPy is more readily oxidised by O_2 in non-aqueous solution than are un-substituted PPys [149] and Masuda observes that PPy/PF_6^- is more stable in dry air than either P(3-MePy) or P(3-OPy) [135, 225]. These three studies indicate, that under the (non-aqueous) conditions employed therein, substituents on the pyrrole ring offer no increased stability to PPy. This was also confirmed here in aqueous solvent under an applied potential. As only 2 % of the charge consumed during growth was required for overoxidation, this process presumably proceeds by a different route for this polymer than for other PPys studied in this work. The possible mechanisms of nucleophilic attack on disubstituted P(MPyC) will be investigated in Chapter 4.

Table 2.19: The supporting electrolyte and its concentration, monomer concentration and solvent employed for galvanostatic growth of P(MPyC) and P(3-OP) polymer films.

Monomer	P(MPyC)		P(3-OPy)	
Anion	DS^-	BF_4^-	pTS^-	DBS^-
Cation	Na^+	TEA^+	Na^+	Na^+
Supporting electrolyte conc (M)	0.1	0.05	0.05	0.05
Monomer conc (M)	0.1	0.2	0.1	0.2
Solvent	30% n-propanol - 70% H_2O	25% CH_2Cl_2 - 75% AcN	25% CH_2Cl_2 - 75% AcN	15% AcN - 85% EtOH

Even though disubstituted PPy offered no significant advantages over unsubstituted pyrroles in terms of overoxidation potential, pyrrole having a hydrophobic β-substituent may enhance the overoxidation potential in aqueous solution [226] due to the increased hydrophobicity this group would impart to the polymer. To this end, P(3-OPy)s incorporating three different anions (BF_4^-, pTS and DBS) were polymerised. These anions were chosen as they themselves have a range of hydrophobicities (BF_4^- < pTS <

DBS) and polymer ordering abilities (DBS ≈ pTS > BF_4^-) [58]. Figure 2.12 presents the LSV / LSR outputs for a galvanostatically grown P(3-OPy)/BF_4 film scanned at 2 mVs^{-1} in 1 M $H_2SO_{4(aq)}$.

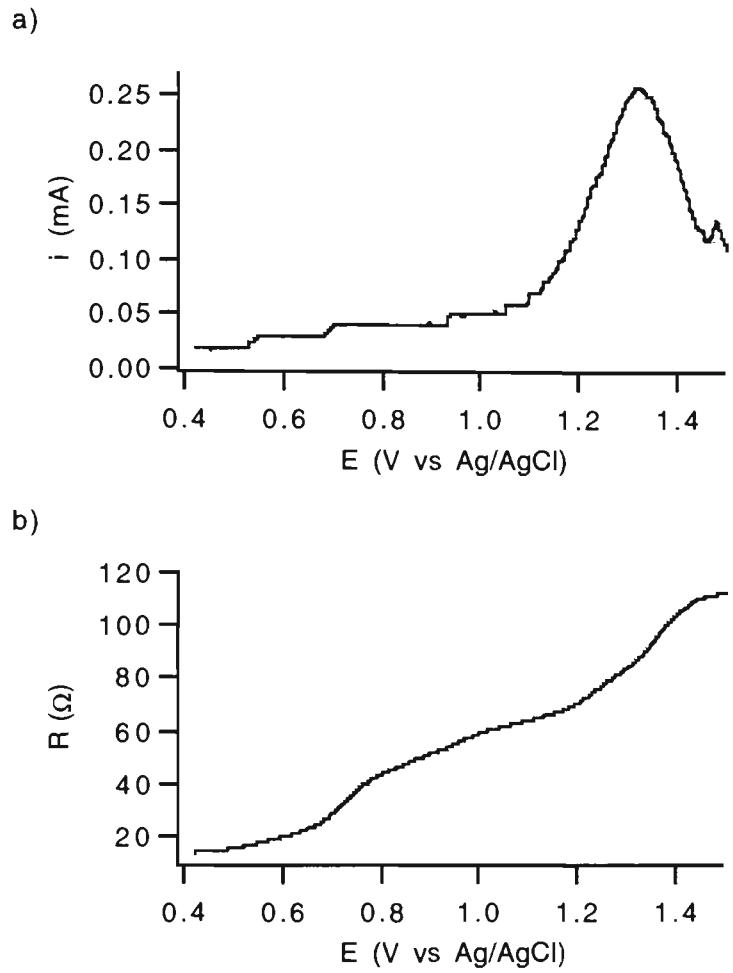

Figure 2.12: (a) LSV and (b) LSR output for 0.75 μm P(3-OPy)/BF_4 film scanned in 1 M $H_2SO_{4(aq)}$ at 2 mVs^{-1}.

As can be seen from Figure 2.12, the resistance began to increase for this P(3-OPy) film at a potential of 0.7 V and then rose rapidly until about 0.8 V. From other LSR experiments the curve shape up to this potential was similar to an un-substituted PPy, but would normally be expected to plateau at this point. However, in this case the resistance continued to increase reasonably rapidly with only slight current flow associated with these changes in resistance. The most likely explanation for this is that the small amount of water trapped in the polymer during growth (there were no special precautions taken to exclude it) is overoxidising part of the polymer. If this is the case then both the resistance and current changes appear normal, but somewhat delayed. This was confirmed by the

observation that the current began to increase, with the resistance curve lagging somewhat behind it, to generate a "normal" overoxidation response from about 1.15 V. As the current peak returned to its baseline, the resistance plateaued, allowing determination of the overoxidation potential at about 1.45 V. It is worth emphasising that even up to 1.60 V there was no apparent oxidation of water, indicating that the film is still coherent and strongly attached to the substrate. This was confirmed by a "scratch test" after the film was removed from the cell. Very good adhesion and a coherent film was found to be a feature of all substituted PPy films, even after they were held at potentials as high as 1.30 V for 60 min or 1.10 V for 180 min. A combination of all of these observations strongly indicates that these highly hydrophobic polymers are stable in water up to 1.1 V, a potential that would normally be regarded as extreme.

As BF_4^- is the least hydrophobic of these anions it was thought that the incorporation of anions having large hydrophobic regions would increase the stability of the P(3-OPy) films even further. This unfortunately was not the case and each of these anions gave very similar overoxidation potentials (1.1 to 1.4 V) and stabilities over extended periods to those determined for BF_4^-. It is possible that BF_4^-, being a small ion with high charge density, happens to be an optimum fit in P(3-OPy) and there is no particular advantage to the incorporation of the larger, more hydrophobic ions.

The overoxidation results determined for P(3-OPy) films were highly variable, as indicated in Table 2.20. This variation in overoxidation potential is largely attributed to the high variation in growth observed in this series of experiments, and could almost certainly be rectified by better solvent selection. However, of utmost importance here is the fact that in all cases where the potential was held below 1.3 V (but above 1 V) the resistance remained near its plateau level (no drop of more than 30% over 60 min) and the film retained excellent adhesion and coherence over periods of up to 180 min.

Table 2.20: Overoxidation potentials determined for various P(3-OPy)/A, approximately 0.7 μm thick, scanned in 1 M H_2SO_4 at 2 mVs^{-1} on GC or Pt.

Anion	Overoxidation Potentials Determined (V vs Ag/AgCl)
BF_4^-	1.2, 1.3, 1.4
pTS	0.8,0.8, 1.1
SDS	0.8, 0.9, 1.1, 1.1

2.4 CONCLUSION

This chapter described a new technique, simultaneous linear sweep voltammetry / resistometry (LSV / LSR), for the determination of the overoxidation potential of the conducting polymer polypyrrole. This technique has an advantage over many others employed for the study of the degradation of CEPs in that it is an in-situ technique able to operate in the environment most relevant to conducting polymer applications - water. This allows direct correlation between any electrical or chemical stimuli and the resistance changes of the bulk polymer. It also has the advantage of being based on a slow, ongoing, linear potential ramp and thus is not limited by the need to increment potential nor switching potentials, as in the case for potential step and cyclic voltammetric determinations, respectively.

The precision of the method was found to be excellent, with relative standard deviations of around ±0.02% being determined for one group of nine PPy films and ±0.03% for a second group of thirteen. It was also found that chemical and physical changes brought about by the application of any potential (eg 0.80 V) below the overoxidation potential were largely reversible in terms of both resistance and current responses. Furthermore, the charge passed during overoxidation, as defined by this technique, was found to be in excellent agreement with literature values (taking into consideration the initial oxidation state of the polymer in each case). Comparison of LSR with two other techniques, RRDE and chronopotentiometry, verified the accuracy of the method and highlighted the

usefulness of simultaneous LSV / LSR in observing the onset, progress and completion of PPy overoxidation. Chronopotentiometry studies also led to the observation that the degree of overoxidation of PPy films is not only dependent on the applied potential, but also the current density; with high current density effectively blowing the molecular wire fuses that are normally the charge carriers.

This new technique was then employed to study the effects of a wide range of variables on the overoxidation potential of polypyrrole: the incorporated counterion; the supporting electrolyte salt; substrate; growing solvent; scan rate; film thickness and ring substituents. With the exception of strong base (which halved the overoxidation potential of one polymer) and the inclusion of a hydrophobic substituent (which increased the overoxidation potential by about 30%), these variables generally altered the overoxidation potential within a range of about ±0.05 V(±5%) of the mean potential for each set. Based on current knowledge of PPy chemistry and the overoxidation mechanism and the chemical and physical properties of the variants within each group, explanations of these results were postulated.

The anions incorporated during growth included: the halogens Br^-, Cl^-, F^- and I^-; small, non-electroactive (in this potential region) mono-anions, NO_3^- and BF_4^-; a dianion, SO_4^{2-}; the sulphonated mono-anions pTS and DS; the sulphonated dianion Tir and the sulphonated multi-anion PVS. Within the halogen group, I^- exhibited the highest overoxidation potential due to its ability to reduce oxidising intermediates, Br^- recorded the lowest due to its high nucleophilicity; and Cl^- and F^- were intermediate, as expected for Cl^-, but not F^-. Fluoride was expected to have an overoxidation potential similar to that of Br^-, due also to its nucleophilic nature. However it was necessary to grow PPy/F potentiostatically instead of galvanostatically, which was believed to alter the stability of the resultant polymer in some way.

The sulphonated anions, including sulphate itself, recorded overoxidation potentials that were related to their charge. Sulphate and all sulphonated anions enhance the degree of molecular order when incorporated into PPy and so were expected to exhibit high overoxidation potentials. This was the case with the sulphonated mono-anions, pTS and DS, which generate highly ordered polymers that limit diffusion during any electrochemical process, including overoxidation. This was reflected in the high overoxidation potentials of these materials. Di- or multi-charged anions, on the other hand, decreased stability once overoxidation commenced due to the disruption caused by the plurality of their charges and the resultant difficulty in compensating these charges in a polymer during overoxidation. Alternatively, multi-anions tend to concentrate the most reactive sites in the polymer chain, the polarons and bipolarons, and this may enhance overoxidation at these sites.

Between these groups, the only obvious trend was that the sulphonated mono-anions generally enhanced the stability of PPy, largely due to the high degree of ordering they impart to the polymer, generally giving PPy/pTS and PPy/DS the highest overoxidation potentials determined for the anions. At the other end of the scale, the effects of the plurality of charge on Tir, PVS and SO_4^{2-} dictated that PPy containing these ions had amongst the lowest overoxidation potentials, with only the strong nucleophile Br^- exhibiting similar ease of overoxidation.

Possibly one of the most significant revelations in this chapter was that the lyotropic series has, when the ions within the series are ranked by a suitable means, direct application to conducting polymer chemistry. The lyotropic series ranks both anions and cations according to their interactions with proteins in solution, with water-ordering kosmotropes encouraging the folding and precipitation of proteins, and water structure-breaking chaotropes encouraging proteins to unfold and solubilise. The ranking of ions within this series is of significance to this study as water (or its derivative OH^-) is the species most likely to initiate overoxidation of PPy. Among the impacts of the lyotropic

series is the organisation of waters around both the hydrophobic region of polymers and in the bulk solution.

Based on interactions with proteins, cations and anions are ranked in the lyotropic series in the following order, kosmotropes to the left, chaotropes to the right:

$$(CH_3)_2 NH_2^+ > NH_4^+ > K^+ \approx Na^+ > Cs^+ > Li^+ > Mg^{2+} > Ca^{2+} > Ba^{2+}$$

$$F^- > PO_4^{3-} > SO_4^{2-} > CH_3COO^- > Cl^- > Br^- > I^- > SCN^-.$$

Among a number of parameters that can be used to rank ions within this series, it was found that the molal surface tension increment (σ) gave excellent agreement with the experimental results obtained in this work on polypyrroles. Within certain limitations, it was found that the lyotropic series based on σ predicted that PPy films would be more readily overoxidised in the presence of NH_4^+ and K^+ compared to Na^+, and of Sr^{2+} and Mg^{2+} compared to Ca^{2+}. This was in perfect agreement with the experimental results.

One of the main advantages of using molal surface tension increments to determine the ranking of ions in the lyotropic series is that it takes into account both the cation and anion of the supporting electrolyte. As such, its application to PPy overoxidation was further validated by its prediction that (again within certain limitations) PPy would be more readily overoxidised in a solution of NO_3^- than one in Cl^-, as was found to be the case.

Considering that anions have larger kosmotropic or chaotropic effects than cations and that the range of anions employed in CEP studies is often broader than the range of cations used, it is expected that the lyotropic series may have a far greater impact on the conformation of conducting polymers than is currently recognised. When the most appropriate determination of the ranking within this series is employed, remembering that it was originally based on the interactions between salts and proteins in solution, it may well have broad application to conducting polymer chemistry.

The effects of strongly acidic and basic conditions on the overoxidation potential were also studied. Based on the assumption that the most significant mechanism of overoxidation of PPy would be nucleophilic attack by OH^-, it was assumed (contrary to a number of other authors who claimed that high concentrations of acid destabilised PPy) that at low pH (approaching 0) overoxidation would be retarded. Again, within certain constraints, this was found to be the case, with PPy films in 1 M acid generally having the highest overoxidation potential within a group of like experiments. The most significant impact on overoxidation potential was found to be that of OH^-, with reasonable concentrations (0.1 M) more than halving the potential at which a film lost the ability to carry current.

Another significant impact on the measured overoxidation potential with possible wider implications was that of the substrate material. It was observed that almost without exception polymers grown on Pt have a lower overoxidation potential than those grown on either Au or GC. This was explained by the ease of aerial oxidation of Pt, allowing the formation of oxygen linkages between PPy and the substrate. Overoxidation was then easier, due to better electron transfer, and possibly better physical contact through these oxygen linkages. The presence of these oxygens on the surface of Pt was also invoked to explain the difficulties of growing hydrophobic (substituted) PPys on this material compared to Au and GC. Finally on the matter of substrates, it was noted that a very high proportion of all non-substituted PPys grown on gold tended to give double or ill-defined resistance "peaks", almost certainly due to the propensity of gold to form stable complexes with a range of chemical species, including Cl^- and possibly some products of the overoxidation of PPy.

As overoxidation involves chemical reactions reliant on diffusion through a solid under the influence of a potential ramp, the effects of film thickness and scan rate were obviously germane. It was found that the overoxidation potential was linearly related to the square root of the scan rate and the square of the film thickness, as expected by

extrapolation of ion diffusion studies in PPy in the normal reversible redox domain. Studies in the current work also proffered a limiting overoxidation potential, *the inherent overoxidation potential*, which, for any given polymer / counterion / supporting electrolyte system, allowed determination of the overoxidation potential at zero scan rate. The plot of scan rate against overoxidation potential for a number of polymer / supporting electrolyte systems also led to clear evidence that (due to the high degree of order created by the counterion employed) PPy/pTS films had a marked stability advantage over other, less ordered polymers regardless of the supporting electrolyte / counterion combinations.

The final factor investigated was the contribution of ring substituents to the overoxidation potential. It was believed that by blocking both the 3- and 4- positions of PPy, overoxidation would be inhibited and the effective working range of these materials could be extended. However, P(MPyC) was found to exhibit a very similar overoxidation potential to unsubstituted PPys examined under similar conditions. Subsequently the overoxidation potential of pyrrole containing a hydrophobic substituent group ($-C_8H_{15}$) was determined. Due to the high hydrophobicity of the side chain, this material was found to have a very high overoxidation potential (up to 1.4 V) and, even after extended periods at potentials of around 1.1 to 1.2 V, retained excellent adhesion to the substrate and constituted a coherent, viable conducting polymer film.

CHAPTER 3: UV-VISIBLE SPECTROSCOPIC STUDIES

3.1 INTRODUCTION

The earliest reports of the use of ultraviolet-visible spectroscopy (UV-vis) to elucidate the changes in structure of electrochemically grown PPy during its oxidation and reduction were by Diaz et al [80], Street [46] and Yakushi et al [116] in the early 1980's. Diaz employed indium - tin oxide (ITO) coated glass substrates for PPy growth. These were largely ex-situ studies, with the polymer being oxidised or reduced before scanning. At about the same time, Feldblum et al reported an in-situ infra-red study of the doping / dedoping of polyacetylene [227], in which the polymer was electrochemically cycled while held in the light path. Since then, UV-vis studies have been applied to PPy for in-situ investigation of: growth [45, 46, 228-230], redox properties [60, 109, 231, 232], conduction mechanism [233, 234], acid / base treatment [22, 61, 121, 123, 144, 235], cast films [236-238], substituent groups [115, 135, 223], structure [124, 239] as well as organometallic copolymers [111, 240-242] and composite materials [243].

The development and commercialisation of the diode array UV-vis spectrometer, capable of collecting the complete spectrum "instantaneously", have allowed the recording of in-situ spectra during electrochemical or chemical processes. These instruments have been employed in studies of PPy by a number authors, including: organometallic copolymers [241] aerial oxidation [244], substituted PPy [115], oxidation and reduction studies [103], stability of reduced PPy [245] and the study of overoxidation [246].

In-situ diode array UV-vis was employed in the current work to monitor the overoxidation of PPy as a function of applied potential and pH. In the first instance a range of fixed potentials (0.60 to 1.10 V vs Ag/AgCl) was applied to films in a constant ionic strength supporting electrolyte (pH of 2.25) and the absorbance between 300 and

820 nm was monitored over time. In the second case a potential of 0.80 V (vs Ag/AgCl) was applied to films in constant ionic strength supporting electrolytes with a range of pHs (0 to 11) and the UV-vis spectra were monitored over time. A later series of experiments were performed in which the absorbance was monitored at a single wavelength under temperature control (±0.2 °C)to allow determination of the rate constant and the activation energy of overoxidation.

3.2 EXPERIMENTAL

3.2.1 Reagents and materials

All chemicals used were analytical reagent grade unless otherwise stated. Pyrrole (Sigma) was distilled before use and stored at -16 °C in the dark under N_2 where necessary. Water was Baker Analysed HPLC Grade (J. T. Baker Inc, USA) or reagent grade obtained from a Millipore Milli-RO/Milli-Q™ water purification system.

Electrodeposition and characterisation of polymer films were carried out on ITO-coated glass with a resistance of 300 Ω/square (Samsung) or 40 Ω/square (Delta Technologies Ltd). ITO has similar advantages to Pt as substrate in that it also forms direct linkages to PPy [247], which gives excellent electrical and physical contact between the film and the substrate. The auxiliary electrode was fabricated from a platinum sheet (Engelhard), by cutting a slot to accommodate the light beam during spectroscopic characterisation. Platinum gauze or sheet (Engelhard) was employed as the auxiliary electrode during polymer growth. All potentials were measured against a narrow diameter Ag/AgCl reference electrode. This was constructed of Ag wire (Engelhard) (previously dipped in concentrated HCl) in 3 M KCl saturated with $AgNO_3$ contained in a 1.5 mm internal diameter glass tubing fitted with a porous frit and heat shrink teflon tube (Hart Analytical, Australia). This electrode was inserted directly into the supporting electrolyte solution.

3.2.2 Instrumentation

Electropolymerisation of polymer films was carried out using either a Yokoyawa Electric Works Ltd (Japan) YEW 2553, or an in-house, galvanostat. UV-vis spectra were collected by a Hewlett Packard (USA) 8452A Diode Array Spectrophotometer with the applied potential controlled by an EG&G Princeton Applied Research (USA) 362 Potentiostat at a laboratory temperature between 29 and 31 °C. Data were collected on a Hewlett Packard PC and processed on a Macintosh (Apple) computer.

Fixed wavelength kinetic studies were carried out on a Shimadzu 1601 Spectrophotometer while the potential was controlled by a BAS CV-27 potentiostat interfaced through a four channel Maclab (ADI, Australia) to a Macintosh (Apple) computer. In these experiments the cell compartment was thermostated (±0.2 °C) to suitable temperatures with a Braun Frigomix temperature control unit.

3.2.3 Procedures

The ITO glass was cut to size (9 x 40 mm), cleaned with chloroform, silanised for 30 s in 10 - 15 % A-189 silanising reagent (Union Carbide, USA) or 10 % 3-glycidoxypropyl-trimethoxy silane (Aldrich) in methanol, dried at 65 °C for 30 min and rinsed with methanol. An area of approximately 2 cm^2 was then masked off with contact adhesive (3M, USA) or teflon tape (T&F, USA) to prevent etching of the ITO at the growing solvent / air interface during growth and to give a reproducible film area.

PPy was electrodeposited galvanostatically with a current density of 1 $mAcm^{-2}$ for 50 s from a solution of 0.36 M pyrrole and 0.036 M counterion in H_2O (unless stated otherwise) to give a film thickness of approximately 0.1 μm. After growth the polymer films were rinsed thoroughly with Milli-Q water and inserted into a 1 cm quartz cuvette fitted with the Pt auxiliary and Ag/AgCl reference electrode, see Scheme 3.1. All growth and characterisation were performed in air, which is claimed not to have a significant impact on the stability and electrochemistry of PPy films [57, 58]. For this and the

remaining chapters no film forming cycles were performed before overoxidation was commenced.

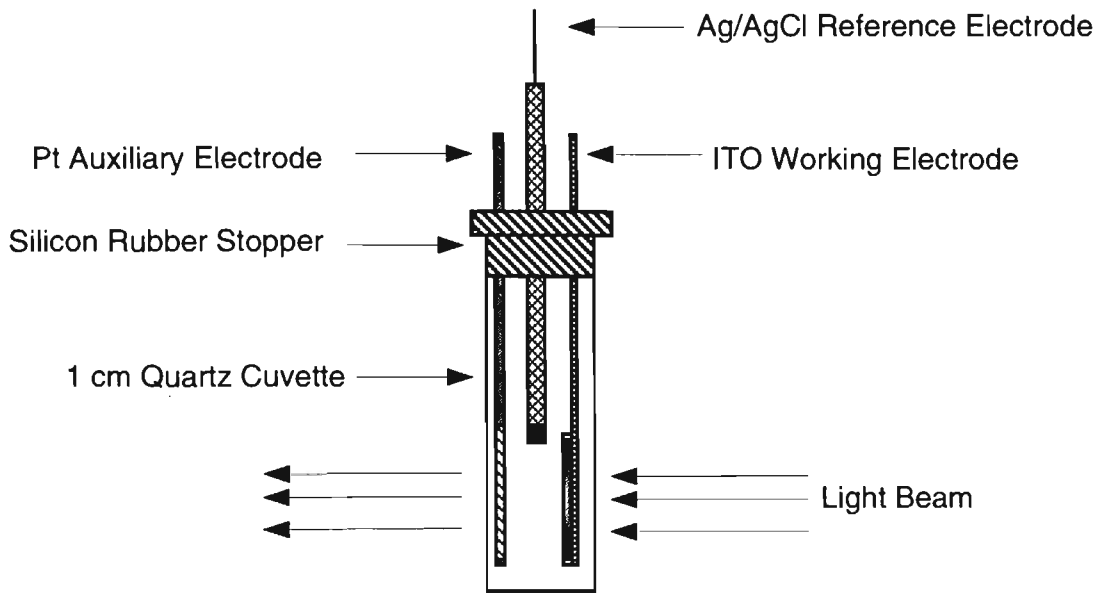

Scheme 3.1: The three electrode cell employed for in-situ UV-vis characterisation, originally reported by Tezuka et al [230].

The films were characterised in solutions of NaCl or Na_2SO_4 having a total ionic strength of 2 M after pH adjustment with HCl (in the case of NaCl), H_2SO_4 (in the case of Na_2SO_4) or NaOH where necessary. The solutions were unbuffered to avoid the presence of ions other than Na^+, Cl^-, SO_4^{2-} or OH^- during characterisation. Table 3.1 lists the concentrations of HCl, NaCl and NaOH used and the measured pHs of these solutions.

Supporting electrolytes based on SO_4^{2-} were made up of 1 M Na_2SO_4 (pH 5.5), 0.90 M Na_2SO_4 / 0.10 M H_2SO_4 (pH 0.7) and 1 M H_2SO_4 (pH ~ 0).

Unless otherwise stated, spectra were collected at the time intervals given in Table 3.2. The "Pristine" spectrum was collected at rest potential immediately after the as-grown film was placed in the relevant supporting electrolyte, throughout this and the remaining chapters the term "Pristine" is used to describe the "As Grown" film, indicating no treatment other than rinsing to remove traces of monomer and excess dopant. The "Time

Zero" spectrum was collected immediately after the appropriate potential was applied. In the case of films that were overoxidised in less than 30 min, scanning was ceased when the absorbance changes appeared to stabilise.

Table 3.1: Concentrations of HCl, NaCl and NaOH employed and the measured pHs of the resulting solutions.

NaCl concentration (M)	HCl concentration (M)	NaOH concentration (M)	Measured pH
0.500	0.500	-	~0
0.950	0.050	-	1.43
0.995	0.005	-	2.25
1.000	-	-	6.24
0.995	-	0.005	11.03

Table 3.2: Time intervals for the collection of UV-vis spectra during overoxidation.

Scan Number	Time (min)	Scan Number	Time (min)	Scan Number	Time (min)
1	Pristine	8	1	15	11
2	0	9	2	16	13
3	0.16	10	3	17	15
4	0.33	11	4	18	20
5	0.50	12	5	19	25
6	0.66	13	7	20	30
7	0.83	14	9		

Based on the work discussed in Chapter 2, 0.8 V (vs Ag/AgCl) was chosen for the "constant potential / variable pH" experiments in the current chapter as it would both allow sufficient time to observe spectrophotometric changes during overoxidation and would completely overoxidise the film in a reasonable time. For similar reasons, after the

constant potential experiments, a pH of 2.25 was chosen for "constant pH / variable potential" experiments.

3.3 RESULTS AND DISCUSSION

3.3.1 Changes in the UV-vis spectra during overoxidation

Figure 3.1 shows the UV-vis spectra obtained during the overoxidation of PPy/DDS with an applied potential of 0.80 V in 1 M Na_2SO_4 at pH 5.5.

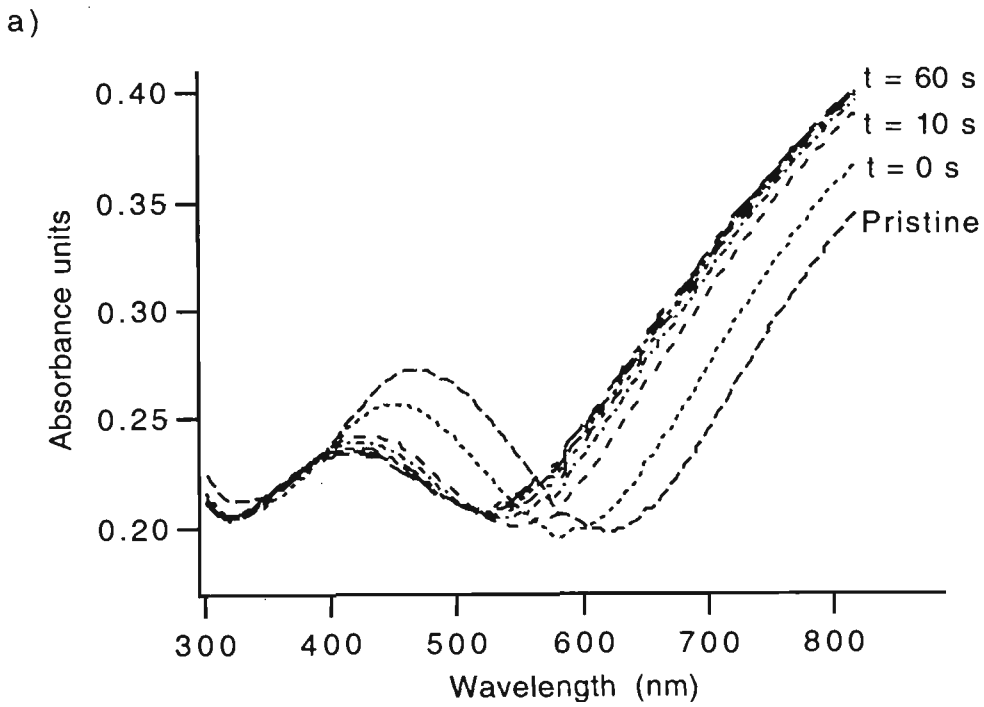

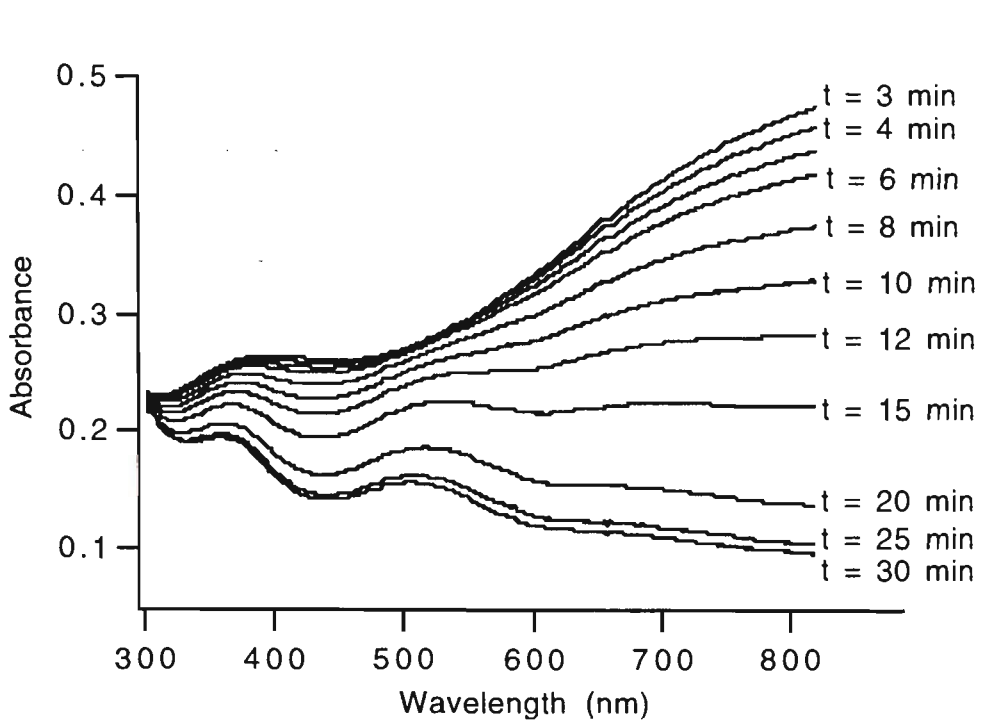

Figure 3.1: PPy/DS on ITO-glass held at 0.80 V (vs Ag/AgCl) in 1 M Na_2SO_4, pH 5.5, (a) spectra collected over the first minute, (b) spectra collected from 3 to 30 min.

Figure 3.1(a) shows the spectra of the pristine film and those collected over the first minute at an applied potential of 0.80 V. These spectra exhibited a number of features associated initially with the progressive doping of the polymer from the as-grown state to a fully doped state, followed by the loss of the highly conjugated system during overoxidation shown in Figure 3.1(b). Among the features associated with full doping is the development of a "free carrier tail", first reported for conducting polymers by Patil, Heeger and Wudl [110], at wavelengths around 800 nm. This peak is associated with valence band to bipolaronic band transitions [45, 108, 242, 245] and, at higher degrees of oxidation, broadens to shorter wavelengths [115]. This hypsochromic peak shift, also observed around 650 nm during the full oxidation of PAni by Brandl [248], is associated with decreasing conjugation length of that polymer as the maximum number of bipolarons are formed.

For scans from t = 10 s to t = 60 s an isosbestic point was observed at about 520 nm (Figure 3.1(a)), indicating that, after the two initial scans, there was no change in

stoichiometry involved in the full doping of the film and that these conversions involve only electron movement [249]. This is expected as the process at this point is simply one of full oxidation. The two initial scans which did not pass through this isosbestic point clearly involve some other chemical process, including a physical change as the film volume increases. This would lead to a change in the chemical environment within the film due to the influx of supporting electrolyte ions associated with full oxidation [41]. Chemical and physical changes during these initial scans are further complicated by the dissimilar anions involved, with DDS incorporated during growth and SO_4^{2-} incorporated from the supporting electrolyte.

The peak at 480 nm in the pristine film corresponds to a valence band to anti-bipolaron band transition [245] in a lightly doped bipolaron state [66]. Decrease in the height of this peak and its associated blue shift are due to reduction in the number of polarons as the polymer is fully doped.

At later reaction times clear isosbestic point was observed at 400 nm, between wavelengths associated with the presence of the neutral polymer and the polaronic state. The $\pi - \pi^*$ transition in the fully conjugated neutral polymer should be observed at 400 to 420 nm [108, 242, 245, 250], but is almost completely absent in the as-grown polymer due to its moderately high oxidation level. Osaka et al report that the absorbance associated with the $\pi - \pi^*$ transition, centred at 390 nm in his work on PPy/Cl in NaCl, increases during a linear scan (at 2 mVs^{-1}) up to 0.7 V [61]. This was also observed in the present work in the first 60 s at 0.80 V, as can be seen in Figure 3.1(a) at 350 to 400 nm.

Osaka further noted that the bipolaron band, centred at 760 nm in his study, increases with potential from -0.6 to 0.7 V, then decreases rapidly from 0.7 to 1.0 V and then more slowly from 1.0 to 1.5 V [61]. This decrease is associated with loss of conjugation and chemical integrity of the polymer as it is overoxidised. Figure 3.1(b) shows such a loss of the bipolaron state during scans from t = 3 min through to t = 30 min for PPy/pTS. The

absorbance approached a minimum at the end of this period as indicated by the closeness of scans at t = 25 and 30 min. During UV-vis studies of extended overoxidation of PPy at 1 V, Park observed a number of overoxidation products in solution, including a carbonyl containing organic group absorbing at 272 nm and a somewhat conjugated material at 217 nm [144]. Even though the current work was limited to a minimum wavelength of 300 nm, it would appear from Figure 3.1(b) that after 30 min at 0.8 V some polaronic (red shifted to about 500 nm [238]) and conjugated (390 nm [61]) species are present either in solution or in the film. In both cases these would be present as short chain length products of overoxidation of the PPy film.

As the bipolaron transition region from 700 to 1300 nm is an excellent indicator of the oxidation state of PPy and is suitable for quantitative studies due to its linear realationship with charge [230], 800 nm was chosen to monitor overoxidation in the remainder of the work to be covered in this chapter.

3.3.2 The role of pH

In this section a constant potential of 0.8 V was applied to PPy films in a constant ionic strength supporting electrolyte of Na_2SO_4 or NaCl with the pH adjusted to various levels between 0 and 11 by the addition of H_2SO_4, HCl or NaOH. The UV-vis spectra of PPy/pTS in NaCl at various pHs collected over 30 min are given in Figure 3.2.

a)

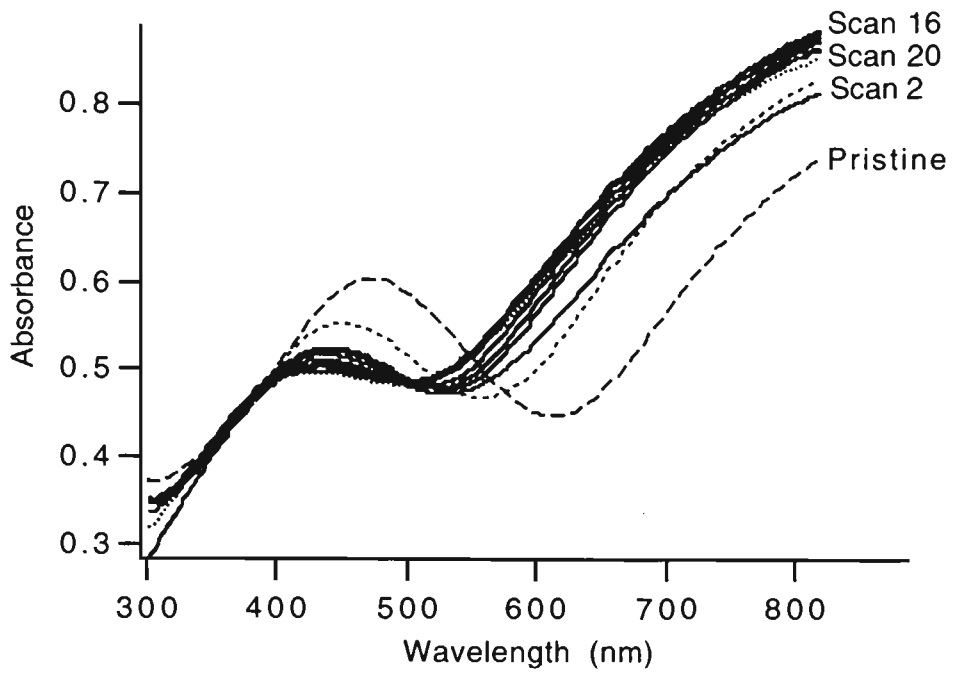
Scan 16
Scan 20
Scan 2
Pristine
Absorbance
0.8
0.7
0.6
0.5
0.4
0.3
300
400
500
600
700
800
Wavelength (nm)

b)

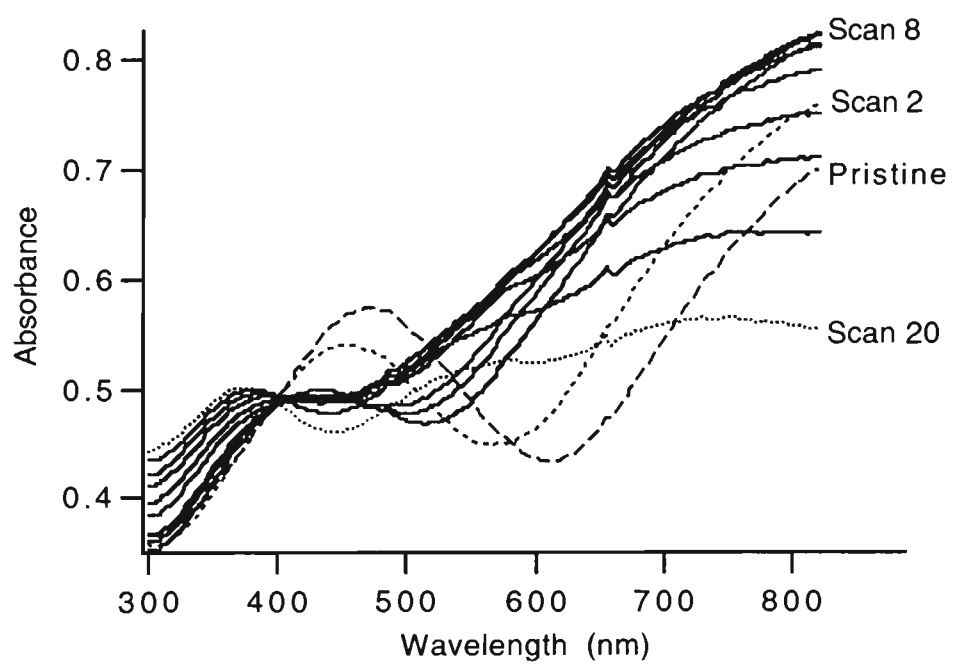
Scan 8
Scan 2
Pristine
Scan 20
Absorbance
0.8
0.7
0.6
0.5
0.4
300
400
500
600
700
800
Wavelength (nm)

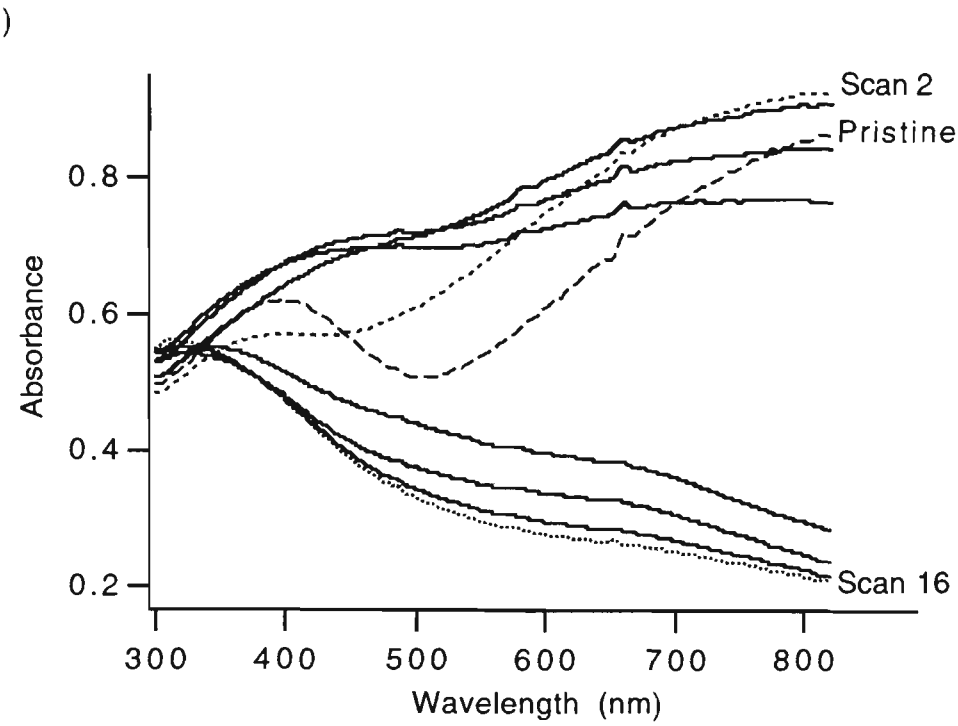

Figure 3.2: PPy/pTS on ITO glass held at 0.80 V (vs Ag/AgCl) in 1 M Cl^- solutions adjusted to a pH of: (a) ~ 0, (b) 2.25 and (c) 11.05. Only every second scan after t = 0 is shown for clarity.

The influence of the supporting electrolyte pH on the rate of overoxidation is clear from Figure 3.2(a), (b) and (c). At pH ~ 0, the bipolaron band around 800 nm barely decreased below the fully doped state after 30 min (Scan 20). In contrast to this, the absorbance at 800 nm had dropped to nearly half of its maximum value after 30 min in pH 2.25, and appeared to approach its minimum after only 13 min at pH 11.05.

At pH ~ 0 the polaron band (400 to 450 nm) was still evident as a shoulder after 30 min, while at pH 2.25, it disappeared completely after about 1 min. It is significant though that this band initially appeared in the same wavelength region (450 to 500 nm) and was blue shifted to the same region (400 to 450 nm) during full doping in both cases. At pH 2.25 a peak also appeared after about 7 min (Scan 13) in the $\pi - \pi^*$ transition region (around 390 nm) as overoxidation progressed and this was not observed at pH ~ 0 even after 30 min. These observations indicate that full doping and the onset of overoxidation at these pHs occur by an identical mechanism, though more quickly at the higher pH.

At pH 11.05 however, it is clear that overoxidation proceeds rather differently. From Figure 3.2(c), full doping (as indicated by the absorbance at 800 nm) occurred very quickly with the maximum reached in Scan 2 (t = 0). Overoxidation then proceeded so quickly that by 13 min the absorbance associated with the bipolaron was approaching a minimum value. Similarly, the absorbances in the polaron and $\pi - \pi^*$ transition regions changed differently than was the case at the lower pHs. It has been observed that during base treatment at rest potential the polaron band is blue shifted to about 380 to 390 nm [22, 119] and that this is associated with dedoping [124] and poorer conjugation [122] of the polymer. In the presence of oxygen the dedoped polymer then undergoes overoxidation more readily [121], particularly under a high applied potential. From the spectra presented in Figure 3.3(c) this hydroxide dedoping followed by rapid overoxidation was also evident here. Even in the scan of the pristine film the polaron peak appeared at 390 to 400 nm and was further blue shifted in the fully doped polymer at time zero. No $\pi - \pi^*$ transition was evident at any stage during the overoxidation, indicating that even short conjugated materials were not present at high levels.

By following the absorbance at 800 nm it is possible to obtain at least a qualitative comparison of the rate of overoxidation of PPy films at various pHs. The results of one such experiment are presented in Figure 3.3. To facilitate discussion of the effects of pH, the maximum absorbance of each film was "normalised" against the maximum of the film with the highest absorbance in the set, as was the case for the remainder of this chapter. As it is the overoxidation stages of the reaction that are of interest here, the readings obtained during the initial "full doping" period (when the absorbance at 800 nm was increasing with time) have been omitted from the Figures for clarity.

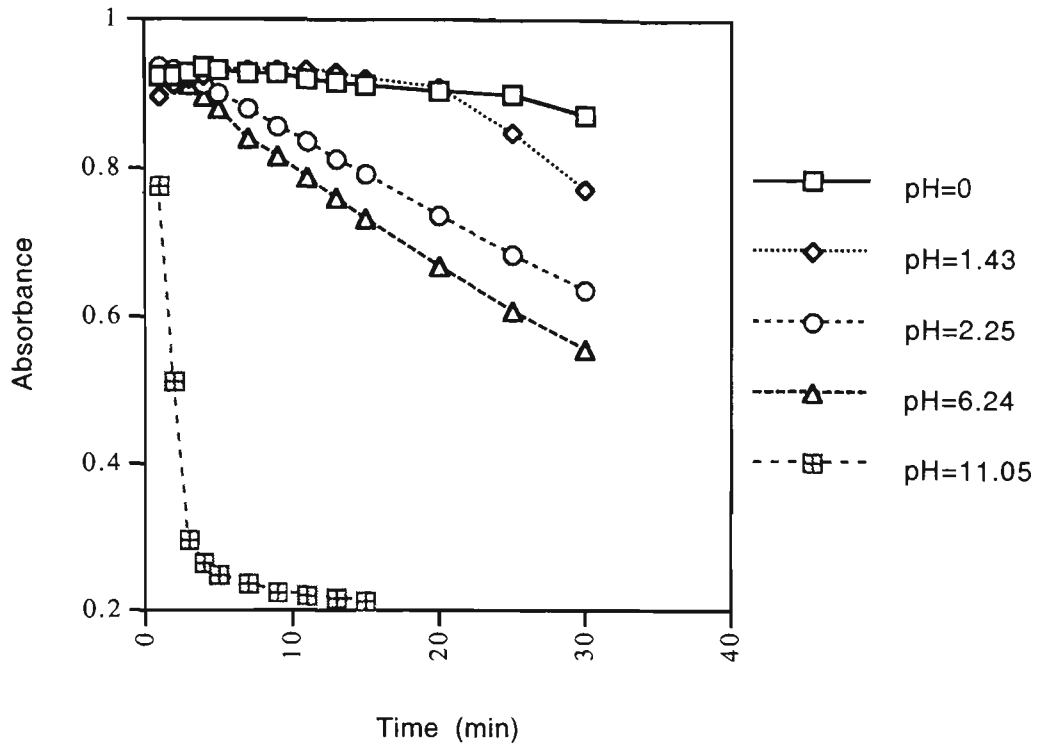

Figure 3.3: Normalised absorbance at 800 nm vs time for PPy/pTS films overoxidised at 0.8V in NaCl adjusted to various pHs. Results of Scans 1 to 8 have been omitted for clarity.

It is again apparent from Figures 3.3 and 3.4 that pH has a critical role in the overoxidation of PPy. At a pH approaching zero the extent of overoxidation is almost negligible for both PPy/pTS and PPy/Cl in Cl^-, as indicated by only small decreases in their absorbances over this period. However, even at a moderate pH of 6.24 (around the pH of most "neutral" aqueous solutions) these films lose about 50% of the absorbance associated with the bipolaron band in 30 min at 0.8 V. At pH 11.05 they approach total loss of this feature in about 10 min, as indicated by the absorbance approaching a minimum at this time. It is also clear from these figures that PPy/pTS is somewhat more stable than PPy/Cl, as discussed previously in Section 2.3.5.4, with smaller changes in absorbance over time for the same pH. Once begun, however, overoxidation in PPy/pTS appears to proceed linearly with time, as evidenced by a linear decrease in absorbance after 25 min at pH 0, 20 min at pH 1.43, 3 min at pH 2.25, 1 min at pH 1.43 and 20 s at pH 11.05. With the exception of pH 11.05 in Cl^- this phenomenon was not observed at

all in PPy/Cl. This indicates that the ordered, tightly packed structure of PPy/pTS initially resists overoxidation, presumably due to limited diffusion of the requisite ions or the increased hydrophobicity associated with the aromatic group. However, once the structure is opened up by the onset of overoxidation, it proceeds freely throughout the polymer.

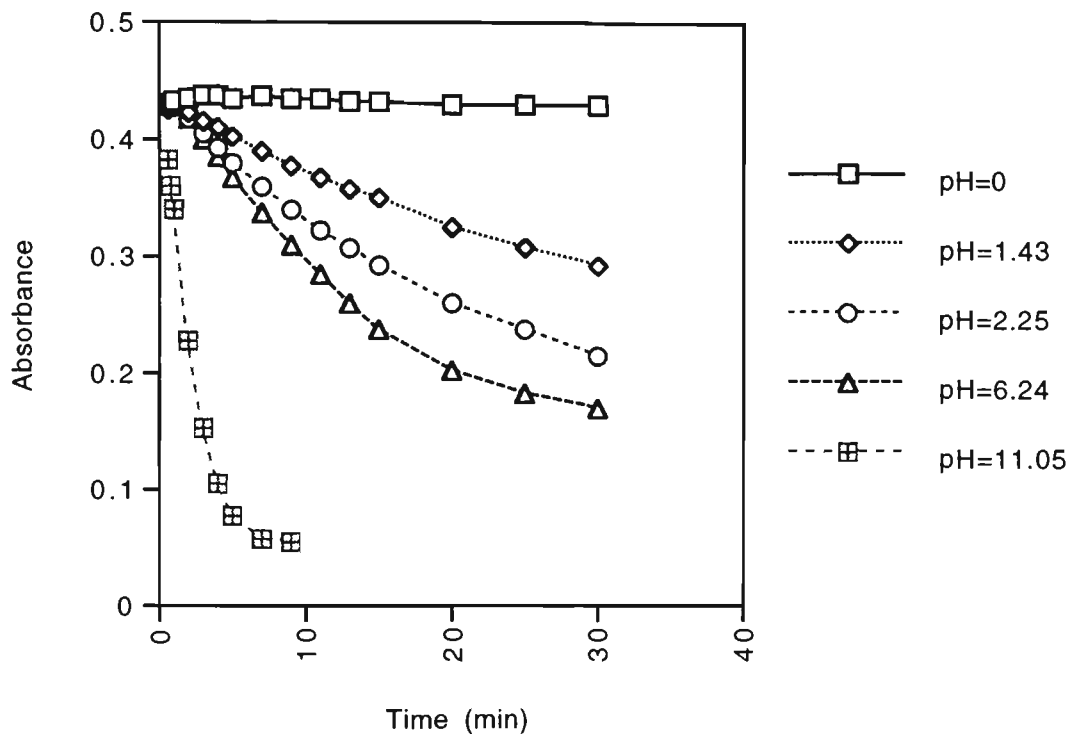

Figure 3.4: Normalised absorbance at 800 nm vs time for PPy/Cl films overoxidised at 0.8 V in NaCl adjusted to various pHs. Results of Scans 1 to 6 have been omitted for clarity.

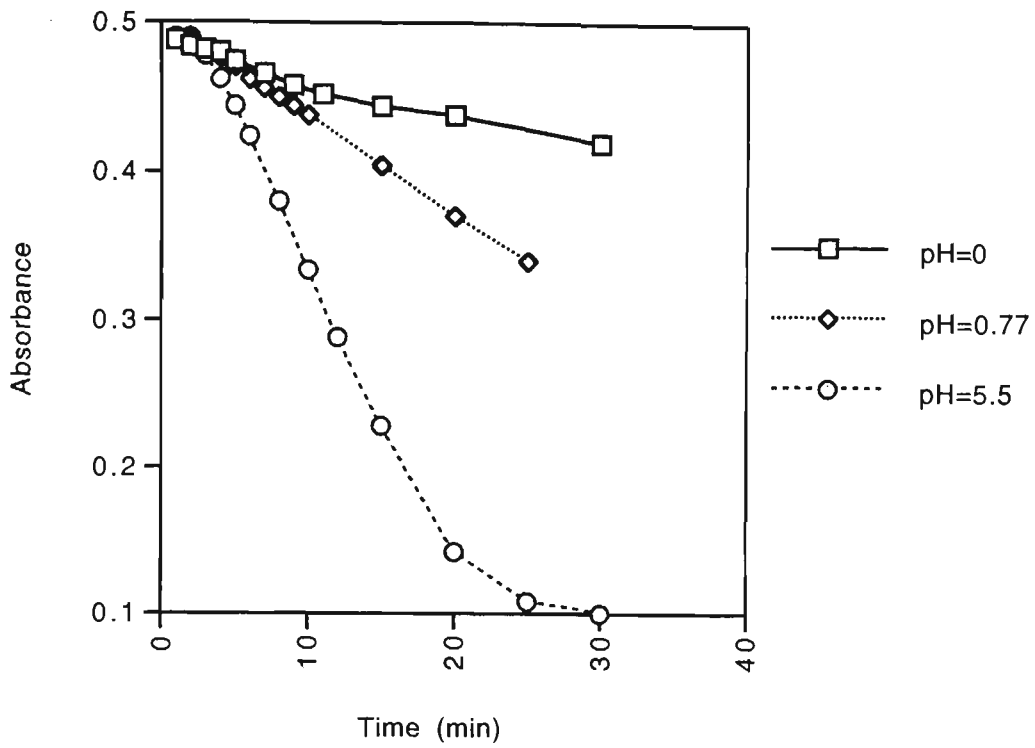

Figure 3.5: Normalised absorbance at 800 nm vs time for PPy/DS films overoxidised at 0.8V (vs Ag/AgCl) in H_2SO_4 adjusted to various pHs. Results of Scans 1 to 5 have been omitted for clarity.

In comparison to Figures 3.3 and 3.4, the results plotted in Figure 3.5 clearly show the disruptive nature of SO_4^{2-} when employed as a supporting electrolyte anion, as also discussed in Section 2.3.5.4. Even at a pH approaching zero (1 M H_2SO_4) overoxidation progressed more rapidly, as indicated by a decrease in absorbance of about 15% over 30 min, than was observed in 1 M HCl (with a decrease of about 7% over 30 min). At pH 0.77 the degree of overoxidation in SO_4^{2-} approaches that measured at pH 2.25 in the presence of Cl^-, while at pH 5.5 it approaches that determined at pH 11.05 in the chloride system. This is despite the fact that PPy/DS is among the most ordered, close packed and stable polypyrroles, with a degree of ordering approaching that of PPy/pTS and greater than PPy/Cl [58]. The increased ease of overoxidation in SO_4^{2-} media then is directly associated with the ingress of these ions during overoxidation and its effects on charge balance or charge carrier concentration in the polymer during overoxidation.

From this work, it is obvious that pH has a significant influence on the rate of overoxidation of PPy. However despite considerable effort it was not possible to establish a clear mathematical relationship between the two. This will be pursued in Section 3.3.5 by employing an broader range of pHs monitored only at 800 nm under rigorous temperature control.

3.3.3 The role of applied potential

In this section UV-vis spectra were collected during the application of various constant potentials to PPy/pTS films in a constant ionic strength Cl^- supporting electrolyte solution at a pH of 2.25. Figure 3.5 presents the spectra collected at 0.60, 0.90 and 1.10 V.

Even at a low applied potential (0.6 V) in acidic conditions (pH 2.25), the film showed (Figure 3.5(a)) a small but discernible amount of overoxidation after 30 min. This was indicated by a small decrease in the bipolaron absorbance at 800 nm towards the end of this period. The presence of a blue shifted polaron band, initially at 450 to 500 nm, and the small increase in the $\pi - \pi^*$ band around 390 nm, also indicated that overoxidation was in its initial stages.

a)

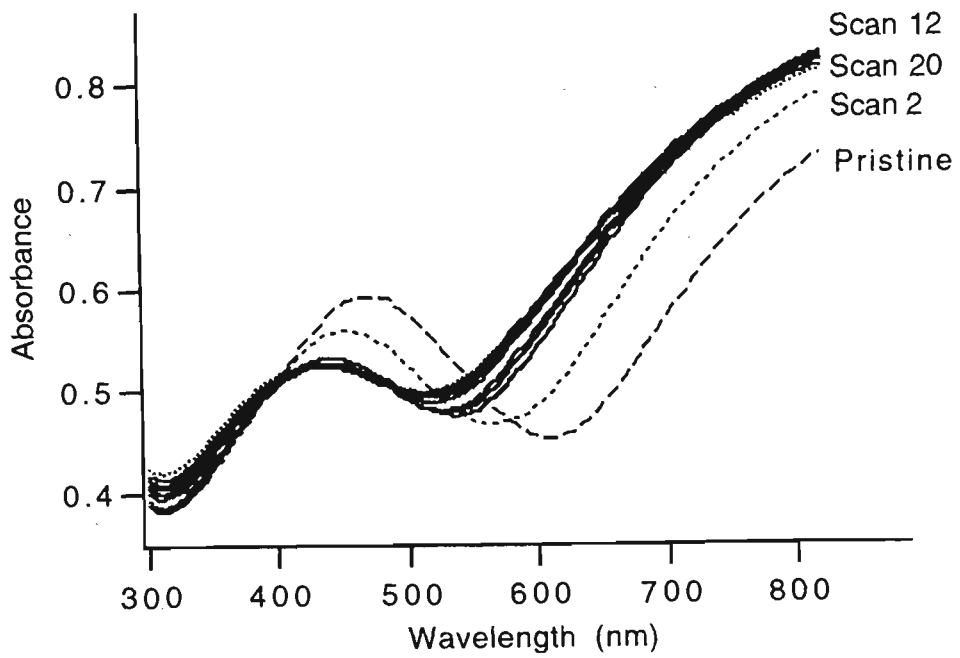
Scan 12
Scan 20
Scan 2
Pristine
Absorbance
0.8
0.7
0.6
0.5
0.4
300
400
500
600
700
800
Wavelength (nm)

b)

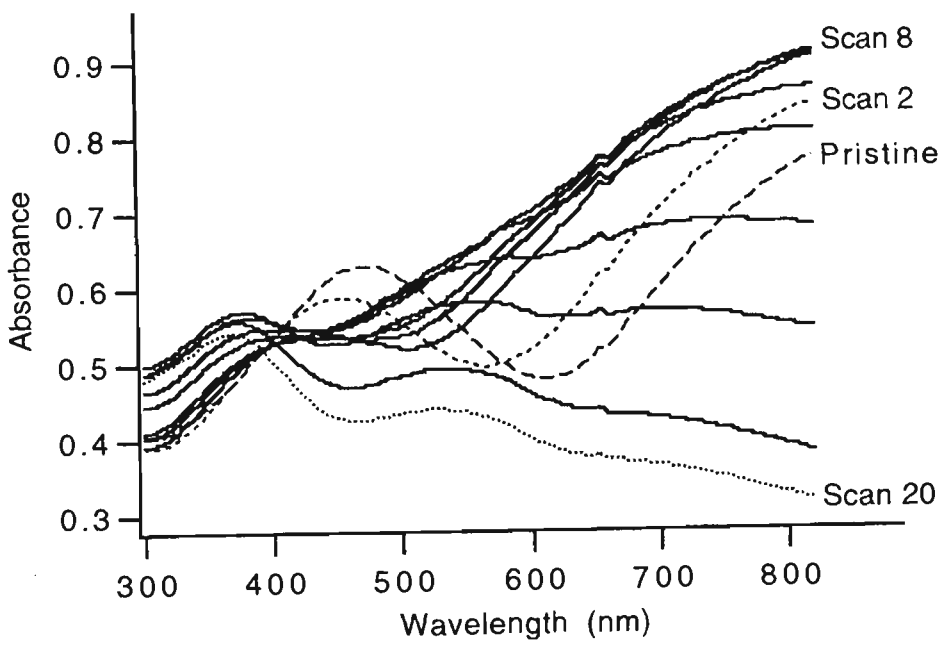
Scan 8
Scan 2
Pristine
Scan 20
Absorbance
0.9
0.8
0.7
0.6
0.5
0.4
0.3
300
400
500
600
700
800
Wavelength (nm)

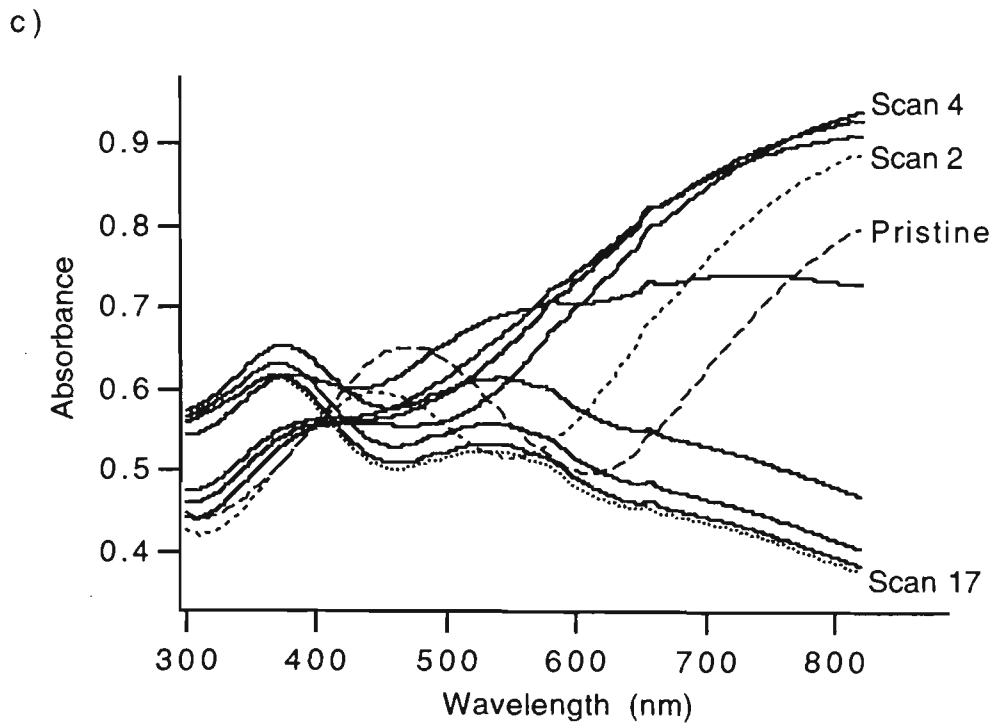

Figure 3.5: PPy/pTS on ITO glass overoxidised in 1 M NaCl at pH 2.25 with an applied potential of: (a) 0.6 V, (b) 0.9 V and (c) 1.1 V (vs Ag/AgCl). Only every second scan after t = 0 is shown for clarity.

Figures 3.5 (b) and (c) clearly show the increasing rate of overoxidation with increasing potential. For the former, the bipolaron band reached a maximum absorbance after only 8 scans (60 s) and the latter required only 4 scans (0.33 s). This band then decreases in intensity as overoxidation proceeds and effectively attained its minimum after only 15 min at 1.1V. Associated with this, and also indicating rapid overoxidation, was the complete disappearance of the polaron band (450 - 500 nm) after only 2 scans in both cases with no apparent blue shifted stage (around 390 nm). The neutral $\pi - \pi^*$ band and the red shifted polaron band (500 - 550 nm), indicative of poor doping levels [249], was observed from scan 10 in both cases, growing more rapidly under the higher potential.

As was done in Section 3.3.2 plots of "normalised" absorbance at 800 nm against time to allow an analysis of the effects of applied potential on the rate of overoxidation of PPy. Again, readings obtained during the initial "full doping" period, where absorbance at 800

nm increases with time, have been omitted from the graphs for clarity. Figure 3.6 gives such plots for a range potentials applied to a PPy/pTS film in NaCl at pH 2.25.

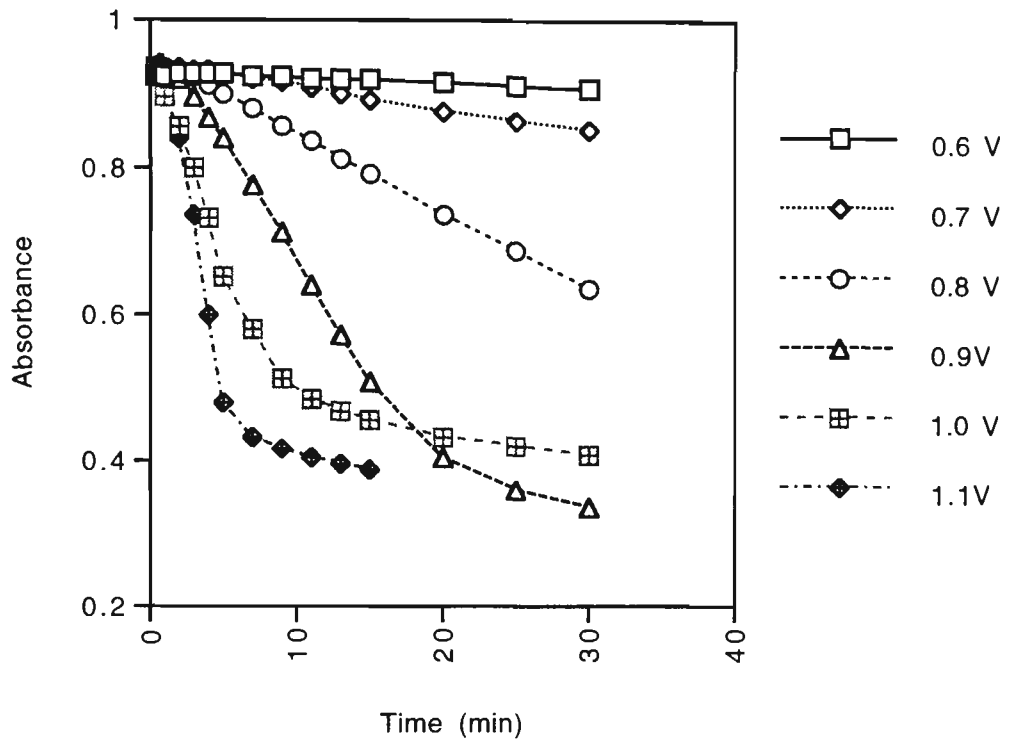

Figure 3.6: Normalised absorbance at 800 nm vs time for PPy/pTS films overoxidised at various potentials (vs Ag/AgCl) in 1 M NaCl at pH 2.25. Results of Scans 1 to 4 have been omitted for clarity.

From Figure 3.6 it is apparent that increasing potential markedly increases the rate of overoxidation. At 0.6 V there was little overoxidation evident after 30 min, whereas at 1.0 V overoxidation appeared to be nearing completion after this period and at 1.1 V it was effectively complete after 15 min. The quantitative relationship between the rate of overoxidation and applied potential will be examined in Section 3.3.5.

3.3.4 Substituted PPy

In Chapter 2 it was observed that the disubstituted pyrrole 3-methylpyrrole-carboxylic acid (MPyC) offered no appreciable advantage over non-substituted PPy with regard to overoxidation stability. It was also noted that the mono-substituted 3-octylpyrrole (3-

OPy) exhibited a relatively high overoxidation potential, presumably due to its increased hydrophobicity compared to a non-substituted PPy. The UV-vis spectral changes of these two polymers during overoxidation are investigated in this section. Figure 3.7 gives the UV-vis spectra collected over 30 min during the application of 0.8 V to a P(MPyC)/BF_4 film grown galvanostatically at 1 $mAcm^{-2}$ from 0.05 M MPyC / 0.02 M TEA-BF_4 in 1:1 CH_2Cl_2:AcN solution.

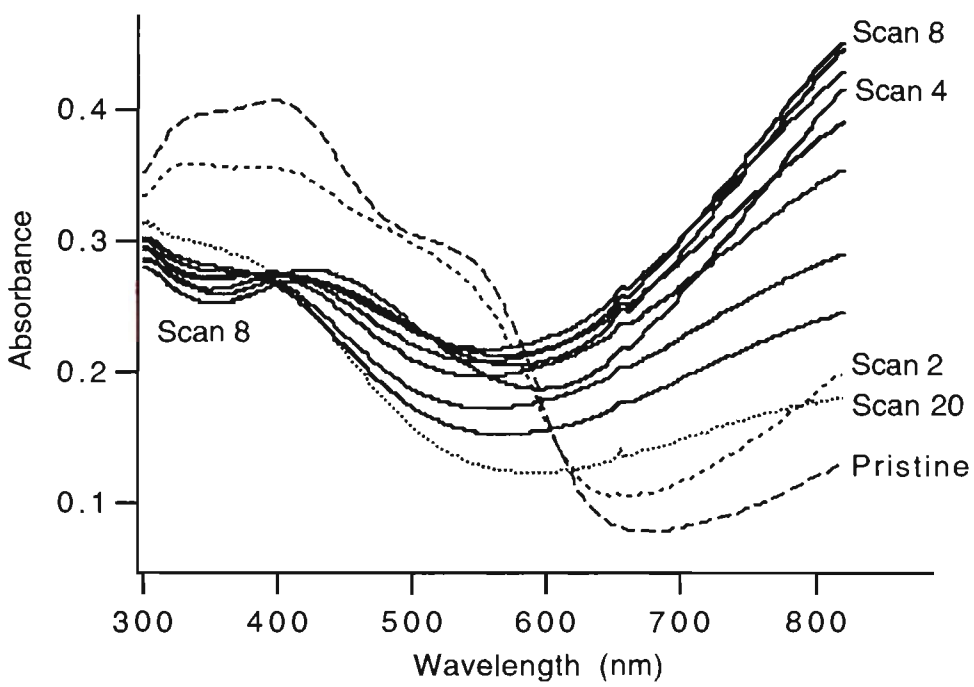

Figure 3.7: P(MPyC)/BF_4 galvanostatically grown from 0.05 M MPyC / 0.02 M TEA-BF_4 in 1:1 CH_2Cl_2:AcN on ITO glass and overoxidised in 1 M NaCl at pH 2.25 under an applied potential of 0.8 V (vs Ag/AgCl). Only every second scan after t = 0 is shown for clarity.

From the spectrum of pristine film in Figure 3.7, it is apparent that as grown P(MPyC)/BF_4 is very poorly doped. This is evidenced by very weak absorbance in the bipolaron region around 800 nm, very strong absorbance around 400 nm associated with the $\pi - \pi^*$ transition in the neutral polymer, and the presence of the polaron band at 500 - 550 nm as merely a shoulder on the $\pi - \pi^*$ peak. This low level of doping is presumably due to a combination of the broad range of conjugation lengths associated with substituted

pyrroles [135], the strong electron withdrawing nature of the carboxyl group [206] and poor planarity brought about by steric hindrance caused by the ring substituents.

As this polymer approached a fully doped state, as determined by the absorbance at 800 nm, its UV-vis spectrum more closely resembles that of a non-substituted PPy. In Scan 4 (Figure 3.7), along with significant absorbance at 800 nm, it exhibited a definite broad peak in the polaron region (400 - 450 nm) and the absorbance decreased around 350 nm. These absorbances were also roughly in the ratio expected for a fully doped non-substituted PPy. However, once the polymer reached the fully doped state, overoxidation proceeded quite rapidly, as indicated by the loss of absorbance at 800 and 400 - 450 nm and an associated increase in the region of 350 nm. Figure 3.8 displays the change in normalised absorbances at 800 nm for two P(MPyC)/BF_4 films in 1 M NaCl at pH 2.25 with applied potentials of 0.80 and 1.10 V.

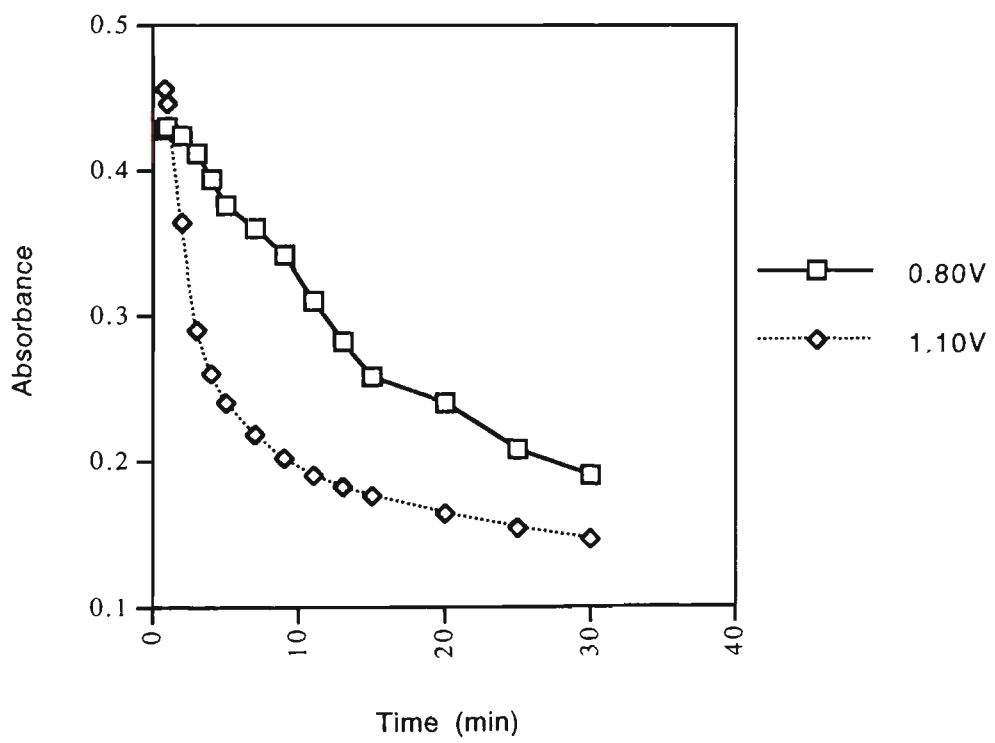

Figure 3.9: Normalised absorbance at 800 nm versus time for P(MPyC)/BF_4 films overoxidised at various potentials (vs Ag/AgCl) in 1 M NaCl at pH 2.25. Results of Scans 1 to 4 have been omitted for clarity.

Figure 3.8 emphasises the fact that P(MPyC), even though both the 3- and 4-positions are occupied, is more readily overoxidised than a non-substituted PPy. Over 30 min the absorbances at 800 nm for both 0.8 and 1.1 V decreased more rapidly than in the equivalent determinations given in Figures 3.4 (PPy/Cl) and 3.6 (PPy/pTS). However, as the UV-vis spectra after full doping and during overoxidation were almost identical to those obtained for non-substituted PPy during overoxidation, no explanation for this can be offered at this stage. This will be again considered in the Raman studies in Chapter 4.

Figure 3.9 gives the UV-vis spectra recorded over 30 min during the application of 1.1 V to P(3-OPy)/BF_4 grown galvanostatically at 1 $mAcm^{-2}$ from 0.05 M 3-OPy / 0.02 M TEA-BF_4 in 1:1 CH_2Cl_2:AcN on ITO glass.

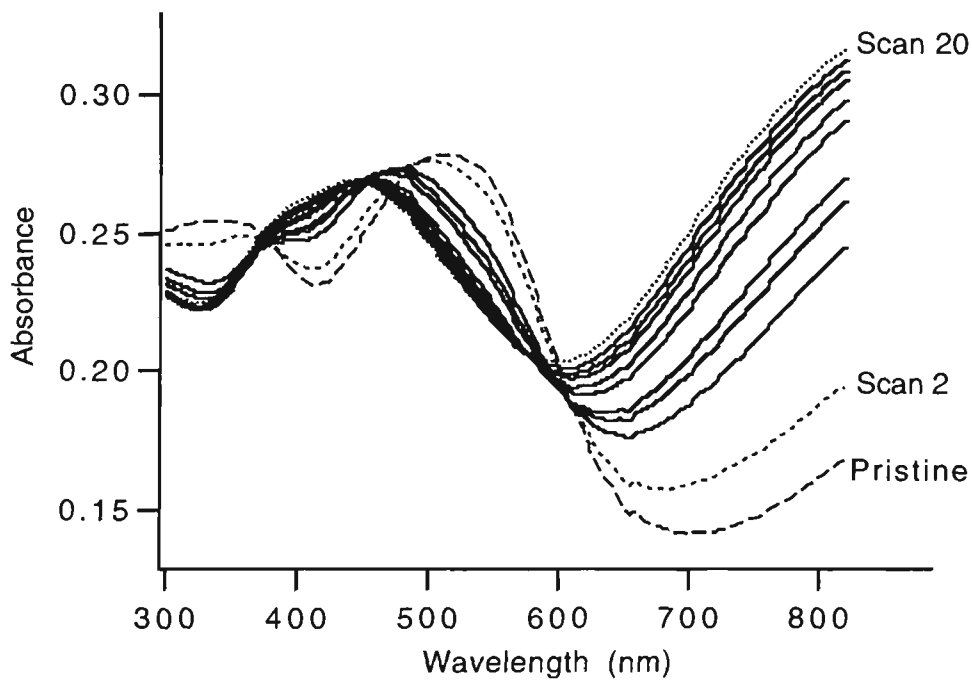

Figure 3.9: P(3-OPy)/BF_4 galvanostatically grown from 0.05 M 3-OPy / 0.02 M TEA-BF_4 in 1:1 CH_2Cl_2:AcN on ITO glass overoxidised in 1 M NaCl at pH 2.25 under an applied potential of 1.1 V (vs Ag/AgCl). Only every second scan after t = 0 is shown for clarity.

As opposed to the results for P(MPyC)/BF_4 discussed above, the spectra given in Figure 3.9 displayed the excellent stability of P(3-OPy)/BF_4 at potentials as high as 1.1 V. Similarly to P(MPyC), P(3-OPy) in the as-grown state exhibited low levels of doping, as indicated again by the lack of absorbance at 800 nm. However, in the latter case a strong band is observed in the polaron region at 500 - 550 nm with a diminished peak in the $\pi - \pi^*$ transition region at 300 - 400 nm, showing that P(3-OPy) is more highly doped than P(MPyC). Nevertheless, the red shift of the polaron peak in comparison to the pristine polymers in Figures 3.2 and 3.5 indicates that the polymer is still not as highly doped as a non-substituted PPy [249]. Again, this is most likely caused by poor planarity and the large range of conjugation lengths associated with substituted polypyrroles. The very low level of doping in P(MPyC) was brought about by the combined effects of poor planarity and the electron withdrawing carboxy group.

The normalised absorbances at 800 nm for two P(3-OPy)/BF_4 films in 1 M NaCl at pH 2.25 are displayed in Figure 3.10. This figure conclusively shows that P(3-OPy) is stable to overoxidation at potentials as high as 1.1 V for periods exceeding 30 min in aqueous solution of moderate pH. This confirms that, as stated in Chapter 2, it is has the highest overoxidation potential of any of the polypyrroles examined in this work. This appears to contradict Masuda's report that P(3-OPy) has a lower stability in air than either PPy or P(3-MePy) [135]. However, in an aqueous environment the hydrophobicity of P(3-OPy) would lessen the diffusion of the causal agent (water) through it, while no such limitation would apply to aerial oxygen in the dry state.

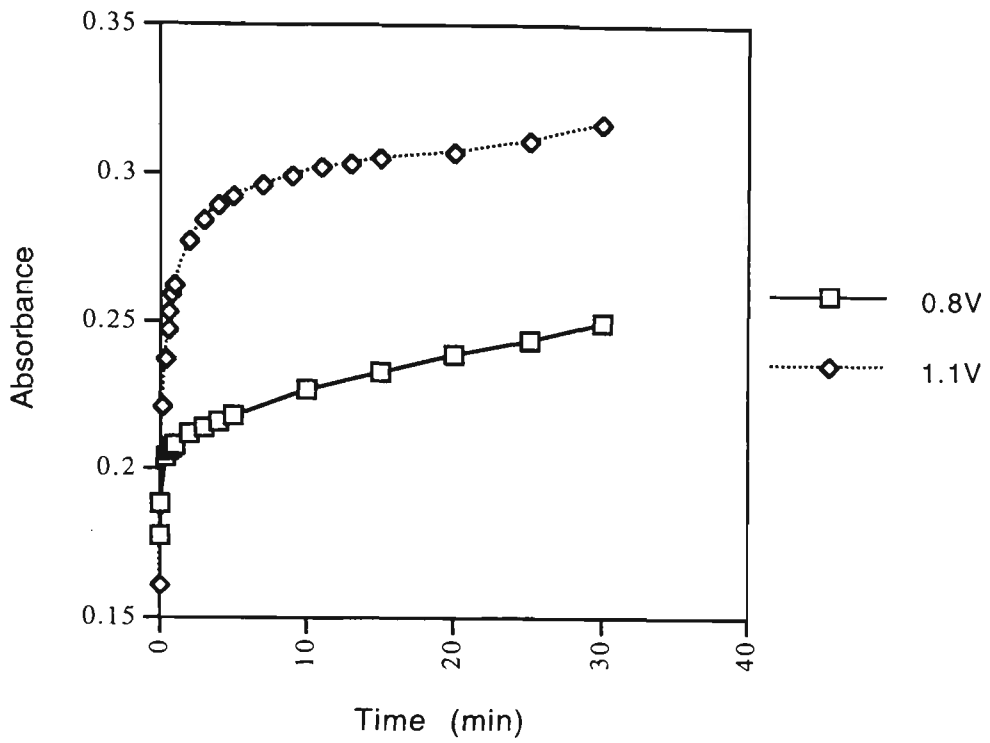

Figure 3.10: Normalised absorbance at 800 nm versus time for P(3-OPy)/BF_4 films overoxidised at various potentials (vs Ag/AgCl) in 1 M NaCl at pH 2.25. Results of Scans 1 to 4 have been omitted for clarity.

3.3.5 The kinetics of overoxidation in aqueous solution

Chen [142], Cheah [118] and Moss [131] report first order kinetics for the stability of PPy in air. Pseudo-first order kinetics are observed for the formation of products of chemical and electrochemical overoxidation of PPy by Thieblemont [156] and Park [180], respectively. Unfortunately, Park's study was performed only in a very aggressive environment of 1 M H_2SO_4 at applied potentials between 0.8 and 1.4 V (vs Ag/AgCl). However, Cheah found that aerial oxidation is a two stage process and both processes follow pseudo-first order kinetics. Similarly, Beck has also noted two consecutive pseudo-first order processes in the "corrosion", ie open circuit acid or base treatment, of polypyrrole [57, 146].

This section examines kinetic parameters for the overoxidation of PPy under conditions more typical for many of its applications. Unlike previous studies, overoxidation will be

monitored by following the decrease of the 800 nm UV-vis absorption band associated with PPy bipolarons.

For any chemical reaction, A ---> B + C, where a reactant A decomposes to give products B and C, the rate of the reaction is given by $d[A]/dt = -k_r [A]^n$, where n is the order of the reaction and k_r is the rate constant [251]. For a first order reaction where n = 1, this equation may be transformed to: $\ln[A]_t = -kt + \ln[A]_o$, where $[A]_o$ is the initial concentration and $[A]_t$ is the concentration at any time, t. In this case a plot of $\ln[A]_t$ against t is linear and has a slope of k, the rate constant. UV-vis absorbance changes may be employed for many reactions to monitor $[A]_t$ over time and, assuming the reaction obeys Beers Law, the observed rate constant, k_{obs}, can be determined from the slope of $-\ln(A_t - A_\infty)$ against time, where A_t is the (decreasing) absorbance at any time t and A_∞ is the final absorbance.

The kinetics of the overoxidation of solid polypyrrole may be determined if it is assumed that the absorbance at 800 nm is proportional to the "concentration" of bipolarons in the solid, and that the bipolaron concentration is a true indicator of the degree of overoxidation of the polymer. As the work in this and the previous chapters implies that these assumptions are reasonable, this approach will be adopted.

Figure 3.11 shows a plot of $-\ln(A_t - A_\infty)$ versus time for a 0.1 μm PPy/pTS film on ITO glass held at 0.8 V in 1 M NaCl at pH 8.1 and 28.8 °C.

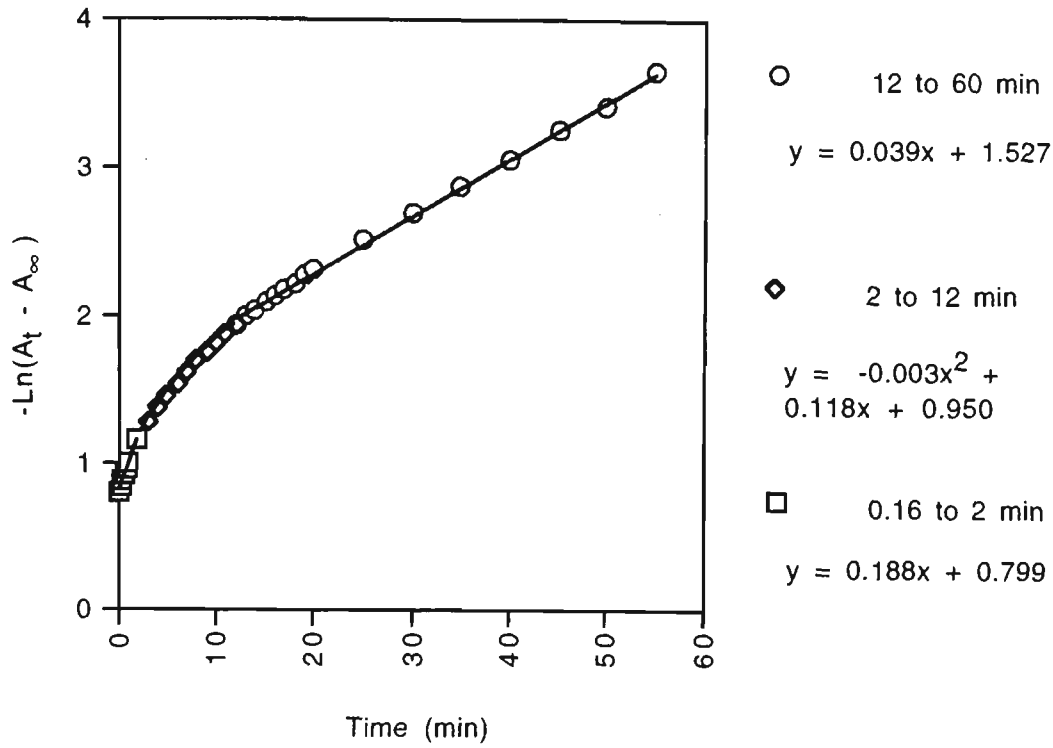

Figure 3.11: Plot of -ln(A$_t$ - A$_\infty$) at 800 nm vs time for a 0.1 μm PPy/pTS film on ITO glass held at 0.8 V in 1 M NaCl at pH 8.1 and 28.8 °C.

From Figure 3.11 it can be seen that the plot of -ln(A$_t$ - A$_\infty$) against time has two linear regions. This is consistent with two consecutive processes in which the bipolaron state of polypyrrole (**1**) is converted via an intermediate species (**2**) to the final overoxidised product (**3**) (Equation 1).

1 --k_1--> **2** --k_2--> **3** .....(1)

From the slopes of the two linear regions of Figure 3.11, the following apparent rate constants can be calculated for these stages: k_{1obs} = 0.188 min^{-1}, k_{2obs} = 0.039 min^{-1}. The intervening curved region, from two to twelve minutes, is presumably caused by an overlap of the two linear regions, where both first order processes are occurring simultaneously. The linear regions parallel the two consecutive pseudo-first order reactions determined by Beck [57, 146] for open circuit "corrosion" and [118] for aerial degradation of PPy, Stilwell [252] for PAni and Beck [253] for PTh degradation.

Beck and Stilwell interpreted the first of these regions as being the fast nucleophilic attack by solvent on the PPy leading to dedoping / overoxidation of the polymer. The second reaction was described as a vague, chemical overoxidation process, also relying on the transfer of electrons from the substrate to the polymer during overoxidation. Based on this, and the results presented in the next three sections, it is now proposed to consider the original overoxidation scheme of Beck et al [21] in terms of two stages. Scheme 3.2 gives this generally accepted overoxidation scheme for PPy, commencing with the bipolaron formed initially the high anodic potential. The Scheme includes the proposed separation into two distinct kinetic sections: Stage 1 is the fast nucleophilic attack at the bipolaron to produce pyrrolin-3-one (**2**) and Stage 2 is the slow "chemical" reaction of 4-hydroxylation of (**2**) to give 4-hydroxypyrrolin-3-one (**3**).

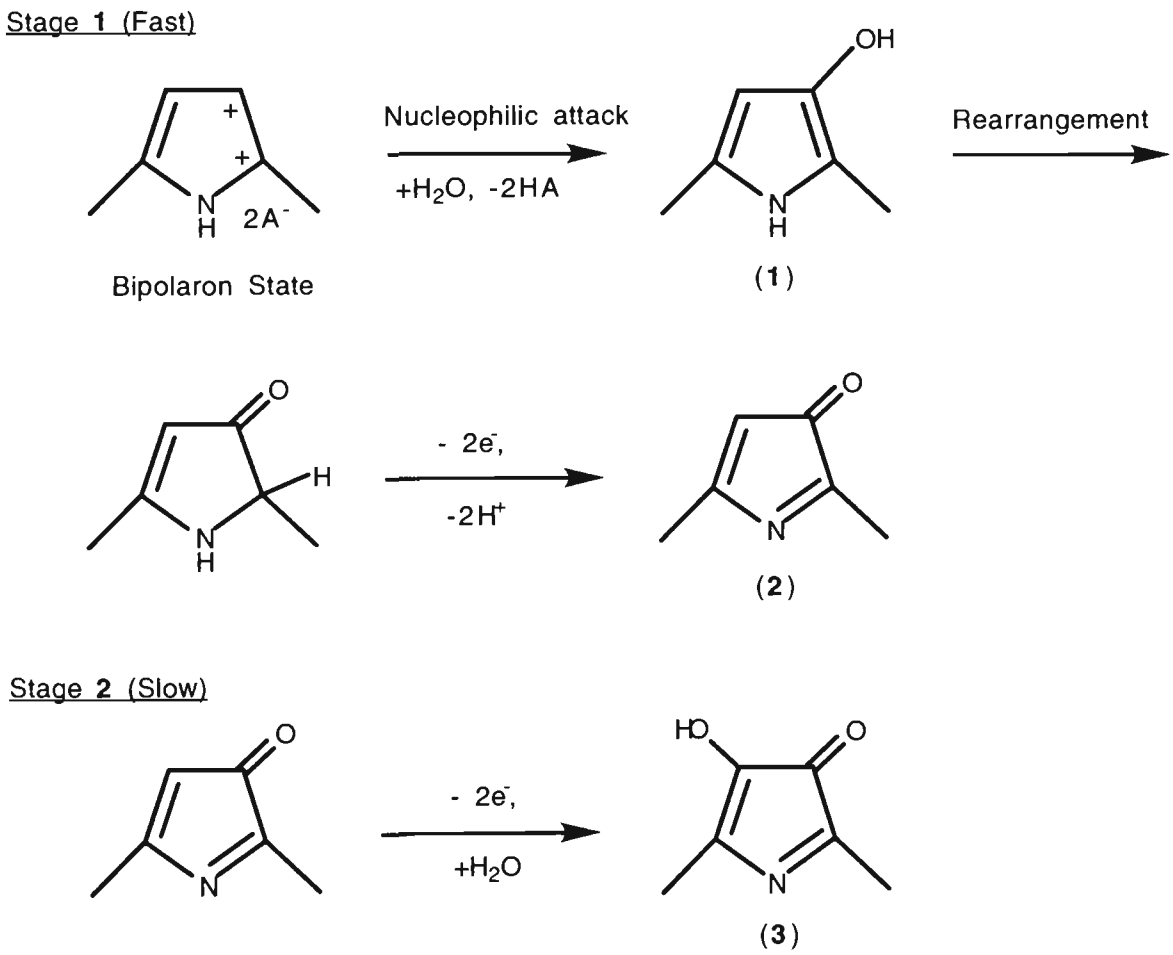

Scheme 3.2: Overoxidation mechanism of PPy after Beck [21] including the steps proposed in the current work as being the fast and slow overoxidation processes.

Supporting evidence for this can be seen in Figure 3.12, a plot of {(Absorbance at 800 nm) / (Charge passed during overoxidation (mC)} against time for a 0.1 μm PPy film overoxidised at 0.8 V in 1 M NaCl at pH 8.1 and 28.8 °C. The sharp initial decrease observed in this graph indicates that the absorbance changes over the first 2 min are not limited by charge flow as the absorbance changes per mC occur very quickly. This is to be expected for the ready nucleophilic attack by the strong nucleophile OH^- at the fully doped bipolaron. It does not imply that little or no current flows during this process, only that it occurs very rapidly. In fact, in this 2 min period 54 % of the charge passed during the entire overoxidation is consumed, (41 of 76 mC). This is very close to the theoretical charge consumed in Step 1 of Scheme 3.2 where the polymer is firstly full doped followed by carbonyl formation, ie 3 of the total of 5 electrons needed for full overoxidation.

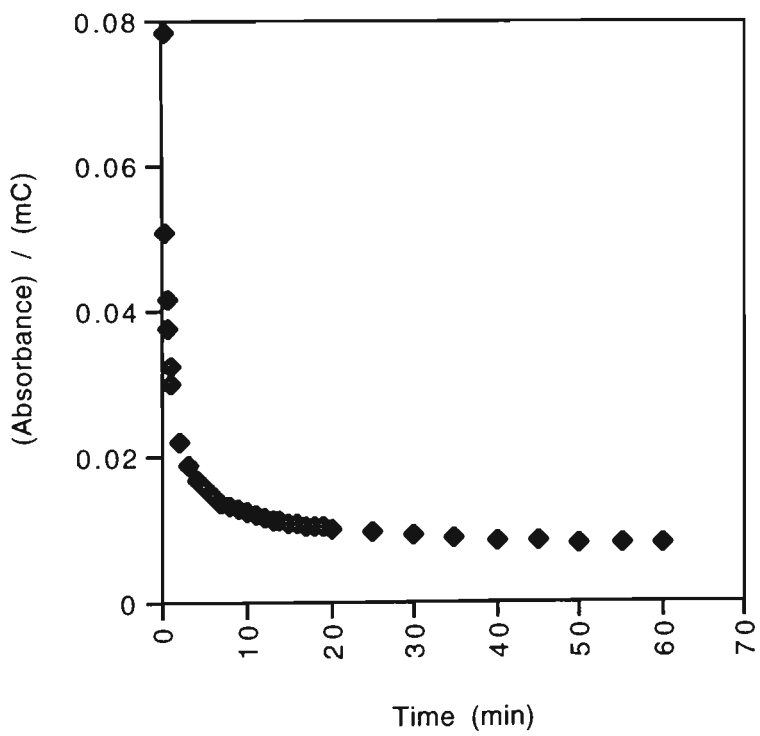

Figure 3.12: Plot of {(Absorbance at 800 nm) / (Charge passed during overoxidation (mC))} against time for a 0.1 μm PPy/pTS film on ITO glass held at 0.8 V in 1 M NaCl at pH 8.1 and 28.8 °C.

After a transition period from fast to slow reactions, indicated by the gentle sweep from 2 min to about 18 min, the absorbance changes are directly related to the consumption of charge, leading to the flat final section in Figure 3.12. When 4-hydroxylation does occur, it consumes two moles of electrons per mole of the product (**3**) and so charge is directly related to changes in absorbance. The times of these vertical, curved and flat regions correspond exactly to the linear and curved regions of the curve given in Figure 3.11.

It is also possible that Stage 1 (the initial nucleophilic attack step of Stage 1) is, at least in part, reversible. It is conceivable that 3-hydroxy pyrrole (**1**) or its rearrangement product may be the species proposed in Chapter 2 during the resistometry studies of the reversibility of overoxidation. The rearrangement product would certainly increase the film resistance, but could return to (**1**) when the cell is switched to open circuit to give a polymer with some conductivity and electroactivity.

For the remainder of this Section, plots of absorbance versus time were constructed to investigate the effects of pH, potential and temperature on the overoxidation of PPy and to determine the rate constants and activation energies for the two pseudo-first order reactions.

3.3.5.1 The effects of pH

The k_{obs} values determined from the slopes of $-\ln(A_t - A_\infty)$ versus time plots for the two overoxidation steps of PPy/pTS at various pHs are given in Table 3.3.

Even after allowance for the small temperature difference, these are appreciably higher than those reported by Beck et al [57] at 23 °C for open circuit corrosion namely: $k_{1obs} \leq 1.8 \times 10^{-3}$ min^{-1} and $k_{2obs} = 1.8 \times 10^{-5}$ min^{-1} at pH 1; $k_{1obs} = 1.2 \times 10^{-1}$ min^{-1} and $k_{2obs} = 1.2 \times 10^{-3}$ min^{-1} at pH 9. This was expected as the work of Beck et al was performed on

thick (3 - 10 μm) films at rest potential. The exception to this is their value for k_{1obs} at pH 9, which is almost identical to the result given in Table 3.3. The substantial increase in k_{1obs} found by Beck et al at pH 9 (70 times higher than at pH 1) indicated that in the absence of an applied potential, the strong nucleophile OH^- plays a major role in overoxidation when at relatively high concentration.

Park et al [180], in a study involving UV-vis spectral analysis of the supporting electrolyte solution during overoxidation, reported single k_{obs} values of 5.5 x 10^{-4} and 6.2 x 10^{-4} min^{-1} at pHs of 4.3 and 9.0, respectively, for 0.32 μm films at 1 V (vs Ag/AgCl). Again these are appreciably lower than the results obtained in the current work, even if k_{1obs} and k_{2obs} are averaged at each pH. This may be due to the different monitoring technique employed by Park et al, namely the UV-vis absorption of the maleimide and succinimide overoxidation products. This technique would rely on diffusion of the UV-vis absorbing overoxidation products into the bulk supporting electrolyte, a process that must have some finite time associated with it.

Table 3.3: k_{1obs} and k_{2obs} for a 0.1 μm PPy/pTS film on ITO glass held at 0.8 V (vs Ag/AgCl) in 1 M NaCl, pH = 8.1, temperature = 32.0 °C.

Supporting Electrolyte pH	k_{1obs} (min^{-1})	k_{2obs} (min^{-1})	Supporting Electrolyte pH	k_{1obs} (min^{-1})	k_{2obs} (min^{-1})
1.0	0.100	0.009	6.1	0.169	0.042
2.2	0.159	0.006	8.1	0.168	0.043
3.1	0.141	0.007	8.9	0.150	0.047
4.2	0.139	0.016	10.5	0.208	0.078
5.3	0.171	0.023	11.6	0.388	0.144

The significance of the variation in k_{obs} with pH may be more clearly seen from the half life associated with each value. From the data in Table 3.3 the half life ($t_{1/2} = (0.693/k_{obs})$

for a first order reaction [254]) may be readily calculated and found to vary from 1.9 min at pH 11.6 2 (at 0.8 V and 32 °C) up to 6.9 min at a pH 1.0 for Stage 1. Similarly $t_{1/2}$ changed from 6 to 77 min for Stage 2 under these experimental conditions. The results in Table 3.3 are presented graphically in Figure 3.13 as a plot of k_{obs} against pH.

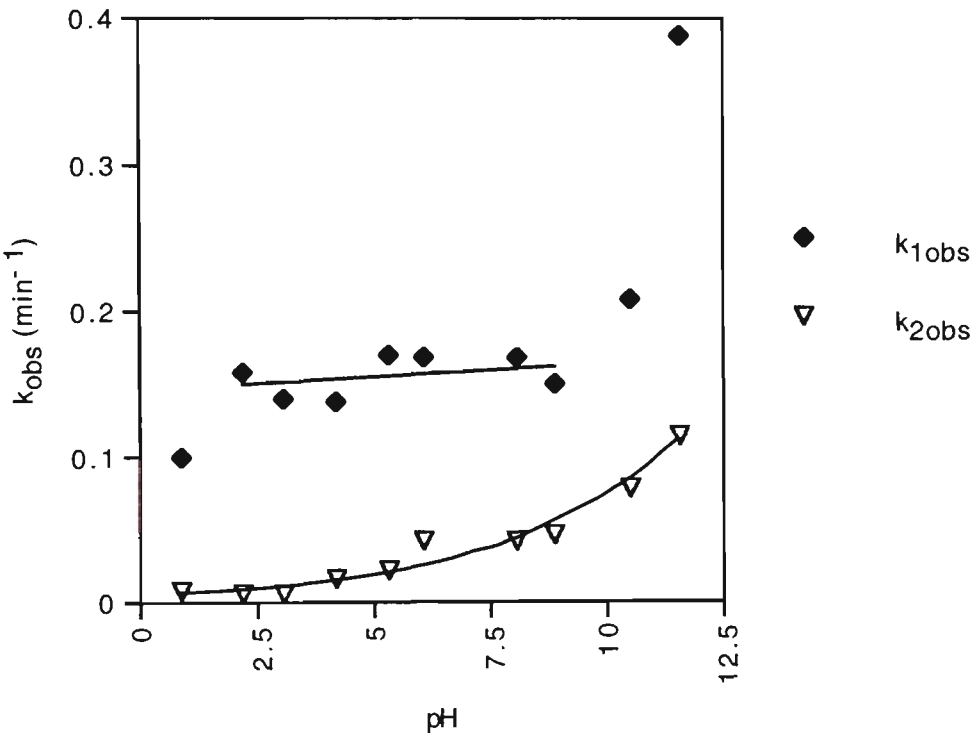

Figure 3.13: Plot of k_{obs} against pH for 0.1 μm PPy/pTS films on ITO glass held at 0.8 V in 1 M NaCl at various pHs. Temperature 32 °C.

In the case of the fast Stage 1 nucleophilic attack process, k_{1obs} is effectively independent of pH over the pH range of 2.2 to 8.9. This is consistent with an S_N1 mechanism for the reaction of OH^- on the bipolaron. If either the subsequent rearrangement of the intermediate (1), or the electron transfer (oxidation) to give (2) is rate-determining, then no dependence of k_{1obs} on [OH^-] would be expected for either an S_N1 or S_N2 mechanism for nucleophilic attack. Table 3.3 reveals a small increase in k_{1obs} at higher pHs (increasing from 0.15 M min^{-1} at pH 8.9 to 0.388 M min^{-1} at pH 11.6). However, in general the results in Table 3.3 and Figure 3.13 reveal the almost total independence of

k_{1obs} from [OH^-] over a pH range of 2.2 to 11.6. This dependence is significantly lower than previously reported by Beck et al [57].

Similarly, the results in Table 3.3 and Figure 3.13 again show only a small dependence of k_{2obs} on [OH^-] over a wide pH range. However, a sixteen-fold increase in k_{2obs} was noticed on increasing the pH from 1.0 to 11.6, indicating a somewhat higher impact of [OH^-] on the slower Stage 2 process compared to Stage 1 in Scheme 3.2.

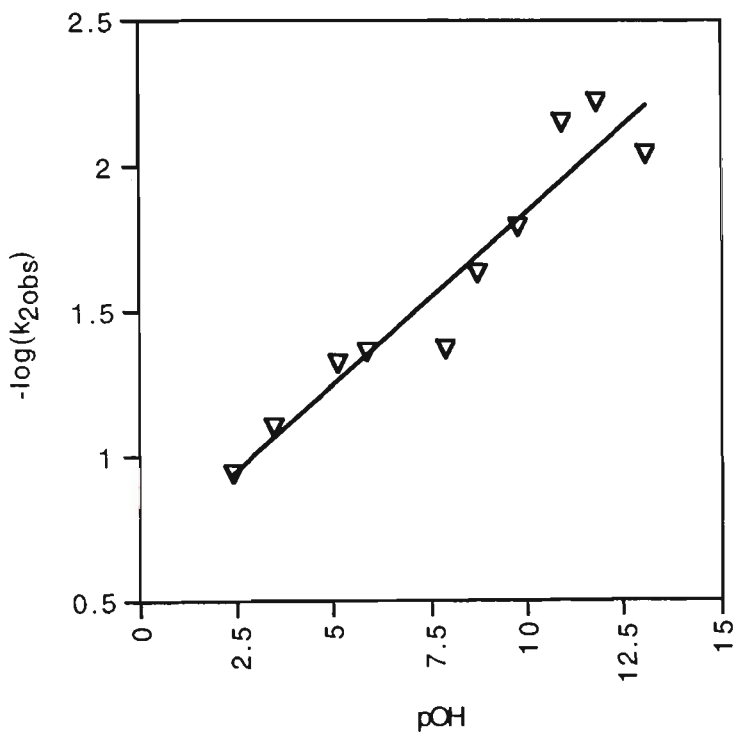

Figure 3.14: Plot of -log(k_{2obs}) versus pOH for 0.1 μm PPy/pTS films on ITO glass held at 0.8 V in 1 M NaCl at various pHs. Temperature 32.0 °C.

Although Figure 3.14 shows an apparent linear relationship between log(k_{2obs}) and pH, the significance of this is uncertain. The over-riding conclusion from these results is the extremely small dependence of k_{2obs} on [OH^-] is inconsistent with the rate-determining step being nucleophilic attack by OH^- on (**2**). It is therefore possible that the weaker nucleophiles H_2O and O_2 (both of which are at higher concentrations than OH^- here) have

a more significant impact than OH^- or that the concomitant oxidation process (electron transfer) is rate-determining for Stage 2.

3.3.5.2 The effect of applied potential

The k_{obs} values determined from the slopes of $-\ln(A_t - A_\infty)$ versus time plots for the two overoxidation steps of PPy/pTS at various applied potentials are given in Table 3.4.

Table 3.4: k_{1obs} and k_{2obs} for a 0.1 μm PPy/pTS film on ITO glass at various applied potentials in 1 M NaCl, pH = 8.1, temperature = 32 °C.

E (V vs Ag/AgCl)	k_{1obs} (min^{-1})	k_{2obs} (min^{-1})	E (V vs Ag/AgCl)	k_{1obs} (min^{-1})	k_{2obs} (min^{-1})
0.70	0.055	0.030	0.85	0.255	0.028
0.75	0.105	0.034	0.90	0.382	0.025
0.80	0.141	0.007			

Figure 3.15 graphically presents these data as a plot of k_{obs} against applied potential for PPy/pTS films in 1 M NaCl. This graph shows that the fast initial step, nucleophilic attack on the bipolaron, is highly dependent on the potential at which the polymer is poised. At higher potentials the film is more amenable to this mechanism of degradation as the polaron is not sufficiently reactive to undergo electroorganic oxidation [21]. As rapid nucleophilic attack will only occur at the bipolaron and the number of bipolarons will be maximised at higher applied potential, k_{1obs} will increase with an increase in applied potential.

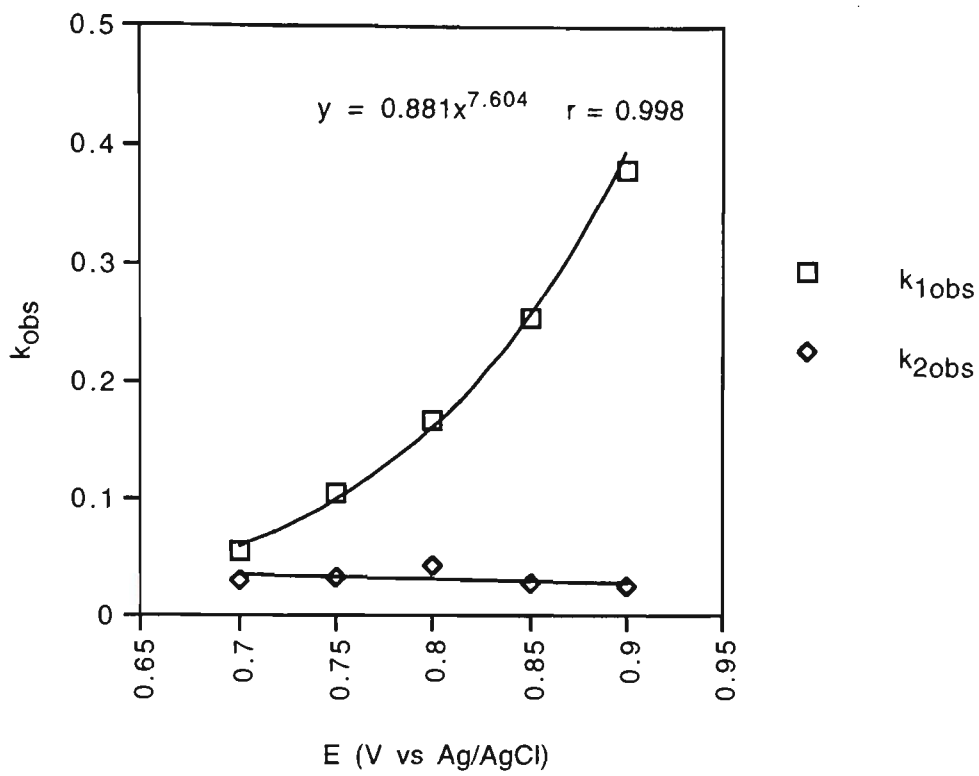

Figure 3.15: Plot of k_{obs} against applied potential for 0.1 μm PPy/pTS films on ITO glass at various potentials in 1 M NaCl. Temperature 32 °C, pH 8.1.

As was mentioned in Section 3.3.3, a clear linear relationship between the quantitative rate of overoxidation and potential to the eighth power was observed. The equation of the line fitted to k_{1obs} in Figure 3.15 is given by $y = 0.88.x^{7.6}$ ($r = 0.998$). The rate of this reaction increases by a factor of 6.9 over a range of only 0.2 V with an associated drop in the half life from 12.6 min at 0.7 V to 1.8 min at 0.9 V at pH 8.1 and 32 °C.

The plot of k_{2obs} against potential in Figure 3.15 indicates that, as expected from Scheme 3.2, potential plays little role in Stage 2 of overoxidation. This is expected as this step is not reliant on the reactant pyrrolinone being driven to a higher oxidation state before the reaction can commence.

3.3.5.3 The effect of temperature

The k_{obs} values determined from the slopes of $-\ln(A_t - A_\infty)$ against time plots, for the two overoxidation steps of PPy/pTS at various temperatures in 1 M NaCl at pH 8.1 and 0.8 V are given in Table 3.5.

Table 3.5: k_{1obs} and k_{2obs} for a 0.1 μm PPy/pTS on ITO glass at various temperatures in 1 M NaCl, pH = 8.1, applied potential 0.8 V (vs Ag/AgCl).

Temperature (°C)	k_{1obs} (min^{-1})	k_{2obs} (min^{-1})	Temperature (°C)	k_{1obs} (min^{-1})	k_{2obs} (min^{-1})
29.8	0.144	0.038	39.3	0.250	0.039
32.8	0.168	0.043	44.7	0.296	0.043
34.5	0.178	0.045			

These results are presented graphically in Figure 3.16 as a plot of k_{obs} against temperature for PPy/pTS films in 1 M NaCl. This graph clearly shows that temperature has a significant effect on the fast initial step, but only a minor impact on the slow process.

For the faster Stage 1 process an Arrhenius plot of $\ln(k_{1obs})$ against 1/T was linear (see Figure 3.16). An activation energy (E_a) of 39 $kJmol^{-1}$ was calculated from the slope of this plot (from the Arrhenius equation, $k = A \cdot e^{(-E/RT)}$). This is similar (though somewhat smaller) than the activation energies reported by Moss [131] (56 kJ mol^{-1} for the aerial oxidation of PPy), Chen [142] (45 kJ mol^{-1} for the chemical overoxidation of PPy) and Otero [176] (17 to 44 kJ mol^{-1} for the oxidation of PPy from a fully reduced state). The value determined in this work was expected to be lower than these reported results, as overoxidation here was carried out under the application of an external potential, which overcame a large amount of the activation energy required for the insertion of oxygen into a PPy chain.

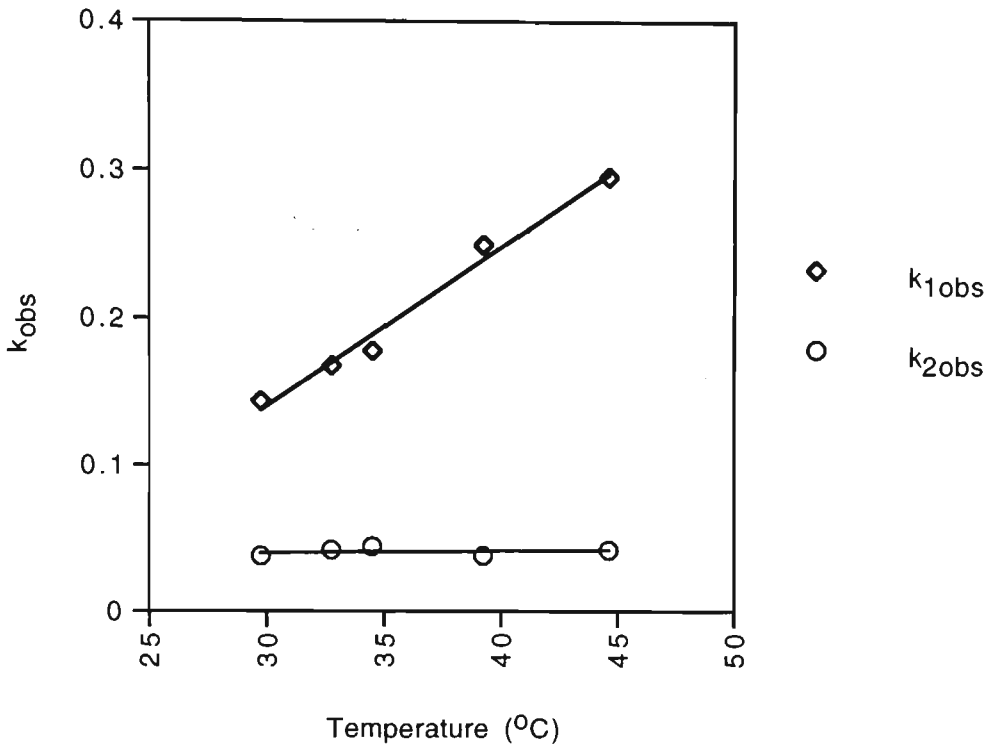

Figure 3.16: Plot of k_{obs} against temperature for 0.1 μm PPy/pTS films on ITO glass at 0.8 V (vs Ag/Cl) in 1 M NaCl adjusted to pH 8.1.

Interestingly, the slower Stage 2 showed an extremely small dependence of k_{2obs} on temperature (Table 3.5, Figure 3.17). This would appear to be inconsistent with a rate-determining S_N1 nucleophilic attack on (**2**), since this would involve an energetically demanding C-H bond cleavage in the transition stage. It may arise from a two step process for Stage 2 involving an initial rapid pre-equilibrium with a negative enthalpy change prior to the rate determining step.

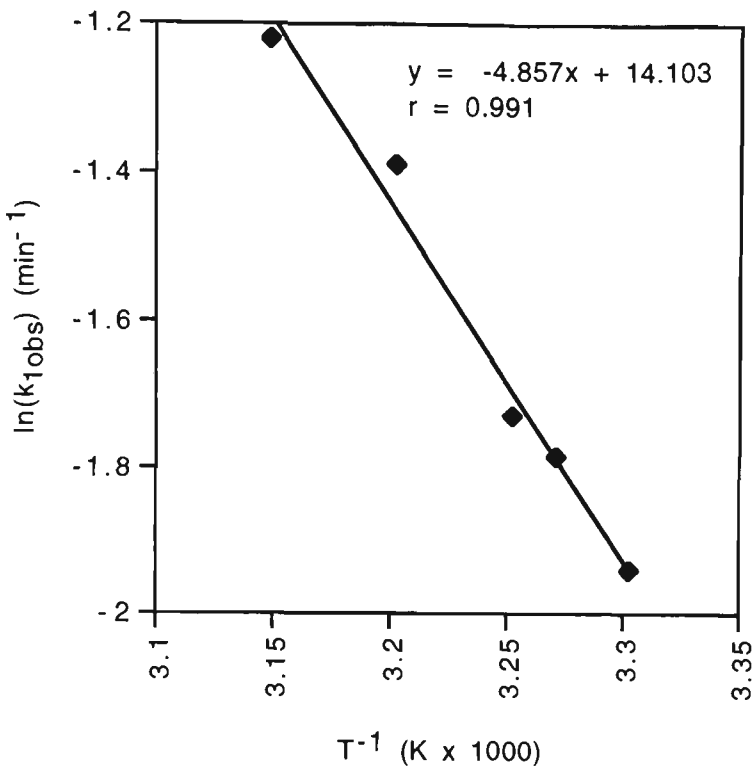

Figure 3.17: Arrhenius plot for 0.1 μm PPy/pTS films on ITO glass at various temperatures in 1 M NaCl adjusted to pH 8.1.

3.4 CONCLUSION

This chapter employed in-situ UV-vis spectrometry to investigate the overoxidation of polypyrrole in an aqueous environment. It was found that during the application of a potential sufficiently high to induce overoxidation, the polymer firstly went through a fully doped stage, as indicated by an increase in absorbance in the bipolaron band region (around 800 nm) with concomitant decrease in the polaron and neutral $\pi - \pi^*$ regions. This full doping is a prerequisite for overoxidation in the current work due to the poor nucleophilicity of the solvent water nucleophiles and the relatively low concentration of hydroxide. The progress of the subsequent overoxidation can be then readily followed by a decrease in absorbance of the bipolaron band around 800 nm with an associated increase in the (red shifted) polaron and (blue shifted) $\pi - \pi^*$ transition bands.

The influence of pH on the overoxidation process was observed. For example, at pH approaching zero little evidence for overoxidation was seen over 30 min at 0.8 V. However, at pH around 11, overoxidation proceeds so readily at this applied potential that it is effectively complete after 10 to 15 min. However, in general there was a remarkably small effect of [OH^-] on the rate of the overoxidation process over the pH range 1.0 to 11.6, indicating a minor role for OH^- in the rate determining step(s).

However, the role of pH in overoxidation was shown to be overshadowed by that of applied potential, which was found to have a marked effect on the rate of the Stage 1 process. A linear relationship between the observed rate constant (k_{1obs}) for the first stage of overoxidation and potential to the eighth power was observed.

The destabilising nature of SO_4^{2-} as a supporting electrolyte ion was again shown, even when employed with the very highly ordered polypyrrole PPy/DS and overoxidation was performed at 0.8 V with supporting electrolyte pH between 0 and 0.77. This effect is so strong that overoxidation in sulphate solution at pH 5.5 occurred as readily as at pH 11 in a chloride solution.

P(MPyC) again exhibited a surprising ease of overoxidation even though both β-carbons are occupied by substituents. No insight into the mechanism of this overoxidation could be established. However, it was observed that despite the polymer exhibiting a very low doping level in the as-grown state, it showed consistent UV-vis features after full doping and through overoxidation. The other substituted PPy studied here, P(3-OPy) exhibited its impressive stability to overoxidation in an aqueous environment, almost certainly due to its high hydrophobicity. Even though this polymer also exhibited poor doping levels in the as-grown form, once it was fully oxidised no further changes in its UV-vis spectra were observed, even at 1.1 V over 30 min.

The detailed spectroscopic and kinetic studies of the overoxidation of PPy/pTS in Cl^- supporting electrolyte, were consistent with the reaction mechanism suggested by Beck et al. Two clear stages were observed leading to two clear first order rates constants. The first of these is believed to be fast nucleophilic attack on the fully doped PPy to yield a pyrrolinone, with an associated pseudo first order rate constant k_{1obs}. The slower second is considered to involve nucleophilic attack on the pyrrolinone to yield a 4-hydroxylated pyrrolinone with an associated first order rate constant k_{2obs}. The rate constants for both steps were determined under a variety of pH, potential and temperature conditions and vary from $k_{1obs} = 0.388\ min^{-1}$ ($t_{1/2} = 1.9$ min) at a pH of 11.6 and potential of 0.8 V down to $k_{2obs} = 0.009\ min^{-1}$ ($t_{1/2} = 77$ min) at pH ~ 0 and potential of 0.8 V. Faster kinetics were observed than those reported by other authors. This was expected as no other reports of direct, in-situ determination of the overoxidation of PPy under an applied potential have been published. As the in-situ UV-vis technique allows direct, real time probing of the polymer during overoxidation, it was anticipated that any rate constants determined here would more truly represent the real rates of overoxidation.

Determination of the rate constant k_{1obs} at various temperatures allowed the estimation of the activation energy of 39 kJ mol^{-1} for the fast stage in the overoxidation process. The somewhat lower activation energy compared to literature values was again rationalised on the basis of the measurement being carried out in-situ with an applied potential which helped to partly overcome the activation energy for the reaction.

CHAPTER 4: RAMAN SPECTROSCOPY STUDIES

4.1 INTRODUCTION

Absorption of electromagnetic radiation (light) in the UV-vis region (200 to 800 nm), which corresponds to transitions of valence shell electrons of an atom or molecule, was employed to determine the oxidation state of polypyrrole in the last chapter. Spectroscopic investigation of the precise chemical structure of this molecule requires the use of other interactions between electromagnetic radiation and the molecule. One such technique is infrared absorption spectroscopy (IR), in which light in the infrared region (around 2,500 to 100,000 nm, ie 4000 to 100 cm^{-1}) is absorbed by exciting a range of molecular vibrations that have corresponding frequencies. However, IR spectroscopy has limited application as an in-situ technique in aqueous systems due to the strong absorbance by the O-H stretch. Raman spectroscopy, though providing similar structural information, has no such limitations as water exhibits very weak Raman scattering [30].

As the transitions responsible for the Raman effect are of the same type as those involved in IR absorbance, the Raman shift spectra observed for any particular molecule should be similar to its IR absorbance spectra obtained under the same experimental conditions, assuming that the molecule is both IR and Raman active [255]. Even though Zerbi reported few coincidences between IR and Raman spectra of PPy, whenever peaks do appear in both spectra, their frequencies are in good agreement [256]. This allows the use of IR assignments for any peaks that have not previously been observed in Raman spectra, as may happen during overoxidation studies.

The Raman technique monitors the scattering of light by the relaxation of an induced polarised state to an allowed energy level other than its original [255, 257]. As the induced polarised state does not correspond to any quantised energy level of the molecule,

Raman scattering can be produced by an excitation source of any wavelength [255]. This is unlike both UV-vis and IR absorption spectrometries which rely on the incident light exactly matching the frequency of the electronic transitions or molecular vibrations, respectively.

However, the frequencies of Raman scattered light are dependent on the frequency of the incident light. The frequencies of scattered light are given by $\nu_{obs} = (\nu_o - \nu_{vib})$ and $(\nu_0 + \nu_{vib})$, where ν_0 is the excitation frequency and ν_{vib} the molecular vibrational frequency, known as Stokes and anti-Stokes scattering, respectively [257]. Stokes scattering is about an order of magnitude greater that of anti-Stokes scattering and, as such, it is the former that is normally employed for practical purposes. To overcome this dependence of the emitted light frequency on the excitation frequency, Raman spectra are normally plotted as intensity (of the scattered light) versus frequency shift, $\Delta\nu = \nu_o - \nu_{obs}$, where $\Delta\nu$ is frequency shift of the Raman scattered light [255].

Even though the frequency shift, $\Delta\nu$, is expected to be independent of the frequency of the excitation source, it is anticipated that the intensity of the emission band will show dependence on this frequency [257]. This dependence of intensity on wavelength at different excitation wavelengths has been observed specifically in conducting polymers by Lapkowski et al [258], Fukuda et al [259] and Quillard et al [260] for PAni, Trznadel et al [261], Louarn et al [262], Bazzaoui et al [263] and Agosti and Zerbi [264] for PTh and Vigmond et al [265], Blanking [107] and Zerbi et al [256] for PPy.

Vigmond et al also noted [265] variation of up to 30 cm^{-1} in the frequency of the Raman shift at different excitation wavelengths for PPy. He reported Raman shifts associated with the C=C stretch at 1575 cm^{-1} when an excitation source of 514.5 nm was employed, at 1560 cm^{-1} for 568 nm, 1590 cm^{-1} for 752 nm and 1580 cm^{-1} for the non-resonance 1064 nm source. Resonance Raman enhancement occurs when the excitation frequency corresponds to an electronic absorption band of the sample. When this occurs the

polarizability of the molecule is greatly increased, resulting in greater intensity of the Raman scattering [107]. As discussed in Chapter 3, PPy absorbs strongly in the visible region due to valence band to anti-bipolaron band transitions. This leads to resonance enhancement of PPy Raman spectra when employing an excitation source between 450 and 650 nm, making these sources ideal for studies of PPy in the doped state. Similarly though, as the bipolaron absorbs strongly at wavelengths above 700 nm due to valence band to bipolaron band transitions, resonance enhancement could occur in a fully doped PPy when a 1064 nm source is employed.

In the four studies involving polythiophenes, the frequency shift of the Raman peaks determined with non-resonance excitation source (1064 nm) shifted to a lower frequency than with resonance sources. The C=C stretch was red shifted by about 40 cm^{-1}, in comparison to the resonance sources (457.9, 488, 514.5 or 632.8 nm), which all exhibited this peak around 1450 cm^{-1}. As long as caution is exercised in band assignment, the non-resonant excitation line offers no particular disadvantages with respect to the sensitivity and assignment of the Raman spectra over any of the resonant lines.

However, the 1064 nm excitation source offers some distinct advantages over visible region sources in the study of PPy: it should limit fluorescence [106, 256]; it allows the use of Fourier Transform techniques with the associated benefits of improved signal-to-noise ratio and decreased signal strength requirements [106]; it exhibits inherent frequency accuracy and allows rapid data collection [265]; due to the strong absorption of the bipolaron above 800 nm it may also have improved sensitivity for highly oxidised forms of PPy due to resonance enhancement. This wavelength is reported by Trznadel et al [261] to reveal vibrations associated with doped segments of PTh more effectively than shorter wavelength excitation lines, and as both PTh [261] and PPy [124] exhibit strong absorbances around 1200 nm in the fully doped state, this should also apply to PPy.

The 1064 nm excitation source, combined with Fourier Transform processing, has been reported for studies of PPy including: structure [106, 256], chemical interactions [265], doping [237], synthesis [266] and substrate dependence [267].

4.2 EXPERIMENTAL

4.2.1 Reagents and materials

All chemicals used were analytical reagent grade unless otherwise stated. Pyrrole (Sigma) was distilled before use and stored at -16 °C in the dark under N_2 where necessary. Water was Baker Analysed HPLC Grade (J. T. Baker Inc, USA).

Electrodeposition and characterisation of polymer films was carried out on platinum sheet (9 x 40 mm), with an auxiliary electrode of the same material and dimensions. All potentials were measured against a narrow diameter Ag/AgCl reference electrode fabricated as described in Chapter 3. This electrode was inserted directly into the supporting electrolyte solution.

4.2.2 Instrumentation

Electropolymerisation of polymer films was carried out using a Yokoyawa Electric Works Ltd (Japan) YEW 2553 galvanostat. FT-Raman spectra were collected by a Perkin Elmer System 2000 FT-Spectrometer employing an Nd:YAG source (1064 nm) and 50 mW power. Overoxidation potentials were applied by an EG&G Princeton Applied Research (USA) 362 Potentiostat at a laboratory temperature between 29 and 31 °C. Data was collected on a Hewlett Packard PC and processed on a Macintosh (Apple) computer.

4.2.3 Procedures

The Pt sheet working electrode was cleaned in chromic acid and rinsed with water then methanol before use. An area of approximately 1 cm^2 was then taped off with teflon tape (T&F, USA) to give a reproducible film area and the reverse side was masked with tape along its length to prevent deposition on that side.

PPy was electrodeposited galvanostatically with a current density of 1 $mAcm^{-2}$ for 50 s from a solution of 0.36 M pyrrole and 0.036 M counterion in H_2O (unless stated otherwise) to give a film thickness of approximately 0.1 μm. After growth the polymer films were rinsed thoroughly with water and fitted into a 1 cm quartz cuvette with the Pt auxiliary and Ag/AgCl reference electrode, see Scheme 4.1. All growth and characterisation was performed in air, while all characterisation was done in solutions of 0.005 M HCl / 0.095M NaCl, with a measured pH of 2.25.

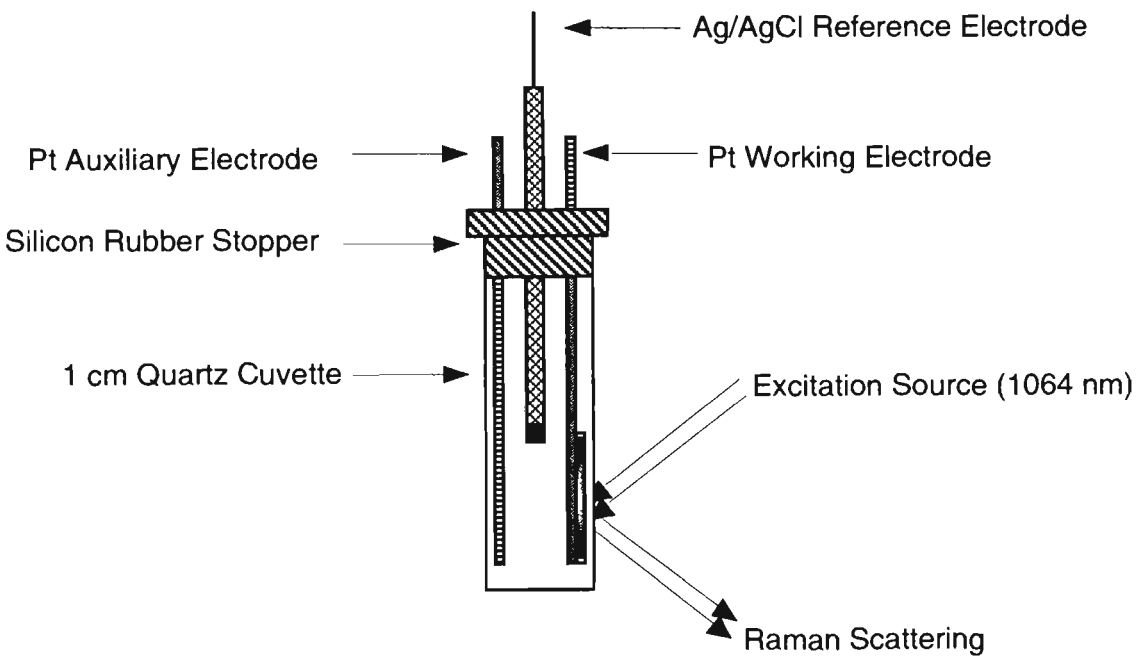

Scheme 4.1: The three electrode cell employed for in-situ Raman characterisation, after Tezuka et al [230].

As the accumulation of data by FT-Raman spectroscopy is relatively slow, requiring about 2 min for 10 scans from 3600 to 220 cm^{-1}, the applied potential was either held constant at 0.8 V (vs Ag/AgCl) or ramped at 0.1 mVs^{-1}. In the former case, spectra were collected firstly of the pristine film, followed by an initial spectrum at 0.8 V (t = 0) and then at times of 5, 10 15, 30 and 60 min. In the instance of the application of a linear potential ramp, a spectrum of the pristine film was collected at rest potential before the potential ramp was initiated. The t = 0 spectrum was collected as the ramp was initiated (at

400 mV) and then spectra were collected each 50 mV up to 900 mV, unless otherwise stated.

4.3 RESULTS AND DISCUSSION

4.3.1 Polypyrrole

4.3.1.1 Overoxidation at a constant potential

Figure 4.2 displays the Raman spectra of a PPy/pTS film in 1 M NaCl at a pH of 2.25 held at an applied potential of 0.8 V (vs Ag/AgCl) for 60 min. The individual spectra have been scaled to give a similar peak height for peak "j" (1230 cm^{-1}) and any comparison of the peak size changes in this section are referenced to this peak. Peak "j" was chosen as inspection of the raw spectra indicated that it remained reasonably constant throughout the time period of the experiment.

The assignments of the Raman peaks marked in Figure 4.2 are given in Table 4.1. In general, the Raman shifts given in Figure 4.2 are very close to the literature values employed for their assignment, allowing for variations in wavelengths observed between IR and the various Raman excitation sources. This generally leads to an unambiguous assignment of the group that generates the Raman shift. For example, Cheung et al [66] assigned the 1072 cm^{-1} band to C-H bending in a resonance Raman study employing a 482.5 nm excitation source. Jenden et al [106] and Vigmond et al [265] assigned this band specifically to C-H in-plane bending in a PPy ring in the bipolaron state. Jenden noted the band at 1091 cm^{-1} for a 1064 nm excitation source [106] and Vigmond at 1082 cm^{-1} when either 752 or 1064 nm [265] excitation sources were used. Hence, Peak "k" at 1082 cm^{-1} was confidently assigned as a C-H bending band in the current work.

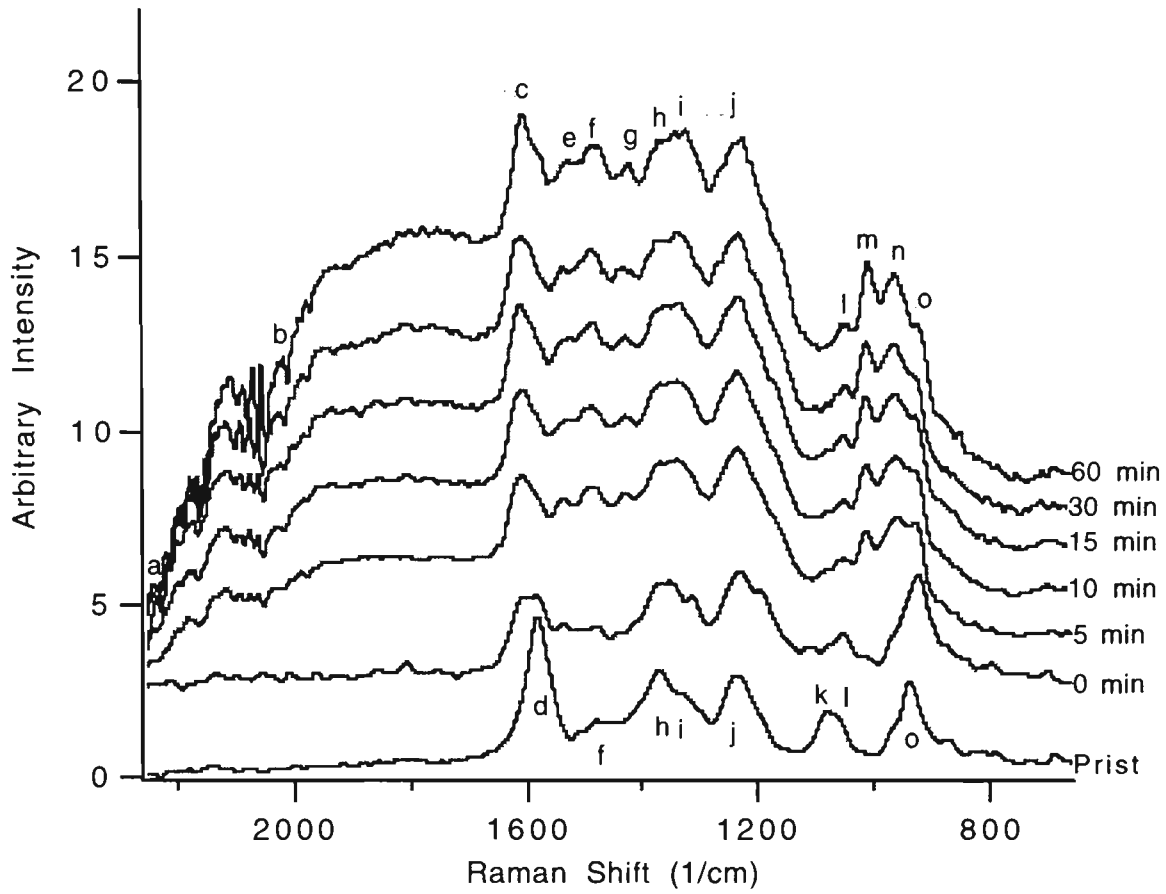

Figure 4.2: Raman spectra of PPy/pTS held at 0.8 V (vs Ag/AgCl) in 1 M NaCl with a pH of 2.25. The spectra have been scaled to peak "j" to allow comparison of peak intensities. The times given are for the start of collection of each spectrum.

Some ambiguity exists regarding the assignment of Peak "l" (1055 cm^{-1}) as it has previously been has been assigned to two distinct molecular transitions. Cheung et al [66] assigned this band to an N-H in-plane deformation in PPy/pTS, while according to Gonzalez-Tejera et al, in an FTIR study of PPy/PSS [160], this deformation is observed at 1025 cm^{-1}. On the other hand, Jenden et al [106] reported C-H in-plane bending in PPy in the polaron state at 1060 cm^{-1}, while according to Vigmond et al [265] this band appears at 1055 cm^{-1}.

In the current work, it was observed that the peak at 1055 cm^{-1} (Peak "k", Figure 4.2), assigned as a polaron C-H deformation by both Vigmond and Jenden, decreases in size relative to Peak "j", whilst the second peak assigned to a polaron (Peak "n", 932 cm^{-1}) grows over time. In the pristine film Peak "n" is observed only as a shoulder on Peak

"o", while at 60 min it is of a comparable size to the other peaks in the spectrum. It would appear unlikely that one peak associated with the polaron state would decrease (Peak "k") as another appears and then grows (Peak "n"). If the Raman scattering at 1055 cm^{-1} (Peak "l") is assigned to an N-H deformation, its decrease during overoxidation is predicted by Ge et al who note that the level of N-H bonding decreases during this process, with an associated increase in -N= nitrogen [55]. As such, Cheung et al's assignment of the 1055 cm^{-1} band as N-H deformation was chosen as being the most likely.

Table 4.1: Assignments of Raman bands in Figure 4.2, the overoxidation of PPy/pTS at 0.8 V(vs Ag/AgCl) in 1 M NaCl with a pH of 2.25.

Peak	Raman shift (cm^{-1})	Assignment	Ref	Peak	Raman shift (cm^{-1})	Assignment	Ref
a	2240	NA	-	i	1330	Ring str	[66]b
b	2026	NA	-	j	1230	Ring str	[66]b
c	1610	C=O str	[268]c	k	1082	C-H bend	[265]a
d	1581	C=C str	[265]a	l	1055	N-H def	[66]b
e	1530	C=C/C=N substit PPy	[147]c	m	1011	C-O str	[144]c
f	1481	Ring str	[66]b	n	968	Pol ring def	[106]a
g	1428	PPy neutral	[107]b	o	932	Bip ring def	[106]a
h	1374	C-N str	[106]a				

[a] Raman data, 1064 nm excitation

[b] Raman data, other excitation sources

[c] IR data

PPy neutral: reduced PPy

substit PPy: in-plane vibration in substituted PPy

def: deformation

str: stretch

Pol: Polaron

Bip: Bipolaron

NA: Not assigned

Similarly, the 1236 cm^{-1} band (Peak "j") was assigned by Cheung et al as ring stretching [66], but as C-H in-plane deformation by Ohtsuka et al [242] and Jenden et al [106] in Raman studies and Cheung et al in an earlier FTIR study [159]. Though observed at all four excitation frequencies employed, it was not assigned by Vigmond et al [265] in their study. In the current work, this band was assigned to ring stretching, and not a C-H stretch, as no decrease in its intensity was observed in the non-substituted polymers during overoxidation. This decrease would be expected as C-H bonds are broken during nucleophilic attack at the β-carbons of the PPy ring. Hence, increases in the intensities of C=O and C-O stretching bands during overoxidation would be accompanied by a decrease in the intensity of the C-H stretching band.

In the spectra of the four overoxidation experiments presented in this work, all exhibit four peaks (not indicated individually) between Peaks "a" and "b". Even though it was not possible to assign these weak peaks, they are present in all substituted polymers, whether part of the initial structure (P(3-OPy), P(MePyC)) or due to overoxidation. These peaks are not reported elsewhere, but are possibly associated with the formation of a highly substituted PPy and are reproducible within 10 cm^{-1} in each case.

The most significant changes between the Pristine film and the film at t = 0 at 0.8 V are observed in Peaks "k" (C-H stretch) and "d" (C=C stretch) (Figure 4.2). The former peak greatly decreased in size over the 2 min taken for the collection of the spectrum, indicating breaking of the C-H bond in the bipolaron. In Section 3.3.2 it was observed that the UV-vis absorbance associated with the bipolaron peak increased over the first minute at 0.8 V in pH 2.25, and then decreased as overoxidation commenced. This is in full agreement with the decrease in the Peak "k" as the C-H bonds are broken over a similar period. The decrease in intensity of Peak "d", assigned to C=C stretch in the polymer backbone, and the development of Peak "c" (C=O stretch) indicate again that over the first 2 min at 0.8 V appreciable levels of C=O have formed and that the conjugation of the polymer has decreased. This is also supported by the appearance of a small peak (Peak "e", 1530 cm^{-1},

C=C/C=N stretch in a substituted PPy) in the scan at t = 0, indicating that substitution has indeed occurred [147]. As was reported in Chapter 2, the short time over which the onset of overoxidation manifests itself, even at moderate potentials and pHs, is surprising.

Unfortunately changes in relative peak intensities in the 1330 to 960 cm^{-1} region are not as easily explained. In agreement with Section 3.3.1, Peak "o" (932 cm^{-1}, bipolaron ring deformation) increases over the first 2 min indicating increased doping levels, even though the bipolaron C-H stretch at 1082 cm^{-1} has decreased, as discussed above. This indicates that the more reactive of the β-carbons (possibly those nearer the polymer surface or those with a higher electrochemical poise) react over this short period. However, as the peak remains throughout the 60 min, bipolarons continue to be generated over the entire period.

Further evidence for the formation of these carbonyl groups at some type of especially reactive site, even for a bipolaron, is found in the absence of a peak associated with C-OH in the t = 0 scan. Peak "m" (1011 cm^{-1}, C-O stretch) is not apparent until the scan commenced at 5 min, the same scan that contains the first peak associated with the polaron state (Peak "n", 968 cm^{-1}). It would appear that, as the hydrogen is lost prior to nucleophilic attack, the deformation of the ring increases and this deformation has similar Raman shifts to the polaron state.

This indicates that overoxidation now proceeds through the hydroxypyrrole intermediate and that the formation of this material causes dedoping of the polymer. It so effectively dedopes the film that a peak associated with the completely neutral polymer (Peak "g", 1428 cm^{-1}) also appears in the spectrum commenced at 5 min, which is unexpected considering that the polymer was held at 0.8 V throughout. These three peaks grew throughout the remaining 55 min of the experiment, along with Peaks "c" and "e", as overoxidation proceeded. However, there is no evidence for ring opening, as both Peaks

"h" (1310 cm^{-1}, ring stretch) and "j" (1143 cm^{-1}, C-N stretch, constant in the raw data) remained reasonably constant throughout.

Changes in the relative sizes of four other peaks are worthy of mention. Peak "l" (1055 cm^{-1}, N-H deformation) decreased over the 60 min period as the nitrogen changes its chemical environment. Ge et al reported that nitrogen is found in an as grown PPy film in either the -N= form (about 3% of the total), -NH- (68%) or $-NH^{+}-$ (29%), while in an overoxidised film these levels change to 14% -N=, 73% -NH- and 13% $-NH^{+}-$ [55]. This decrease in N-H bonding is reflected in the decrease in the relative size of this peak from 10 min onwards as overoxidation progresses. Peaks "f" (1481 cm^{-1}, ring stretch) and "i" (1330 cm^{-1}, ring stretch) both increased in intensity as the polymer is overoxidised, due to the decrease in conjugation as the C=O is formed. At the same time, the third peak assigned to ring stretching (Peak "j", 1230 cm^{-1}) remains constant (even in the raw data) throughout.

This would appear to discredit the assignment of these three frequencies to the same phenomena. However, it may simply indicate that these peaks are related to stretching of different regions of the PPy ring.

4.3.1.2 Overoxidation with a potential ramp

Figure 4.3 displays the Raman spectra of a PPy/pTS film collected each 50 mV during the application of a potential ramp from 0.4 to 0.9 V at 0.1 mVs^{-1}. The supporting electrolyte used was 1 M NaCl at a pH of 2.25. The individual spectra have again been scaled to give a similar peak height for peak "j" (1230 cm^{-1}, due to its constant intensity in the raw spectra) and any comparison of the peak size changes in this section will use this peak as a reference point. The assignments of the Raman peaks of Figure 4.3 are given in Table 4.2.

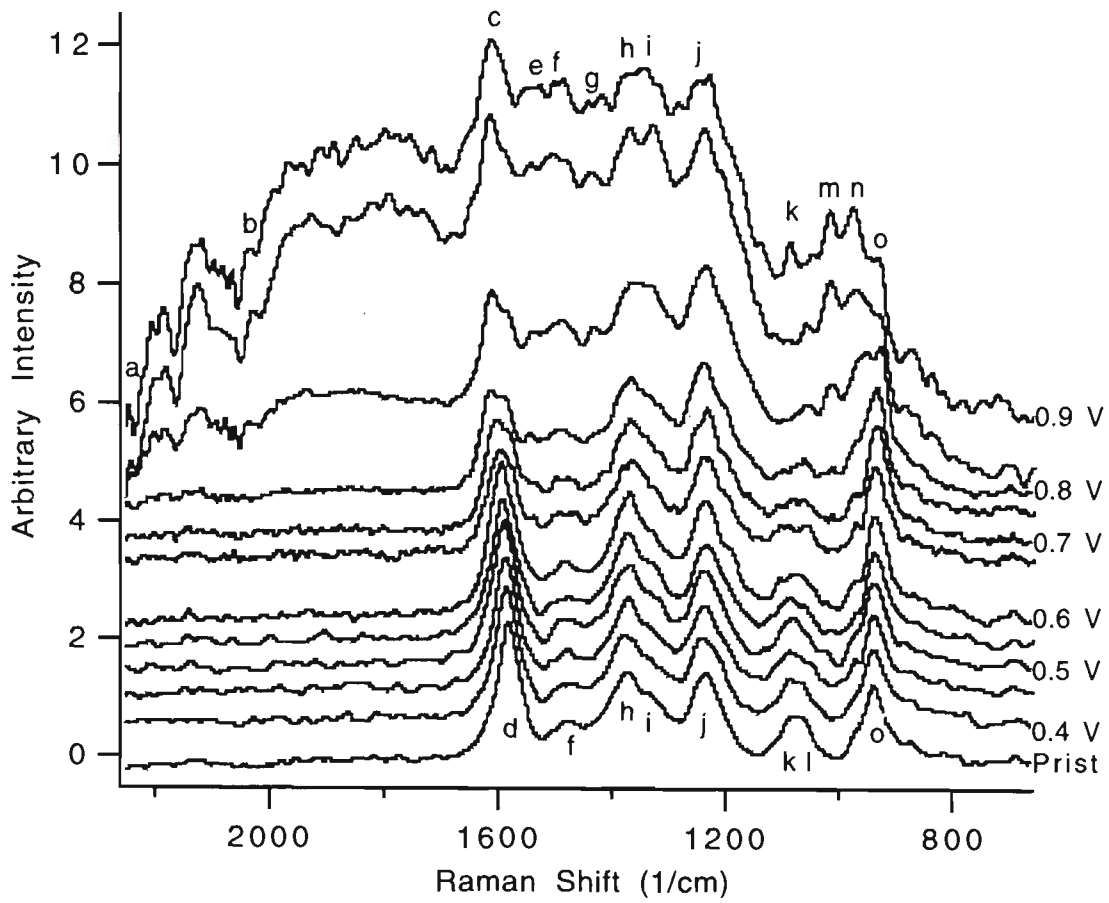

Figure 4.3: Raman spectra of PPy/pTS scanned from 0.4 to 0.9 V (vs Ag/AgCl) at a scan rate of 0.1 mVs^{-1} in 1 M NaCl with a pH of 2.25. The spectra have been scaled to peak "j" for to allow comparison of peak intensities. The potentials given are for the start of collection of each spectrum.

As expected the general profile of this figure closely resembles that of Figure 4.2. The spectrum of the pristine film and the film at 0.9 V are almost identical to the initial and final spectra when PPy was overoxidised at a constant 0.8 V. The only noticeable exception to this is the appearance of Peak "k" (1082 cm^{-1}, C-H deformation) and the more complete loss of Peak "d" (1580 cm^{-1}, C=C stretch in the polymer backbone) in the spectrum at 0.9 V. This indicates that more C-H bonds were forming, logically at the sites of chain scission, and that the polymer backbone was losing its integrity. The combination of these two features would indicate that the polymer chain is disintegrating at this potential. This would suggest some chain breaking mechanism, possibly the formation of maleimide and succinimide as observed by Park and Shim [144].

Table 4.2: Assignments of Raman bands in Figure 4.3, the overoxidation of PPy/pTS with potential ramped at 0.1 mVs^{-1} in 1 M NaCl with a pH of 2.25.

Peak	Raman shift (cm^{-1})	Assignment	Ref	Peak	Raman shift (cm^{-1})	Assignment	Ref
a	2241	NA	-	i	1340	Ring str	[66]b
b	2037	NA	-	j	1230	Ring str	[66]b
c	1610	C=O str	[268]c	k	1082	C-H bend	[265]a
d	1580	C=C str	[265]a	l	1061	N-H def	[66]b
e	1520	C=C/C=N substit PPy	[147]c	m	1011	C-O str	[144]c
f	1480	Ring str	[66]b	n	970	Pol ring def	[106]a
g	1444	PPy neutral	[107]b	o	937	Bip ring def	[106]a
h	1375	C-N str	[106]a				

[a] Raman data, 1064 nm excitation

[b] Raman data, other excitation sources

[c] IR data

PPy neutral: reduced PPy

substit PPy: in-plane vibration in substituted PPy

def: deformation

str: stretch

Pol: Polaron

Bip: Bipolaron

NA: Not assigned

No noticeable changes are apparent in Figure 4.3 between the pristine and 0.4 V spectra, however, at 0.45 V a small shoulder appears at 970 cm^{-1} on Peak "o", assigned as polaron ring stretch. It was noted above (at a constant 0.8 V) this feature was observed prior to the appearance of a C-O stretch band at 1011 cm^{-1}. However, at potentials appreciably lower than 0.8 V, it is obvious that changes in the ring conformation are actually a precursor for nucleophilic attack. Even though the polaron ring stretch band appears at 0.45 V, no carbon - oxygen bonds are observed until 0.65 V, as indicated by the presence of a small peak at 1011 cm^{-1} at this potential. The broadening of Peak "d" (1580 cm^{-1}, C=C stretch) and the development of the C=O stretching peak (Peak "c",

1610 cm^{-1}) and C=C / C=N band in a substituted PPy (Peak "e") are also apparent for the first time at this potential. As both C-O and C=O features are present at 0.65 V, it can be said that irreversible overoxidation has commenced at this potential.

Between 0.65 and 0.85 V all of the features associated with the progress of overoxidation can be observed: loss of N-H bonds (Peak "l"); development of polaron deformation (Peak "n"), C-O groups (Peak "m"), C=O groups (Peak "c"), C=C / C=N in a substituted PPy (Peak "e") and ring stretch (Peak "i"); as well as the loss of C=C in the polymer backbone (Peak "d").

4.3.2 Overoxidation of the disubstituted pyrrole poly(3-methylpyrrole carboxylic acid)

Poly(3-methylpyrrole carboxylic acid) (P(MePyC)/BF_4) was galvanostatically grown from a solution of 0.05 M 3-methylpyrrole carboxylic acid and 0.02 M TEA BF_4 in 50% CH_2Cl_2 : AcN. The Raman spectra collected every 50 mV during the application of a potential ramp from 0.4 to 0.9 V at 0.1 mVs^{-1} are given in Figure 4.4. No spectrum was collected at 0.55 V. On this occasion, the individual spectra have been scaled to give a similar peak height for peak "h" (1375 cm^{-1}), due to its constant intensity in the raw spectra. Any comparison of the peak size changes in this section will use this peak as reference point. The assignments of the Raman peaks indicated in Figure 4.4 are shown in Table 4.3.

The Pristine spectrum exhibits a number of features not seen in the non-substituted PPys above. The broad peak centred at 790 cm^{-1} (Peak "p") is reported by Beck (Beck, 19) to be symptomatic of a substituted PPy, though it is present as a small peak in all other spectra given in the current work. Peak "m" (1025 cm^{-1}, C-O stretch) is also apparent in the pristine film and is presumably due to the carboxylic acid substituent and not an oxygen attached directly to the ring. The final additional band is Peak "k" (1200 cm^{-1}, CH_3 bend), due to the substituent methyl group.

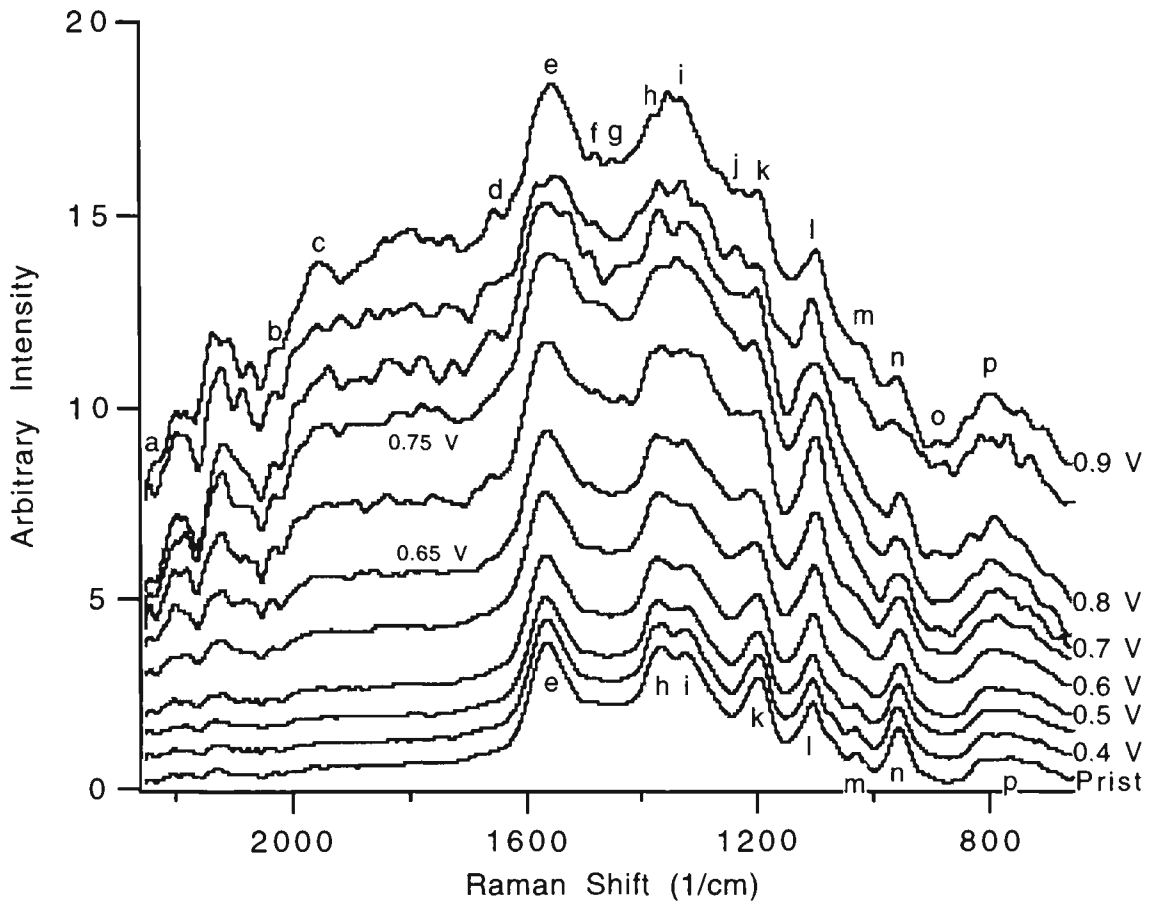

Figure 4.4: P(MPyC)/BF4, scanned at 0.1 mVs^{-1}. Figure 4.3: Raman spectra of PPy/pTS scanned from 0.4 to 0.9 V (vs Ag/AgCl) at 0.1 mVs^{-1} in 1 M NaCl with a pH of 2.25. The spectra have been scaled to peak "h" to allow comparison of peak intensities. The potentials given are for the start of collection of each spectrum.

However, due to the disubstitution of the pyrrole ring, a number of the bands have been shifted to somewhat different frequencies. The N-H deformation band (Peak "I") shifts from 1061 cm^{-1} given in Tables 4.1 and 4.2 to 1105 cm^{-1}, as explained in Note 2 of Table 4.3. Support for this assignment comes from Park and Shim [144] who note that the N-H stretch in a mixture of the overoxidation products of PPy, namely disubstituted maleimide and succinimide, occurs at 1100 cm^{-1} in an FT-IR study. As a result of lattice dynamical calculations Tian and Zerbi assign a frequency of 1134 cm^{-1} [269] to this deformation, thus its appearance at 1105 cm^{-1} does not represent an extreme shift.

Table 4.3: Assignments of peaks indicated in Figure 4.4 for P(MPyC)/BF_4 scanned at 0.1 mVs^{-1} in 1 M NaCl at a pH of 2.25.

Peak	Raman shift (cm^{-1})	Assignment	Ref	Peak	Raman shift (cm^{-1})	Assignment	Ref
a	2240	NA	-	i	1330	Ring str	[66]b
b	2024	NA	-	j	1231	Ring str	[66]a
c	1950	NA	-	k	1200	CH_3 bend	Note 1
d	1655	C=O	[123]c	l	1105	N-H def	Note 2
e	1560	C=C str	[265]a	m	1025	C-O str	[144]c
f	1480	Ring str	[66]b	n	961	Pol ring def	[106]a
g	1448	PPy neutral	[107]b	o	888	Ring def	[269]c
h	1375	C-N str	[106]a	p	790	Ring vib substit PPy	[21]c

[a] Raman data, 1064 nm excitation

[b] Raman data, other excitation sources

[c] IR data

NA Not assigned

PPy neutral: reduced PPy

substit PPy: in-plane vibration in substituted PPy

def: deformation

vib: vibration

str: stretch

Pol: Polaron

Bip: Bipolaron

Note 1: This assignment pertains to the hydrogens in the substituent methyl group, as the PPy ring has only hydrogens attached directly at the α-carbons of the terminal pyrroles. Socrates reports that the H-C-H bend in a methyl group is typically observed between 1490 and 1150 cm^{-1} [270]. Some confirmation of this comes from FT-IR spectra of poly(dimethylpyrrole) presented by Ribo et al [271] which indicates a peak at 1200 cm^{-1}.

Note 2: It is assumed that the frequency of this band has moved from its normal position in PPy as this material is disubstituted. Ribo et al [271] note that disubstitution modifies the positions of peaks around this frequency in PPy.

One of the signature frequencies of polypyrrole, the C=C backbone stretching band, was also found at a slightly different frequency than its normal Raman shift of around 1580 cm^{-1} [66, 106, 265]. This band was shifted to a lower frequency of 1560 cm^{-1} in pristine P(MePyC). This was not unexpected as this band is believed to be an overlap of polaron and bipolaron bands [106] and, as was discussed in Chapter 3, this polymer is in a very low oxidation state in the as-grown form. It would be anticipated that this low level of doping would bias the position of this band one way or the other.

The doping of this film was so poor that no bipolaron ring deformation band is evident in the scan of the pristine film. Based on PPy and P(3-OPy) this band would be expected around 900 to 930 cm^{-1}. The only possibilities near these frequencies are a small shoulder in the scan initiated at 0.85 V, or a mis-assignment of the small Peak "o", which appears at 0.65 V. In either case, it could be said that the peaks are almost insignificant and that effectively no bipolaron species are identified throughout the experiment.

The C=C/C=N stretching band of a substituted PPy at 1530 cm^{-1} [147] was also absent in the scan of the pristine film, presumably as it falls under the C=C stretch (Peak "e") due to the red shift of this band. However, as the potential, and hence the doping level, was increased the more normal 1580 cm^{-1} C=C and 1530 cm^{-1} C=C/C=N stretches appeared. These were first observed in the scan initiated at 0.75 V. At a somewhat lower potential of 0.65 V two new peaks arose for the first time: a new ring deformation band (Peak "o", 888 cm^{-1}), indicating a change in the ring structure, and a new ring-carbon C=O (Peak "d", 1655 cm^{-1}), indicating that one of the substituent groups has been replaced by a direct oxygen linkage. At the same time the C-O stretching band (Peak "m", 1025 cm^{-1}) became vanishingly small. In other words, overoxidation was well underway, even before the polymer was fully doped with no C-O formation as a precursor to C=O.

From Figure 4.4 it can be seen that the peak assigned to the substituent methyl group (Peak "k", 1200 cm^{-1}) remained reasonably constant at these potentials. However, as mentioned above, the peak assigned to the substituent carboxylic acid group (Peak "m", 1025 cm^{-1}, C-O stretch) had been totally lost. This implies not only that overoxidation was initiated by the loss of the carboxylic acid group, but also that it proceeded by some mechanism other than nucleophilic attack at a ring carbon. If the latter was not true, the C-O stretch would remain due the attachment of the hydroxyl group.

Overoxidation could have occurred directly by elimination of carbon dioxide (decarboxylation) [206], as presented in Scheme 4.2. At a potential of 0.6 V, the level of doping in the polymer would have increased sufficiently from its very low as-grown level (see Chapter 3) to generate large numbers of polarons. This radical cation could then react with oxygen, followed by elimination of CO_2 then $OH^{\cdot}$ and finally, rearrangement to a substituted pyrrolinone, which has the electron configuration of overoxidised (non-substituted) PPy reported by Beck et al [146]. If the reactions that occurred from the time of oxygen attack and until the elimination of the $OH^{\cdot}$ are quick, no C-O stretch will be observed. This is reasonable as these reactions are quite different to those seen in the rearrangement of the hydroxy species to the ketone in nucleophilic attack.

This mechanism not only fits the changes in the Raman spectra noted above, but also accounts for the observation in Chapter 2 that only 2% of the growth charge is consumed during overoxidation of P(MePyC). It also explains why this disubstituted PPy, with both possible sites for nucleophilic attack blocked, has a much lower overoxidation than anticipated.

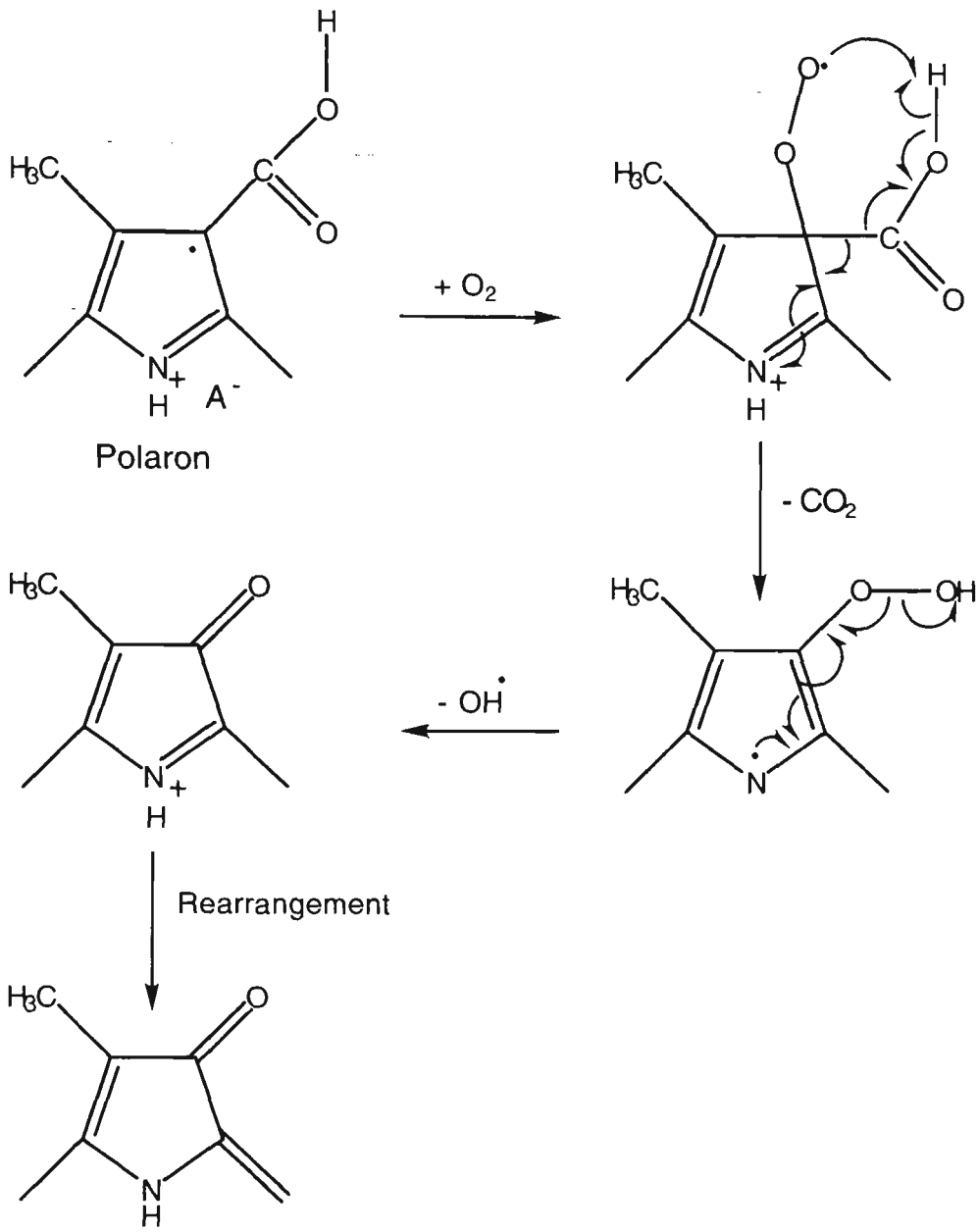

Scheme 4.2: Proposed mechanism for decarboxylation of the P(MePyC) polaron by reaction with oxygen.

Though there is no indication in the Raman spectra, overoxidation based on the decarboxylation of P(MePyC) may proceed through further oxidation of the β-carbon free radical (-C•-) to the carbocation (-C+-) [272, 273]. Reactions between the free radical and an adjacent conjugated carbon, or between the carbocation and a free radical of an adjacent pyrrole, could then lead to cross linking between polymer chains. This may also contribute to the rapid overoxidation of the disubstituted PPy indicated in Chapter 3.

4.3.3 Overoxidation of the monosubstituted pyrrole poly(3-octylylpyrrole)

Poly(3-octylylpyrrole) (P(3-OPy)/BF_4) was grown from a solution of 0.05 M 3-octyl pyrrole and 0.02 M TEA BF_4 in 50% CH_2Cl_2 : AcN. The Raman spectra collected every 50 mV during the application of a potential ramp from 0.4 to 1.1 V at 0.1 mVs^{-1} (in 1 M NaCl with pH adjusted to 2.25) are given in Figure 4.5. Scaling was not necessary for the spectra of this polymer. The assignments of the Raman peaks indicated in Figure 4.5 are given in Table 4.4.

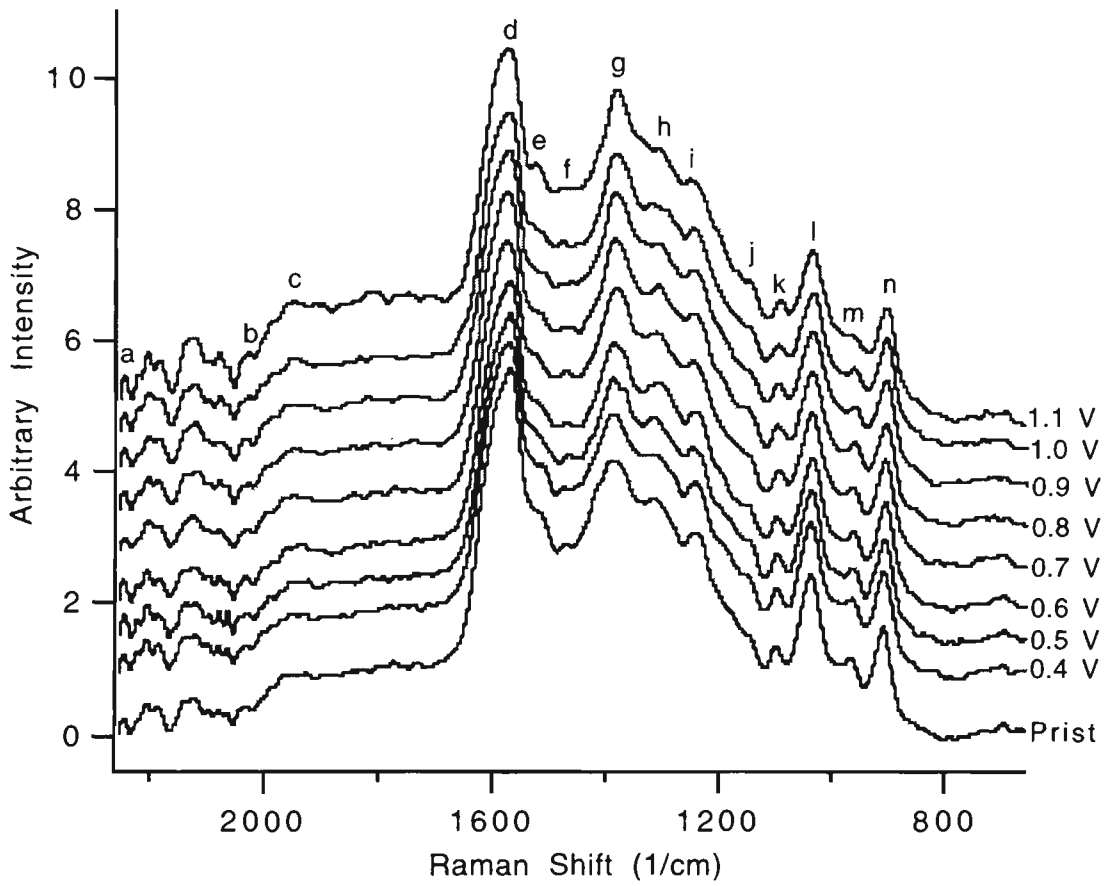

Figure 4.5: Raman spectra of P(3-OPy)/BF_4 scanned from 0.4 to 0.9 V (vs Ag/AgCl) at 0.1 mVs^{-1} in 1 M NaCl with a pH of 2.25. No scaling was necessary for these spectra. The potentials given are for the start of collection of each spectrum.

Compared to the two other polypyrroles studied in this chapter, the spectra of P(3-OPy) show a number of unusual features. In particular, it is the only polymer to display both

prominent polaron (Peak "m", 901 cm^{-1}) and bipolaron (Peak "n", 901 cm^{-1}) ring deformation bands. PPy displayed only a bipolaron stretch in this region and P(MePyC) only a polaron stretch, indicating moderate and low doping levels, respectively. The presence of both in P(3-OPy) confirms the intermediate doping levels of this polymer observed in Chapter 3.

Table 4.4: Assignments of peaks indicated in Figure 4.5 for P(3-OPy)/BF_4 scanned at 0.1 mVs^{-1} in 1 M NaCl at a pH of 2.25.

Peak	Raman shift (cm^{-1})	Assignment	Ref	Peak	Raman shift (cm^{-1})	Assignment	Ref
a	2240	NA	-	h	1310	Ring str	[66]b
b	2027	NA	-	i	1252	Ring str	[66]b
c	1946	NA	-	j	1143	C-N str	[269]b
d	1573	C=C str	[265]a	k	1094	C-H bend	[265]a
e	1524	C=C/C=N substit pol	[147]c	l	1036	N-H def	[66]b
f	1468	Ring str	[66]c	m	961	Pol ring def	[106]a
g	1381	C-N str	[106]a	n	901	Bip ring def	[106]a

[a] Raman data, 1064 nm excitation

[b] Raman data, other excitation sources

[c] IR data

PPy neutral: reduced PPy

substit PPy: in-plane vibration in substituted PPy

def: deformation

str: stretch

Pol: Polaron

Bip: Bipolaron

NA: Not assigned

Another feature only observed in this polymer is the band at 1946 cm^{-1} (Peak "c"). As it not present in pristine nor overoxidised PPy or P(MePyC), it is not associated with either the PPy backbone, substituted or disubstituted of PPy nor counterion bands. As no assignment could made for this peak, it is possibly a Raman shift associated with the octyl

substituent. Based on FT-IR studies, C_8H_{17} should exhibit Raman shifts around 1640 cm^{-1} (C-C stretch) [160] and 1200 cm^{-1} (C-H) [270]. However, neither of these was observed, though the C-C stretch may be subsumed under the strong C=C peak at 1573 cm^{-1}.

Finally, and most importantly, the spectra of P(3-OPy) exhibited minimal chemical changes during the experiment. The only changes observed in Figure 4.5 are small decreases in the intensities of Peaks "f" and "i", both ring stretching bands, and Peak "m", the ring deformation assigned specifically to the polaron oxidation state. These simply indicate that the doping level of the polymer is increasing as the potential increases. From the discussions of this polymer in Chapters 2 and 3, this was not unexpected. As Peak "m" was still evident in the final spectrum, it can be assumed that the polymer has not reached its maximum doping level, even at 1.1 V. The fact that no other changes were observed between the spectrum of the pristine film and that at 1.1 V, again emphasises the incredible stability of this polymer to electrochemical degradation in an aqueous environment.

CONCLUSION

This chapter set out to investigate the chemical changes occurring in polypyrrole (PPy), the mono-substituted polypyrrole P(3-OPy) and the disubstituted polypyrrole P(MePyC) during overoxidation. This was performed in an aqueous environment using Raman spectroscopy to probe the chemical interactions during the application of anodic potentials.

PPy/pTS was found to be in a highly doped state in the as grown form, with strong evidence that the polymer was almost exclusively in the bipolaron state, with no neutral or polaron bands noted. When the polymer was stepped to a potential of 0.8 V (vs Ag/AgCl) it was found that the rapid loss of some bipolaron features was associated with the

formation of the carbonyl group at a ring carbon. This carbonyl formation occurred without any evidence of the normal hydroxyl intermediate of a nucleophilic attack. From 5 min to 60 min at 0.8 V, the more expected route of nucleophilic attack was observed. Raman bands associated with the polaron and C-O linkages developed strongly over this time. At the same time the intensity of the carbonyl group increased and that of the N-H group decreased. In combination these findings offer strong in-situ support for nucleophilic attack proposed by Beck et al.

In the case of a PPy/pTS film scanned slowly from 0.4 to 0.9 V, Raman spectroscopy showed that the development of polarons was a precursor for nucleophilic attack at moderate potentials. The polaronic state was first observed at 0.45 V and this was followed by irreversible overoxidation at 0.65 V (as indicated by the presence of both C-O and C=C groups). One of the other proposed mechanisms of overoxidation of PPy is that of chain breaking. Some evidence of this was noted at a potential of 0.9 V.

The disubstituted polypyrrole P(MePyC) displayed an extremely low level of doping both in the as grown form and under the application of a high anodic potential. No evidence for the bipolaronic state could be found in either environment. Based on the Raman data collected during the application of a slow potential ramp, a mechanism was proposed for the overoxidation of P(MePyC) via a direct decarboxylation reaction. This mechanism explained why this disubstituted PPy, with no obvious sites for nucleophilic attack, has an overoxidation potential not dissimilar to a non-substituted PPy. It also explained the low level of charge consumed for this polymer (Chapter 2) and its rapid rate of overoxidation (Chapter 3).

The stability of P(3-OPy) to electrochemical overoxidation in an aqueous environment was again demonstrated. During the application of a linear potential ramp from 0.4 to 1.1 V, no chemical changes in the polymer structure were detected. The only change in the polymer was determined to be a slight increase in doping level, from an original level

between PPy (mostly bipolaronic) and P(MePyC) (exclusively polaronic). This increase in the doping levels with no detectable overoxidation seems a natural extension of the work in Chapters 2 and 3 on this polymer.

CHAPTER 5: MATRIX-ASSISTED LASER DESORPTION IONISATION MASS SPECTROMETRY STUDIES

5.1 Introduction

The use of matrix assisted laser desorption ionisation (MALDI) as an ionisation technique for introducing large, labile molecules into the gas phase for mass spectrometry (MS) was first reported independently by Tanaka et al and Karas and Hillenkamp ([274] and references therein). The technique involves mixing solutions of the analyte and a suitable matrix compound such that the matrix is in 100 to 50000 fold excess [275]. The solution is then dispensed onto a metal "target" (eg stainless steel) and the solvent is allowed to evaporate causing cocrystallization the sample and matrix. After insertion into the sample port, the sample / matrix is subjected to a series of short laser pulses (337 nm in the current work) to desorb / ionise the sample. The resultant ions are then passed into a mass spectrometer for mass analysis. Though other mass analysers can be used for this purpose, time of flight (ToF) analysers are the most common owing to their high mass range (< 100 to 1,000,000 Da [276]) and excellent sensitivity [277, 278]. Synchronisation of the detector and the laser pulses allows precise measurement of the time of flight and, hence, the mass-to-charge ratio (m/z) of the ions. The advantages of MALDI include generation of almost exclusively singly charged (z = 1) ions, generally either hydrogen $(M+H)^+$ or sodium $(M+Na^+)$ adducts [279].

The matrix is generally thought to have several roles [275, 276, 280], namely:

(i) to absorb energy from the laser pulse and convert this into excitation energy to evaporate the matrix;

(ii) to isolate the sample molecules to reduce intermolecular forces [280];

(iii) to supply photoexcited acidic and basic sites to generate protonated or deprotonated species via ion / molecule collisions in the gas phase.

(These processes are represented schematically in Figure 5.1.) These requirements are met by a number of large organic acids containing one or more benzene rings [281], including: sinapinic acid, 2,5-dihydroxybenzoic acid, caffeic acid, vanillic acid and nicotinic acid [275, 280]. Of these, the former three absorb strongly at the N_2-laser wavelength of 337 nm.

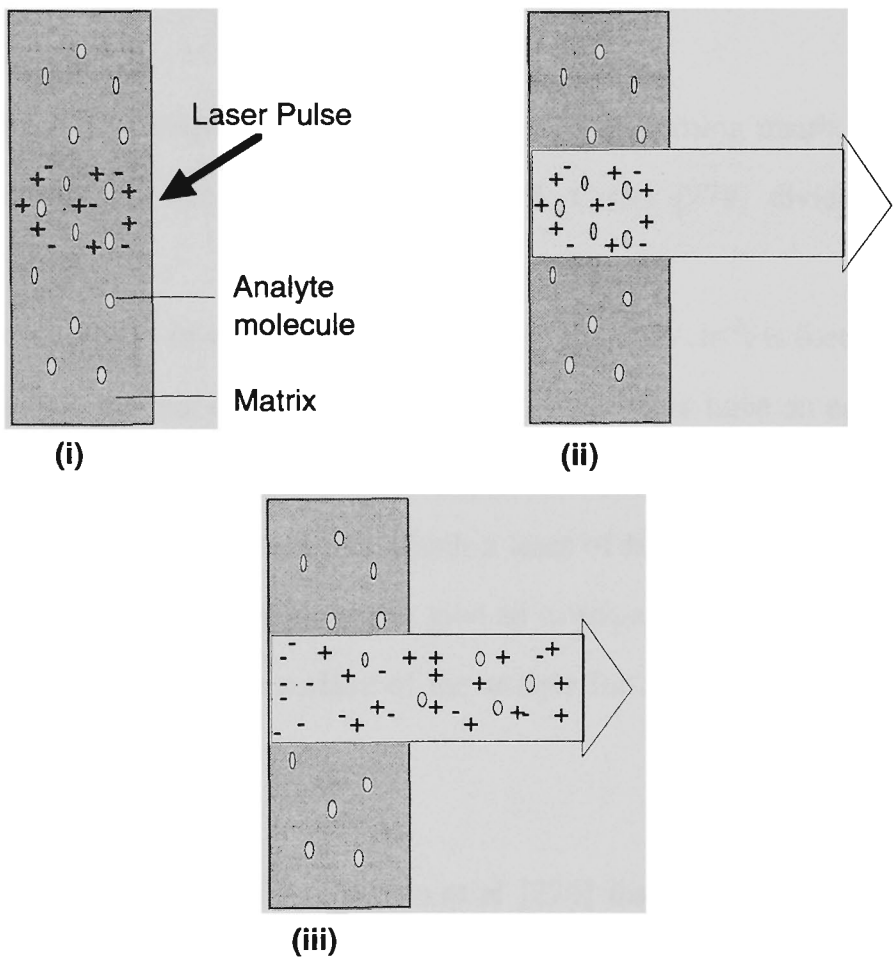

Figure 5.1: Matrix assisted laser desorption ionisation mechanism. (i) absorption of UV radiation by matrix leading to ionisation of matrix, (ii) dissociation of the matrix, phase change to supercompressed gas and transfer of charges to the analyte matrix, (iii) entrapment of analyte in rapidly expanding matrix plume and transfer of charges to analyte molecules (from Fenselau [276]).

Owing to the low laser intensity per unit area (irradiance) employed in this technique and the strong resonance absorption of the sample / matrix at the laser wavelength, this "soft ionisation" technique yields largely molecular ions with little fragmentation. It is important

to note however, that a sharp irradiance threshold has been observed. Levels appreciably above the threshold level result in extensive fragmentation, with increasing formation of nonspecific low-mass ions (thought to be recombination products from a laser-induced plasma) [280]. Soft ionisation is limited to a quite small irradiance range, at or slightly above the threshold level, with fragmentation / degradation of the sample at high laser irradiances.

Laser desorption techniques that do not employ a UV absorbing matrix to transfer energy to the analyte have also been commonly used. Cotter [278] divides these into two categories:

(i) microprobes - in which a pulsed laser (10^6 to 10^7 Wcm^{-2}) is focussed on an area of 1 μm^2 or less on the rear of a thin metal foil support. These have an energy of a few mJ per pulse which burns through the foil and instantaneously thermally desorbs the analyte;

(ii) bulk analysis instruments - in which a laser of higher power (10^8 to 10^{12} Wcm^{-2}) is focussed over the entire target area to give an average pulse energy of about 0.5 J per pulse, which heats the entire surface of the analyte for several microseconds to generate analyte ions.

It has also been recognised by Campana et al [274] that under some circumstances the addition of a matrix material is not necessary or desirable to obtain a mass spectrum of a sample. They give as an example the determination of a UV absorbing additive in a solid paint sample. In this case it is not convenient to alter the sample to introduce a matrix. Instead, a chip of paint can be directly analysed by laser desorption with a UV laser under the same instrumental conditions employed in MALDI-ToF-MS. The short pulses of low power laser light are then absorbed by the UV active component, leading to ionisation of the material followed by ToF analysis in the normal way.

Mass spectrometric techniques in general have found limited use in studies of polypyrrole (PPy). Abel et al [282] and Luk et al [283] have employed Secondary Ion ToF-MS (ToF-

SIMS) to identify dopant ions in various PPys. Dopant loss at elevated temperatures has been monitored by Satoh et al [56] using gas chromatography MS (GC-MS) and Ge and Wallace [130] using fast atom bombardment-MS (FAB-MS). PPy dopant ions have also been studied by Raynor and Schlindwein [284] with direct insertion probe Electron Impact-MS (EI-MS). Mass spectrometric studies of the soluble degradation products of PPy have been carried out by Park and Shim [144] and Chen and Rajeshwar [285], with the latter employing GC-MS. Structural information on the PPy backbone was obtained by Cheung et al [66], who observed pyrrole dimers, trimers and hexamers with FAB-MS.

Though MALDI-ToF MS has been applied to a wide range of biological molecules [275, 276, 280] and commodity plastics [274, 281, 286, 287] no reports of its application to PPy have yet been published.

5.2 EXPERIMENTAL

5.2.1 Reagents and materials

All chemicals used were analytical reagent grade unless otherwise stated. Pyrrole (Sigma) was distilled before use and stored at -16 °C in the dark under N_2 where necessary. Water was reagent grade obtained from a Millipore Milli-RO/Milli-Q™ water purification system.

Electrodeposition, overoxidation and characterisation of polymer films were carried out on 2 cm diameter stainless steel MALDI targets (Bruker). Platinum gauze (Engelhard) was used as an auxiliary electrode throughout. All potentials were measured against a Ag/AgCl reference electrode (Hart Analytical) via a salt bridge containing 0.1 $NaNO_3$.

5.2.2 Instrumentation

Electropolymerisation of polymer films was carried out using an in-house galvanostat. Overoxidation was performed using a CV-27 (BAS) Potentiostat. Data was collected by a Macintosh (Apple) computer interfaced through a MacLab (ADI, Australia) four channel interface.

Mass spectra were obtained on a Bruker Biflex MALDI operating in the positive ion mode reflectror using an N_2-laser (337 nm, pulse length ~ 3 ns, target area 10^4 μm^2, laser irradiance 10^6 to 10^7 Wcm^2). The instrument was calibrated with polyethylene glycol (average molecular weight 600, Polymer Laboratories) and data was processed on a Sun Sparc Station 5. The spectra were generated with between 15 and 50 laser shots, with an attenuation of 40 to 50 % of the laser irradiance.

5.2.3 Procedures

The electrodes were firstly polished, initially on 1 μm and then 0.3 μm Al_2O_3 slurry, followed by ultrasonication for 30 s in Milli-Q water and rinsing with water. One half of the face and the entire back of the target were masked with contact adhesive (3M, USA) to give a reproducible growing area of 1.07 cm^2. PPy was electrodeposited galvanostatically using a standard three-electrode cell with a current density of 1 $mAcm^{-2}$ for 30 min from a solution of 0.2 M pyrrole and 0.2 M NapTS in H_2O. This generated films of approximately 4.5 μm thickness which were rinsed thoroughly with Milli-Q water. The films were then either:

i) allowed to dry in air.

ii) overoxidised in 0.2 M NapTS (pH 5.2) at an applied potential of 0.9 V (vs Ag/AgCl) for 12 or 30 min.

iii) allowed to age in air for 6 months.

iv) base treated by soaking in 0.1 M NaOH (pH 12.7) for 12 min.

v) overoxidised in 0.1 M NaOH (pH 12.7) at an applied potential of 0.9 V (vs Ag/AgCl) for 2 min.

All growth and film treatment was performed in air.

5.3 RESULTS AND DISCUSSION

Initial investigations employing sinapinic acid as quasi-matrix spread thinly over a PPy film were not encouraging. Presumably this was because the PPy was an insoluble film under the matrix and thus was neither isolated within, nor in intimate contact with, the matrix molecules. These results were so poor that it was felt that reliance on the UV absorption of PPy itself may produce better results, as suggested by Campana et al [274] in the example mentioned in Section 5.1. As discussed in Chapter 1, PPy absorbs strongly around 310 [39, 103] and 390 nm [109, 135].

Preliminary experiments with 1 μm thick films gave promising results, but raised two further issues:

(i) for the purposes of the generation of a useful signal, it was critical to find the "threshold irradiance" mentioned in the Introduction to this chapter. Below this level, no signal was observed, while above it peaks owing to the degradation of the sample were observed at all mass-to-charge values, in accord with Karas et al [280] as mentioned above. The optimum range was found to be within around +/- 1 % attenuation of the threshold value, which varied from sample to sample;

(ii) even at the low laser irradiance employed in a MALDI instrument, 1 μm films were, from time to time, completely ablated to expose the stainless steel substrate. As a result, all further studies were performed on 4.5 μm films which eliminated this problem.

The mass spectrum of a 4.5 μm, as-grown PPy/pTS film is given in Figure 5.2. This mass spectrum, showed no peaks that could be attributed to molecular ions of PPy species. This indicates that the pristine polymer was sufficiently stable that laser excitation was unable to ionise complete molecules and only produced fragments, which appear as "nonspecific low mass ions" along the mass to charge (m/z) axis [280]. Another

possibility is that molecules were desorbed into the gas phase, but were not ionised and, hence, not detected. This was reported by Belu et al [281] as serious limitation of the MALDI technique for straight hydrocarbon polymers (eg polybutadiene and polyethylene). However, considering the ease of protonating / deprotonating the nitrogen in PPy and the nature of the polymer backbone itself, it seems unlikely that molecules desorbed from this polymer would lack an effective site for ionisation.

MALDI mass spectra of a number of PPy samples subjected to overoxidation at 0.9 V (vs Ag/AgCl), base treatment or long term ageing are given in Figures 5.2 - 5.7. All of these spectra show a series of intense peaks that are readily distinguished from the background. Proposed structures to account for the masses of the major peaks in these spectra are given in Schemes 5.1 - 5.3. After either overoxidation at 0.9 V (vs Ag/AgCl), base treatment or long term ageing, all samples submitted to the MALDI yielded reasonable spectra. It would appear that the polypyrrole which has not been affected by overoxidation may be acting as the "matrix" for the overoxidised components. That is, absorbing UV radiation and transferring this energy to the isolated overoxidised segments.

Considering first the mass spectrum of PPy/pTS overoxidised at 0.9 V (vs Ag/AgCl) for 12 min in 0.2 M NapTS (Figure 5.3). In this spectrum the major peaks observed at m/z 39, 413 and 429, the former due to the ubiquitous K^+ ions. The peak at m/z corresponds to the sodium adduct {$(M+Na)^+$ ion} of an non-substituted PPy chain comprising six monomer units less two hydrogen atoms. A possible structure for this ion (i), in which the hexamer contains two imine-nitrogens (-N=), is given in Scheme 5.1. The presence of two imine nitrogens is consistent with the observations of Ge et al [55] and Malitesta et al [154] that imine-N increased significantly during overoxidation. Ge et al have reported that an as-grown polymer has approximately 1 imine-N for each 20 monomer units and that after overoxidation this rises to 1 per 7 units. Malitesta et al claimed that the level of this moiety rises from 1 in 20 to nearly 1 in 5 during this process. It is not unreasonable

to assume that these imine-nitrogens do not occur evenly along the chain, but may be concentrated at sections of the polymer undergoing overoxidation, though the mass spectra provide no evidence of the location of the imine groups.

Structures (ii) and (iii) are sodium adducts of two possible tautomers of an oxygen-substituted, six monomer PPy chain that would give rise to an ion of m/z 429. This chain length coincides with that reported by Cheung et al [66] in a Fast Atom Bombardment - MS study of PPy/pyrenesulphonate. According to this group, the largest polymeric unit observed was the hexamer, with dimers and trimers also seen.

The structures are consistent with work described in earlier chapters, which provided strong evidence that oxygen is incorporated during overoxidation. One of these may represent the earlier stages of overoxidation (Structure (i), containing C-OH) and the other of the latter stages (Structure (ii), containing C=O). However, strong support for Structure (ii) came again from Malitesta et al [154] (though not in agreement with Ge et al on this occasion) who report that the level of C=O rises from 1 carbonyl per 25 Py units to 1 in 7.5 during overoxidation. Along with Palmisano et al [153] these authors also claimed that this oxygen will be attached to an α-carbon, leading to breaking of the PPy chain. Based on Structure (i), this may be induced by the presence of two imine nitrogens at the end of a six unit chain.

The major peaks in the spectrum of a highly overoxidised film (0.9 V for 30 min in 0.2 M Na/pTS, Figure 5.4) occur at m/z 194, 217, 232, 241, 367, 413, 429 and 477. The peaks at m/z 413 and 427 are attributed to an unsubstituted and an oxidised hexamer described above for the less overoxidised film. In this case though the oxygen substituted hexamer has three imine-nitrogens (Scheme 5.3, Structure (viii)). It is also apparent that their relative intensities have considerably altered. Whereas in the less overoxidised film the peak at m/z 413 was approximately twice the intensity of m/z 427, they now have similar

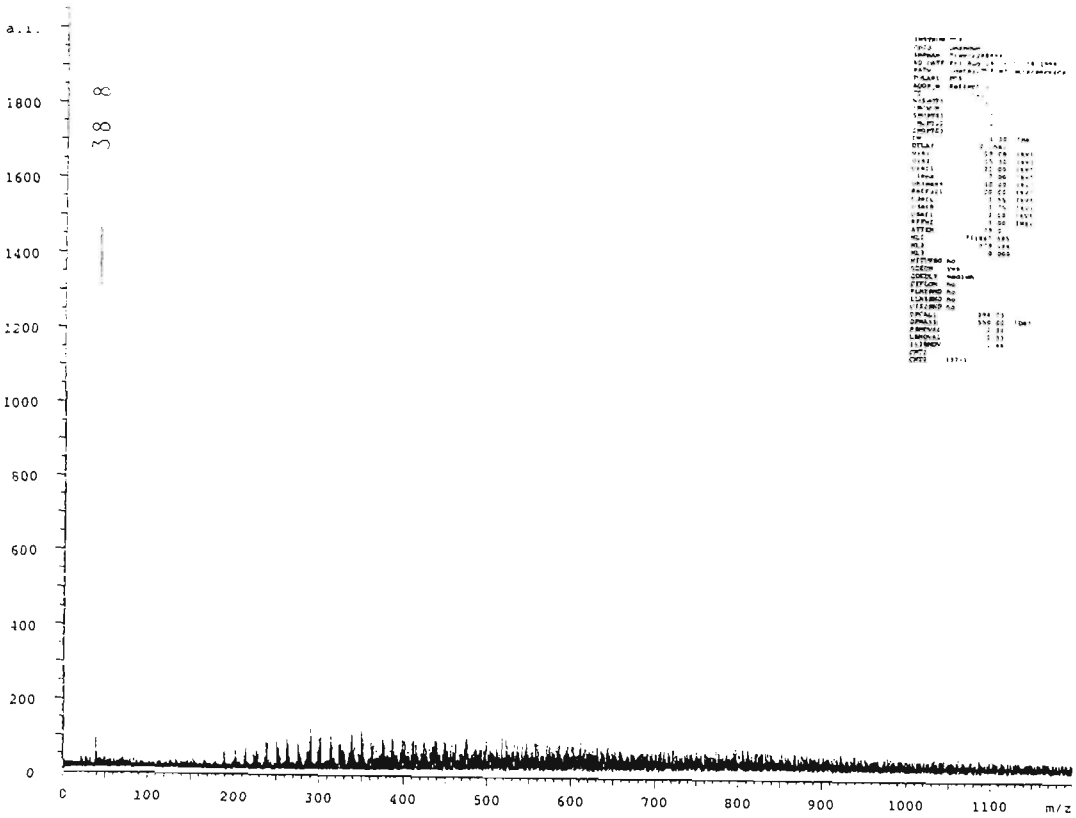

Figure 5.2: MALDI-ToF mass spectrum of a 4.5 υm pristine PPy/pTS film. Attenuation 39 arbitrary units; 20 shot average.

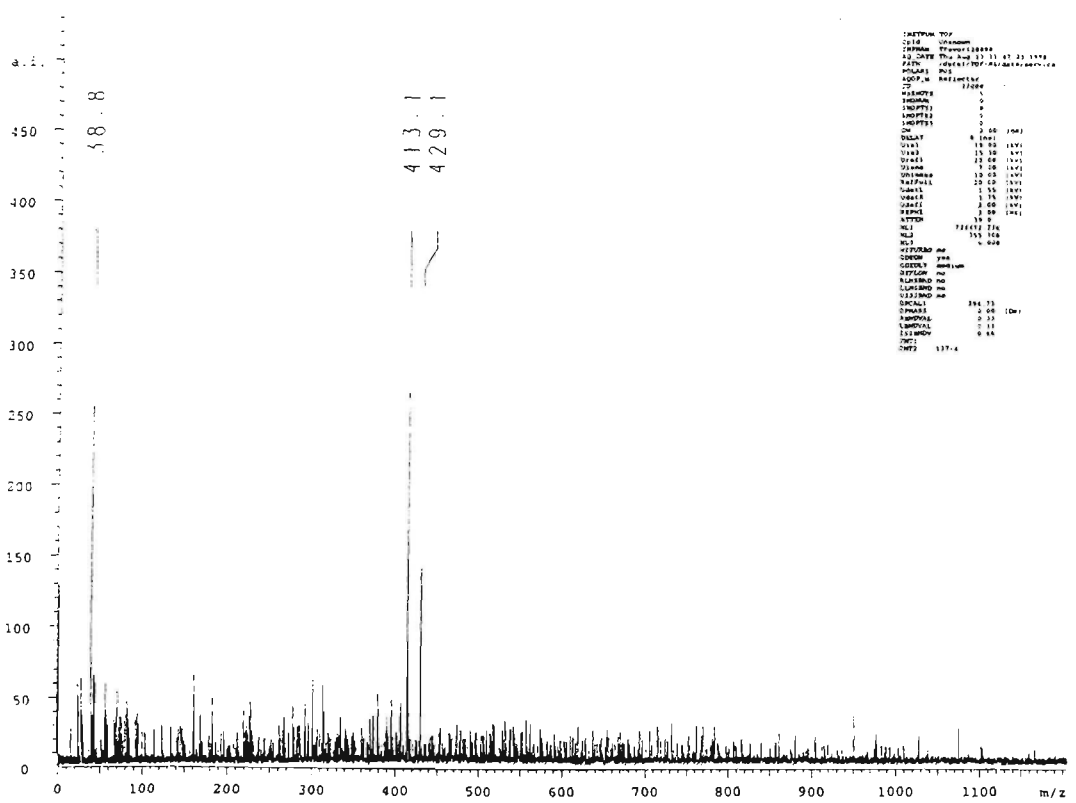

Figure 5.3: MALDI-ToF mass spectrum of a 4.5 υm PPy/pTS film overoxidised at 0.9 V (vs Ag/AgCl) for 12 min in 0.2 M NapTS. Attenuation 51 arbitrary units; 50 shot average.

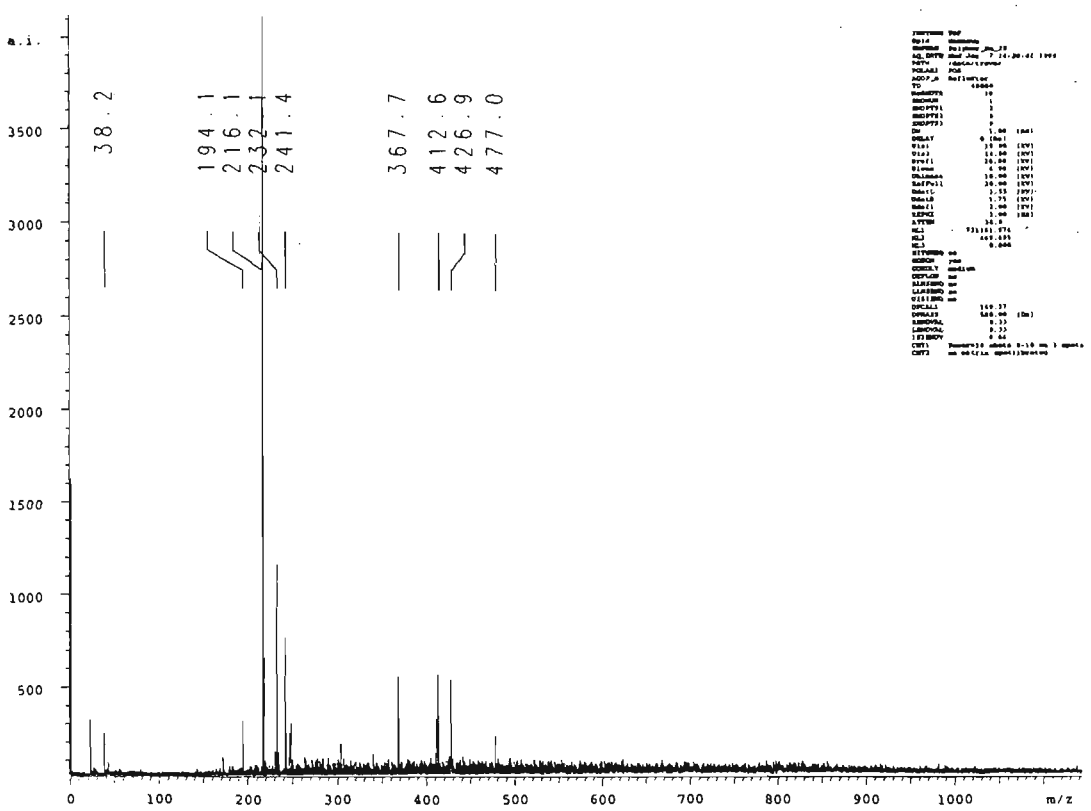

Figure 5.4: MALDI-ToF mass spectrum of a 4.5 υm PPy/pTS film overoxidised at 0.9 V (vs Ag/AgCl) for 30 min in 0.2 M NapTS. Attenuation 36 arbitrary units; 30 shot average.

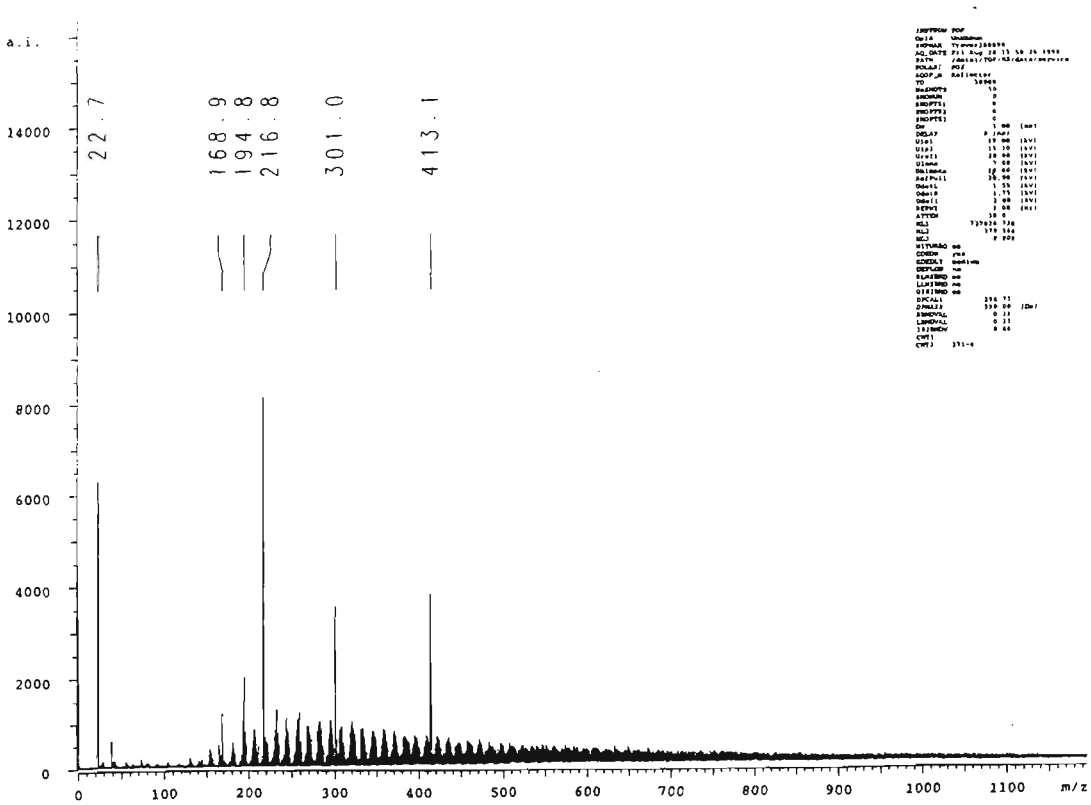

Figure 5.5: MALDI-ToF mass spectrum of a 4.5 υm PPy/pTS film aged in air for 6 months. Attenuation 38 arbitrary units; 50 shot average.

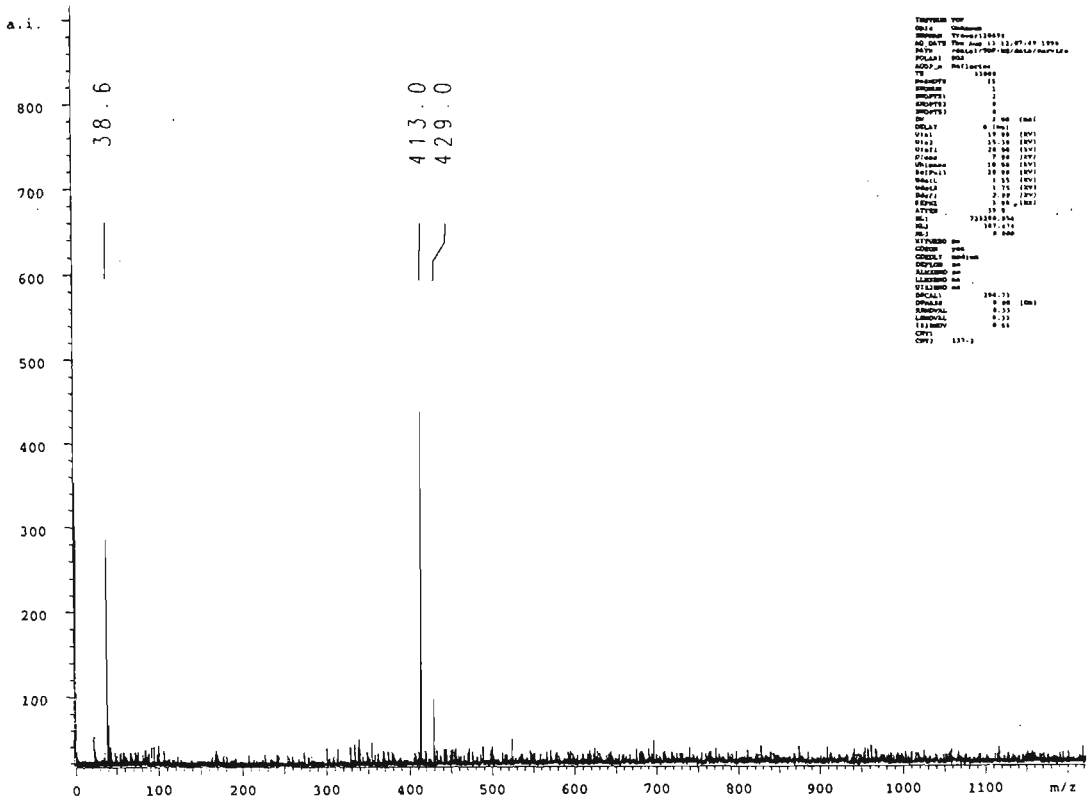

Figure 5.6: MALDI-ToF mass spectrum of a 4.5 υm PPy/pTS film base treated in 0.1 M NaOH for 12 min. Attenuation 38 arbitrary units; 50 shot average.

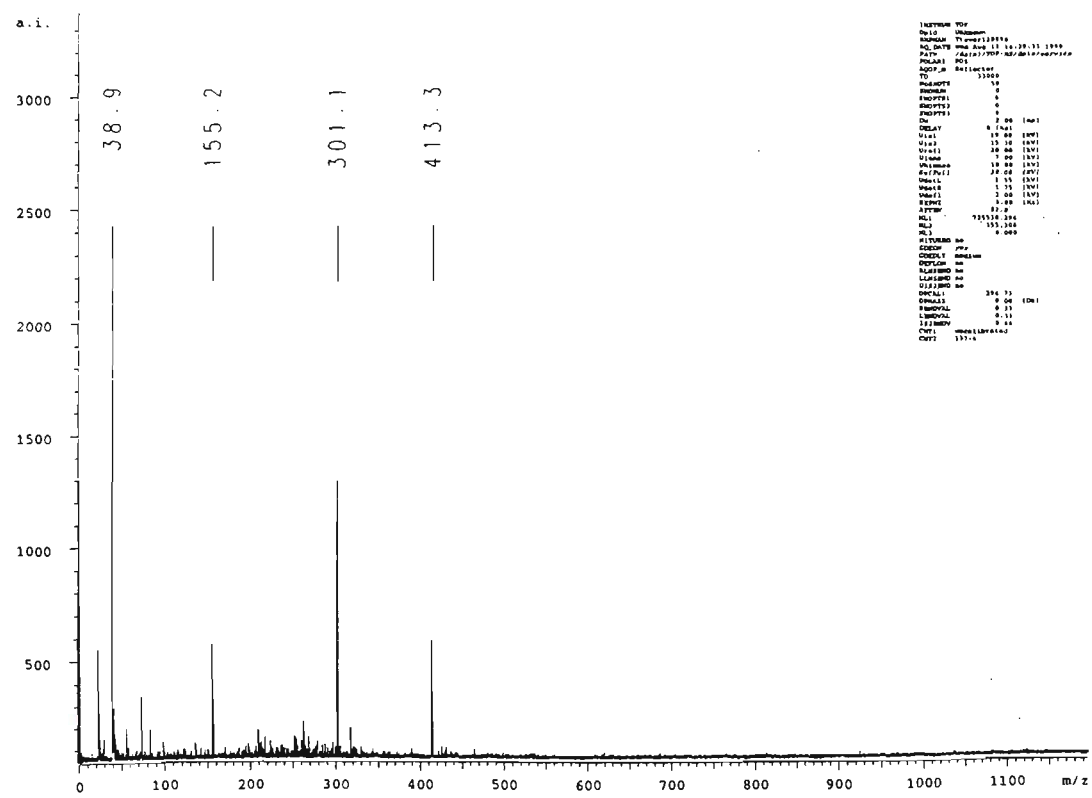

Figure 5.7: MALDI-ToF mass spectrum of a 4.5 υm PPy/pTS film overoxidised at 0.9 V (vs Ag/AgCl) for 2 min in 0.1 M NaOH. Attenuation 51 arbitrary units; 50 shot average.

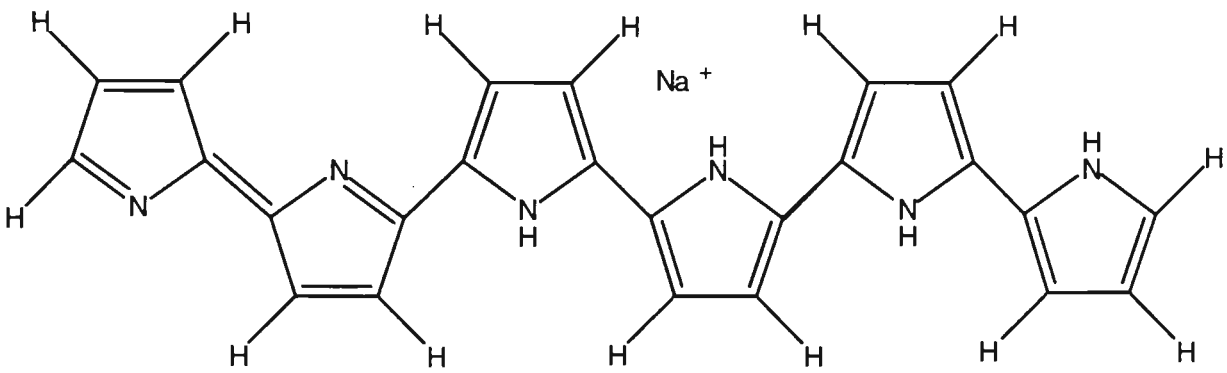

Structure (i)

$C_{24}H_{18}N_6Na^+$

M Wt = 413 Da

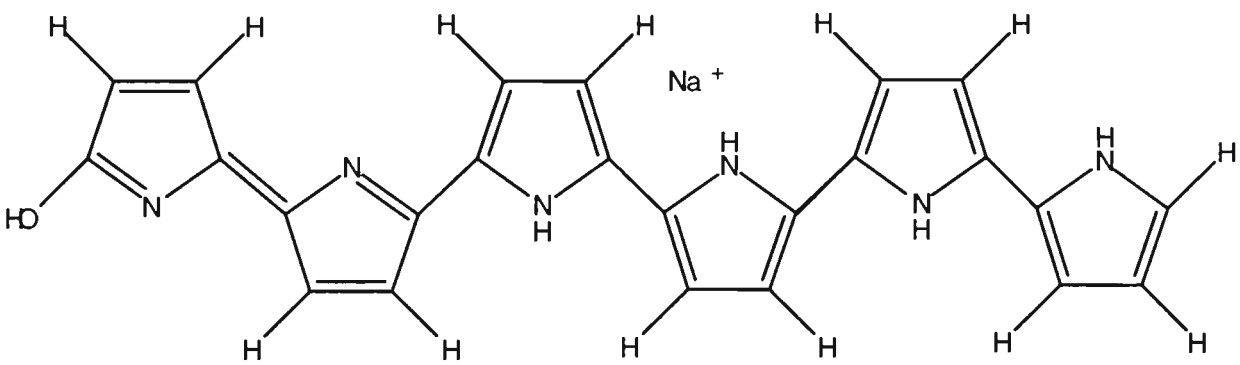

Structure (ii)

$C_{24}H_{18}N_6ONa^+$

M Wt = 429 Da

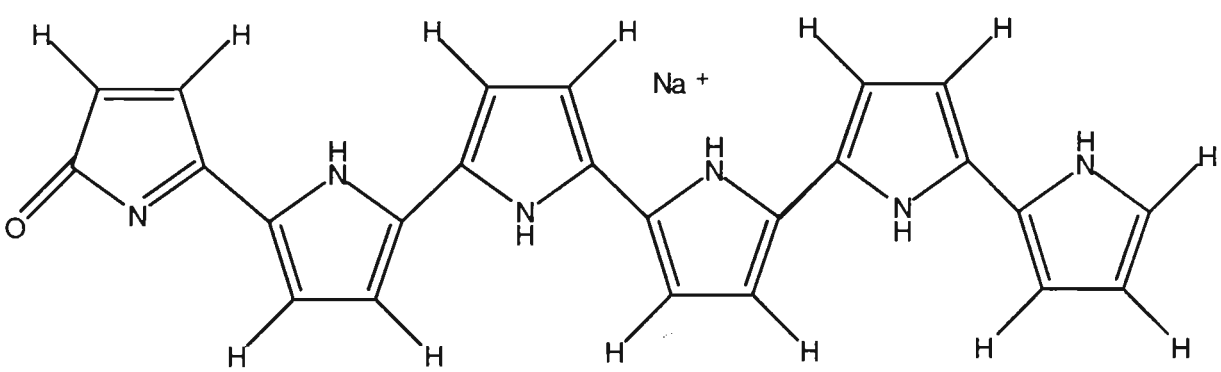

Structure (iii)

$C_{24}H_{18}N_6ONa^+$

M Wt = 429 Da

Scheme 5.1: Possible structures with m/z 413 and 429 Da.

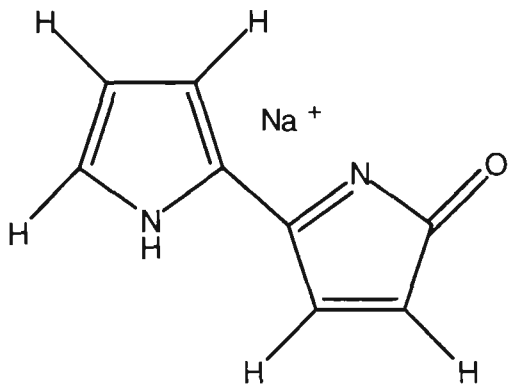

Structure (iv)

$C_8 H_6 N_2 O\ Na^+$

M Wt = 169 Da

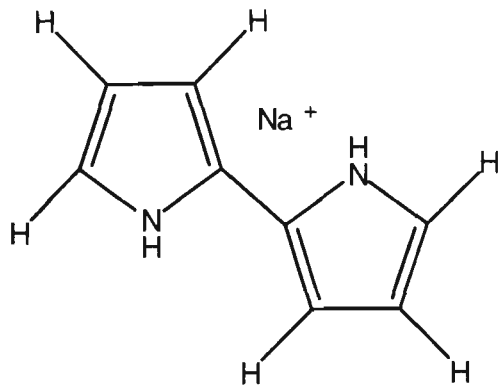

Structure (v)

$C_8 H_8 N_2\ Na^+$

M Wt = 155 Da

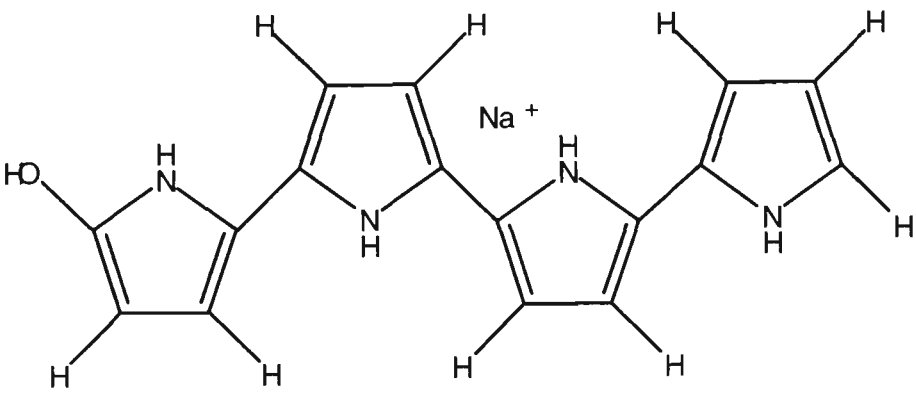

Structure (vi)

$C_{16} H_{14} N_4 O\ Na^+$

M Wt = 301 Da

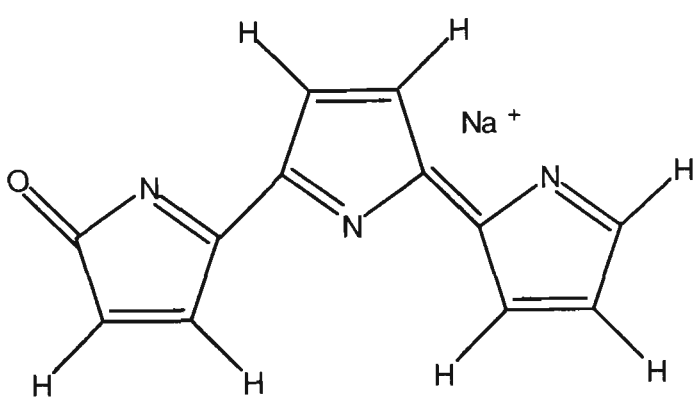

Structure (vii)

$C_{12} H_7 N_3 O\ Na^+$

M Wt = 232 Da

Scheme 5.2: Possible structures with m/z 169, 155, 301 and 232 Da.

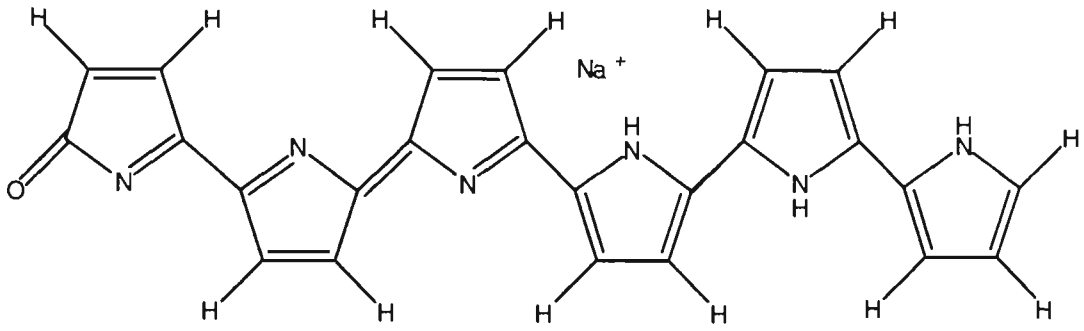

Structure (viii)

$C_{24}H_{16}N_6ONa^+$

M Wt = 427 Da

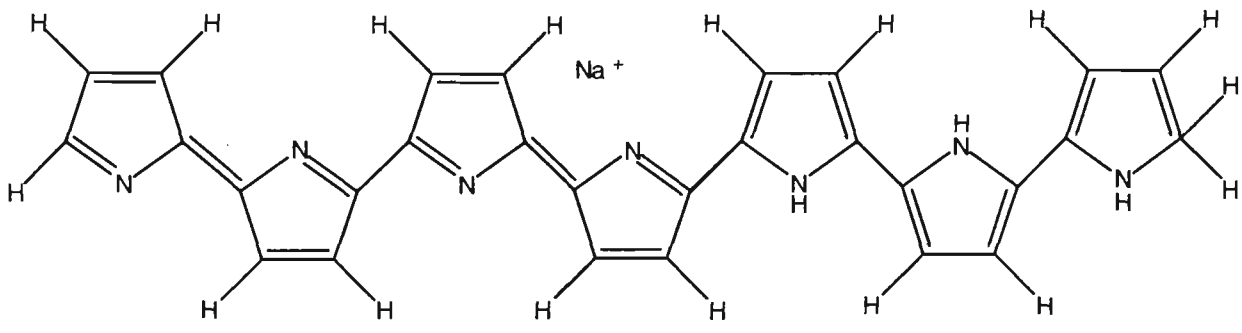

Structure (ix)

$C_{28}H_{20}N_7Na^+$

M Wt = 477 Da

Scheme 5.3: Possible structures with m/z 427 and 477 Da.

intensities. This clearly indicates that the proportion of oxygen substituted hexamers has increased significantly. Assuming equal desorption efficiency, about half of the hexamers now contain oxygen substituents. This is presumably related to the high number of imine-nitrogens formed over this extended period at 0.9 V. It is also worth of noting that no di-substituted hexamers are observed as predicted by Beck et al [253] for highly overoxidised PPy. The peak at m/z 477 would fit the sodium adduct of a PPy chain with seven monomer units, four of which have imine-nitrogens with no oxygen substitution (Scheme 5.3, Structure (ix)).

Peaks at m/z 194, 216 and 368 appear to derive from sodium adducts of the pTS counterion: 194 approximately corresponds to $\{NaHpTS\}^+$ (actual mass 195 Da), 216 to $\{Na_2\ pTS\}^+$ (actual mass 217 Da) and 368 to $\{Na\ (HpTS)_2\}^+$ (actual mass 367).

Unfortunately these variations from the expected masses cannot be explained however, it will be assumed they are pTS adducts.

The fact that no pTS peaks were observed in the less overoxidised film, implies that it is only released from the polymer matrix at higher levels of overoxidation. This may account for the lack of peaks owing to pTS in the pristine and lightly overoxidised films. It could imply that both pTS and PPy are bound strongly into the polymer matrix that neither can be desorbed.

It was not possible to propose a reasonable structure to the m/z 241 peak. Considering the very high intensity of the m/z 216 peak assigned to pTS, m/z 241 may be some recombination or reaction product of this ion. Abel et al [282] reported that Secondary Ion Mass Spectrometry (SIMS) of PPy/pTS yields not only the pTS anion, but also SO_3^-, SO_2^-, SO^-, S^-, HSO_4^- (due to recombination in the gas phase), pTS^- and traces of Br^-, Cl^- and F^-. Though SIMS is a much harsher ionisation technique, it may be possible that similar reactions occur in the laser plume in the MALDI instrument.

The structure proposed to account for the remaining peak (m/z 232) is given in Scheme 5.2, Structure (vii). Again it is a pyrrolinone formed by α-substitution to explain the shortening of the polymer chain to only three Py units. Looking at the intensity of this peak, it is evident that this now represents the major product of overoxidation. This indicates that continued overoxidation breaks chains into shorter lengths as opposed to adding a second oxygen to form hydroxy-pyrrolinones as proposed by Beck et al.

Of the peaks apparent in the film aged in air for six months (Figure 5.5) reasonable structures can be proposed for those at m/z 169, 195, 217, 301 and 413. Of these, m/z 195 and 217 are likely to be pTS adducts and m/z 413 the six membered PPy chain containing two imine-nitrogens. Structure (iv), a sodium adduct of pyrrole dimer with a carbonyl group at one of the α-carbons would account for the ion at m/z 169 and m/z 301

corresponds to a four membered PPy with a hydroxy group substituted at an α-carbon. These results suggest that even under aerial oxidation alone (in the presence of atmospheric oxygen and water), PPy undergoes gradual overoxidation via a chain breaking mechanism. During this process the pTS dopant is released, adjacent imine-nitrogens are formed and oxygen attack occurs as a two step process with the formation of C-OH and C=O.

From Figure 5.6 it is clear that short term base treatment (0.1 M NaOH for 12 min in air) leads to breaking of the polymer chain via formation of adjacent imine-nitrogens with a small degree of oxygen insertion at an α-carbon. These phenomena are evidenced by m/z 413 (Structure (i)) and 429 (Structure (iii)), respectively. This is in excellent agreement with the observations of Neoh et al [22] that dedoping with NaOH leads to polymer in the neutral state and subsequent oxygen attack forms C=O and C-OH. They also report that C-OH is not prominent in an FTIR study of the overoxidised film, again in agreement with the observations here. A number of reports also note that PPy/pTS is dedoped quite quickly in strong base [73, 75, 121] and the spectrum given in Figure 5.6 indicates that is also the case here. The very clean spectrum also indicates that no further degradation of the polymer occurs over this period.

The final spectrum (Figure 5.7) is of a film overoxidised at 0.9 V in an extremely harsh environment of 0.1 M NaOH. This spectrum is also surprisingly clean, with only three peaks associated with PPy observed (m/z 155, 301 and 413). It would appear that under these severe conditions, no oxygen substituted hexamer is formed, indicating that chain breaking occurs in preference. In other words, the hexamer with adjacent imine-nitrogens (m/z 413, Structure (i)) forms and breaks directly into a dimer (m/z 155, Structure (v)) and an oxygen substituted tetramer (m/z 301, Structure (vi)).

5.4 CONCLUSION

From the work described in this Chapter, it is apparent that MALDI-MS has application to the elucidation of the structure(s) of polypyrrole subject to different oxidation conditions. Though the as-grown film is not amenable to the MALDI technique, it is potentially a very important tool for improving understanding of the numbers and location of imine-nitrogen, and its role in overoxidation. It would appear that sections of the polymer that are not affected by the MALDI process may act as an energy absorbing and dispersing matrix in place of the more common organic acid groups.

It would also seem that electrochemical overoxidation proceeds via the formation of adjacent imine-nitrogen groups over six monomer units in the polymer. The formation of this structural feature encourages substitution of oxygen at this point, probably by a chain breaking mechanism, ie α-substitution as proposed by Maltitesta et œal [154]. This leads to the formation of a pyrrolinone on the end group of PPy hexamer. Overoxidation either over extended periods, or in extreme environments proceeds, by repetitive chain breaking to yield shorter chain lengths of both oxygen containing and oxygen free pyrrole dimers, trimers and tetramers. No evidence was found to indicate the formation of di-oxygen containing Py units (ie hydroxy-pyrrolinones [253] and succinimide and maleimide [152, 180]) and instead, further chain breaking was apparent from these data.

Under simple base dedoping, the polymer undergoes complete dedoping and reasonably clean degradation. This yields only the PPy hexamer with either adjacent imine-nitrogens or carbonyl at an α-carbon at one end.

CHAPTER 6: OVEROXIDATION IN A TWO ELECTRODE SYSTEM

7.1: INTRODUCTION

The final experimental chapter is a brief study of the overoxidation of polypyrrole in a polymer device where both electrodes are conducting polymers. Proposed applications include dual polymer-membrane transport cells [288] and electromechanical actuators [16, 289-298]. The work presented here focuses on the electrochemical stability of polypyrrole employed as an active component in electromechanical actuators. Recent proposals for practical applications of polypyrrole based actuators include steerable microcatheters [299] and micro-fingers for handling small objects [300].

Ion movement during the oxidation and reduction of free standing PPy films leads to appreciable changes in the volume of these films, for example the oxidation of PPy/PTS in $NaNO_3$ solution produces a longitudinal contraction of about 1% in a PPy film [301]. If the films are grown on a conducting flexible substrate, the expansion and contraction associated with the redox process is converted into actuation by bending the CEP/substrate material [296, 298]. Improvements in the force generation capabilities of these devices have been achieved by employing conducting polymer films as both electrodes in such a devices [16, 291]. If a solid ion source / sink is inserted between the polymer films, eg polyacrylonitrile based solid polymer electrolyte (SPE) [294] or a water based polyacrylamide hydrogel [293], a free-standing device can be fabricated. The current work is directed towards establishing appropriate potentials for application to a solid state device employing a polyacrylonitrile SPE.

An SPE can be thought of as a solution of an ionic salt (eg $NaClO_4$) in a long-chain polymeric material (eg polyacrylonitrile) which has both crystalline and amorphous regions and acts as an immobile solvent [302]. Linford also notes that both cations and

anions are mobile in such systems and that the mechanical properties may be improved by the addition of organic plasticisers (eg propylene and ethylene carbonates). The conductivity of a polyacrylonitrile SPE employing $LiClO_4$ and propylene and ethylene carbonates as solvents has been reported to be as high as 1.7×10^{-3} Scm^{-1} at 20 °C [303].

Free-standing devices employing solid state, non-aqueous ion sources and sinks, will generally operate simply with a potential difference applied between the electrodes. That is without a reference electrode to control the potential applied to the working electrode. In an electrochemical cell where both electrodes are of equivalent size and composition and where potential is applied only as a potential difference between the electrodes the terms "working electrode" and "auxiliary electrode" are a little misleading. However, for the sake of clarity during discussions on these systems, "working" and "auxiliary" will be used to indicate the PPy film connected to the working (w) or auxiliary (a) outputs of a potentiostat, respectively. In a two electrode system the "auxiliary" electrode should be more correctly called the "counter" electrode, however, to retain consistent naming throughout, the term "auxiliary" electrode will be used.

From the point of view of overoxidation studies, any two electrode system where both electrodes are conducting polymers presents special problems. While one electrode is oxidised at an anodic potential, the other is reduced at a necessarily cathodic potential. At a potential of around -0.8 V (vs SCE) the conductivity of the PPy auxiliary electrode will decrease by up to five orders of magnitude from that observed in its oxidised state at 0.4 V [168]. As the auxiliary electrode is the source of potential and carries any current, changes in its conductivity are critical.

In a three electrode cell the potential of the working electrode is measured against a reference electrode and the auxiliary electrode will apply any potential necessary (within the compliance voltage of the potentiostat) to achieve the set potential. If the auxiliary electrode is a poor conductor, a significant potential loss will occur within the electrode

itself. This could lead to potentiostat driving the auxiliary electrode to ±100 V (in the case of the PAR 273 potentiostat used in this work) in order to reach the desired potential at the working electrode. Though the PPy working electrode may not be degraded under these conditions, the PPy auxiliary certainly will be.

However, in a two electrode cell no reference electrode is employed (a simple potential difference is applied between the electrodes) and the potential at the working electrode may be far lower than anticipated. Potential losses between the electrodes may be caused by resistance in the supporting electrolyte solution or solid state electrolyte, or by any resistive losses in the auxiliary electrode. As such, changes in the conductivity of the auxiliary electrode have a major impact on the potential of the working electrode.

To gain the maximum degree of actuation from these devices it is necessary to extend the potential range as far as possible. This ensures complete oxidation and reduction of the PPy electrodes, which maximises ion movement, and hence actuation, in each of the active components. The aim of the work reported in this chapter is to investigate these potential limits employing both aqueous and propylene carbonate supporting electrolyte solutions and the solid polymer electrolyte, polyacrylonitrile.

6.2 EXPERIMENTAL

6.2.1 Reagents and materials

All chemicals used were analytical reagent grade unless otherwise stated. Propylene carbonate (BDH) and ethylene carbonate (BDH) were General Purpose Reagent grade and used as received. Pyrrole (Aldrich) was distilled before use and stored at -16 °C in the dark under N_2 where necessary. Water was reagent grade obtained from a Millipore Milli-RO/Milli-Q™ water purification system.

Electrodeposition and characterisation of polymer films was carried out on gold coated mylar (Au-mylar) sheets (Cortaulds Advanced Products) (10 x 40 mm). PPy films on gold coated mylar were used as the working and auxiliary electrodes. In instances where a three-electrode cell was employed a 17.5 cm^2 gold coated mylar film was used an auxiliary electrode. The reference electrode, when employed, was Ag/AgCl (Hart Analytical). This electrode was inserted into the supporting electrolyte solution via a salt bridge containing 1 M $NaNO_3$.

6.2.2 Instrumentation

Electropolymerisation and characterisation of polymer films were performed on an EG&G Princeton Applied Research (USA) 273 Potentiostat - Galvanostat. Data was collected on a Hewlett Packard 7090A Plotter, downloaded onto a Delta Systems PC and processed on a Macintosh (Apple) computer.

6.2.3 Procedures

6.2.3.1 PPy growth

The Au-mylar film electrodes were ultrasonicated in methanol before use. An area of approximately 1 cm^2 was then taped off with contact adhesive (3M, USA) to give reproducible film areas. PPy was electrodeposited galvanostatically from a solution of 0.1 M pyrrole, 1 M $NaClO_4$ and 0.1 M NapTS in H_2O. pTS was included to give the films the mechanical properties required of an actuator, whilst the bulk of the doping / dedoping involves the $NaClO_4$ employed as the ionic species in the SPE. A current density of 1 $mAcm^{-2}$ was applied for 5 min to give 1 μm thick films for characterisation in solution, or 30 min to give 6 μm thick films for characterisation as a component of a free-standing device. After growth the polymer films were rinsed thoroughly with water. All growth was carried out in air.

6.2.3.2 Fabrication of a solid state device

2.2 g sodium perchlorate were dissolved in 7.4 g ethylene carbonate and 7.4 g propylene carbonate by heating at 90 to 100 ^{0}C with stirring at 30 - 40 rpm with a mechanical stirrer. After complete dissolution, 2.4 g polyacrylonitrile was added in small increments over 15 minutes. Stirring was continued until the polyacrylonitrile had completely dissolved (up to 2 hr). The SPE was allowed to cool to room temperature and stored in a sealed container. For the preparation of a conducting polymer device, a small section was cut from the mass prepared above and heated to melting with a hair drier (~ 60 °C). The melted SPE was then spread on a PPy on Au-mylar sample to a thickness of about 2 mm. A second PPy on Au-mylar sample was placed the SPE and pressed gently with a glass slide to ensure good adhesion and to give a final SPE thickness of about 1 mm. The device (Scheme 6.1) was the left to set for at least 24 h.

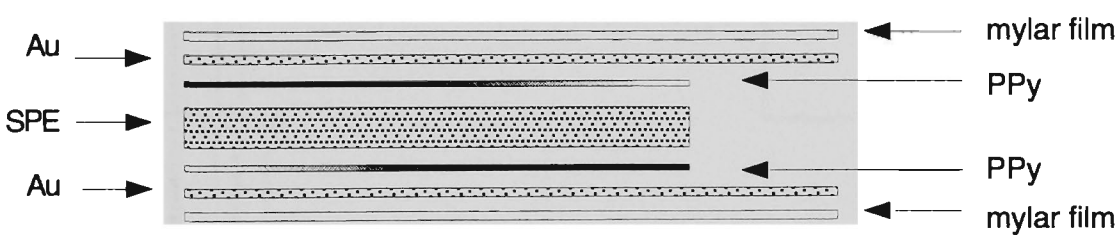

Scheme 6.1: Solid state CEP device based on PPy on gold coated mylar film and polyacrylonitrile solid polymer electrolyte (SPE).

6.2.3.2 Characterisation

6.2.3.2.1 Characterisation in a supporting electrolyte solution

Characterisation was carried out in air in aqueous and propylene carbonate solutions of 1 M $NaClO_4$ without pH adjustment. The films were characterised in one of two cell configurations:

i) A standard three-electrode cell was used to check films before and after an overoxidation experiment in one of the other cell configurations. This cell employed the

PPy on Au-mylar as a working electrode, a Au-mylar film as an auxiliary and a Ag/AgCl reference.

ii) A two-electrode cell employing PPy on Au-mylar as both working and auxiliary electrodes was used for a number of the overoxidation studies. In practical terms this is done by shorting the reference electrode connection of a three cell potentiostat directly to the auxiliary lead as shown in Scheme 6.2.

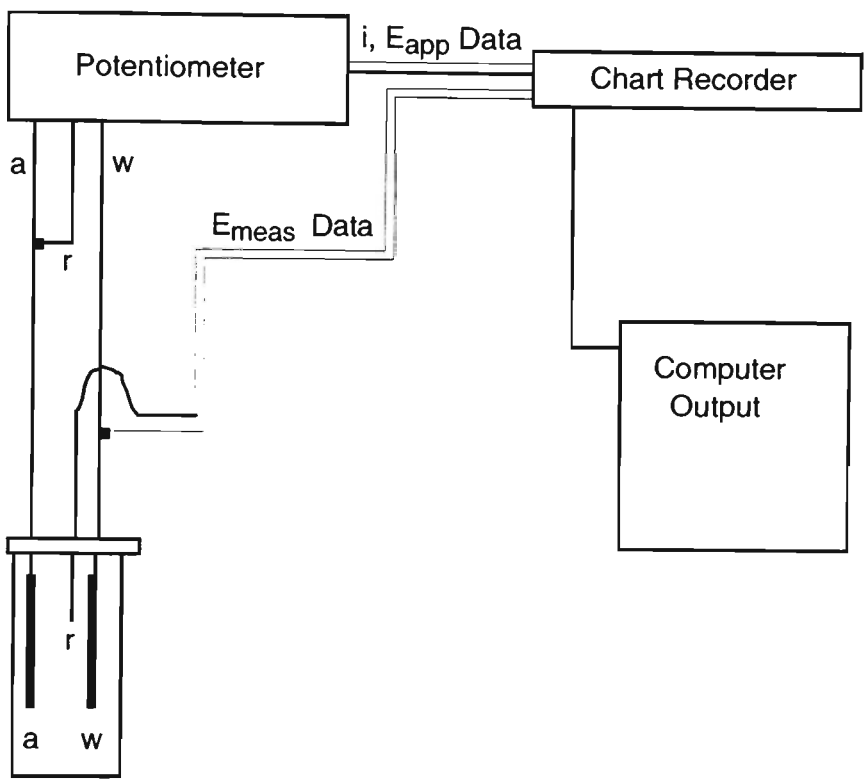

Scheme 6.2: Scheme of the two-electrode cell configuration with working electrode potential monitoring; "a" auxiliary, "w" working and "r" reference, "i" current, "E_{app}" applied potential, "E_{meas}" measured potential.

In order to monitor the potential of the working electrode (E_{meas}) in the two electrode cell, the potential was measured against a Ag/AgCl reference electrode independently of the potentiostat. The impedance of a Hewlett Packard 7090A Plotter is sufficiently high to monitor the potential difference between the working and reference electrodes directly. (It is worth emphasising that the potential was only monitored at the working electrode and not fed back to the potentiostat for potential control purposes.) In these experiments the

switching potentials of a triangular waveform were stepped in 0.1 V increments after three cycles at any given potential. The current, potential difference (E_{app}), measured working electrode potential (E_{meas}) and time were recorded to allow the generation of two-electrode CVs of E_{app} and E_{meas} against current.

6.2.3.2.2 Characterisation in a solid state device

The suitability of the potential difference determined in Section 6.2.3.2.1 for application to a solid state device was checked with the instrumental set up shown in Scheme 6.3. Connections were made directly to the gold substrate and the device was characterised in air.

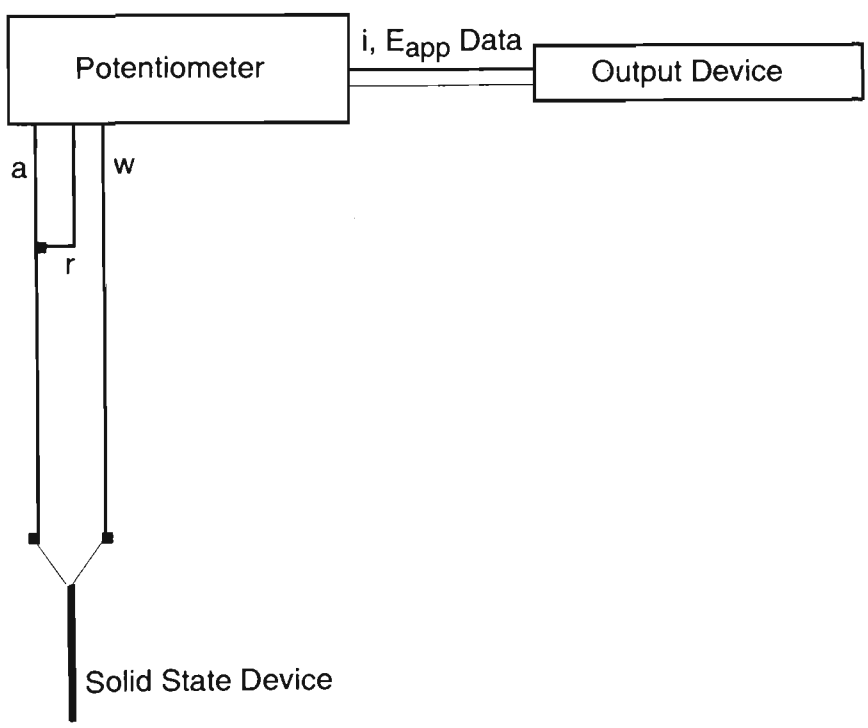

Scheme 6.3: Scheme of the two-electrode configuration employed to characterise a solid state device; "a" auxiliary, "w" working and "r" reference, "i" current, "E_{app}" applied potential.

6.3 RESULTS AND DISCUSSION

6.3.1 Solution supporting electrolyte studies

To illustrate the problems associated with the use of conducting polymers as electrodes in a two-electrode cell, a single PPy film on Au-mylar was fitted as the working electrode with an auxiliary electrode of Au-mylar. Figure 6.1 displays the potential versus time plots of the applied and measured potentials obtained from this cell.

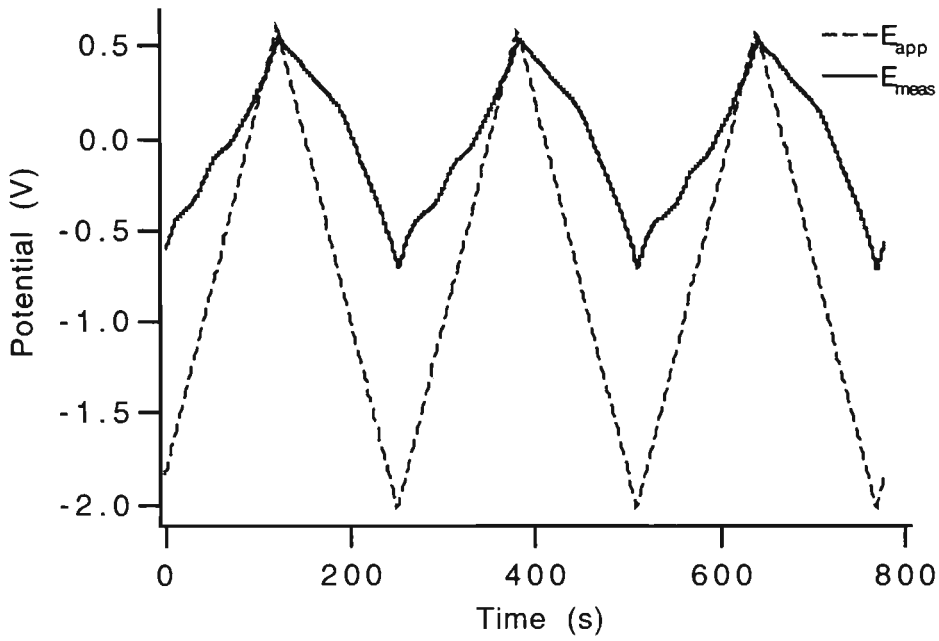

Figure 6.1: Applied potential (E_{app}) and measured potential (E_{meas} vs Ag/AgCl) vs time in a two-electrode cell with potential monitored at the working electrode. Working electrode, PPy/ClO_4/pTS; auxiliary electrode, Au-mylar; supporting electrolyte, 1 M $NaClO_{4(aq)}$; applied potential limits, -2.0 and 0.6 V; scan rate 20 mVs^{-1}.

In this example the potential measured at the working electrode (0.55 V) at the anodic limit closely approximates the applied potential (0.60 V). At this point the PPy film is fully oxidised and at its most conductive. However, at the other extreme of the applied potential, when the film is fully reduced and at its lowest conductivity, the measured potential (-0.68 V) is far removed from that applied (-2.0 V). At this potential the resistance of the film leads to a significant potential loss, effectively forming an insulating layer across the conducting substrate. This is reflected in the lag times between the measured and applied potential curves. As it should be, the applied potential curve is linear with time. At higher anodic potentials ($E_{meas} > 0.17$ V), when the film is conductive,

the measured potential approximates this behaviour. On the other hand, at potentials (E_{meas} < 0.17 V) the measured potential lags appreciably behind the applied potential as the conductivity of the PPy film decreases and ultimately the measured potential is limited by this poor conductivity.

These problems are compounded in a two electrode system where the conductivity of both electrodes is potential dependent. Figure 6.2 presents plots of applied and measured potentials against time when PPy was employed as both electrodes.

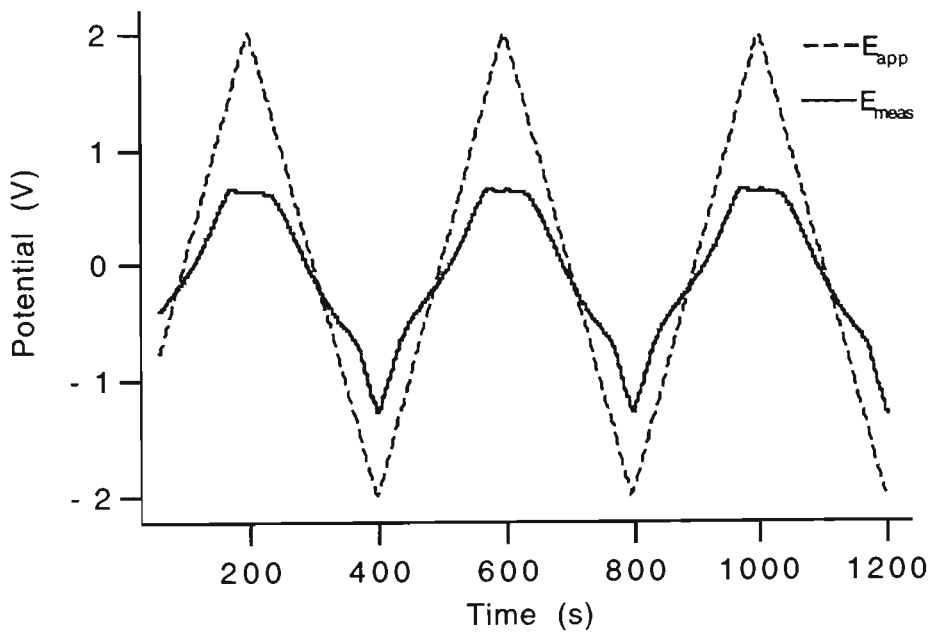

Figure 6.2: Applied potential (E_{app}) and measured potential (E_{meas} vs Ag/AgCl) vs time in a two-electrode cell with potential monitored at the working electrode. Working and auxiliary electrodes, PPy/ClO_4/pTS; supporting electrolyte, 1 M $NaClO_{4(aq)}$; applied potential limits, -2.0 and 2.0 V; scan rate 20 mVs^{-1}.

Again, the effect of the changes in conductivity of the working electrode film are apparent, though on this occasion exacerbated by the changes in conductivity of the auxiliary electrode. Even at an applied potential of 2.0 V, the measured potential at the working electrode is -1.2 V, due to the PPy working electrode being in a reduced (non-conducting) state. On this occasion the conductivity of the PPy at the auxiliary electrode is

not a factor, as this material is in its most conductive state. At the other potential limit, the effect of changes in the conductivity of the auxiliary electrode PPy is noticed. In this case, even though the working electrode is oxidised, it is now the auxiliary (potential source) electrode PPy that is resistive and, hence, potential limiting. This limits the maximum measured potential at the working electrode to 0.66 V, a potential at which only slow overoxidation would be expected. An inherent advantage of a two-electrode system may be that it is self limiting with regard to the true potential the polymer will experience. It seems possible that changes in conductivity of the polymer modified electrodes prevent the application of extreme potentials and will, therefore, limit the rate of overoxidation.

Even though the system, in some ways, is self limiting, it was found that if the reference electrode was not shorted to the auxiliary and the full 100 V compliance voltage of the PAR 273 was applied to the films, "rapid catastrophic deactivation" [138] of the polymers ensued.

Figure 6.2 also indicates the importance of recognising that polymer electrodes have a significant impact on the true working electrode potential in a two electrode system. Only at one point in each the anodic and cathodic scans does the measured potential correspond to the applied potential. As such, if the operation of a CEP device is reliant on full oxidation / reduction of the polymers, the applied potential limits must considerably exceed the oxidation and reduction potentials of the PPy components.

The extent of the self limiting effect was investigated (Figure 6.3) by measuring the maximum and minimum potentials at the working electrode during the application of a triangular waveform (20 mVs^{-1}) to a two-electrode cell in which both electrodes were PPy/ClO_4/pTS films on Au-mylar. The limiting potentials were stepped in 0.1 V increments after each 3 cycles.

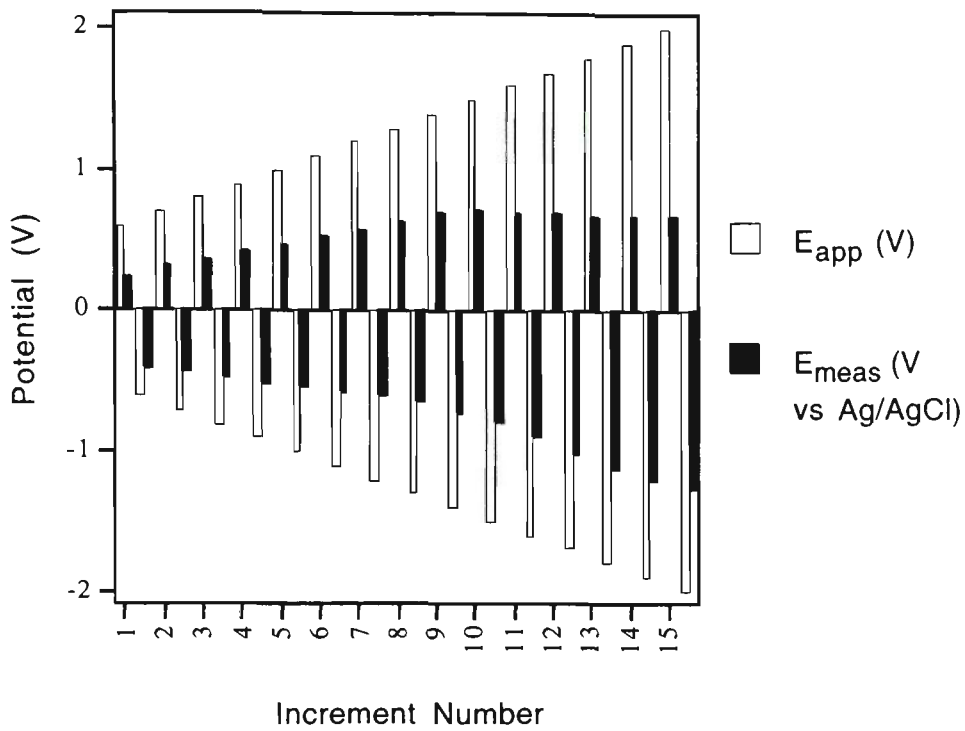

Figure 6.3: Measured potential (E_{meas} vs Ag/AgCl) and applied potential (E_{app}) for a two-electrode cell in 1 M $NaClO_{4(aq)}$ supporting electrolyte. Working and auxiliary electrodes PPy/ClO_4/pTS on Au-mylar. E_{app} was stepped in ±0.1 V increments, E_{meas} was monitored at the working electrode.

When a reasonably slow scan rate of 20 mVs^{-1} was used, overoxidation would appear to commence at an applied potential of 1.5 V. At this applied potential the measured potential at the working electrode reached its maximum value of 0.7 V. The potential measured at the working electrode during subsequent potential steps then decreased slowly as overoxidation occurs and the electrode coating becomes resistive.

However, the potentials measured during the application of negative applied potentials appear to have to retained a direct relationship with the applied potential. Presumably this indicates that the small number of overoxidised segments in the working electrode film do not add to the resistivity of the fully reduced state. Thus, the effects of overoxidation were noticed when the remainder of the film is in the conductive oxidised state, but the overoxidised segments have little impact on conductivity when the bulk of the film is in the non-conductive reduced state.

To investigate the extent of overoxidation at these high potential limits, the cyclic voltammogram (E_{meas} against current) of two PPy/ClO_4/pTS electrodes scanned from E_{app} of -2.0 to 2.0 V is given in Figure 6.4. The films were characterised individually by three cycles between -1.0 and 0.6 V in a standard three-electrode cell before use in the two-electrode cell. They were then again individually characterised in a standard three-electrode cell (see Figure 6.5).

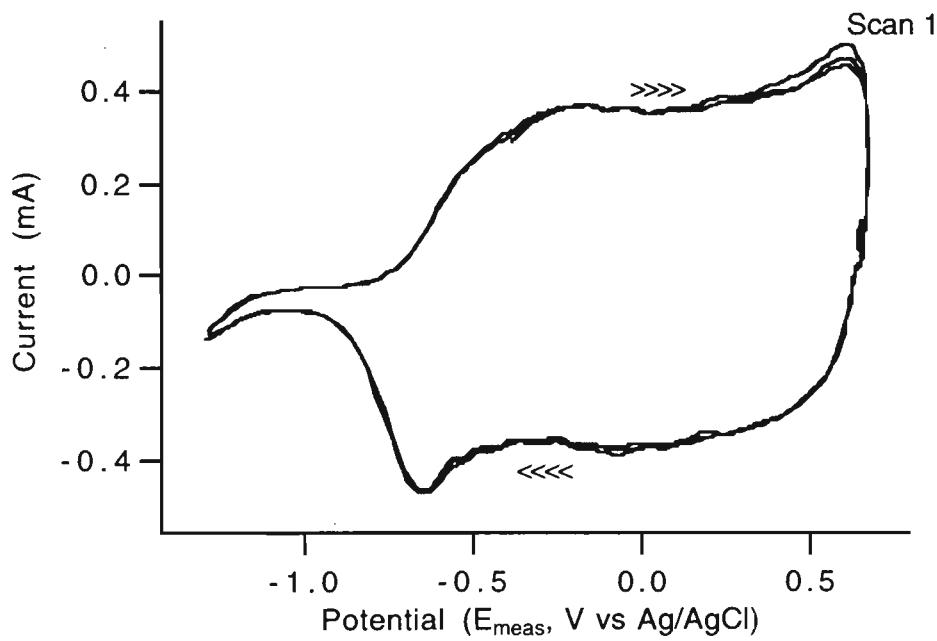

Figure 6.4: Cyclic voltammogram (E_{meas} against i) obtained from a two-electrode cell employing two PPy/ClO_4/pTS electrodes. Applied potential (E_{app}) limits ± 2 V; E_{meas} vs Ag/AgCl; supporting electrolyte, 1 M $NaClO_{4(aq)}$; scan rate 20 mVs^{-1}.

These figures together show that very little overoxidation of the polymer film has occurred during the three cycles between switching potential of ±2.0 V. Figure 6.4 shows no indication of an overoxidation peak at its anodic limit. It also shows little change between cycles 1 and 3. The two-electrode CV and the three-electrode CV of the working electrode after the experiment both show good electroactivity. Clear oxidation and reduction peaks are evident in both. The reduction peak typical of PPy/ClO_4, normally observed around -0.5 V [72, 86], is present in the as grown film, but is not seen in the

CVs during and after the application ±2.0 V. Iseki [72] reported that this peak is totally lost from the CV of PPy/pTS in less than 10 cycles (-1.0 to 0.5 V vs Ag/AgCl) in $NaNO_3$. Thus, the absence of this peak indicates that the film has now exchanged the pTS for ClO_4^-. The redox peaks in the film after exposure to ±2.0V, closely resemble those expected of PPy/ClO_4 in an aqueous $NaClO_4$ solution [86] though shifted to rather more cathodic potentials than reported by Tamm. However, Novak [140] observed that a shift of redox peaks in an anodic direction is indicative of overoxidation, so the position of these peaks at least indicates that degradation was not significant.

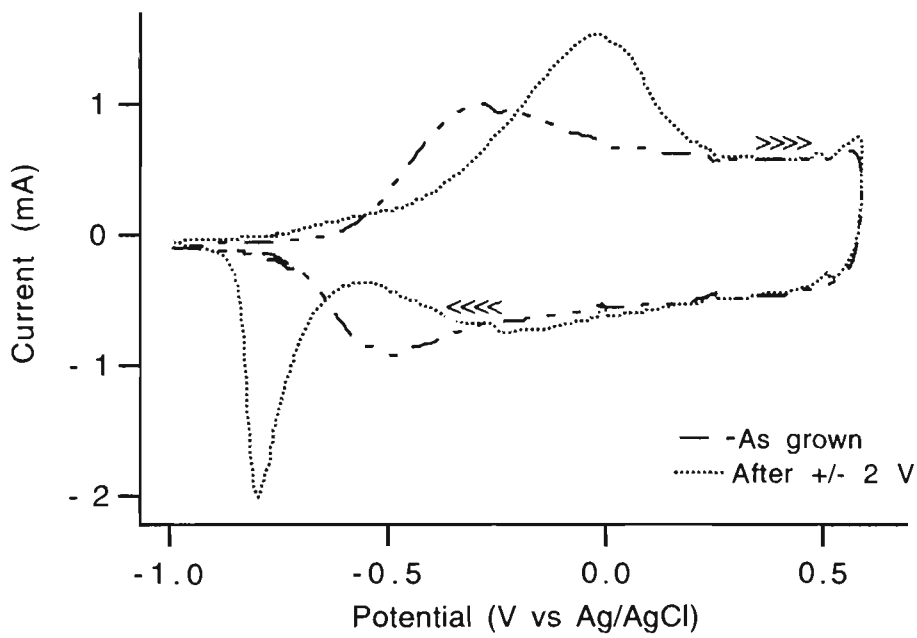

Figure 6.5: Standard three-electrode cyclic voltammogram of the PPy working electrode used to generate Figure 6.4. Supporting electrolyte, 1 M $NaClO_{4(aq)}$; scan rate 20 mVs^{-1}; reference Ag/AgCl; auxiliary electrode Au-mylar.

The three-electrode CVs of the auxiliary electrode film before and after cycling in the two-electrode cell were identical to the corresponding CVs of the working electrode presented in Figure 6.5. This implies that both the working and auxiliary polymer films are stable at the potentials used during the two-electrode experiment.

In an application such as electromechanical actuators, the polymer electrodes could be subjected to repetitive switching from one potential limit to the other. To examine the longer term stability of polymer electrodes in these circumstances, a pair of PPy electrode films were subjected to 30 s potential steps between ±1.7 V. The results for steps 13 to 35 are given in Figure 6.6. It is clear from this figure that the electrode system is not stable at these potential limits over this period. This is evidenced by the decreasing maxima and increasing minima observed in E_{meas} towards the end of the cycling. Over the initial scans these maxima and minima were reached immediately the potential was stepped. The increase in the time to reach the final potentials and the final potentials themselves are indicative of the increasing resistivity, and hence degradation, of the polymer electrodes at these applied potentials.

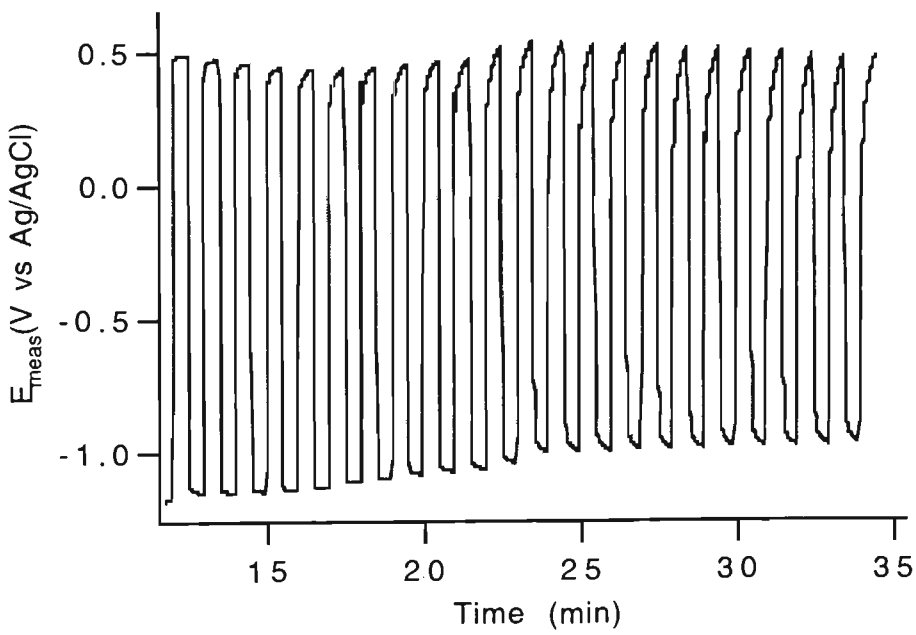

Figure 6.6: E_{meas} (vs Ag/AgCl) for a series of applied potential steps from -1.7 to 1.7 V. Working and auxiliary electrodes PPy/ClO_4/pTS; supporting electrolyte 1 M $NaClO_{4(aq)}$; step duration 30 s. The first 12 steps have been omitted.

From this work, it was considered that a more appropriate potential difference for long term application may be 1.5 V. This is also, coincidently, a standard commercial battery voltage and represents a convenient potential source for free standing devices. This was

trialed on two PPy films in 1 M $NaNO_3$ in propylene carbonate, a major component of the ultimate liquid phase in contact with a two electrode device. Figure 6.7 presents the potential measured at the working electrode during potential steps from -1.5 to 1.5 V. Each potential was applied for 2 min and steps 6 to 20 are shown for clarity.

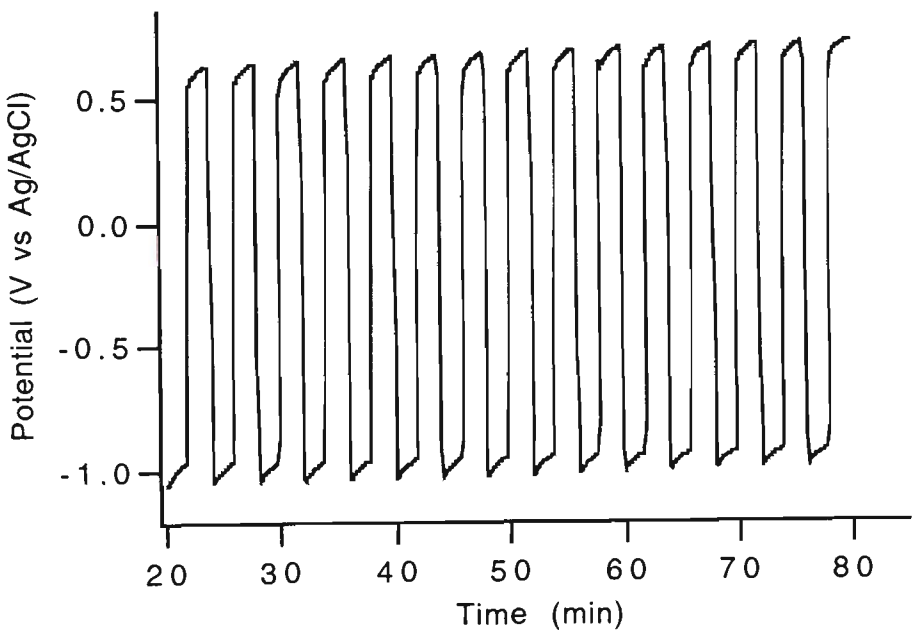

Figure 6.7: E_{meas} (vs Ag/AgCl) for a series of applied potential steps from -1.5 to 1.5 V. Working and auxiliary electrodes PPy/ClO_4/pTS; supporting electrolyte 1 M $NaClO_4$ in PC; step duration 2 min. The first 12 steps have been omitted.

Figure 6.7 shows that a two polymer electrode system is very stable under a potential difference of ±1.5 V. After forty cycles, each with a hold time of 2 min, there is no indication of changes in the resistivity of either PPy film. In this case the fact that the potentials do not reach their limiting potential immediately is presumably due to the lower rates of diffusion of counterions into and out of the polymer in this solvent.

To ensure that this potential range was sufficient to fully oxidise and reduce the polymer films, a cyclic voltammogram of two fresh films was run between applied potential limits of ±1.5 V. From the CV, given in Figure 6.8, it would appear that these potential limits

are again quite suitable. A broad oxidation peak is apparent around -0.2 V and electrochemical processes appear to be complete before the switching potentials are reached.

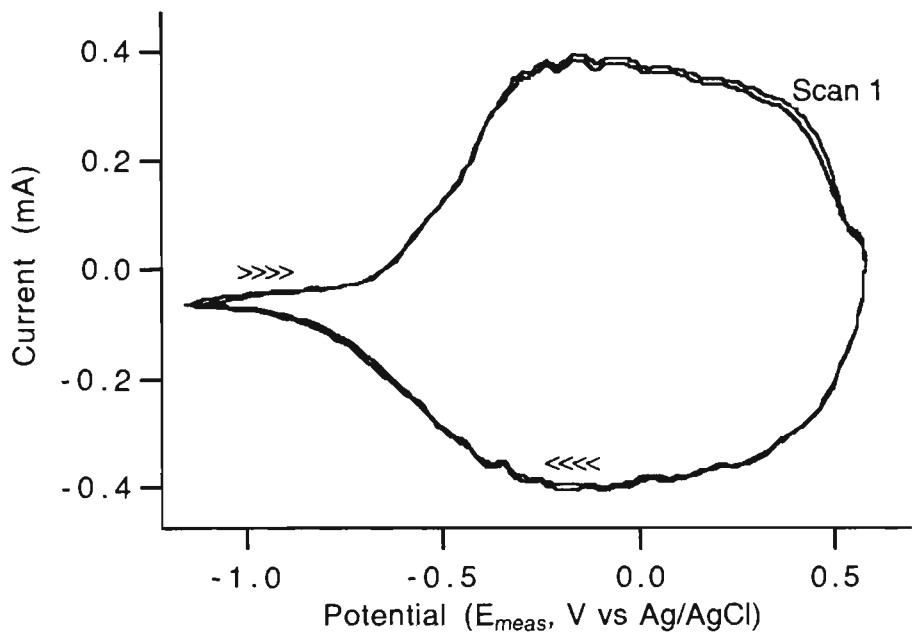

Figure 6.8: Cyclic voltammogram (E_{meas} against i) obtained from a two-electrode cell employing two PPy/ClO_4/pTS electrodes. Applied potential (E_{app}) limits ± 1.5 V; E_{meas} vs Ag/AgCl; supporting electrolyte, 1 M $NaClO_4$ in PC; scan rate 20 mVs^{-1}.

6.3.2 Solid state device studies

The final experiment in this work was to verify that a potential difference of ±1.5 V was suitable for application to a complete, solid state device. This was performed with two 1 cm^2 PPy/ClO_4/pTS films adhered to either side of a polyacrylonitrile solid polymer electrolyte. This employed 1 M $NaClO_4$ as the mobile ionic species and propylene carbonate / ethylene carbonate as a plasticiser. The resultant CV, in this case applied potential against current, is shown in Figure 6.9.

From this figure, it is apparent that the switching potentials are sufficient to allow these processes to occur. Towards each potential limit the current associated with the reversible oxidation and reduction of PPy subsides. Subsequent cycles up to higher potential limits (±1.8 V) verified that no further electrochemical processes occurred past these potentials.

An increase in the potential limits simply extended the region of very low current flow seen at either end of Figure 6.9.

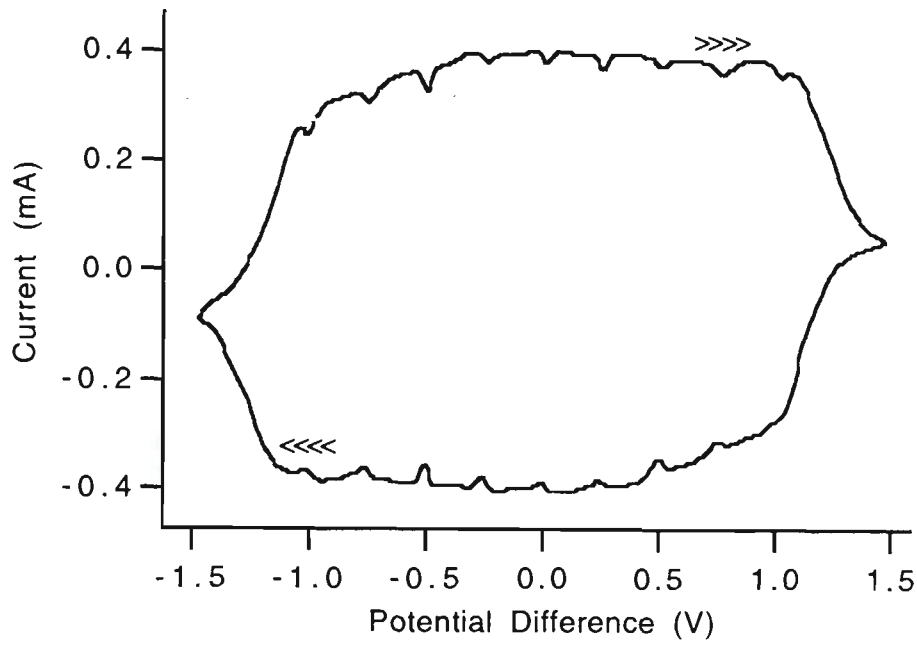

Figure 6.9: Cyclic voltammogram (Potential Difference vs i) obtained from a two-electrode cell employing two PPy/ClO_4/pTS electrodes. Applied potential (E_{app}) limits ± 1.5 V; supporting electrolyte, 1 M $NaClO_4$ in SPE; scan rate 20 mVs^{-1}.

6.4 CONCLUSION

In this chapter the potential limits suitable for application to two electrode all polymer devices was investigated. These devices require a delicate balance between extending the potential limits as far as possible to allow full oxidation and reduction, while ensuring that the potentials at which overoxidation will occur are not reached. The concept of monitoring the potential at the working (electrically passive) electrode was introduced to allow the determination of the actual potential at this electrode during the application of a potential difference.

The determination of the actual potential at this electrode is significant as the conductivities of both electrodes change with changing potential. This leads to a partially effective potential limiting mechanism in a two-electrode cell which retards the overoxidation at seemingly extreme applied potentials. At an applied potential of -2 V, the potential

measured at the working electrode was found to be only 0.69 V (vs Ag/AgCl) with only slight overoxidation evident. At the other applied potential extreme, +2 V, a potential of -1.3 V was measured at the working electrode, indicating on this occasion that little overoxidation had occurred at the auxiliary electrode. Comparison of the standard three-electrode cyclic voltammetry of both electrodes before and after the application of this potential also showed only slight overoxidation.

However, as a decrease in the measured potential at the working electrode was evident at potential differences above ±1.5 V, it was considered that this potential may be more suitable for long term applications of polymer films. This potential difference was applied over an extended period in a series of potential steps to a two electrode device in a propylene carbonate solution and found to have no deleterious effects on the polymer electrodes. It was also shown that this potential difference was sufficient to fully oxidise and reduce PPy both in a supporting electrolyte solution and as a component of a two-electrode solid state device.

CHAPTER 7: GENERAL CONCLUSION

Practical applications of the conducting polymer polypyrrole (PPy) are often limited by the longevity of the material under normal operating conditions. Many applications require the polymer to be subjected to an applied potential when in contact with air and / or water. Under these conditions polypyrrole will often be irreversibly degraded or "overoxidised", losing the very properties that suited it for the particular application, eg conductivity, charge storage ability, electrochromism, electroactivity and mechanical properties. This thesis set out to elucidate the nature of this degradation using a range of instrumental techniques that would allow in-situ, real-time monitoring of the process. These techniques were chosen to allow consideration of a number of parameters known to affect the degradation of polypyrrole in an aqueous environment, including applied potential, solute anions and cations, pH and substrate. The exception to this was an investigation of the solid products of overoxidation by MALDI-MS, which allowed a new insight into the chemical structure of these products. In combination these techniques should allow a better understanding of the mechanism of overoxidation and establish realistic limits for the operation of polypyrrole in both an aqueous environment and as components of free-standing polymer devices.

The first experimental chapter described a new technique, simultaneous linear sweep voltammetry / resistometry for the determination of the overoxidation potential of polypyrrole with a precision of better than ±0.03 %. The technique was employed to study the effects of a wide range of variables on the overoxidation potential of polypyrrole: incorporated counterion, supporting electrolyte salt, substrate, growing solvent, scan rate, film thickness and ring substituents. With the exception of strong base, which halved the overoxidation potential of one polymer and the inclusion of a hydrophobic substituent which increased the overoxidation potential by about 30%, these variables had little effect on the overoxidation potential.

An important finding of this chapter was that the lyotropic series, which ranks anions and cations according to their "water ordering" ability, has direct application to conducting polymer chemistry. Based on this series, the overoxidation potential of PPy should be in the order $NH_4^+ \approx K^+ < Na^+$ and $Sr^{2+} \approx Mg^{2+} < Ca^{2+}$. This prediction was found to be in agreement with the experimental results. This series also predicts that PPy would be more readily overoxidised in a solution of NO_3^- than one of Cl^-, as was found to be the case.

It was also observed that acid concentrations of around 1 M stabilise PPy against overoxidation. On the other hand, overoxidation of PPy in moderate concentrations of base (0.1 M) more than halved the potential at which the film was overoxidised. The effect of the substrate on the overoxidation potential was also considered and it was found that films grown on platinum have a lower overoxidation potential than those grown on either gold or glassy carbon. It was noted that overoxidation potential is linearly related to the square root of the scan rate and the square of the film thickness. This section also showed that PPy/pTS films had a marked stability advantage over other, less ordered polymers regardless of the supporting electrolyte / counterion combinations.

The final factor investigated in this chapter was the contribution of ring substituents to the overoxidation potential. P(MPyC) was found to exhibit a very similar overoxidation potential to unsubstituted PPys examined under similar conditions. However, the overoxidation potential of polypyrrole containing the hydrophobic substituent group (-C_8H_{15}) was found to be around 1.4 V. The increased stability of this polymer was attributed to its high hydrophobicity, which reduces intimate contact between it and the aqueous phase (containing the nucleophiles H_2O and OH^-). The decreased contact between the P(MPyC) and any strong nucleophile allowed the application of an appreciably higher potential before irreversible overoxidation was observed.

Chapter 3 employed in-situ UV-vis spectrophotometry to monitor the relative levels of neutral, polaronic and bipolaronic polypyrrole. The levels of these oxidation states were

followed during the application of both a constant potential and a potential ramp over a range of pHs. In a separate set of experiments, the decay of the characteristic bipolaron was used to determine the rate constants and activation energy for PPy overoxidation.

From the first section of this chapter the role of pH in overoxidation was observed. While at pH ≈ 0 little overoxidation was seen over 30 min at 0.8 V, at pH around 11 overoxidation proceeded almost to completion after 10 to 15 min. In this section it was also noted that the magnitude of the applied potential plays an even more significant role in overoxidation than pH. The rate of overoxidation was observed to increase to eighth power with applied potential. The destabilising nature of SO_4^{2-} as a supporting electrolyte ion was also shown, on this occasion for very highly ordered PPy/DS. This effect is so strong that overoxidation in sulphate solution at pH 5.5 occurs as readily as at pH 11 in a chloride solution.

The ease of overoxidation of P(MPyC) and the stability of P(3-OPy) were confirmed. Even though the latter polymer exhibited poor doping levels in the as-grown form, once it was fully oxidised its UV-vis spectrum remained constant, even at 1.1 V over 30 min.

In the kinetic study of the overoxidation of PPy/pTS in Cl^- supporting electrolyte, the reaction mechanism suggested by Beck et al was elaborated into two stages: fast nucleophilic attack on the fully doped PPy to yield a pyrrolinone (rate constant k_{1obs}), followed by slow nucleophilic attack on the pyrrolinone to yield a 4-hydroxylated pyrrolinone (rate constant k_{2obs}). The rate constants were determined under a variety of pH, potential and temperature conditions and varied (at E_{app} = 0.8 V vs Ag/AgCl) from k_{1obs} = 0.388 min^{-1} ($t_{1/2}$ = 1.9 min) at pH = 11.6 down to k_{2obs} = 0.009 min^{-1} ($t_{1/2}$ = 77 min) at pH ~ 0. Determination of the rate constant k_{1obs} at various temperatures allowed the estimation of the activation energy of the fast step in the overoxidation process. This was calculated as 39 kJ mol^{-1}.

Raman spectroscopy was used to investigate the chemical changes at the molecular level, occurring in PPy, P(MePyC) and P(3-OPy) during overoxidation. Application of a constant potential of 0.8 V (vs Ag/AgCl) led directly to carbonyl formation in PPy/pTS, with no evidence of the normal hydroxyl intermediate of a nucleophilic attack. However, the C-O linkages developed strongly over the next 5 to 60 min. At the same time the intensity of the carbonyl group increased and that of the N-H group decreased.

In the case of a PPy/pTS film scanned from 0.4 to 0.9 V, Raman spectroscopy showed that nucleophilic attack at moderate potentials was accompanied by the formation of polarons. The polaronic state was first observed at 0.45 V, followed by irreversible overoxidation at 0.65 V (as indicated by the presence of both C-O and C=O groups). Some evidence of chain breaking was noted at a potential of 0.9 V.

Based on the Raman data collected during the application of a slow potential ramp, a mechanism was proposed for the overoxidation of P(MePyC) via a direct decarboxylation reaction. This mechanism explained why this disubstituted PPy, with no obvious sites for nucleophilic attack, has an overoxidation potential close to a non-substituted PPy.

The stability of P(3-OPy) to electrochemical overoxidation in an aqueous environment was again demonstrated. During the application of a linear potential ramp from 0.4 to 1.1 V, no chemical changes in the polymer structure were detected. The only change in the polymer was determined to be a slight increase in doping level, from an original level between PPy (mostly bipolaronic) and P(MePyC) (exclusively polaronic).

One of the aims of this work was to establish reasonable anodic operating limits for PPy in an aqueous environment. Though this issue is complicated by the effects of the range of parameters discussed, it is possible to make some general recommendations. Firstly, the most stable non-substituted polypyrroles are those incorporating the mono-anionic sulphonates pTS and DS as dopants. Based on these dopants, the operating limits for

long term use in moderately acidic conditions (0.1 to 1 M) should be set at 0.5 V (vs Ag/AgCl). Certainly, even under the most favourable conditions, overoxidation was observed in non-substituted polypyrroles at 0.6 V over a period of minutes. In less favourable conditions, around pH ≈ 10, even 0.5 V would lead to rapid overoxidation in these polymers. On the other hand, the substituted polymer P(3-OPy) was stable over periods of up to 1 h in neutral conditions at potentials as high as 1.1 V (vs Ag/AgCl).

In Chapter 5, MALDI-MS studies, led to the conclusion that overoxidation proceeds via the formation of adjacent imine-nitrogens. This encourages substitution of oxygen at this point, probably by a chain breaking mechanism, ie α-substitution, leading to the formation of a pyrrolinone on the end group of a pyrrole hexamer. Overoxidation over either extended periods or in extreme environments proceeds by repetitive chain breaking to yield both oxygen containing and oxygen free pyrrole dimers, trimers, tetramers and heptamers. Under simple base dedoping, the polymer undergoes complete dedoping and reasonably clean degradation. This yields only the PPy hexamer with either adjacent imine-nitrogens or carbonyl at an α-carbon at one end.

In the final experimental chapter the potential limits suitable for application to two-electrode all polymer devices were investigated. The concept of monitoring the potential at the working (electrically passive) electrode was introduced. This was necessary to determine the actual potential "seen" by this electrode during the application of a potential difference. At an applied potential of -2 V in a propylene carbonate based supporting electrolyte, the potential measured at the working electrode was found to be only 0.69 V (vs Ag/AgCl) with only slight overoxidation evident. However, it was considered that a potential difference of ±1.5 V was more suitable for long term applications in a two-electrode cell where both electrodes are PPy. It was also shown that this potential difference was sufficient to fully oxidise and reduce PPy both in a supporting electrolyte solution and as a component of a two-electrode solid state device.

REFERENCES

1. B.R. Saunders, R.J. Fleming, and K.S. Murray, *Chemistry of Materials*, 1995, **7**(6): 1082-1094.
2. R. McNeil, R. Siudak, J. Wardlaw, and D. Weiss, *Australian Journal of Chemistry*, 1963, **16**: 1056-75.
3. A. Dall'Olio, G. Dascola, V. Varracca, and V. Bocchi, *C. R. Acad. Sci., Paris, Ser. C.*, 1968, **267**(6): 433-5.
4. A. Diaz and K. Kanazawa, *Journal of the Chemical Society, Chemical Communications*, 1979, **14**: 635-6.
5. P. Janda and J. Weber, *Journal of Electroanalytical Chemistry Interfacial Electrochemistry*, 1991, **300**(1-2): 119-27.
6. M. Umana and J. Waller, *Analytical Chemistry*, 1986, **58**(14): 2979-83.
7. A. Ivaska, *Electroanalysis*, 1991, **3**(4-5): 247-54.
8. H.L. Ge and Y.C. Lin, *Sensors & Actuators B Chemical*, 1994, **21**(1): 57-63.
9. A. Haimerl and A. Merz, *Journal of Electroanalytical Chemistry*, 1988, **220**: 55-65.
10. J. Prejza, I. Lundstrom, and T. Skotheim, *Journal of the Electrochemical Society*, 1982, **129**: 1685-1689.
11. J. Rodriguez, H. Grande, T.F. Otero, T. Trigaud, and J.P. Moliton, *Synthetic Metals*, 1996, **83**(3): 201-203.
12. Y. Kudoh, M. Fukuyama, and S. Yoshimura, *Synthetic Metals*, 1994, **66**(2): 157-164.
13. G. Troch-Nagels, R. Winand, A. Weymeersch, and L. Renard, *Journal of Applied Electrochemistry*, 1992, **22**(8): 756-64.
14. B. Scrosati, in *Modern Batteries*, C. Vincent and B. Scrosati, Editors. 1997, Arnold: London.
15. J.M. Kim, S.M. Chang, H.W. Lee, Y.S. Kwon, and Y.H. Oh, *Synthetic Metals*, 1997, **85**(1-3): 1371-1372.

16. R. Baughman and L. Shacklette, in *Science and Application of Conducting Polymers*, W. Salanek, D. Clark, and E. Samuelson, Editors. 1990, Adam Hilger: New York. 47-61.

17. F. Jonas and L. Schrader, *Synthetic Metals*, 1991, **41-43**: 831-836.

18. T. Otero, C. Santamaria, E. Angulo, and J. Rodriguez, *Synthetic Metals*, 1991, **41-43**: 2947-2952.

19. T. Otero, E. Angulo, C. Santamaria, and J. Rodriguez, *Synthetic Metals*, 1993, **54**: 217-222.

20. J. Schlenoff and H. Xu, *Journal of the Electrochemistry Society*, 1992, **139**(9): 2397-2401.

21. F. Beck, P. Braun, and M. Oberst, *Ber. Bunsenges. Phys. Chem.*, 1987, **91**: 967-974.

22. K.G. Neoh, T.T. Young, E.T. Kang, and T. Kang, *Journal of Applied Polymer Science*, 1997, **64**(3): 519-526.

23. A.A. Pud, *Synthetic Metals*, 1994, **66**(1): 1-18.

24. M. Freund, L. Bodalbhai, and A. Brajter-Toth, *Talanta*, 1991, **38**(1): 95-99.

25. C.C. Hsueh and A. Brajtertoth, *Analytical Chemistry*, 1994, **66**(15): 2458-2464.

26. K. Pihel, Q.D. Walker, and R.M. Wightman, *Analytical Chemistry*, 1996, **68**(13): 2084-2089.

27. Z.Q. Gao, J. Bobacka, A. Lewenstam, and A. Ivaska, *Synthetic Metals*, 1994, **62**(2): 117-123.

28. D. Centonze, A. Guerrieri, C. Malitesta, F. Palmisano, and P. Zambonin, *Fresenius Journal of Analytical Chemistry*, 1992, **342**: 729-733.

29. A.M. Farrington and J.M. Slater, *Electroanalysis*, 1997, **9**(11): 843-847.

30. J. Schlenoff, Y. Fong, and C. Shen, *Macromolecules*, 1991, **24**: 6791-6793.

31. A. Asarvapirivamont, G. Chandler, G. Gunaworden, and D. Pletcher, *Journal of Electroanalytical Chemistry Interfacial Electrochemistry*, 1984, **177**: 229-244.

32. S. Armes, in *Handbook of Conducting Polymers*, T. Skotheim, R. Elsenbaumer, and J. Reynolds, Editors. 1998, Marcel Dekker: New York.

33. R. John and G. Wallace, *Journal of Electroanalytical Chemistry*, 1991, **306**(1-2): 157-67.

34. R. Waltman and J. Bargon, *Tetrahedron*, 1984, **40**(20): 3963-70.

35. A. Diaz and J. Bargon, in *Handbook of Conducting Polymers*, T. Skoteim, Editor. 1986, Marcel Dekker: New York.

36. D.J. Fermin and B.R. Scharifker, *Journal of Electroanalytical Chemistry*, 1993, **357**(1-2): 273-287.

37. B. Scharifker and D. Fermin, *Journal of Electroanalytical Chemistry*, 1994, **365**(1-2): 35-39.

38. R. Bilger and J. Heinze, *Synthetic Metals*, 1993, **55**(2-3): 1424-1429.

39. Y. Kim, R. Collins, K. Vedam, and D. Allara, *Journal of the Electrochemical Society*, 1991, **138**(11): 3266-3275.

40. D. Mukherjee, *Progress in Rubber and Plastics Technology*, 1990, **6**(1): 30-49.

41. P. Christensen and A. Hamnett, *Electrochimica Acta*, 1991, **36**(8): 1263-1286.

42. J.-R. Rau, S.-C. Chen, and P.-H. Liu, *Journal of Electroanalytical Chemistry*, 1991, **307**: 269-274.

43. T.F. Otero and C. Santamaria, *Solid State Ionics*, 1993, **63-65**: 810-815.

44. G. Maia, E.A. Ticianelli, and F.C. Nart, *Zeitschrift fur Physikalische Chemie International Journal of Research in Physical Chemistry & Chemical Physics*, 1994, **186**(Part 2): 245-257.

45. B.S. Kim, W.H. Kim, S.N. Hoier, and S.M. Park, *Synthetic Metals*, 1995, **69**(1-3): 455-458.

46. G. Street, T. Clarke, M. Krounbi, K. Kanazawa, V. Lee, P. Pfluger, J. Scott, and G. Weiser, *Molecular Crystals Liquid Crystals*, 1982, **83**: 253-264.

47. P. Pfluger, M. Krounbi, and G. Street, *Journal of Chemical Physics*, 1983, **78**(6): 3212-3218.

48. J. Lei, W. Liang, and C. Martin, *Synthetic Metals*, 1992, **48**: 301-312.

49. J. Lei and C. Martin, *Synthetic Metals*, 1992, **48**: 331-336.

50. J.T. Lei and C.R. Martin, *Chemistry of Materials*, 1995, **7**(3): 578-584.

51. X. Zhang, E.T. Kang, K.G. Neoh, K.L. Tan, D.Y. Kim, and C.Y. Kim, *Journal of Applied Polymer Science*, 1996, **60**(4): 625-636.

52. E.T. Kang, K.G. Neoh, X. Zhang, K.L. Tan, and D.J. Liaw, *Surface & Interface Analysis*, 1996, **24**(1): 51-58.

53. M. Schirmeisen and F. Beck, *Journal of Applied Electrochemistry*, 1989, **19**: 401-409.

54. Y.F. Li and J. Yang, *Journal of Applied Polymer Science*, 1997, **65**(13): 2739-2744.

55. H. Ge, G. Qi, E. Kang, and K. Neoh, *Polymer*, 1994, **35**(3): 504-508.

56. M. Satoh, H. Ishikawa, H. Yageta, K. Amano, and E. Hasegawa, *Synthetic Metals*, 1997, **84**(1-3): 167-168.

57. F. Beck, U. Barsch, and R. Michaelis, *Journal of Electroanalytical Chemistry*, 1993, **351**(1-2): 169-184.

58. L. Warren, J. Walker, D. Anderson, and C. Rhodes, *Journal of the Electrochemical Society*, 1989, **136**(8): 2286-2295.

59. D.A. Kaplin and S. Qutubuddin, *Polymer*, 1995, **36**(6): 1275-1286.

60. J. Mostany and B.R. Scharifker, *Electrochimica Acta*, 1997, **42**(2): 291-301.

61. T. Osaka, T. Momma, S. Komaba, H. Kanagawa, and S. Nakamura, *Journal of Electroanalytical Chemistry*, 1994, **372**(1-2): 201-207.

62. W. Wernet and G. Wegner, *Macromolecular Chemistry*, 1987, **188**: 1465-1475.

63. J. Mostany and B.R. Scharifker, *Synthetic Metals*, 1997, **87**(3): 179-185.

64. R. John and G.G. Wallace, *Journal of Electroanalytical Chemistry*, 1993, **354**(1-2): 145-160.

65. S. Kuwabata, J. Nakamura, and H. Yoneyama, *Journal of the Electrochemical Society*, 1990, **137**(6): 1788-1792.

66. K. Cheung, D. Bloor, and G. Stevens, *Journal of Materials Science*, 1990, **25**: 3814-3837.

67. V. Krishna, Y.-H. Ho, S. Basak, and K. Rajeshwar, *Journal of the American Chemical Society*, 1991, **113**: 3325-3333.

68. Y. Lin, P. Riley, and G. Wallace, *Analytical Letters*, 1989, **22**(3): 669-81.

69. S. Adeloju, S. Shaw, and G. Wallace, *Analytica Chimica Acta*, 1997, **341**: 155-60.

70. R. John, M. Spencer, G. Wallace, and M. Smyth, *Analytica Chimica Acta*, 1991, **249**: 381-85.

71. A. Hodgson, M. Spencer, and G. Wallace, *Reactive Polymers*, 1992, **18**: 77-85.

72. M. Iseki, K. Saito, M. Ikematsu, Y. Sugiyama, K. Kuhara, and A. Mizukami, *Journal of Electroanalytical Chemistry*, 1993, **358**(1-2): 221-233.

73. G. Zotti, G. Schiavon, and N. Comisso, *Synthetic Metals*, 1991, **40**: 43-316.

74. M. Yamaura, K. Sato, and T. Hagiwara, *Synthetic Metals*, 1991, **41-43**: 439-442.

75. M. Forsyth and V.T. Truong, *Polymer*, 1995, **36**(4): 725-730.

76. S. Pruneanu, W. Graupner, L. Oniciu, M. Brie, and R. Turcu, *Materials Chemistry & Physics*, 1996, **46**(1): 55-60.

77. M. Grzeszczuk and G. Zabinskaolszak, *Journal of Electroanalytical Chemistry*, 1997, **427**(1-2): 169-177.

78. J.R. Reynolds, M. Pyo, and Y.J. Qiu, *Synthetic Metals*, 1993, **55**(2-3): 1388-1395.

79. D. Walton, C. Hall, and A. Chyla, *Analyst*, 1992, **117**(8): 1305-1311.

80. A. Diaz, J. Castillo, J. Logan, and W. Lee, *Journal of Electroanalytical Chemistry*, 1981, **129**: 115-132.

81. M. De Paoli, R. Peres, S. Panero, and B. Scrosati, *Electrochimica Acta*, 1992, **37**(7): 1173-1182.

82. D.A. Kaplin and S. Qutubuddin, *Journal of the Electrochemical Society*, 1993, **140**(11): 3185-3190.

83. J. Kaufman, N. Colaneri, J. Scott, and G. Street, *Physical Review Letters*, 1984, **53**(10): 1005-1008.

84. H.W. Rhee, J.M. Ko, J.K. Kim, and C.Y. Kim, *Molecular Crystals & Liquid Crystals*, 1993, **227**: 207-218.

85. S. Kuwabata, J. Nakamura, and H. Yoneyama, *Journal of the Electrochemical Society*, 1990, **137**(7): 2147-2150.

86. J. Tamm, A. Hallik, A. Alumaa, and V. Sammelselg, *Electrochimica Acta*, 1997, **42**(19): 2929-2934.

87. J. Schlenoff and C. Chien, *Journal of the American Chemical Society*, 1987, **109**: 6269-6274.

88. T. Matencio, M.A. Depaoli, R.C.D. Peres, R.M. Torresi, and S.I.C. Detorresi, *Synthetic Metals*, 1995, **72**(1): 59-64.

89. T. Amemiya, K. Hashimoto, and A. Fujishima, *Journal of Physical Chemistry*, 1993, **97**: 4187-4191.

90. T. Amemiya, K. Hashimoto, and A. Fujishima, *Journal of Electroanalytical Chemistry*, 1994, **377**(1-2): 143-148.

91. Y.F. Li and R.Y. Qian, *Synthetic Metals*, 1994, **64**(2-3): 241-245.

92. R.M. Torresi, S.I.C. Detorresi, T. Matencio, and M.A. Depaoli, *Synthetic Metals*, 1995, **72**(3): 283-287.

93. J.S. Wainright and C.A. Zorman, *Journal of the Electrochemical Society*, 1995, **142**(2): 384-388.

94. J. Tamm, A. Hallik, and A. Alumaa, *Synthetic Metals*, 1993, **55**(2-3): 1473-1476.

95. Q. Pei and Q. Renyang, *Electrochimica Acta*, 1992, **37**(6): 1075-1081.

96. F. Beck and M. Dahlhaus, *Journal of Electroanalytical Chemistry*, 1993, **357**(1-2): 289-300.

97. D.Y. Kim, J.K. Kim, J.Y. Lee, H.W. Rhee, and C.Y. Kim, *Polymers for Advanced Technologies*, 1997, **8**(4): 184-188.

98. D. Bott, in *Handbook of Conducting Polymers*, T. Skotheim, Editor. 1986, Marcel Dekker: New York.

99. T.L. Brown and H.E. LeMay, *Chemistry The Central Science*. 3rd ed. 1985, Englewood Cliffs: Prentice-Hall.

100. J. Kane and M. Sternheim, *Physics S. I. Version.* 1980, New York: John Wiley & Sons.

101. G.F. McCann, G.J. Millar, G.A. Bowmaker, and R.P. Cooney, *Journal of the Chemical Society Faraday Transactions*, 1995, **91**(23): 4321-4328.

102. D. Walton, *Materials and Design*, 1990, **11**(3): 142-52.

103. D.J. Fermin, H. Teruel, and B.R. Scharifker, *Journal of Electroanalytical Chemistry*, 1996, **401**(1-2): 207-214.

104. M. Forsyth, V.T. Truong, and M.E. Smith, *Polymer*, 1994, **35**(8): 1593-1601.

105. M. Kertesz, *Synthetic Metals*, 1995, **69**(1-3): 641-644.

106. C. Jenden, R. Davidson, and T. Turner, *Polymer*, 1993, **34**(8): 1649-1652.

107. J.R. Blanking, G.J. Millar, G.A. Bowmaker, and R.P. Cooney, *Journal of Raman Spectroscopy*, 1993, **24**(8): 523-526.

108. J. Bredas, J. Scott, Y. K., and G. Street, *Physical Review B*, 1984, **30**(2): 1023-1025.

109. E. Genies and J. Pernaut, *Journal of Electroanalytical Chemistry*, 1985, **191**: 111-126.

110. A. Patil, A. Heeger, and F. Wudl, *Chemistry Reviews*, 1988, **88**: 183-200.

111. A. Hourch, A. Rakotondrainibe, B. Beden, B. Beden, P. Croigneau, J.-M. Leger, C. Lamy, A. Tanaka, and E. Gonzalez, *Electrochimica Acta*, 1994, **39**(7): 889-898.

112. Y. Furukawa, *Journal of Physical Chemistry*, 1996, **100**(39): 15644-15653.

113. R. Singh, R. Tandon, V. Panwar, and S. Chandra, *Journal of Applied Physics*, 1991, **70**(1): 243-245.

114. P. Pfluger, G. Weiser, J. Scott, and G. Street, in *Handbook of Conducting Polymers*, T. Skotheim, Editor. 1986, Marcel Dekker: New York.

115. W.A. Goedel, G. Holz, G. Wegner, J. Rosenmund, and G. Zotti, *Polymer*, 1993, **34**(20): 4341-4346.

116. K. Yakushi, L. Lauchlan, T. Clarke, and G. Street, *Journal of Chemical Physics*, 1983, **79**(10): 4774-4778.

117. B. Sixou, N. Mermilliod, and J.P. Travers, *Physical Review B Condensed Matter*, 1996, **53**(8): 4509-4521.

118. K. Cheah, M. Forsyth, V.T. Truong, and C. Olssonjacques, *Synthetic Metals*, 1997, **84**(1-3): 829-830.

119. K.G. Neoh, K.K.S. Lau, V.V.T. Wong, E.T. Kang, and K.L. Tan, *Chemistry of Materials*, 1996, **8**(1): 167-172.

120. K. Tan, B. Tan, E. Kang, and K. Neoh, *Journal of Materials Science*, 1992, **27**(15): 4056-4060.

121. Y. Li and R. Qian, *Synthetic Metals*, 1988, **26**: 139-151.

122. O. Inganas, R. Erlandson, C. Nylander, and I. Lundstom, *Journal of Physics Chemistry of Solids*, 1984, **45**(4): 427-432.

123. G. Gustafsson, I. Lundstrom, B. Liedberg, C. Wu, O. Inganas, and O. Wennerstrom, *Synthetic Metals*, 1989, **31**: 163-179.

124. Y.F. Li and R.Y. Qian, *Journal of Electroanalytical Chemistry*, 1993, **362**(1-2): 267-272.

125. Y. Li and R. Qian, *Synthetic Metals*, 1993, **53**: 149-154.

126. Y.F. Li, R.Y. Qian, K. Imaeda, and H. Inokuchi, *Polymer Journal*, 1994, **26**(5): 535-538.

127. Y.F. Li, *Electrochimica Acta*, 1997, **42**(2): 203-210.

128. G.I. Mathys and V.T. Truong, *Synthetic Metals*, 1997, **89**(2): 103-109.

129. R. Ansari and G. Wallace, *Polymer*, 1994, **35**(11): 2372-2377.

130. H. Ge and G. Wallace, *Polymer*, 1992, **33**(11): 23482352.

131. B. Moss and R. Burford, *Polymer*, 1992, **33**(9): 1902-1908.

132. T. Tansley and D. Maddison, *Journal of Applied Physics*, 1991, **69**(11): 7711-7713.

133. S.P. Khedkar and S. Radhakrishnan, *Polymer Degradation & Stability*, 1997, **57**(1): 51-58.

134. V.T. Truong, B.C. Ennis, and M. Forsyth, *Polymer*, 1995, **36**(10): 1933-1940.

135. H. Masuda and K. Kaeriyama, *Journal of Materials Science*, 1991, **26**(20): 5637-5643.

136. A. Adachi and J. Yamauchi, *Synthetic Metals*, 1995, **73**: 101-105.

137. V. Kras'ko, A. Yakovleva, and Y. Kolotyrkin, *Electrokhimiya*, 1986, **22**: 1432-1434.

138. A.G. Rangamani, P.T. McTigue, and B. Verity, *Synthetic Metals*, 1995, **68**(2): 183-190.

139. M.H. Pyo, J.R. Reynolds, L.F. Warren, and H.O. Marcy, *Synthetic Metals*, 1994, **68**(1): 71-77.

140. P. Novak and W. Vielstich, *Journal of the Electrochemical Society*, 1990, **137**(4): 1036-1042.

141. A. Witkowski, M. Freund, and A. Brajter-Toth, *63*, 1991, (622-626).

142. X.B. Chen, J.P. Issi, J. Devaux, and D. Billaud, *Journal of Materials Science*, 1997, **32**(6): 1515-1518.

143. T. Otero, R. Tejada, and A. Elola, *Polymer*, 1987, **28**: 651-658.

144. D.-S. Park and Y.-B. Shim, *Journal of the Electrochemical Society*, 1993, **140**(3): 609-614.

145. G. Wegner, W. Wernet, D. Glatzhofer, J. Ulanski, C. Krohnke, and M. Mohammadi, *Synthetic Metals*, 1987, **18**: 1-6.

146. F. Beck and R. Michaelis, *Werkstoffe und Korrosion*, 1991, **42**: 341-347.

147. P. Novak, B. Rasch, and W. Vielstich, *Journal of the Electrochemical Society*, 1991, **138**(11): 330-3304.

148. P. Novak, *Electrochimica Acta*, 1992, **37**(7): 1227-1230.

149. M.C. Anglada, J. Claret, and J.M. Ribo, *Synthetic Metals*, 1993, **59**(2): 181-190.

150. P. Novak and W. Vielstich, *Collection of Czechoslovak Chemical Communications*, 1992, **57**(2): 339-348.

151. G. Mengoli, M. Musiani, M. Fleischman, and D. Pletcher, *Journal of Applied Electrochemistry*, 1984, **14**: 285-291.

152. J.C. Thieblemont, J.L. Gabelle, and M.F. Planche, *Synthetic Metals*, 1994, **66**(3): 243-247.

153. F. Palmisano, C. Malitesta, D. Centonze, and P.G. Zambonin, *Analytical Chemistry*, 1995, **67**(13): 2207-2211.

154. C. Malitesta, I. Losito, L. Sabbatini, and P.G. Zambonin, *Journal of Electron Spectroscopy & Related Phenomena*, 1995, **76**: 629-634.

155. V.T. Truong, B.C. Ennis, and M. Forsyth, *Synthetic Metals*, 1995, **69**(1-3): 479-480.

156. J.C. Thieblemont, M.F. Planche, C. Petrescu, J.M. Bouvier, and G. Bidan, *Polymer Degradation & Stability*, 1994, **43**(2): 293-298.

157. X.B. Chen, J. Devaux, J.P. Issi, and D. Billaud, *European Polymer Journal*, 1994, **30**(7): 809-811.

158. D.I. Kang, W.J. Cho, H.W. Rhee, and C.S. Ha, *Synthetic Metals*, 1995, **69**(1-3): 503-504.

159. K. Cheung, D. Bloor, and G. Stevens, *Polymer*, 1988, **29**: 1709-1717.

160. M. Gonzalez-Tejera, M. Delaplaza, E. Delabalanca, and I. Hernandezfuentes, *Polymer International*, 1993, **31**(1): 45-50.

161. S.J. Sutton and A.S. Vaughan, *Synthetic Metals*, 1993, **58**(3): 391-402.

162. B. Feldman, P. Burgamayer, and R. Murray, *Journal of the American Chemical Society*, 1985, **107**: 872-878.

163. E. Kupila and J. Kankare, *Synthetic Metals*, 1993, **55**(2-3): 1402-1405.

164. J.Y. Ouyang and Y.F. Li, *Synthetic Metals*, 1995, **75**(1): 1-3.

165. G. Zotti, G. Schiavon, S. Zecchin, and G. Daprano, *Synthetic Metals*, 1996, **80**(1): 35-39.

166. G. Kittleson, H. White, and M. Wrighton, *Journal of the American Chemical Society*, 1984, **106**: 7389-7396.

167. E. Paul, A. Ricco, and M. Wrighton, *Journal of Physical Chemistry*, 1985, **89**: 1441-1447.

168. W. Zhang and S. Dong, *Electrochimica Acta*, 1993, **38**(2/3): 441-445.

169. R. Deutscher, S. Fletcher, and J. Hamilton, *Electrochimica Acta*, 1986, **31**(5): 585-589.

170. R. John, A. Talaie, G. Wallace, and S. Fletcher, *Journal of Electroanalytical Chemistry*, 1991, **319**: 365-371.

171. A. Talaie and G.G. Wallace, *Solid State Ionics*, 1994, **70**(Part 1): 692-696.

172. A. Talaie and G.G. Wallace, *Synthetic Metals*, 1994, **63**(2): 83-88.

173. M. Montemayor, R. Jimenez, and E. Fatas, *Journal of Electroanalytical Chemistry*, 1993, **361**(1-2): 115-119.

174. B. Sun, J. Jones, R. Burford, and M. Skyllas-Kazacos, *Journal of the Electrochemical Society*, 1989, **136**(3): 698-701.

175. A. Witkowski and A. Brajter-Toth, *Analytical Chemistry*, 1992, **64**: 635-641.

176. T. Otero and E. Angulo, *Solid State Ionics*, 1993, **63**(5): 803-809.

177. Z. Cai and C. Martin, *Journal of Electroanalytical Chemistry*, 1991, **300**: 35-50.

178. T.F. Kang, G.L. Shen, and R.Q. Yu, *Talanta*, 1996, **43**(11): 2007-2013.

179. D. Stilwell and S.-M. Park, *Journal of the Electrochemical Society*, 1989, **136**(3): 688-698.

180. D.S. Park, Y.B. Shim, and S.M. Park, *Journal of the Electrochemical Society*, 1993, **140**(10): 2749-2752.

181. B. Zinger, *Journal of Electroanalytical Chemistry*, 1988, **244**: 115-121.

182. Z.G. Qi, N.G. Rees, and P.G. Pickup, *Chemistry of Materials*, 1996, **8**(3): 701-707.

183. R. Bull, F.-R. Fan, and A. Bard, *Journal of the Electrochemical Society: Electrochemical Science and Technology*, 1982, **129**(5): 1009-1015.

184. D.I. Kang, W.J. Cho, and C.S. Ha, *Molecular Crystals & Liquid Crystals Science & Technology Section A Molecular Crystals & Liquid Crystals*, 1995, **267**: 317-322.

185. H. Yamato, M. Ohwa, and W. Wernet, *Journal of Electroanalytical Chemistry*, 1995, **397**(1-2): 163-170.

186. H.Q. Tang, A. Kitani, and M. Shiotani, *Electrochimica Acta*, 1996, **41**(9): 1561-1567.

187. E.R. Nightingale, *Journal of Physical Chemistry*, 1959, **63**: 1381-1387.

188. R.C. Weast, ed. *CRC Handbook of Chemistry and Physics*. 56th ed. . 1975, CRC Press: Cleveland.

189. G.H. Aylward and T.J. Findlay, eds. *Chemical Data Book*. 2nd ed. . 1964, John Wiley: Sydney.

190. K. Collins and M. Washabaugh, *Quarterly Review of Biophysics*, 1985, **18**(4): 323-422.

191. J. Da Silva, in *New Trends in Bio-inorganic Chemistry*, R. Williams and J. Da Silva, Editors. 1978, Academic Press: London. 449-484.

192. N. Darby and T. Creighton, *Protein Structure*. In Focus, ed. D. Rickwood and D. Male. 1993, Oxford: IRL Press.

193. F. Franks, in *Characterisation of Proteins*, F. Franks, Editor. 1988, Humana Press: Clifton. 53-94.

194. G. Somero, in *Water and Life*, G. Somero, C. Osmond, and C. Bolis, Editors. 1992, Springer-Verlag: Berlin. 3-18.

195. C. Tanford, *Science*, 1978, **200**: 1012-1018.

196. D. Volkin and A. Klibanov, in *Protein Function: a prctical approach*, T. Creighton, Editor. 1989, IRL Press: Oxford. 1-24.

197. F. Franks and D. Eagland, *Critical Reviews in Biochemistrty*, 1975, **3**: 165-219.

198. F. Franks, in *Characterisation of Proteins*, F. Franks, Editor. 1988, Humana Press: Clifton.

199. R. Chicz and F. Regner, in *Guide to Protein Purification*, M. Deutscher, Editor. 1990, Academic Press: San Diego. 392-421.

200. I. Levesque and M. Leclerc, *Journal of the Chenical Society Communication*, 1995, : 2293-2294.

201. A. MacDiarmid and A. Epstein, *Synthetic Metals*, 1994, **65**: 103-116.

202. Y. Xia, A. MacDiarmid, and A. Epstein, *Macromolecules*, 1994, **27**: 7212-7214.

203. Y. Xia, J. Wiesinger, and A. MacDiarmid, *Chemistry of Materials*, 1995, **7**: 443-445.

204. W. Zheng, Y. Min, A. MacDiarmid, M. Angelopoulus, Y.-H. Liao, and A. Epstein, *Synthetic Metals*, 1997, **84**: 63-64.

205. T. Creighton, *Proteins - Structures and Molecular Properties*. 2nd ed. 1990, New York: W. H. Freeman.

206. J. Hendrickson, D. Cram, and G. Hammond, *Organic Chemistry*. 3rd ed. McGraw-Hill Series in Undergraduate Chemistry, ed. Z. Hugus, *et al.* 1970, Tokyo: McGraw-Hill Kogakakusha.

207. W. Melander and C. Horvath, *Archives of Biochemistry and Biophysics*, 1977, **183**: 200-215.

208. V. Lobo and J. Quaresma, eds. *Handbook of Electrolyte Solutions A*. Physical Scinces Data. Vol. Part A. 1989, Elsevier: Amsterdam.

209. V. Lobo, ed. *Handbook of Electrolyte Solutions B*. Physical Scinces Data. Vol. Part B. 1989, Elsevier: Amsterdam.

210. A.D. Lange and G.M. Forker, eds. *Lange's Handbook of Chemistry*. 10th ed. . 1967, McGraw- Hill: New York.

211. B.E. Conway, *Electrochemical Data*. 1952, Amsterdam: Elsevier.

212. E.W. Washburn, ed. *International Critical Tables of Numerical Data, Physics, Chemistry and Technology*. First Edition, Sixth Impression ed. . Vol. 4. 1928, McGraw Hill: New York.

213. C.D. Hodgman, ed. *Handbook of Chemistry and Physics*. 30th ed. . 1946, Chemical Rubber Publishing: Cleveland.

214. G. Jones and W. Ray, *Journal of the American Chemical Society*, 1942, **64**(2): 2744-2745.

215. H. Cupples, *Journal of the American Chemical Society*, 1945, **67**(1): 987-990.

216. P. Teasdale, *Characterisation of the Chemical Properties of Polypyrrole and Polyaniline*, in *Chemistry*. 1993, University of Wollongong: Wollongong.

217. E. Pigois-Landureau, Y.F. Nicolau, and M. Delamar, *Synthetic Metals*, 1995, **72**(2): 111-119.

218. R. McCreery and K. Cline, in *Laboratory Techniques in Electroanalytical Chemistry*, P. Kissinger and W. Heineman, Editors. 1996, Marcel Dekker: New York.

219. D. Sawyer, A. Sobkowiak, and J. Roberts, *Electrochemistry for Chemists*. 2nd ed. 1995, New York: John Wiley &Sons.

220. L. Warren and D. Anderson, *Journal of the Electrochemical Society*, 1987, **134**(1): 101-105.

221. M.D. Levi, C. Lopez, E. Vieil, and M.A. Vorotyntsev, *Electrochimica Acta*, 1997, **42**(5): 757-769.

222. H. Ge, K. Gilmore, and G. Wallace, *Journal of Liquid Chromatography*, 1994, **17**(6): 1301-1316.

223. H. Masuda and K. Kaeriyama, *Synthetic Metals*, 1990, **38**: 371-379.

224. H. Ge, K. Gilmore, S. Ashraf, C. Too, and G. Wallace, *Polymer*, 1993, **34**(9): 2007-2010.

225. S. Ashraf, F. Chen, C. Too, and G. Wallace, *Polymer*, 1996, **37**(13): 2811-2819.

226. A. Ho-Hoang, F. Fache, G. Boiteux, and M. Lemaire, *Synthetic Metals*, 1994, **62**(3): 277-280.

227. A. Feldblum, J. Kaufman, S. Etemad, and A. Heeger, *Physical Review B*, 1982, **26**(2): 815-826.

228. J.K. Avlyanov, H.H. Kuhn, J.Y. Josefowicz, and A.G. Macdiarmid, *Synthetic Metals*, 1997, **84**(1-3): 153-154.

229. P. Rapta, A. Bartl, and L. Dunsch, *Synthetic Metals*, 1997, **84**(1-3): 187-188.

230. Y. Tezuka, K. Aoki, and K. Shinozaki, *Synthetic Metals*, 1989, **30**: 369-379.

231. Y. Son, J.S. Choi, K.S. Jang, J.S. Suh, E.J. Oh, J. Joo, and J.H. Cho, *Synthetic Metals*, 1997, **84**(1-3): 175-176.

232. S.M. Chang, J.M. Kim, J.S. Chang, Y.S. Kwon, H. Muramatsu, and T. Ataka, *Molecular Crystals & Liquid Crystals Science & Technology Section A Molecular Crystals & Liquid Crystals*, 1996, **280**: 151-156.

233. Y. Tezuka, T. Ishii, and K. Aoki, *Journal of Electroanalytical Chemistry*, 1996, **402**(1-2): 161-165.

234. Y. Tezuka, K. Aoki, H. Yajima, and T. Ishii, *Journal of Electroanalytical Chemistry*, 1997, **425**(1-2): 167-172.

235. S. de Marcos and O. Wolfbeis, *Analytical Chimica Acta*, 1996, **334**: 149-153.

236. C.H. Lee, J.Y. Lee, and H. Lee, *Synthetic Metals*, 1997, **84**(1-3): 149-150.

237. D.Y. Kim, J.Y. Lee, C.Y. Kim, E.T. Kang, and K.L. Tan, *Synthetic Metals*, 1995, **72**(3): 243-248.

238. D.Y. Kim, J.Y. Lee, C.Y. Kim, E.T. Kang, and K.L. Tan, *Synthetic Metals*, 1995, **69**(1-3): 501-502.

239. V.P. Menon, J.T. Lei, and C.R. Martin, *Chemistry of Materials*, 1996, **8**(9): 2382-2390.

240. C. Coutanceau, A. Rakotondrainibe, P. Crouigneau, J.M. Leger, and C. Lamy, *Journal of Electroanalytical Chemistry*, 1995, **386**(1-2): 173-182.

241. F. Girard, S.Y. Ye, and D. Belanger, *Journal of the Electrochemical Society*, 1995, **142**(7): 2296-2301.

242. T. Ohtsuka, T. Wakabayashi, and H. Einaga, *Synthetic Metals*, 1996, **79**(3): 235-239.

243. T.F. Otero and M. Bengoechea, *Electrochimica Acta*, 1996, **41**(11-12): 1871-1876.

244. Y. Son and K. Rajeshwar, *Journal of the Chemical Society - Faraday Transactions*, 1992, **88**(4): 605-610.

245. D.Y. Kim, J.Y. Lee, D.K. Moon, and C.Y. Kim, *Synthetic Metals*, 1995, **69**(1-3): 471-474.

246. T.W. Lewis, G.G. Wallace, C.Y. Kim, and D.Y. Kim, *Synthetic Metals*, 1997, **84**(1-3): 403-404.

247. I. Rodriguez, M. Marcos, and J. Gonzalez-Velasco, *Electrochimica Acta*, 1987, **32**(8): 1181-1185.

248. V. Brandl and R. Holze, *Berichte der Bunsen Gesellschaft fur Physikalische Chemie An International Journal of Physical Chemistry*, 1997, **101**(2): 251-256.

249. S. Hoier and S.-M. Park, *Journal of Physical Chemistry*, 1992, **96**: 5188-5193.

250. W. Goedel, V. Enkelman, and G. Wegner, *Synthetic Metals*, 1991, **41-43**: 377-380.

251. H. Avery, *Basic Reaction Kinetics and Mechanisms*. 1974, London: Macmillan.

252. D. Stilwell and S.-M. Park, *Journal of the Electrochemical Society: Electrochemical Science and Technology*, 1988, : 2497-2502.

253. F. Beck and U. Barsch, *Synthetic Metals*, 1993, **55**(2-3): 1299-1304.

254. K. Laidler, *Chemical Kinetics*. 2nd ed. 1965, New York: McGraw-Hill.

255. D. Skoog and D. West, *Fundamentals of Analytical Chemistry*. 1971, New York: Holt, Rinehart, Winston.

256. G. Zerbi, M. Veronelli, S. Martina, A.D. Schluter, and G. Wegner, *Journal of Chemical Physics*, 1994, **100**(2): 978-984.

257. P. Hendra, C. Jones, and G. Warnes, *Fourier Transform Raman Spectrsocopy*. Ellis Horwood Series in Analytical Chemistry, ed. M. Masson and J. Tyson. 1991, New York: Ellis Horwood.

258. M. Lapkowski, K. Berrada, S. Quillard, G. Louarn, S. Lefrant, and A. Pron, *Macromolecules*, 1995, **28**(4): 1233-1238.

259. T. Fukuda, H. Takezoe, K. Ishikawa, A. Fukuda, H.S. Woo, S.K. Jeong, E.J. Oh, and J.S. Suh, *Synthetic Metals*, 1995, **69**(1-3): 175-176.

260. S. Quillard, K. Berrada, G. Louarn, S. Lefrant, M. Lapkowski, and A. Pron, *New Journal of Chemistry*, 1995, **19**(4): 365-374.

261. M. Trznadel, M. Zagorska, M. Lapkowski, G. Louarn, S. Lefrant, and A. Pron, *Journal of the Chemical Society Faraday Transactions*, 1996, **92**(8): 1387-1393.

262. G. Louarn, J.P. Buisson, S. Lefrant, and D. Fichou, *Journal of Physical Chemistry*, 1995, **99**(29): 11399-11404.

263. E.A. Bazzaoui, J.P. Marsault, S. Aeiyach, and P.C. Lacaze, *Synthetic Metals*, 1994, **66**(3): 217-224.

264. E. Agosti and G. Zerbi, *Synthetic Metals*, 1996, **79**(2): 107-113.

265. S.J. Vigmond, V. Ghaemmaghami, and M. Thompson, *Canadian Journal of Chemistry*, 1995, **73**(10): 1711-1718.

266. J.Y. Lee, D.Y. Kim, and C.Y. Kim, *Synthetic Metals*, 1995, **74**(2): 103-106.

267. B.T. Sun and D.P. Schweinsberg, *Synthetic Metals*, 1994, **68**(1): 49-56.

268. S. Dong and J. Ding, *Synthetic Metals*, 1987, **20**: 119-124.

269. B. Tian and G. Zerbi, *Journal of Chemical Physics*, 1990, **92**(6): 3886-3891.

270. G. Socrates, *Infrared Characteristic Frequencies*. 1980, Chichester: John Wiley and Sons.

271. J.M. Ribo, M.C. Anglada, J.M. Tura, and N. Ferreranglada, *Synthetic Metals*, 1995, **72**(2): 173-176.

272. P. Kissinger and W. Heineman, *Laboratory Techniques in Electroanalytical Chemistry*. 2nd ed. 1996, New York: Marcel Dekker Inc.

273. J. March, *Advanced Organic Chemistry*. 4th ed. 1992, New York: John Wiley and Sons.

274. J. Campana, L.-S. Sheng, S. Shew, and B. Winger, *Trends in Analytical Chemistry*, 1994, **13**(6): 239-51.

275. F. Hillenkamp, M. Karas, R. Beavis, and B. Chait, *Analytical Chemistry*, 1991, **63**(24): 1193A-1202A.

276. C. Fenselau, *Analytical Chemistry*, 1997, **69**(21): 661A-665A.

277. R. Cotter, *Analytical Chemistry*, 1984, **56**(3): 485A-503A.

278. R. Cotter, *Analytica Chimica Acta*, 1987, **195**: 45-59.

279. P. Cole-Clark and P. Humphrey, *Testing Technology*, 1996, **4**.

280. M. Karas, U. Bahr, and U. Giebmann, *Mass Spectrometry Reviews*, 1991, **10**: 335-337.

281. A. Belu, J. DeSimone, R. Linton, G. Lange, and R. Friedman, *American Society for Mass Spectrometry*, 1996, **7**: 11-24.

282. M.L. Abel, S.R. Leadley, A.M. Brown, J. Petitjean, M.M. Chehimi, and J.F. Watts, *Synthetic Metals*, 1994, **66**(1): 85-88.

283. S.Y. Luk, W. Lineton, M. Keane, C. Dearmitt, and S.P. Armes, *Journal of the Chemical Society Faraday Transactions*, 1995, **91**(5): 905-910.

284. J. Raynor and W. Schlindwein, *Synthetic Metals*, 1992, **46**(1): 45-51.

285. C.C. Chen and K. Rajeshwar, *Journal of the Electrochemical Society*, 1994, **141**(11): 2942-2946.

286. D. Schriemer and L. Li, *Analytical Chemistry*, 1996, **68**(17): 2721-2725.

287. J. Scrivens, H. Yates, M. Taylor, J. Segal, A. Jackson, A. Russell, and G. Critchly, *the analysis of synthetic polymer formulations by matrix assisted laser desorption ionisation time-of-flight mass spectrometry*, . 1995, VG Organic: Manchester.

288. D. Zhou, H. Zhao, W. Price, and G. Wallace, *Journal of Membrane Science*, 1995, **98**: 173-176.

289. R. Baughman, L. Shacklette, R. Elsenbaumer, E. Plitcha, and C. Becht, in *Conjugated Polymeric Materials: Opportunities in Electronics, Optoelectronics and Molecular electronics*, J. Bredas and R. Chance, Editors. 1990, Kluwer Academic Publishing: Dordrecht. 559-582.

290. P. Chiarelli, A. Della Santa, D. De Rossi, and A. Mazzoldi, *Journal of Material Systems and Structures*, 1995, **6**: 32-37.

291. K. Kaneto, M. Kaneko, Y. Min, and A. MacDiamid, *Synthetic Metals*, 1995, **71**: 2211-2212.

292. T. Lewis, S. Moulton, G. Spinks, and G. Wallace, *Synthetic Metals*, 1997, **85**: 1419-1420.

293. T. Lewis, L. Kane-Maguire, A. Hutchison, G. Spinks, and G. Wallace, *Synthetic Metals*, In Press, .

294. T. Lewis, G. Spinks, G. Wallace, D. De Rossi, and M. Pachetti, *Polymer Preprints*, 1997, **38**(2): 520-521.

295. T. Otero and H.-J. Grande, in *Handbook of Conducting Polymers*, T. Sotheim, R. Elsenbaumer, and J. Reynolds, Editors. 1998, Marcel Dekker Inc: New York.

296. Q. Pei and O. Inganas, *Advanced Materials*, 1992, **4**(4): 277-278.

297. Q. Pei, O. Inganas, and I. Lundstrom, *Smart Materials*, 1993, **2**: 1-6.

298. W. Takashima, M. Kaneko, K. Kaneto, and A. MacDiarmid, *Synthetic Metals*, 1995, **71**(2265-2266).

299. A. Della Santa, A. Mazzoldi, and D. De Rossi, *Journal of Material Systems and Structures*, 1996, **7**(3): 292-300.

300. E. Smela, O. Inganas, and I. Lundstrom, *Journal of Micromechanics and Microengineering*, 1993, : 203-205.

301. M. Ghandi, P. Murray, G. Spinks, and G. Wallace, *Synthetic Metals*, 1995, **73**: 247-256.

302. R. Linford, in *Applications of Electroactive Polymers*, B. Scrosati, Editor. 1993, Chapman & Hall: London.

303. D. Peramunage, D. Pasquariello, and K. Abraham, *Journal of the Electrochemical Society*, 1995, **142**(6): 1789-1798.

" 'There must be someway out of here,' said the joker to the thief,

'There's too much confusion, I can't get no relief.' "

All Along the Watchtower.

Bob Dylan, 1968.